

Development and Application of London Dispersion Corrections for Electronic Structure Methods

Eike-Hanno Jeremias Caldeweyher

Dissertation

Development and Application of London Dispersion Corrections for Electronic Structure Methods

Dissertation
zur
Erlangung des Doktorgrades (Dr. rer. nat.)
der
Mathematisch-Naturwissenschaftlichen Fakultät
der
Rheinischen Friedrich-Wilhelms-Universität Bonn

vorgelegt von
Eike-Hanno Jeremias Caldeweyher
aus Hilden

–2019–

Dekan:	Prof. Dr. Johannes Beck
Erster Gutachter:	Prof. Dr. Stefan Grimme
Zweiter Gutachter:	Prof. Dr. Thomas Bredow
Fachnaher Gutachter:	Prof. Dr. Andreas Gansäuer
Fachfremder Gutachter:	Prof. Dr. Rainer Manthey
Erscheinungsjahr:	2020
Tag der Disputation:	23.04.2020

Angefertigt mit Genehmigung der Mathematisch-Naturwissenschaftlichen
Fakultät der Rheinischen Friedrich-Wilhelms-Universität Bonn

Jana, Uschi und Rainer in Dankbarkeit gewidmet.

Statement of Authorship

I, Eike-Hanno Jeremias Caldeweyher, hereby declare that I am the sole author of this dissertation. The ideas and work of others, whether published or unpublished, have been fully acknowledged and referenced.

Bonn, April 27, 2020

Publications

Parts of this thesis were published in peer-reviewed journals:

- Caldeweyher, E. and Bannwarth, C. and Grimme, S. “Extension of the D3 dispersion coefficient model”, *J. Chem. Phys.* **2017**, *147*, 034112.
- Rösel, S. and Quanz, H. Logemann, C. and Becker, J. and Mossou, E. and Canãdillas-Delgado, L. and Caldeweyher, E. and Grimme, S. and Schreiner, P. R. “London dispersion enabled the shortest intermolecular hydrocarbon H···H contact”, *J. Am. Chem. Soc.* **2017**, *139*, 7428–7431.
- Caldeweyher, E. and Bursch, M. and Hansen, A. and Neugebauer, H. and Ehlert, S. and Grimme, S. “Understanding and quantifying London dispersion effects in organometallic complexes”, *Acc. Chem. Res.* **2019**, *52*, 258–266.
- Caldeweyher, E. and Ehlert., S and Hansen, A. and Neugebauer, H. and Spicher, S. and Grimme, S. “A generally applicable atomic-charge dependent London dispersion correction”, *J. Chem. Phys.* **2019**, *150*, 154122.
- Caldeweyher, E. and Mewes, J.-M., and Ehlert, S. and Grimme, S. “Extension and evaluation of the D4 London dispersion correction for periodic systems”, *ChemRxiv. Preprint*, DOI:10.26434/chemrxiv.10299428.v1 **2019**.

Further publications:

- Grimme, S. and Bannwarth, C. and Caldeweyher, E. and Pisarek, J. and Hansen, A. "A general intermolecular force field based on tight-binding quantum chemical calculations", *J. Chem. Phys.* **2017**, *147*, 161708.
- Caldeweyher, E. and Brandenburg, J. G. "Simplified DFT methods for consistent structures and energies of large systems", *J. Phys. Condens. Matter* **2018**, *30*, 213001.
- Pracht, P. and Caldeweyher, E. and Ehlert, S. and Grimme, S. "A robust non-self-consistent tight-binding quantum chemistry method for large molecules", *ChemRxiv. Preprint*, DOI:10.26434/chemrxiv.8326202.v1 **2019**.

Talks:

- "Low-cost dispersion-corrected density functional approaches", *Theoretical chemistry colloquia*, **2017**, Mühlheim an der Ruhr, Germany.
- "DFT-D4: An accurate and generally applicable tight-binding based dispersion correction for DFT", *SPP 1807: Control of London dispersion interactions in molecular chemistry*, **2018**, Hamburg, Germany.
- "An accurate and generally applicable atomic-charge based dispersion correction for density functional theory (DFT-D4)", *Symposium for theoretical chemistry*, **2018**, Halle-Saale, Germany.
- "An accurate and generally applicable atomic-charge based dispersion correction for density functional theory (DFT-D4)", *Bonn international graduation school*, **2018**, Bonn, Germany.

Posters:

- "Development and implementation of HSE-3c: A dispersion and counterpoise corrected range-separated hybrid functional", *Symposium for theoretical chemistry*, **2016**, Bochum, Germany.
- "Extension of the D3 dispersion coefficient model", *Sanibel symposium*, **2017**, Saint Simons Island, Georgia, USA.
- "Extension of the D3 dispersion coefficient model", *Computational molecular science*, **2017**, Warwick, United Kingdom.

- “An accurate *ab-initio* parametrization of density functional dispersion correction (DFT-D4) for the 86 elements H-Rn”, *SPP 1807: Control of London dispersion interactions in molecular chemistry*, **2017**, Giessen, Germany.
- “An accurate *ab-initio* parametrization of density functional dispersion correction (DFT-D4) for the 86 elements H-Rn”, *World association of theoretical and computational chemists*, **2017**, Munich, Germany.
- “An accurate *ab-initio* parametrization of density functional dispersion correction (DFT-D4) for the 86 elements H-Rn”, *European summerschool of quantum chemistry*, **2017**, Palermo, Italy.
- “Application and benchmarking of the DFT-D4 Method”, *Winter school in theoretical chemistry: Machine learning*, **2018**, Helsinki, Finland.
- “Extending a generally applicable atomic-charge dependent London dispersion correction with periodic boundary conditions”, *International conference on density-functional theory and its applications*, **2019**, Alicante, Spain.
- “D4 Goes Periodic”, *Atomic simulation environment developer meeting*, **2019**, Göteborg, Sweden.

Parts of this thesis were highlighted:

- “London dispersion enables the shortest intermolecular hydrocarbon H···H contact.”, *Computational chemistry highlights*, **2017**.
- “Hydrogens set a short-distance record”, *Chemical&Engineering news*, **2017**, *30*, 8–9.
- “Shortest H···H contact between hydrocarbon molecules”, *ChemistryView*, **2017**.
- “Simplified DFT methods for consistent structures and energies of large systems”, Ψ_k — *Scientific highlight of the month*, **2019**, *144*.
- “Fixing a Failure of Density Functional Theory”, *ChemistryView*, **2019**.

Abstract

Mean-field electronic structure methods like *Hartree–Fock* (HF) or *Kohn–Sham* (KS) *Density Functional Theory* (DFT) do not account for long-range correlation effects and consequently not for *London Dispersion* (LD). These LD forces contribute significantly to the interaction between molecular aggregates and are thus mandatory for a quantitative comparison of *in silico* predictions with experimental observations. Casimir and Polder formulated long-range correlation in terms of dynamic polarizabilities and established the foundation of all LD corrections within a DFT framework. This dissertation develops an efficient correction scheme, termed DFT-D4, for the accurate calculation of LD correlation effects in combination with *Density Functional Approximations* (DFAs) or other mean-field electronic structure methods. The presented scheme is an extension of the well-established DFT-D3 LD correction. In DFT-D3, the Coulomb operator is expanded into multipoles where a coarse-grain partitioning to atomic polarizabilities enables the calculation of interatomic dipole-dipole dispersion coefficients. *Fractional Coordination Numbers* (CNs) are used as a measure of the hybridization to efficiently calculate hybridization dependent dispersion coefficients from dynamic *Atom-in-Molecule* (AIM) polarizabilities.

In order to better account for non-additive AIM-polarizability effects, DFT-D4 additionally uses atomic oxidation state information. Those oxidation state information are of particular importance in systems like organometallic or charged complexes and improve their description of noncovalent interactions substantially. The oxidation-state dependency is implemented by an empirical function which uses atomic charge information for the scaling of reference polarizabilities. This scaling procedure is shown to be well suited to incorporate the most significant electronic effects into the reference values. The DFT-D4 default method uses a classical charge model, however, other charge schemes are implemented as well. A D3-like interpolation scheme incorporates those scaled references and generates hybridization and oxidation state dependent dynamic polarizabilities. DFT-D4 is shown to yield excellent molecular polarizabilities and dispersion coefficients. On a database of 1225 intermolecular dispersion coefficients the *Mean Absolute Deviation* (MAD) from experimental references is 3.8%. When combined with appropriate DFAs, noncovalent interaction energies for large complexes have MADs well below 10% and rotational constants (measure for the molecular size) have

Abstract

the accuracy of high-level correlated methodologies.

For certain metal-ions in highly polar and periodic environments, DFT-D methods obtain too large atomic polarizabilities compared to *Time-Dependent Density Functional Theory* (TD-DFT) values (*e.g.*, Na⁺ in crystalline NaCl). A more in-depth analysis shows that the absence of suitable reference systems causes the identified problem. In periodic environments, the CNs quickly approach values far beyond those for which reference polarizabilities are available. This absence leads to CNs extrapolations of polarizabilities, which are not reliable. The periodic DFT-D4 removes this drawback by extending the scope of reference polarizabilities for highly coordinated systems. For this purpose, dynamic polarizabilities for pseudo-periodic references with high CNs are calculated. The addition of such references to the D4-reference pool enables the physically reasonable calculation of atomic polarizabilities in dense solids. Such improved polarizabilities are shown to be beneficial for obtaining high-quality adsorption energies.

Comparing the computational costs of several dispersion corrections shows large differences in terms of efficiency. While the computational costs of the DFT-D4 method are negligible with respect to the underlying DFT calculation, some correction methods become the computational bottleneck.

The second part of the thesis consists of two application studies of LD corrected DFT methods. In the first case study, LD driven packing effects lead to the shortest intermolecular H···H contact reported to date. The attractive interactions between ^tBu groups cause this unusual binding situation. A periodic dispersion corrected DFT composite scheme verifies the experimental finding and an energy decomposition analysis quantifies the importance of LD interactions. The DFT structure determined by this composite scheme agrees very well with the structure determined from a low-temperature neutron diffraction experiment (intermolecular hydrogen-hydrogen bond length deviate by ≈ 1 pm from the experimental one). The second case study investigates LD interactions in organometallic complexes. Properly accounting for LD is shown to be important for predicting reaction paths, *e.g.* for the design of dispersion-controlled reaction sequences in homogeneous catalysis. In other systems like in the $[[\text{Rh}(\text{CNPh})_4]_2]^{2+}$ dication, LD contributions are able to compensate substantial repulsive electrostatic interactions. Additionally, LD interaction energies are compared to values obtained by a *Local Energy Decomposition* (LED) employing a local coupled-cluster theory. In combination with certain DFAs, the LD energies are in good agreement with the values of the LED partitioning.

In summary, the DFT-D4 LD correction is recommended as a standard tool in computer-assisted chemistry of molecular and periodic systems due to its high accuracy and computational efficiency.

Kurzreferat

Mean-Field-Elektronenstrukturmethoden wie *Hartree–Fock* (HF) oder *Kohn–Sham* (KS) *Dichtefunktionaltheorie* (DFT) sind nicht befähigt langreichweitige Korrelationseffekte und somit auch keine *London Dispersion* (LD) zu beschreiben. Solche LD Kräfte tragen signifikant zu der Interaktion molekularer Aggregate bei und sind deshalb obligatorisch für einen quantitativen Vergleich zwischen *in silico*-Vorhersagen und experimentellen Beobachtungen. Casimir und Polder haben langreichweitige Korrelationseffekte anhand dynamischer Polarisierbarkeiten hergeleitet und damit die Grundlage aller DFT-basierten LD Korrekturen errichtet. Die vorliegende Dissertation entwickelt ein effizientes Korrekturschema, namens DFT-D4, für die genaue Berechnung von LD Korrelationseffekten in Kombination mit *Dichtefunktionalnäherungen* (DFAs) oder anderen Mean-Field-Elektronenstrukturmethoden. Das präsentierte Schema ist eine Erweiterung der etablierten DFT-D3 London Dispersionskorrektur. In DFT-D3 wird der Coulomb-Operator in Multiple entwickelt, wobei eine coarse-grain Partition auf atomare Polarisierbarkeiten die Berechnung von interatomaren Dipol-Dipol Dispersionskoeffizienten ermöglicht. *Fraktionelle Koordinationszahlen* (CNs) gelten hierbei als Maß für die Hybridisierung von Atomen und werden zur effizienten Berechnung von hybridisierungsabhängigen Dispersionskoeffizienten ausgehend von dynamischen *Atom-in-Molekül* (AIM) Polarisierbarkeiten verwendet.

Für eine weitere Verbesserung von solchen nicht additiven AIM-Polarisierbarkeits-effekten, verwendet DFT-D4 zusätzlich Informationen über den atomaren Oxidationszustand. Solche Oxidationszustandsinformationen sind besonders in Systemen wie Organometallkomplexen oder geladenen Komplexen von ausgesprochener Wichtigkeit und verbessern die Beschreibung von deren nichtkovalenten Wechselwirkungen substantiell. Diese Oxidationszustandsabhängigkeit wird anhand einer empirisch ermittelten Funktion eingeführt welche atomare Ladungsinformationen für die Skalierung von Referenzpolarisierbarkeiten benutzt. Es wird gezeigt, dass diese Skalierung die wichtigsten Elektronenstruktureffekte in die Referenzwerte einbezieht. Die vorgestellte DFT-D4 Standardmethode benutzt ein klassisches Ladungsmodell für Skalierungszwecke, wobei auch andere Ladungsmodelle implementiert sind. Ein D3-artiges Interpolationschema verwendet die skalierten Referenzen und erstellt hybridisierungs- und oxidationsabhängige dynamische Polarisierbarkeiten. Desweiteren wird gezeigt, dass DFT-D4 exzellente molekulare

Polarisierbarkeiten und Dispersionskoeffizienten berechnet. Auf einer Datenbank von 1225 intermolekularen Dispersionskoeffizienten erzielt DFT-D4 eine *mittlere absolute Abweichung* (MAD) von 3.8% im Vergleich zu experimentellen Referenzen. Wenn geeignete DFAs mit DFT-D4 gekoppelt werden, weisen nichtkovalente Interaktionsenergien für große Komplexe MADs unter 10% auf und Rotationskonstanten (Meßgröße für die molekulare Größe) besitzen die Genauigkeit von hochgenauen korrelierten Wellenfunktionsmethoden.

Für gewisse Metallionen in hochpolaren und periodischen Umgebungen berechnen DFT-D Methoden zu große atomare Polarisierbarkeiten verglichen mit *zeitabhängigen Dichtefunktionaltheorie* (TD-DFT) Werten (z.B. für Na⁺ im NaCl-Kristall). Eine gründliche Untersuchung zeigt, dass die Abwesenheit von zweckmäßigen Referenzsystemen diese identifizierten Probleme verursacht. Innerhalb periodischer Umgebungen können CNs-Werte erreicht werden, die weit von den Werten abweichen, für welche Referenzpolarisierbarkeiten vorhanden sind. Dieses Fehlen von Interpolationspunkten sorgt für eine Extrapolation von Polarisierbarkeiten, welche nicht zuverlässig ist. Das periodische DFT-D4 beseitigt diesen Nachteil, indem es den Umfang der Referenzpolarisierbarkeiten für hoch koordinierte Systeme erweitert. Zu diesem Zweck werden dynamische Polarisierbarkeiten für pseudoperiodische Referenzen mit hohen CNs berechnet. Die Aufnahme solcher Referenzen in den D4-Referenzpool ermöglicht die physikalisch sinnvolle Berechnung der atomaren Polarisierbarkeiten in dicht gepackten Festkörpern. Diese verbesserten Polarisierbarkeiten erweisen sich als vorteilhaft für den Erhalt hochwertiger Adsorptionsenergien.

Der Vergleich der Rechenkosten mehrerer Dispersionskorrekturen zeigt große Unterschiede in Bezug auf ihre Effizienz. Während die Rechenkosten der DFT-D4-Methode im Vergleich zur zugrunde liegenden DFT-Berechnung vernachlässigbar sind, werden einige Korrekturmethode zum Rechenengpass.

Der zweite Teil der Arbeit besteht aus zwei Anwendungsstudien von LD-korrigierten DFT-Methoden. In der ersten Fallstudie sorgen LD-induzierte Packungseffekte zu dem bisher kürzesten ermittelten intermolekularen H···H-Kontakt. Die attraktiven Wechselwirkungen zwischen den ^tBu-Gruppen der Substituenten verursachen diese ungewöhnliche Bindungssituation. Ein periodisch dispersionskorrigiertes DFT-Kompositschema verifiziert den experimentellen Befund und eine Energiezersetzungsanalyse quantifiziert die Bedeutung von LD-Interaktionen. Die ermittelte DFT-Struktur stimmt sehr gut mit der durch ein Neutronenbeugungsexperiment bestimmten Struktur überein (intermolekulare Wasserstoff-Wasserstoff Bindungslänge weicht ≈1 pm vom experimentellen Befund ab). Die zweite Fallstudie untersucht LD-Interaktionen in metallorganischen Komplexen. Die korrekte Berücksichtigung von LD erweist sich als wichtig für die Vorhersage von Reaktion-

spfad, z.B. für die Gestaltung von dispersionsgesteuerten Reaktionsabläufen in der homogenen Katalyse. In anderen Systemen wie in dem $[[\text{Rh}(\text{CNPh})_4]_2]^{2+}$ Dikation sind LD-Beiträge in der Lage, erhebliche abstoßende elektrostatische Wechselwirkungen zu kompensieren. Zusätzlich werden LD-Interaktionsenergien mit Werten verglichen, die durch eine *lokale Energieersetzung* (LED) unter Verwendung einer lokalen Coupled-Cluster-Theorie erhalten werden. In Kombination mit bestimmten DFAs stehen die LD-Energien in guter Übereinstimmung mit den Werten der LED-Partitionierung.

Zusammenfassend wird die DFT-D4 London Dispersionskorrektur aufgrund ihrer hohen Genauigkeit und Recheneffizienz als Standardwerkzeug in der computergestützten Chemie von molekularen und periodischen Systemen empfohlen.

Contents

Publications	ix
Abstract	xiii
Kurzreferat	xv
Introduction	1
Theoretical Background	7
0.1. Definition of the Electronic Hamiltonian	7
0.2. Hartree–Fock Theory and Electron Correlation	9
0.3. Density Functional Theory	13
0.4. Long-Range Correlation	21
0.5. Semi-Classical London Dispersion Corrections	25
I. Development of the DFT-D4 London Dispersion Correction	29
1. Extension of the D3 Dispersion Coefficient Model	33
1.1. Introduction	34
1.2. Theory	35
1.2.1. General	35
1.2.2. Dispersion Coefficients	36
1.2.3. Dispersion Energy	38
1.2.4. Technical Details	39
1.3. Results	39
1.3.1. Molecular C_6 Coefficients	39
1.3.2. Atoms-in-Molecules Polarizabilities	40
1.3.3. Li^+ -benzene: An Electronically Complicated Example System	41
1.3.4. Noncovalent Interaction Energies	43
1.4. Summary and Conclusion	43
1.5. Acknowledgments	44

Contents

1.6. Appendix A1	44
2. A Generally Applicable Atomic-Charge Dependent London Dis-	
persion Correction	45
2.1. Introduction	46
2.2. Theory	48
2.2.1. Classical Environment Dependent Partial Charges	55
2.2.2. Two-body Dispersion Energy	57
2.2.3. Three-body Dispersion and Efficient Geometry Optimizations	58
2.2.4. Many-body Dispersion Energy	59
2.2.5. Definition of the D4 Default Model and Use of Alternative	
Charges	60
2.2.6. Technical Details	61
2.3. Results	63
2.3.1. Molecular Dispersion Coefficients	63
2.3.2. Noncovalent Interactions and Conformational Energies . .	66
2.3.3. Thermochemistry	69
2.3.4. Covalent and Noncovalent Structures	73
2.4. Summary and Conclusions	75
2.5. Acknowledgments	77
2.6. Appendix A2	77
3. Extension and Evaluation of the D4 London Dispersion Model for	
Periodic Systems	79
3.1. Introduction	80
3.2. Theory	83
3.2.1. Dynamic Polarizabilities from Cluster Extrapolation	83
3.3. Results	86
3.3.1. Polarizabilities and Refractive Indices	86
3.3.2. Molecular Crystals	91
3.3.3. Adsorption on Surfaces	97
3.3.4. Timings	100
3.4. Summary and Conclusions	102
3.5. Acknowledgments	103
3.6. Appendix A3	103

II. Applications of London Dispersion Corrections in Molecular Systems	105
4. London Dispersion Enables the Shortest Intermolecular Hydrocarbon H···H Contact	109
4.1. Acknowledgments	116
4.2. Appendix A4	117
5. Understanding and Quantifying London Dispersion Effects in Organometallic Complexes	119
5.1. Introduction	121
5.2. Theory and Methods	124
5.3. Applications	126
5.4. Summary and Perspective	132
5.5. Appendix A5	133
Final Summary and Conclusion	136
Bibliography	141
A1. Supporting Information to Chapter 1	164
A1.1. Extension of the D3 Dispersion Coefficient Model	164
A1.2. D4 Definition	164
A1.3. Parametrization of the ζ Scaling Function	171
A1.4. Extended Statistical Measures	171
A1.5. Cation- π Dissociation	172
A1.6. BJ-Damping Parameter	173
A2. Supporting Information to Chapter 2	174
A2.1. A Generally Applicable Atomic-Charge Dependent London Dispersion Correction	174
A2.2. Classical Partial Charges	174
A2.3. Many-Body Dispersion Theory	180
A2.4. Tight-Binding Two-Body Dispersion Potential (GFN2-xTB)	183
A2.5. Double Hybrid Density Functionals	185
A2.6. BJ-Damping Parameters	185
A2.7. Timings of Energy and Gradient Calls	193
A2.8. Extended Statistical Measures	193

A3. Supporting Information to Chapter 3	214
A3.1. Extension and Evaluation of the D4 London Dispersion Model for Periodic Systems	214
A3.1.1. Periodic DFT-D4 Methodologies	214
A3.1.2. Periodic Electronegativity Equilibration Model	216
A3.1.3. Dispersion Energy	219
A3.1.4. Theory of the Quasi-Harmonic Approximation	221
A3.1.5. Technical Details	222
A3.1.6. Computational Details	223
A4. Supporting Information to Chapter 4	225
A4.1. London Dispersion Enables the Shortest Intermolecular Hydrocarbon H···H Contact	225
A4.2. Computations	225
A4.2.1. Crystal Structure	226
A4.2.2. Gas Phase Structures	235
A4.2.3. Determination of the Dissociation Energies	237
A4.3. Interaction Energies	243
A4.3.1. Energy Decomposition Analysis	243
A5. Supporting Information to Chapter 5	245
A5.1. Understanding and Quantifying London Dispersion Effects in Organometallic Complexes	245
A5.1.1. Computational Details	245
A5.1.2. Benchmark Data	246
A5.1.3. LED	249
A5.1.4. Timings	250
A5.1.5. Indenyl Complexes	250
Acknowledgements	252
Abbreviations	253

Introduction

Quantum Mechanical (QM) models are used in chemistry and physics to rationalize experimental findings, *i. e.*, to explain reactivity or spectroscopic properties of compounds of various kind.¹⁻³ Typically their predictive power is verified in benchmark studies or blind competitions. Examples are the assessment of protein and ligand modeling,^{4,5} the prediction of crystal structures,^{6,7} or the calculation of intermolecular interaction energies.⁸ Nowadays, theoretical modeling has become accurate enough to be incorporated as an integral part of many developments in both science and industry.⁹⁻¹¹ One example is the discovery process of new materials. When searching for materials with specific properties, one has to choose from a vast pool of possible candidates. Since the experimental investigation of many materials is practically and economically demanding, electronic structure methods are used to efficiently reduce the search space and guide through the material design process.

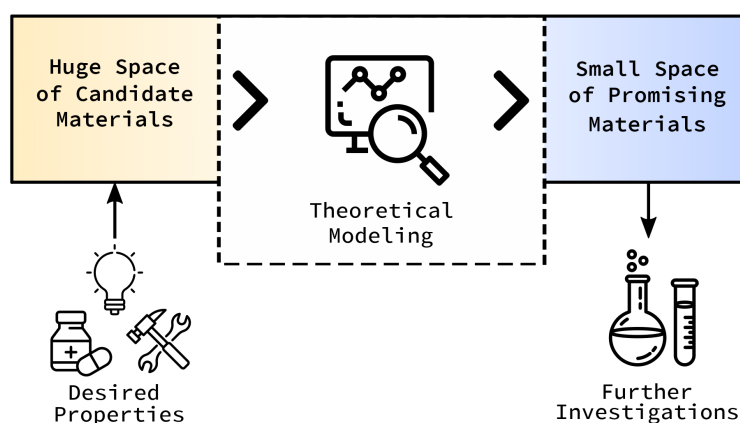


Figure 0.1.: Sketch of a possible material discovery work-flow.

Figure 0.1 exemplifies a practical, quantum-mechanically driven material discovery process. Different branches of industry impose specific conditions on new materials which are determined by their chemical and physical properties. As the available space of new materials is immense, theoretical models are used to identify promising candidates,^{12,13} which can be further investigated experimentally.

0. Introduction

In this context, the three-dimensional (molecular) structure plays a crucial role as it strongly influences physical and chemical properties. Experimentally, the X-ray method is routinely used to determine the structure of the corresponding molecular crystal of organic or biomolecular compounds. However, this requires the formation of an ordered crystal structure of the considered compound. Even if the crystallization was successful, it is questionable whether the conformation of the molecule in the crystal structure represents the molecular geometry adopted in solution.¹⁴ To resolve this issue, QM simulations allow to describe the structure for the respective compound in different aggregate types, *i. e.*, within the gas phase, a solution, or a solid state. Here, the accurate modeling of the structure requires the proper description of covalent and *Noncovalent Interactions* (NCIs).

The *Symmetry-Adapted Perturbation Theory* (SAPT)^{15,16} allows the separation of the *total interaction energy* (INT) into several energetic contributions. Those contributions are *Electrostatics* (ES), *Pauli Exchange Repulsion* (EXR), *Induction* (IND), and LD.

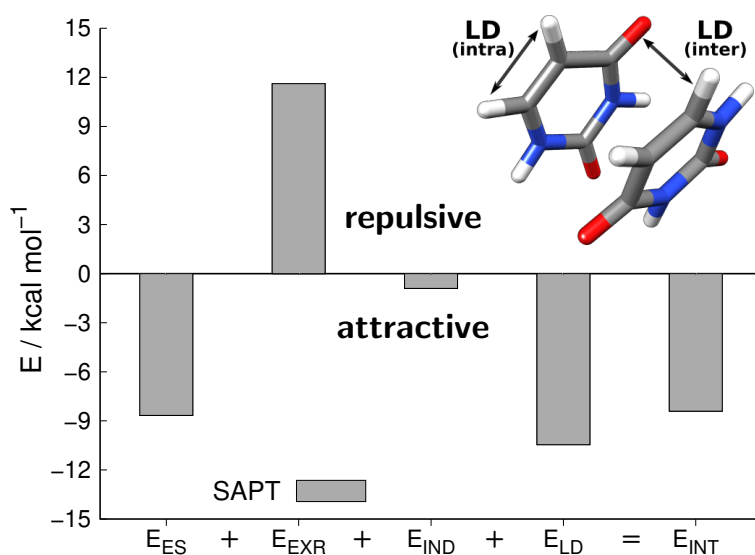


Figure 0.2.: Energetic decomposition of the π -stacked uracil dimer INT using the SAPT method (AC-PBE0/def2-QZVP level of theory). Figure created in analogy to Figure 6 of Ref. 17.

Figure 0.2 shows such a decomposition for the INT of the π -stacked uracil dimer using SAPT. Usually, the EXR is the largest (and often only) repulsive contribution. The ES and LD terms are of similar magnitude, whereas the IND terms are smaller. Apparently, the LD is a very important interaction in this system, and its accurate prediction is necessary for accurate QM predictions.

Solving the many-particle Schrödinger equation would seamlessly cover all these covalent and NCIs. However, this is prohibitive for realistic systems. Therefore, formal approximations of either the Hamiltonian or the many-particle wave function

exist. The desired accuracy of the results can be used to select different electronic structure methods, ranging from fast, low-cost methods¹⁸ to more involved high-level methods. In recent years new developments introduced an impressive impact in the field of high-level *Wave Function Theory* (WFT). Embedding techniques^{19–21} and local variants of coupled-cluster theory^{22–24} have made the “gold standard” of quantum chemistry CCSD(T) feasible for molecular systems up to several hundred atoms and molecular crystals of small organic compounds.^{25,26} Furthermore, new algorithms extended the field of quantum Monte–Carlo simulation. This led to substantial time savings achieving even high-precision lattice energies of molecular crystals calculated in a reasonable amount of time.²⁷ Other commonly used many-body correlation methods are the *Random Phase Approximation* (RPA)²⁸ and the *Møller–Plesset Perturbation Theory of Second-Order* (MP2). Along with the availability of more powerful computers,²⁹ the development of efficient electronic structure methods, in particular, has established computational chemistry as a fundamental part of chemistry in recent decades.^{30,31} Herein especially effective one-particle methods such as HF or DFT have become the “workhorse”³² of computational chemistry.

Hohenberg and Kohn (HK) introduced DFT as the mapping of the electron density $n(\mathbf{r})$ to the electronic energy,³³ which makes this approach particularly cost-effective (wavefunction $\Psi \in \mathcal{R}^{3N}$ versus electron density $n \in \mathcal{R}^3$). However, the exact HK density functional is unknown. Therefore, it is common practice to use DFAs in the picture of KS-DFT. Such DFAs express the electron correlation in semi-local frameworks allowing for a good description of ES, IND, and EXR effects. However, they do not describe the LD contribution, which is a nonlocal, long-range correlation effect. Conventional hybrid functionals (including nonlocal Fock exchange) do not describe such LD contributions either.^{34–37} This inability roots in the missing $-C_6/R^6$ dependence and is known as the “dispersion problem”.³⁸ The missing long-range correlation of semi-local DFT was subject of early studies, e. g., in rare-gas dimers,³⁹ in base pair stacking,⁴⁰ or in N_2 dimers.⁴¹ Cohen and Pack showed that the application of an atom pairwise dispersion correction combined with a density functional type interaction potential partly cures the dispersion problem. In their work,⁴² they used the so-called Gordon–Kim model and applied a dispersion correction of the form

$$E_{\text{DISP}}(R) = -\frac{C_6}{R^6} - \frac{C_8}{R^8} - \frac{C_{10}}{R^{10}}, \quad (0.1)$$

with R being the interatomic distance. At the same time several other dispersion corrections were developed for the description of NCIs in bio-organic systems, e. g., by the groups of Yang,⁴³ Elstner/Hobza,⁴⁴ or Scoles⁴⁵. Newer generations of dispersion corrections have nowadays become standard tools in the field of

0. Introduction

computational chemistry.^{46–52}

Among these models are the DFT-D corrections (namely DFT-D,⁵³ DFT-D2,⁵⁴ and DFT-D3⁴⁶), which are based on a semi-classical treatment of dispersion interactions. The wording “semi-classical” means that the dispersion contribution is expressed in classical terms, although this contribution is a pure quantum mechanical effect. DFT-D models couple the resulting dispersion potential with conventional QM methods and are predicated on an atom pairwise additive treatment of the dispersion energy (for HF analogue see Ref. 55,56). Benchmarking of the third DFT-D version (DFT-D3) revealed high accuracies for all test cases and no outliers.⁴⁶ DFT-D3 thus enables the accurate prediction of noncovalent geometries and dispersion interactions as highlighted in figure 0.3.

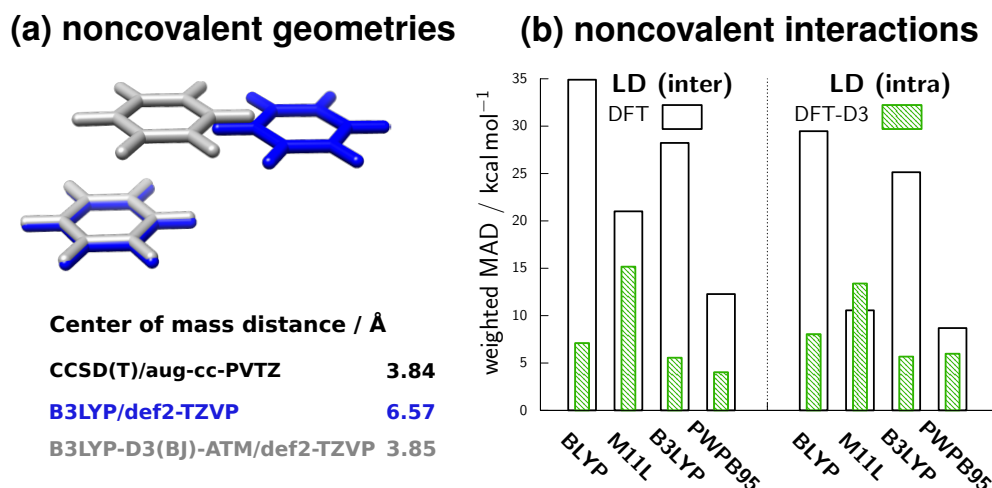


Figure 0.3.: Noncovalent geometries (a) and NCIs⁵⁷ (b) for D3 corrected DFAs.

The wide spread use of this method is reflected in its growing citation numbers (*cf.* figure 0.4). Furthermore, this correction scheme is available in several leading codes as ORCA,⁵⁸ TURBOMOLE,⁵⁹ GAUSSIAN,^{60,61} VASP,^{62–66} PSI4,⁶⁷ MOLPRO,⁶⁸ ADF,⁶⁹ QCHEM,⁷⁰ CRYSTAL17,⁷¹ CP2K,⁷² and many more, demonstrating a broad acceptance in the community.

Since the bottleneck of the calculation remains the self-consistent field procedure, the coupling of semi-local DFT with DFT-D3 does not come with any additional computational costs. Due to the popularity and excellent quality, which makes this method the *de facto* standard approach for treating NCIs in molecular systems, an important question arises:

“Can this model be further improved while maintaining its efficiency?”

Instead of a simple reparametrization of the damping scheme—as proposed by

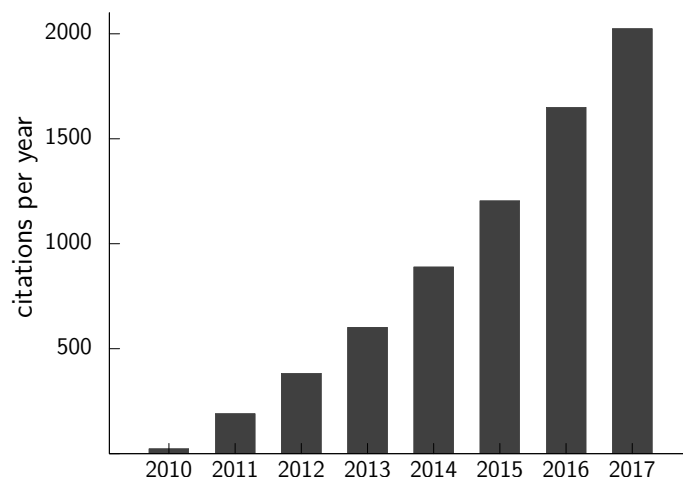


Figure 0.4.: Citations of the DFT-D3 method within recent years.

groups of Schwabe,⁷³ Sherrill,⁷⁴ or Head-Gordon⁷⁵—the main topic of the present work is the partial inclusion of electronic structure to improve the D3 methodology itself.

The present dissertation develops an “improved DFT-D3 method”. This improved method includes electronic structure contributions in the derivation of dynamic polarizabilities while keeping up the efficiency of the original model. In analogy with earlier DFT-D revisions, the new method is called DFT-D4. The intention is to provide an extension of the original model by means of partitioned charge information in order to achieve higher accuracies especially in situations where charge information is different from that of the D3-references, *e. g.*, in organometallic or charged complexes. In the following an overview of QM methods is given that are important for this dissertation, focusing on DFT and the description of long-range correlation effects in terms of *Rayleigh–Schrödinger Perturbation Theory* (PT). Furthermore, the semi-classical DFT-D3 LD correction is introduced, which provides the foundation for the development of the successor method.

Part I discusses the DFT-D4 method in detail. Chapter 1 introduces hybridization and oxidation state dependent dynamic polarizabilities. Those polarizabilities are obtained by extending the hybridization-only scheme of DFT-D3 with a charge-scaling concept. Chapter 2 describes a generalization of this charge-scaling concept, resulting in a significant reduction of empirical parameters. Afterwards, Chapter 3 discusses the extension of the molecular DFT-D4 method with *Periodic Boundary Conditions* (PBCs). Such an extension is essential for representing LD effects in solid states, on surfaces, or in simulations applied with PBCs. Several applications, like the calculation of lattice energies and volumes of molecular crystals, show small but consistent improvements when applying the periodic DFT-D4 method compared to other dispersion correction schemes. We also analyze ad-

0. Introduction

sorption of small organic molecules on different surfaces. A computational timings analysis shows that the DFT-D4 method is convincing in terms of its accuracy/-cost ratio.

Part II highlights two applications of dispersion-corrected DFT methods. Chapter 4 demonstrates the importance of LD effects within a molecular crystal synthesized by the Schreiner group.⁷⁶ This overcrowded molecular crystal exhibits the shortest intermolecular H \cdots H contacts reported so far, which may correspond either to potential energy minima or conformational transition states.⁷⁷ DFT schemes are used to identify the origin of these short H \cdots H contacts.

Afterwards, several organometallic complexes are investigated concerning their structural and energetic properties. Several examples are presented, *e.g.*, the analysis of transition metal thermochemistry and NCIs for small, heavy element containing main group compounds (Chapter 5). These examples show that charge-dependent polarizabilities are beneficial to describe properties of organometallic complexes more accurately.

Theoretical Background

The following chapters provide an overview of the theoretical background of QM methods that are of special importance for this dissertation. After defining the electronic Hamiltonian, the HF theory is explained in Chapter 0.2 and the concept of dynamic electron correlation is explained. Chapter 0.3 introduces the KS-DFT and gives an overview of various classes of DFAs. Mean-field electronic structure methods such as HF and KS-DFT generally do not account for long-range electron correlation. Such mean-field methods share the common feature that a set of N one-particle functions is optimized for the considered N electrons and that the total energy depends exclusively on the occupied orbitals. The remaining functions that are left over in the variational optimization are the virtual orbitals. These virtual orbitals contain information about excitation energies and can be used to model the response of the system with respect to external perturbations, *e.g.*, caused by electromagnetic fields. This is exploited in wave function theories since the virtual orbitals are used to construct an improved wavefunction by inclusion of excited determinants.⁷⁸ However, neither virtual orbitals nor non-local density information is used within mean-field approaches which is the root cause for their missing ability to describe LD correlation. The concept of long-range dynamic correlation is defined in Chapter 0.4. Based on these theoretical fundamentals, a semi-classical scheme is introduced in Chapter 0.5 which enables the approximated inclusion of LD interactions in mean-field electronic structure approaches. Semi-classical correction schemes calculate the pairwise dispersion energy contribution, which is added to the electronic energy of the particular mean-field approach. The term “semi-classical” arises from the fact that the dispersion energy is effectively expressed in terms of classical interactions between atoms or molecules, although LD itself is intrinsically a pure quantum mechanical effect.

0.1. Definition of the Electronic Hamiltonian

Molecular systems consist of bonded atoms that comprise negatively charged electrons and positively charged nuclei. The Hamiltonian defines the sum of the kinetic and the potential energies of all particles within such systems. In the following, indices e and n refer to electrons and nuclei, respectively. The time-independent,

0. Theoretical Background

non-relativistic Hamiltonian is given by

$$\hat{H} = \hat{H}_e + \hat{T}_n + \hat{V}_{n-n} (+\hat{V}_{n\text{-field}}), \quad (0.2)$$

with \hat{H}_e being the electronic Hamiltonian defined as

$$\hat{H}_e = \hat{T}_e + \hat{V}_{n-e} + \hat{V}_{e-e} (+\hat{V}_{e\text{-field}}). \quad (0.3)$$

If not noted otherwise, atomic units are used throughout. The kinetic energy of the K nuclei of the system \hat{T}_n is defined by

$$\hat{T}_n = \sum_{a=1}^K \frac{-\nabla_{\mathbf{R}_a}^2}{2M_a}, \quad (0.4)$$

where \mathbf{R}_a denotes the Cartesian coordinates of the nucleus a with mass M_a and $\nabla_{\mathbf{R}_a} = \partial/\partial\mathbf{R}_a$. The nucleus-nucleus potential \hat{V}_{n-n} represents the repulsion between the nuclei⁷⁹ (with nuclear charges Z_a and Z_b)

$$\hat{V}_{n-n} = \sum_{a=1}^{K-1} \sum_{b>a}^K \frac{Z_a Z_b}{|\mathbf{R}_a - \mathbf{R}_b|}. \quad (0.5)$$

The electronic Hamiltonian \hat{H}_e is decomposed into the kinetic energy of the N electrons (note that $\nabla_i \equiv \nabla_{\mathbf{r}_i}$, with \mathbf{r}_i being the position of electron i)

$$\hat{T}_e = \sum_{i=1}^N \frac{-\nabla_i^2}{2}, \quad (0.6)$$

the interaction between electrons and nuclei

$$\hat{V}_{n-e} = \sum_{a=1}^K \sum_{i=1}^N \frac{Z_a}{|\mathbf{R}_a - \mathbf{r}_i|}, \quad (0.7)$$

and the interaction between electrons

$$\hat{V}_{e-e} = \sum_{i=1}^{N-1} \sum_{j>i}^N \frac{1}{|\mathbf{r}_i - \mathbf{r}_j|}. \quad (0.8)$$

After a transformation into the center-of-mass, the Hamiltonian separates into parts of the nuclei and the electrons. This separation leads to an electronic problem in which the nuclear charge enters as a static external field. However, this practical factorization is lost as soon as the system to be considered is composed of several atoms. In such systems the dynamic coupling between electrons and nuclei has

0.2. Hartree–Fock Theory and Electron Correlation

to be taken into account, *e. g.*, by solving the Schrödinger equation

$$\hat{H}|\Psi\rangle = E|\Psi\rangle. \quad (0.9)$$

The first step towards a solution to equation 0.9 is the decoupling of the electron from the nuclear motion, which relies on the different time scales of the two types of motion. This is known as the *Born–Oppenheimer Approximation* (BOA).⁷⁹ The BOA factorizes the total wavefunction Ψ into a nuclear wavefunction Ψ^n and an electron wavefunction Ψ_k^e

$$\begin{aligned} \Psi(\mathbf{R}_1, \dots, \mathbf{R}_K; \mathbf{r}_1\sigma_1, \dots, \mathbf{r}_N\sigma_N) \\ = \Psi^n(\mathbf{R}_1, \dots, \mathbf{R}_K) \Psi_k^e(\mathbf{R}_1, \dots, \mathbf{R}_K; \mathbf{r}_1\sigma_1, \dots, \mathbf{r}_N\sigma_N), \end{aligned} \quad (0.10)$$

where σ denotes the spin-state of an electron. The electron wavefunction depends on the position of the nuclei and satisfies the Schrödinger equation

$$\hat{H}_e|\Psi_k^e\rangle = E_k|\Psi_k^e\rangle, \quad (0.11)$$

which represents a stationary eigenvalue problem for any given set of \mathbf{R}_α . E_k is the electronic energy of the stationary electronic state k with corresponding wavefunction Ψ_k^e . The nuclei are moving in a potential field created by the nucleus–nucleus repulsion (*cf.*, equation 0.5) and the potential generated by the electrons. Within the BOA, the contribution from \hat{V}_{n-n} becomes an additive constant.

0.2. Hartree–Fock Theory and Electron Correlation

The most common and simplest approximate solution of equation 0.11 is the HF method, which assumes the ground state wave function $\Psi_{k=0}^e$ to be a single Slater determinant composed of single-particle states

$$\begin{aligned} \Psi_{k=0}^e &\approx \Phi_{1\dots N}(\mathbf{r}_1\sigma_1, \dots, \mathbf{r}_N\sigma_N) \\ &= \frac{1}{\sqrt{N!}} \begin{vmatrix} \phi_1(\mathbf{r}_1\sigma_1) & \cdots & \phi_N(\mathbf{r}_1\sigma_1) \\ \vdots & & \vdots \\ \phi_1(\mathbf{r}_N\sigma_N) & \cdots & \phi_N(\mathbf{r}_N\sigma_N) \end{vmatrix}. \end{aligned} \quad (0.12)$$

The HF approach determines the N single-particle states ϕ_i in the approximate ground state wavefunction $\Phi_{1\dots N}$ variationally. This is realized by forming the expectation value of the Hamilton operator with respect to the wave function $\Phi_{1\dots N}$. We obtain the following result by assuming orthogonal single-particle

0. Theoretical Background

states

$$\begin{aligned}
\langle \Phi_{1\dots N} | \hat{H} | \Phi_{1\dots N} \rangle &= \sum_{i=1}^N \sum_{\sigma=\uparrow,\downarrow} \int d^3r \phi_i^*(\mathbf{r}\sigma) \left[\frac{-\nabla^2}{2} + v_{\text{ext}}(\mathbf{r}) \right] \phi_i(\mathbf{r}\sigma) \\
&+ \frac{1}{2} \sum_{i,j=1}^N \sum_{\sigma,\sigma'=\uparrow,\downarrow} \int d^3r \int d^3r' \phi_i^*(\mathbf{r}\sigma) \phi_j^*(\mathbf{r}'\sigma') w(\mathbf{r}, \mathbf{r}') \\
&\times [\phi_i(\mathbf{r}\sigma) \phi_j(\mathbf{r}'\sigma') - \phi_j(\mathbf{r}\sigma) \phi_i(\mathbf{r}'\sigma')],
\end{aligned} \tag{0.13}$$

where $v_{\text{ext}}(\mathbf{r}) = -\sum_{\alpha=1}^K Z_{\alpha}/|\mathbf{R}_{\alpha} - \mathbf{r}|$ denotes the total potential generated by the nuclei and $w(\mathbf{r}, \mathbf{r}') = 1/|\mathbf{r} - \mathbf{r}'|$ the electron-electron interaction. This method incorporates orthonormality by introducing a set of Lagrange multipliers $\{\varepsilon_i\}$ and minimizing the energy expression with respect to this constraint.

$$\mathcal{L}(\{\phi_i\}) = \langle \Phi_{1\dots N} | \hat{H} | \Phi_{1\dots N} \rangle - \sum_{i=1}^N \varepsilon_i \left(\sum_{\sigma} \int d^3r |\phi_i(\mathbf{r}\sigma)|^2 - 1 \right) \tag{0.14}$$

A set of real and diagonal multipliers is sufficient as the resulting single-particle Hamiltonian determining the ϕ_i turns out to be Hermitian, which ensures the orthogonality of the ϕ_i . The set of single-particle states corresponding to the diagonal Lagrange multiplier matrix is called canonical. This constraint leads to the HF equations (for $i = 1, \dots, N$)

$$\frac{-\nabla^2}{2} \phi_i(\mathbf{r}\sigma) + \sum_{\sigma'=\uparrow,\downarrow} \int d^3r' v_{\text{eff}}^{\text{HF}}(\mathbf{r}\sigma, \mathbf{r}'\sigma') \phi_i(\mathbf{r}'\sigma') = \varepsilon_i \phi_i(\mathbf{r}\sigma). \tag{0.15}$$

The effective HF potential is given as

$$v_{\text{eff}}^{\text{HF}} = \delta_{\sigma\sigma'} \delta^{(3)}(\mathbf{r} - \mathbf{r}') \{v_{\text{ext}}(\mathbf{r}) + v_{\text{H}}(\mathbf{r})\} + v_{\text{X}}^{\text{HF}}(\mathbf{r}\sigma, \mathbf{r}'\sigma'). \tag{0.16}$$

δ_{KL} is the Kronecker delta which equals unity for $K = L$ and zero for $K \neq L$ and $\delta^{(3)}$ is the Dirac delta-function. This potential is non-local and contains three terms, the potential generated by the nuclei (see above), the Hartree potential (Coulomb interactions between electrons)

$$v_{\text{H}}(\mathbf{r}) = \int d^3r' w(\mathbf{r}, \mathbf{r}') \sum_{\sigma'=\uparrow,\downarrow} \sum_{i=1}^N |\phi_i(\mathbf{r}'\sigma')|^2, \tag{0.17}$$

and the non-local exchange potential

$$v_X^{\text{HF}}(\mathbf{r}\sigma, \mathbf{r}'\sigma') = -w(\mathbf{r}, \mathbf{r}') \sum_{j=1}^N \phi_j(\mathbf{r}\sigma) \phi_j^*(\mathbf{r}'\sigma'), \quad (0.18)$$

which depend on the solutions to be determined by the HF equations. We overcome this nonlinearity by iterating equation 0.15 self-consistently where each step determines first the ϕ_i corresponding to the current potential followed by generating the updated potentials from these ϕ_i . We stop the self-consistent treatment once the iterative procedure reached a suitable accuracy limit (*i.e.*, obtaining self-consistency). The introduced Slater determinant (equation 0.12) satisfies the requirement of antisymmetry and therefore incorporates correlation between *Same-Spin* (SS) electrons better known as Fermi correlation. This determinant does, however, not include the correlation resulting from the interaction between the *Opposite-Spin* (OS) electrons. In the HF approach each electron experiences the average field of the complete electron cloud. The actual motion of an electron, however, depends on the individual positions of all other electrons which is known as Coulomb correlation. Including Coulomb correlation into the many-body wavefunction needs representation by more than a single Slater determinant. The complete solutions of the HF equations not only provides the N occupied single-particle states included in the HF ground state, but also a finite (to infinite) number of unoccupied states (the other eigenstates of the differential equation in equation 0.15). We build the complete basis N -particle Hilbert space from the set of all such single-particle state determinants using a *Configuration Interaction* (CI) approach. This enables the description of correlated wavefunctions in terms of a series of excited determinants (single excitations, double excitations, \dots , N -tuple excitations) where p, q represent occupied and r, s virtual orbitals

$$|\Psi_k\rangle = \underbrace{c_0 |\Phi_0\rangle}_{\text{ground state}} + \underbrace{\sum_{pr} c_p^r |\Phi_p^r\rangle}_{\text{singles}} + \underbrace{\sum_{pqrs} c_{pq}^{rs} |\Phi_{pq}^{rs}\rangle}_{\text{doubles}} + \dots \quad (0.19)$$

Several strategies are developed to calculate the expansion coefficients c differently.^{80,81} So-called correlated *ab initio* methods are obtained by forming the expectation value of the Hamiltonian with respect to correlated wavefunctions. Modern computer architectures and efficient numerical implementations allow the application of correlated *ab initio* methods to more extensive system sizes. Nevertheless, there is a fundamental drawback which seriously limits their range of applicability. To understand this, we need to introduce the concept of algorithm complexity. Using mathematical nomenclature, fast algorithms refer to low-complexity algorithms (*e.g.*, fast Fourier transform,⁸² the multigrid method,⁸³ and the fast

0. Theoretical Background

multipole method⁸⁴). Generally, the complexity of an algorithm relates to its asymptotic behavior. If the computing time grows as $T_{\text{CPU}} \propto \text{prefactor } M^k$ in the limit of large systems, the scaling behavior of the method is proportional to $\mathcal{O}(M^k)$ where M resembles the total size of the system. For QM methods the system size is given by the total number of, *e. g.*, atomic orbitals, plane waves, or a similar concept used for the expansion of the single-particle orbitals that construct the wavefunction. A typical expansion of the single-particle orbitals uses *Linear Combinations of Atomic Orbitals* (LCAO-MO).^{80,85,86}

$$\phi_i(\mathbf{r}\sigma) = \sum_{k=1}^M b_{i,k\sigma} \psi_k(\mathbf{r}). \quad (0.20)$$

From equation 0.20, the problem of calculating the HF molecular orbitals reduces to the problem of calculating the set of expansion coefficients $b_{i,k\sigma}$. Multiplying by $\langle \psi_k |$, turns the integro-differential equation into an algebraic eigenvalue problem (Roothaan–Hall formalism). Here, the b (equation 0.20) and the c (equation 0.19) coefficients are determined either sequentially or simultaneously. For instance, in the case of an effective single-particle problem, like in HF, this results in

$$\sum_{l=1}^M \sum_{\sigma'} \left[\left\langle \psi_k \left| \frac{-\nabla^2}{2} \delta_{\sigma\sigma'} + \hat{v}_{\text{eff},\sigma\sigma'} \right| \psi_l \right\rangle - \varepsilon_i \langle \psi_k | \psi_l \rangle \delta_{\sigma\sigma'} \right] b_{i,l\sigma'} = 0, \quad (0.21)$$

where $\hat{v}_{\text{eff},\sigma\sigma'}$ is the total effective potential which the electrons experience. In order to make a statement about the applicability of QM methods, one compares their scaling behavior with the size M of the basis set. The following list gives an overview about the scaling behavior of different established QM methods.⁸⁷

Table 0.1.: Scaling behavior for QM methods with respect to system size M .

Method	Scaling	Description
HF	$\mathcal{O}(M^4)$	Standard implementation
MP2	$\mathcal{O}(M^5)$	Møller-Plesset perturbation theory of 2 nd order on HF basis
RPA	$\mathcal{O}(M^5)$	Random phase approximation using the matrix sign function by Furche ⁸⁸
CCSD(T)	$\mathcal{O}(M^7)$	Coupled Cluster: projection allowing single (S), double (D) and selected triple (T) particle-hole excitations from HF ground state
FCI	$\mathcal{O}(M!)$	Full CI: energy minimization allowing all N -tuple excitations from the HF ground state with N electrons

While the exact range of applicability of *ab initio* methods is hard to assess, there will always be interesting systems whose size is beyond their scope. For this reason, a method is chosen that offers the best possible scaling to describe large and complex systems. Table 0.1 reveals that the standard scaling behavior of the HF method is sufficient for conducting larger computational studies. However, within HF the electron motion is practically uncorrelated (particle moves within an averaged effective potential of all other). Thus the question arises whether it is possible at all to map the complete many-body problem onto an effective single-particle theory, which incorporates parts of Coulomb correlation.

0.3. Density Functional Theory

One method that aims for the mapping of the many-body problem onto an effective single-particle theory is DFT. The foundations of DFT are based on the theorems of HK,^{33,89} which assure that a stationary many-particle system is completely described by its ground state density. The Hamiltonian of a stationary system with N interacting electrons is given as

$$\hat{H}_e = \hat{T}_e + \hat{V}_{\text{ext}} + \hat{W}_{e-e}, \quad (0.22)$$

where \hat{T}_e represents the kinetic energy operator of the electrons, \hat{V}_{ext} represents the interaction of the electrons with external sources characterized by time-independent potentials $v_{\text{ext}}(\mathbf{r})$, and \hat{W}_{e-e} the electron-electron interaction. The many-body eigenstates $|\Psi_k^e\rangle$ corresponding to this Hamiltonian are obtained by solving the stationary Schrödinger equation given in equation 0.11.

Consider the set of all Hamiltonians of this form, *i.e.*, the set of all local potentials v_{ext} for which equation 0.11 leads to $|\Psi_{k=0}^e\rangle$, while fixing the electron-electron interaction. This set contains apart from physically realizable potentials also an infinite number of mathematical constructs. Additionally, it contains an infinite number of copies of any given $v_{\text{ext}}(\mathbf{r})$, which are obtained by simply adding a constant. All such copies lead to the same ground state and are therefore physically equivalent. The solution of the Schrödinger equation can therefore be interpreted as a map between the set \mathcal{V} of external potentials which differ by more than a constant

$$\mathcal{V} = \left\{ v_{\text{ext}} \mid \text{with: } v_{\text{ext}} \text{ multiplicative, corresponding } |\Psi_{k=0}^e\rangle \text{ exists,} \right. \\ \left. v'_{\text{ext}}(\mathbf{r}) \neq v_{\text{ext}}(\mathbf{r}) + \text{const.} \right\} \quad (0.23)$$

0. Theoretical Background

and the set \mathcal{G} of resulting ground states³²

$$\mathcal{G} = \left\{ |\Psi_{k=0}^e\rangle \mid \text{with: } |\Psi_{k=0}^e\rangle \text{ ground state corresponding to one element of } \mathcal{V}, \right. \\ \left. |\Psi_{k=0}^{e'}\rangle \neq \exp(i\theta) |\Psi_{k=0}^e\rangle \text{ with } \theta \text{ being some global phase} \right\}. \quad (0.24)$$

The map from \mathcal{V} to \mathcal{G} is termed A . The associated ground state density n_0 is defined as

$$n_0(\mathbf{r}) = \langle \Psi_{k=0}^e | \hat{n}(\mathbf{r}) | \Psi_{k=0}^e \rangle \\ = N \sum_{\sigma_1 \dots \sigma_N} \int d^3 r_2 \dots d^3 r_N |(\mathbf{r}_1 \sigma_1, \dots, \mathbf{r}_N \sigma_N) | \Psi_{k=0}^e \rangle|^2. \quad (0.25)$$

The second map from \mathcal{G} to \mathcal{N} is termed B where the ground state densities are obtained as

$$\mathcal{N} = \left\{ n_0 \mid n_0(\mathbf{r}) = \langle \Psi_{k=0}^e | \hat{n}(\mathbf{r}) | \Psi_{k=0}^e \rangle, |\Psi_{k=0}^e\rangle \in \mathcal{G} \right\}. \quad (0.26)$$

The complete surjective mapping is shown below.

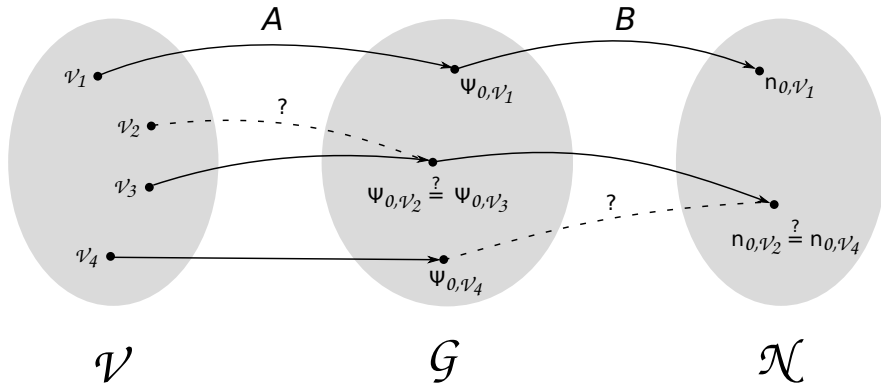


Figure 0.5.: Connection between external potential v_i , associated ground states Ψ_{0,v_i} , and ground state densities n_{0,v_i} . Figure created in analogy to Figure 2.1 of Ref. 32.

HK observed that both mappings (A and B) are injective³³ (proof by contradiction) and thus unique (paths with question marks are not possible). This means there exists a direct correspondence between the external potential v_{ext} in the Hamiltonian, the ground state $|\Psi_{k=0}^e\rangle$ resulting from solution of the Schrödinger equation and the associated ground state density n_0 . Furthermore, the ground state is a unique and universal functional of the ground state density. As a consequence of the unique relation between n_0 and $|\Psi_{k=0}^e\rangle$ and the Ritz variational

principle, a minimum principle for $E[n]$ is introduced

$$E[n] = \langle \Psi_{k=0}^e[n] | \hat{H}_e | \Psi_{k=0}^e[n] \rangle. \quad (0.27)$$

If n_0 is the ground state density corresponding to v_{ext} , one has for other densities $n'(\mathbf{r}) \neq n_0(\mathbf{r})$

$$E[n_0] < E[n'] \iff E_0 = \min_{n \in \mathcal{N}} E[n]. \quad (0.28)$$

Unfortunately, the HK theorems give no further information about the exact form of $E[n]$.⁹⁰ The connection between the existence theorems and a mapping of the interacting N-particle problem onto an effective noninteracting system is provided by the KS-DFT scheme.^{91,92} This scheme uses a model system of noninteracting electrons ($\hat{W}_{e-e} = 0$) by employing a multiplicative external potential v_s .

$$\hat{H}_S = \hat{T}_e + \hat{V}_s \quad \text{with} \quad \hat{V}_s = \int d^3r \hat{n}(\mathbf{r}) v_s(\mathbf{r}) \quad (0.29)$$

The N-particle ground state $\Phi_{1\dots N}$ is a single Slater determinant constructed from the energetically lowest solutions ϕ_i of the single-particle Schrödinger equation (for $i = 1, \dots, N$)

$$\left\{ \frac{-\nabla^2}{2} + v_s(\mathbf{r}) \right\} \phi_i(\mathbf{r}\sigma) = \varepsilon_i \phi_i(\mathbf{r}\sigma). \quad (0.30)$$

The introduced HK theorem is valid for arbitrary many-particle systems, irrespective of their particle-particle interaction (interacting particles or noninteracting particles). The ground state of a noninteracting system is a unique functional of the ground state density $|\Phi[n]\rangle$ for which the HK ground state energy functional of a noninteracting system is given as

$$E_s[n(\mathbf{r})] = \langle \Phi[n(\mathbf{r})] | \hat{T} | \Phi[n(\mathbf{r})] \rangle + \int d^3r v_s(\mathbf{r}) n(\mathbf{r}). \quad (0.31)$$

KS worked out an effective potential v_s – by restricting the variation of $E[n]$ to fixed particle numbers – which is given by

$$v_s(\mathbf{r}) = v_{\text{ext}}(\mathbf{r}) + v_H[n_0(\mathbf{r})] + v_{\text{XC}}[n_0(\mathbf{r})], \quad (0.32)$$

where v_H is the Hartree (Coulomb) potential

$$v_H[n(\mathbf{r})] = \int d^3r' w(\mathbf{r}, \mathbf{r}') n(\mathbf{r}'), \quad (0.33)$$

and v_{XC} the *Exchange-Correlation* (XC) potential given as functional derivative of

0. Theoretical Background

the XC energy functional

$$v_{\text{XC}}[\mathbf{n}(\mathbf{r})] = \frac{\delta E_{\text{XC}}[\mathbf{n}(\mathbf{r})]}{\delta \mathbf{n}(\mathbf{r})}. \quad (0.34)$$

By inserting equation 0.32 into equation 0.30 one obtains the KS equations⁹² where the starting potential is typically constructed by some trial density $\mathbf{n}^{(1)}(\mathbf{r})$ (e. g., superposition of atomic densities)

$$\left\{ \frac{-\nabla^2}{2} + v_{\text{ext}}(\mathbf{r}) + v_{\text{H}}[\mathbf{n}^{(1)}(\mathbf{r})] + v_{\text{XC}}[\mathbf{n}^{(1)}(\mathbf{r})] \right\} \phi_i(\mathbf{r}\sigma) = \varepsilon_i \phi_i(\mathbf{r}\sigma). \quad (0.35)$$

Those equations have to be solved self-consistently, similar to the HF equations. The XC energy functional is composed of an exchange $E_{\text{X}}[\mathbf{n}(\mathbf{r})]$ and a correlation $E_{\text{C}}[\mathbf{n}(\mathbf{r})]$ functional part, though these are not necessarily separable.^{93,94} Given the exact XC functional one would yield the correct *Exchange* (X) and *Correlation* (C) energy.^{33,95} In this case, a system of noninteracting fermionic particles would yield the same density and energy as the fully interacting N-electron system.^{92,93} This way, KS-DFT offers an appealing alternative to treat electron correlation within a mean-field approach. Since the exact functional of an arbitrary density is unknown, DFAs are used.^{96,97} Herein, the XC energy has to be approximated, which is regularly classified according to the Jacob's ladder hierarchy as introduced by Perdew.^{98,99} Within Jacob's ladder, DFAs are categorized into rungs of that ladder. The higher the rung, the more information of the systems is used in the functional, ascending from the so-called "Hartree hell" to the "Heaven of chemical accuracy" as depicted in figure 0.6.

The simplest approximation assumes a (locally) uniform electron density and is thus dubbed *Local Spin Density Approximation* (LSDA). In the frame of this approximation, the expression for the XC energy is given by

$$E_{\text{XC}}^{\text{LSDA}}[\mathbf{n}(\mathbf{r})] = \int d^3\mathbf{r} \mathbf{n}(\mathbf{r}) \varepsilon_{\text{XC}}^{\text{LSDA}}[\mathbf{n}(\mathbf{r})]. \quad (0.36)$$

Here, $\varepsilon_{\text{XC}}^{\text{LSDA}}$ is the XC energy density per particle of an electron gas with uniform spin densities.¹⁰⁰ LSDA is still used in the solid state community with recent extensions to finite temperature free energies.¹⁰¹ While extended metallic systems can be described reasonably well by LSDA, typical molecular systems require inclusion of the density gradient $\nabla \mathbf{n}(\mathbf{r})$ as in the *Generalized Gradient Approximation* (GGA).

$$E_{\text{XC}}^{\text{GGA}}[\mathbf{n}(\mathbf{r})] = \int d^3\mathbf{r} \varepsilon_{\text{XC}}^{\text{LSDA}}[\mathbf{n}(\mathbf{r})] g(\mathbf{n}(\mathbf{r}), \nabla \mathbf{n}(\mathbf{r})) \quad (0.37)$$

Different expressions are possible for the so-called enhancement factor g . The most prominent GGAs are the *Perdew–Burke–Enzerhof* (PBE)¹⁰² exchange and

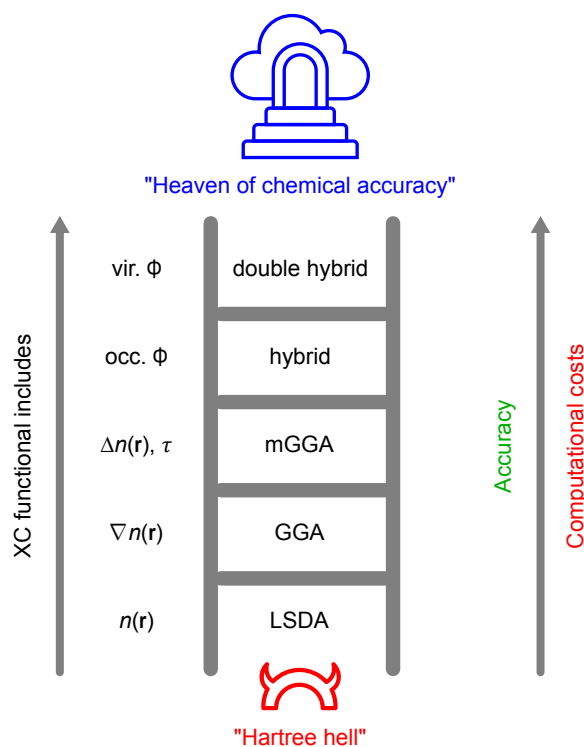


Figure 0.6.: Perdew and Schmidt's "Jacob's ladder" of DFAs.

correlation functionals and the *Becke Exchange* (B88)¹⁰³ combined with the *Lee–Yang–Parr* (LYP)¹⁰⁴ correlation functional. A natural extension to GGAs is to use higher-order derivatives of the electron density or other semilocally-available information, leading to the *meta-GGA* (mGGA) class. A typically employed variable is the KS kinetic energy density

$$\tau = \sum_i \frac{|\nabla\phi_i|^2}{2}. \quad (0.38)$$

Popular mGGAs are the *Tao–Perdew–Staroverov–Scuseria* (TPSS)¹⁰⁵ functional and the Minnesota functionals M06L,¹⁰⁶ M11L,¹⁰⁷ and MN12L¹⁰⁸ by Truhlar and co-workers. A recently introduced empirical mGGA with a smoothness constraint and a VV10 long-range dispersion correction (long-range dispersion effects see below), B97M-V, was presented by Mardirossian and Head-Gordon.¹⁰⁹ Constraint-satisfaction based mGGA functionals have gained more attention^{110–113} with a most recent development being the *Strongly Constrained and Appropriately Normed* (SCAN)¹¹⁴ functional. Driven from the fact that LSDA and GGAs suffer from *Self-Interaction Error* (SIE)¹¹⁵ techniques have been developed for constructing functionals which combine a fractional amount α_X of nonlocal (one-determinantal) HF exchange with local XC functionals. Such hybrid functionals have reduced SIE

0. Theoretical Background

which drastically improved, e. g., the description of band-gaps of periodic materials, thermochemistry, and kinetics of chemical reactions. These hybrid DFAs were originally introduced by Becke and are motivated by the adiabatic connection.⁹³ The hybrid energy expression is given as

$$E_{XC}^{\text{hybrid}} = (1 - \alpha_X) E_X^{\text{GGA}} + \alpha_X E_X^{\text{HF}} + E_C^{\text{GGA}}. \quad (0.39)$$

In principle, any semi-local XC component can be combined with Fock exchange, popular ones are PBE0¹¹⁶ and B3LYP.^{117,118} Heyd and co-workers decomposed the Coulomb operator into *Short-Range* (SR) and *Long-Range* (LR) contributions of the form

$$\frac{1}{|\mathbf{r} - \mathbf{r}'|} = \frac{\text{erf}(\omega|\mathbf{r} - \mathbf{r}'|)}{|\mathbf{r} - \mathbf{r}'|} + \frac{1 - \text{erf}(\omega|\mathbf{r} - \mathbf{r}'|)}{|\mathbf{r} - \mathbf{r}'|}, \quad (0.40)$$

where erf is the normal error function and ω is an adjustable range separation parameter.¹¹⁹ Those *Range-Separated Hybrids* (RSH) have the energy expression

$$E_{XC}^{\text{RSH}} = (1 - \alpha_X) E_X^{\text{GGA,SR}}(\omega) + \alpha_X E_X^{\text{HF,SR}}(\omega) + E_X^{\text{GGA,LR}} + E_C^{\text{GGA}}. \quad (0.41)$$

In molecular calculations especially long-range corrected functionals are widely used in the calculation of excited states by means of TD-DFT because the orbital energies obtained with them are much more amenable for such calculations.^{120–123} The highest rung of Jacob's ladder corresponds to a non-local treatment of exchange and correlation, where the latter is achieved by including virtual orbital information, e. g., by means of MP2^{124–129} or RPA theory.^{130–134} However, these so-called double-hybrid functionals are no longer pure mean-field approaches since they go beyond the zeroth-order term in the many-body perturbation series (see section 0.4 for more details).

In the procedure of solving the KS-DFT equations in systems with translational invariance, several simplifications can be applied due to symmetry. The effective potential v_s , which enters the KS Hamiltonian, is periodic with respect to translations

$$v_s(\mathbf{r}) = v_s(\mathbf{r} + \mathbf{T}), \quad (0.42)$$

where \mathbf{T} is the Bravais lattice vector of the solid. Those PBCs lead to Bloch's theorem which states that the periodicity of the bulk material constrains the one-electron wave function to obey

$$\phi_{i,\mathbf{k}}(\mathbf{r} + \mathbf{T}) = \exp(i\mathbf{k}\mathbf{T}) \exp(i\mathbf{k}\mathbf{r}) u_{i,\mathbf{k}}(\mathbf{r}) = \exp(i\mathbf{k}\mathbf{T}) \phi_{i,\mathbf{k}}(\mathbf{r}), \quad (0.43)$$

where \mathbf{k} is the vector of reciprocal space and $\phi_{i,\mathbf{k}}(\mathbf{r})$ a product of a lattice-periodic Bloch function $u_{i\mathbf{k}}(\mathbf{r})$ and a single-particle basis set. Translational symmetry now ensures that one has to consider only \mathbf{k} -vectors which lie inside the *First Brillouin*

Zone (FBZ)¹³⁵ when solving the KS equations under PBCs. The integration in the FBZ is then replaced by an integration over a \mathbf{k} -point mesh (special point theorem^{136,137}).

Different expansions are possible to represent the single-particle basis set of equation 0.43. One possibility is to solve the KS equations directly by using a grid where functions are represented by their value over a set of points in real space.¹³⁸ Furthermore, *Numerically Tabulated Atom-Centered Orbitals* (NAOs) are well known in the literature allowing the creation of optimized element-dependent basis sets that are compact as well as accurate in production calculations with respect to total energy convergence.¹³⁹ Conceptually somehow different are the so-called Daubechies wavelets which have the characteristic that they form an orthogonal and smooth basis set, localized both in real and Fourier spaces.¹⁴⁰ Another possibility in generating orbitals relies on an expansion in *Slater Type Orbitals* (STOs) where integrals may be calculated numerically¹⁴¹ or in a mixed scheme with analytical and recursion/expansion-based evaluations.¹⁴² Most quantum chemical codes use *Gaussian Type Orbitals* (GTOs) to solve integrals analytically^{59,60,143–145} while others use a combination of GTOs with *Projector Augmented-Wave* (PAW) methods.^{72,146} Especially the PAW ansatz is often used in material science^{66,147} and will thus be discussed in more detail.

In the PAW method the *All-Electron* (AE) wave function $|\Phi_N\rangle$ is transformed into the so-called *Pseudo Hilbert Space* (PHS) by means of a linear transformation

$$|\Phi_N\rangle = |\tilde{\Phi}_N\rangle + \sum_{\mathbf{r}} (|\phi_{\mathbf{r}}\rangle - |\tilde{\phi}_{\mathbf{r}}\rangle) \langle \tilde{p}_{\mathbf{r}} | \tilde{\Phi}_N \rangle. \quad (0.44)$$

Here, the PHS wave functions $|\tilde{\Phi}_N\rangle$ are the variational quantities and \mathbf{r} is an abbreviation for the atomic site. The AE partial waves $|\phi_{\mathbf{r}}\rangle$ are obtained for a reference atom whereas the PHS partial waves $|\tilde{\phi}_{\mathbf{r}}\rangle$ are equivalent to the AE partial waves outside a defined radius.¹⁴⁸ The projector functions \tilde{p} are dual to the partial waves

$$\langle \tilde{p}_{\mathbf{r}} | \tilde{\phi}_{\mathbf{s}} \rangle = \delta_{\mathbf{r}\mathbf{s}}. \quad (0.45)$$

By incorporating equation 0.44, one is able to show that in the PAW method the AE charge density is given by

$$\mathbf{n}(\mathbf{r}) = \tilde{\mathbf{n}}(\mathbf{r}) + \mathbf{n}^1(\mathbf{r}) - \tilde{\mathbf{n}}^1(\mathbf{r}), \quad (0.46)$$

where $\tilde{\mathbf{n}}(\mathbf{r})$ is the soft pseudo-charge-density calculated directly from the pseudo-wave-functions on a plane-wave grid

$$\tilde{\mathbf{n}}(\mathbf{r}) = \sum_{\mathbf{N}} f_{\mathbf{N}} \langle \tilde{\Phi}_{\mathbf{N}} | \mathbf{r} \rangle \langle \mathbf{r} | \tilde{\Phi}_{\mathbf{N}} \rangle. \quad (0.47)$$

0. Theoretical Background

Here, f_N denotes the occupation number. The onsite charge densities $n^1(\mathbf{r})$ and $\tilde{n}^1(\mathbf{r})$ are treated on a radial support grid.^{62,64,65} Both charge densities are defined as

$$n^1(\mathbf{r}) = \sum_{(r,s)} \rho_{rs} \langle \phi_r | \mathbf{r} \rangle \langle \mathbf{r} | \phi_s \rangle, \quad (0.48)$$

and

$$\tilde{n}^1(\mathbf{r}) = \sum_{(r,s)} \rho_{rs} \langle \tilde{\phi}_r | \mathbf{r} \rangle \langle \mathbf{r} | \tilde{\phi}_s \rangle, \quad (0.49)$$

where ρ_{rs} are the occupancies of each augmentation channel (r, s) which are calculated from the pseudo-wave-functions applying the projector functions

$$\rho_{rs} = \sum_N f_N \langle \tilde{\Phi}_N | \tilde{p}_r \rangle \langle \tilde{p}_s | \tilde{\Phi}_N \rangle. \quad (0.50)$$

It is common practice to expand only those plane-waves-functions which exhibit small kinetic energies. Hence, the plane-wave basis set can be truncated to include only plane-wave-functions within a particular cutoff energy. The truncation of the basis set at a finite cutoff energy will lead to errors in the computation of the energy and its derivatives. To minimize this error in a systematic way, it is recommended to increase the value of the cutoff energy until the calculated total energy converges within a required tolerance. For states with metallic characteristics and small fluctuations in the charge density, very few plane-waves are sufficient. In contrast, systems with a rather localized electron density as in molecular crystals, large plane-wave basis sets are needed which make the DFT calculation rather costly.¹⁴⁹

In these situations, atom centered functions like GTOs can significantly reduce the number of basis functions. This approach is based on the expansion of orbitals in Bloch sums

$$\phi_{i,\mathbf{k}}(\mathbf{r}) = \sum_{\mu} c_{\mu i}(\mathbf{k}) \phi_{\mu,\mathbf{k}}(\mathbf{r}) \quad \mu = 1, \dots, M, \quad (0.51)$$

where μ labels all *Atomic Orbitals* (AOs) in the reference primitive cell and the Bloch functions are created in an LCAO-MO ansatz

$$\phi_{\mu,\mathbf{k}}(\mathbf{r}) = \sum_{\mathbf{T}} \exp(i\mathbf{k}\mathbf{T}) \chi_{\mu}(\mathbf{r} - \mathbf{A}_{\mu} - \mathbf{T}). \quad (0.52)$$

GTOs benefit from a fast convergence behavior for describing the core electrons due to strong localization. However, in contrast to plane-waves, small AO basis sets strongly suffer from *Basis Set Incompleteness Error* (BSIE), and especially from the *Basis Set Superposition Error* (BSSE). Already semi-diffuse AOs can exhibit near linear dependencies in periodic calculations which directly excludes the reduction of the BSSE by a systematic increase of the AO basis. To overcome

this problem, a general geometrical procedure has been developed in 2012 which corrects for the BSSE in a semi-empirical way¹⁵⁰ which has been further extended to be applicable to periodic systems in 2013.¹⁵¹

0.4. Long-Range Correlation

A drawback about mean-field electronic structure methods like HF or semi-local DFT is the fact that these methods do not describe long-range electronic correlation effects, and hence they cannot account for LD effects.¹⁷ Such interactions are mandatory for describing the chemistry or physics of large or condensed-phase systems in an accurate and asymptotically correct way. This chapter describes how PT captures such long-range correlation effects, giving rise to the theoretical framework of LD.

Given a Hamiltonian \hat{H} that is too complicated to be handled directly, it is supposed that it differs by a small “perturbation” (obtaining \hat{H}') from a related unperturbed zeroth-order Hamiltonian \hat{H}_0 describing the following problem

$$\hat{H} = \hat{H}_0 + \lambda \hat{H}' \quad (0.53)$$

λ is the strength of the perturbation ranging from the unperturbed problem ($\lambda = 0$) to the perturbed problem ($\lambda = 1$). When solving for $\lambda = 0$

$$\hat{H}_0 |\Phi_0\rangle = W_{\Phi}^0 |\Phi_0\rangle, \quad (0.54)$$

one obtains the eigenfunctions of the unperturbed problem $|\Phi_0\rangle$ with eigenvalues W_{Φ}^0 . The desired solution for $\lambda = 1$ satisfies

$$\hat{H} |\Phi\rangle = W_{\Phi} |\Phi\rangle, \quad (0.55)$$

where the eigenfunctions of the perturbed problem $|\Phi\rangle$ as well as its eigenvalues W_{Φ} are to be obtained. For this purpose both quantities are expanded as a power series in λ as shown below:

$$\begin{aligned} |\Phi\rangle &= |\Phi_0\rangle + \lambda |\Phi'\rangle + \lambda^2 |\Phi''\rangle + \dots \\ W_{\Phi} &= W_{\Phi}^0 + \lambda W'_{\Phi} + \lambda^2 W''_{\Phi} + \dots \end{aligned} \quad (0.56)$$

Orthonormality is required (intermediate normalization), *i.e.*,

$$\langle \Phi_0 | \Phi' \rangle = \langle \Phi_0 | \Phi'' \rangle = \dots = 0 \quad \text{and} \quad \langle \Phi_0 | \Phi_0 \rangle = \langle \Phi' | \Phi' \rangle = \dots = 1. \quad (0.57)$$

0. Theoretical Background

By substituting the expanded $|\Phi\rangle$ and W_Φ into $(\hat{H} - W_\Phi)|\Phi\rangle = 0$, we get

$$\begin{aligned} & \left((\hat{H}_0 + \lambda \hat{H}') - (W_\Phi^0 + \lambda W_\Phi' + \lambda^2 W_\Phi'' + \dots) \right) \\ & \times (|\Phi_0\rangle + \lambda |\Phi'\rangle + \lambda^2 |\Phi''\rangle + \dots) = 0, \end{aligned} \quad (0.58)$$

which is expected to converge for sufficient small λ for which one can equate coefficients in power of λ (up to second-order) as

$$\begin{aligned} \lambda^0 : & (\hat{H}_0 - W_\Phi^0) |\Phi_0\rangle = 0, \\ \lambda^1 : & (\hat{H}_0 - W_\Phi^0) |\Phi'\rangle + (\hat{H}' - W_\Phi') |\Phi_0\rangle = 0, \\ \lambda^2 : & (\hat{H}_0 - W_\Phi^0) |\Phi''\rangle + (\hat{H}' - W_\Phi') |\Phi'\rangle - W_\Phi'' |\Phi_0\rangle = 0. \end{aligned} \quad (0.59)$$

The zeroth-order problem is supposed to be solved already. By multiplying the first-order equation with $\langle \Phi_0 |$ one obtains (exploiting that $\langle \Phi_0 | \hat{H}_0 - W_\Phi^0 | \Psi \rangle = \langle \Psi | \hat{H}_0 - W_\Phi^0 | \Phi_0 \rangle^* = 0$ for any wavefunction Ψ)

$$W_\Phi' = \langle \Phi_0 | \hat{H}' | \Phi_0 \rangle, \quad (0.60)$$

where the first-order energy W_Φ' resembles the expectation value of the perturbation operator for the unperturbed wavefunction. Applying the same procedure to the second-order term one obtains the second-order energy expression

$$W_\Phi'' = \langle \Phi_0 | \hat{H}' | \Phi' \rangle, \quad (0.61)$$

for which the wavefunction $|\Phi'\rangle$ is needed. Here $|\Phi'\rangle$ is expanded in terms of the unperturbed eigenfunctions

$$|\Phi'\rangle = \sum_k' c_k |k_0\rangle, \quad (0.62)$$

where the prime indicates that the term $k = n$ is omitted – ensuring that $\langle \Phi_0 | \Phi' \rangle = 0$. Using this expression within the first-order term – and remembering that $\hat{H}_0 |k_0\rangle = W_k^0 |k_0\rangle$ – gives the following expression

$$\sum_k' c_k (W_k^0 - W_\Phi^0) |k_0\rangle + (\hat{H}' - W_\Phi') |\Phi_0\rangle = 0. \quad (0.63)$$

Multiply by $\langle p_0 |$ and exploiting the orthonormality of the unperturbed eigenfunctions $|k_0\rangle$ one obtains an expression for each c_p coefficient

$$c_p = - \frac{\langle p_0 | \hat{H}' | \Phi_0 \rangle}{W_p^0 - W_\Phi^0}, \quad (0.64)$$

which can be substitute into equation 0.62 to finally obtain the second-order energy expression after substituting $|\Phi'\rangle$ into equation 0.61

$$W''_{\Phi} = \langle \Phi_0 | \hat{H}' | \Phi' \rangle = - \sum_p' \frac{\langle \Phi_0 | \hat{H}' | p_0 \rangle \langle p_0 | \hat{H}' | \Phi_0 \rangle}{W_p^0 - W_{\Phi}^0}. \quad (0.65)$$

Since intermolecular forces are relatively weak it is common practice to model such interactions using PT. If two systems are far enough apart from each other the overlap between their wavefunctions approaches zero (exponential decrease of the electron density). This means that one can identify a set of i electrons belonging to system A and a set of j electrons belonging to system B. Furthermore, one can define a Hamiltonian \hat{H}_A for system A and one \hat{H}_B for system B in terms of their electrons. The unperturbed Hamiltonian now simply is the sum of both Hamiltonians

$$\hat{H}_0 = \hat{H}_A + \hat{H}_B. \quad (0.66)$$

Perturbations are given by electrostatic interactions between particles of system A and particles of system B

$$\hat{H}' = \sum_{i \in A} \sum_{j \in B} \frac{1}{R_{ij}}, \quad (0.67)$$

where R_{ij} resembles the distance between particles on A and particles on B. The unperturbed states are simply the product wavefunction of both systems $\Phi_m^A \Phi_n^B$ which can be abbreviated as $|mn\rangle$

$$\begin{aligned} \hat{H}_0 |mn\rangle &= (\hat{H}_A + \hat{H}_B) |mn\rangle \\ &= (W_m^A + W_n^B) |mn\rangle \\ &= W_{mn}^0 |mn\rangle. \end{aligned} \quad (0.68)$$

The energy expressions up to second-order of the ground state of the system ($m = n = 0$), also known as the ‘‘polarization approximation’’,¹⁵² are given by

$$\begin{aligned} W_{00}^0 &= W_A^0 + W_B^0, \\ W'_{00} &= \langle 00 | \hat{H}' | 00 \rangle, \\ W''_{00} &= - \sum_{mn}' \frac{\langle 00 | \hat{H}' | mn \rangle \langle mn | \hat{H}' | 00 \rangle}{W_{mn}^0 - W_{00}^0}. \end{aligned} \quad (0.69)$$

After expanding \hat{H} in multipole moments the consideration of the dipole-dipole

0. Theoretical Background

term gives to the leading order pairwise dispersion energy expression ¹⁵³

$$\begin{aligned}
 E_{\text{DISP}}^{(6)} &= - \sum_{m_A \neq 0} \sum_{n_B \neq 0} \frac{\langle 0_A 0_B | \hat{\mu}_\alpha^A T_{\alpha\beta} \hat{\mu}_\beta^B | m_A n_B \rangle \langle m_A n_B | \hat{\mu}_\gamma^A T_{\gamma\delta} \hat{\mu}_\delta^B | 0_A 0_B \rangle}{W_{m0}^A + W_{n0}^B} \\
 &= -T_{\alpha\beta} T_{\gamma\delta} \sum_{m_A \neq 0} \sum_{n_B \neq 0} \underbrace{\frac{W_{m0}^A W_{n0}^B}{W_{m0}^A + W_{n0}^B}}_{\text{not factorizable}} \\
 &\quad \times \frac{\langle 0_A | \hat{\mu}_\alpha^A | m_A \rangle \langle m_A | \hat{\mu}_\gamma^A | 0_A \rangle}{W_{m0}^A} \frac{\langle 0_B | \hat{\mu}_\beta^B | n_B \rangle \langle n_B | \hat{\mu}_\delta^B | 0_B \rangle}{W_{n0}^B}, \tag{0.70}
 \end{aligned}$$

with $W_{m0}^A = W_m^A - W_0^A$. Expression 0.70 cannot be completely factorized, which has been solved in two ways. The first solution has been introduced by London ¹⁵⁴ which makes use of the Unsöld approximation ¹⁵⁵ to replace the highlighted term by an empirical one constructed from average excitation energies (U_A and U_B). Here, one obtains the London formula by factoring out the sum-over-states expression for the polarizabilities ($\alpha_{\alpha\gamma}^A$ and $\alpha_{\beta\delta}^B$)

$$\begin{aligned}
 E_{\text{DISP}}^{(6)} &\approx - \frac{U_A U_B}{4(U_A + U_B)} T_{\alpha\beta} T_{\gamma\delta} \alpha_{\alpha\gamma}^A \alpha_{\beta\delta}^B \\
 &= - \frac{U_A U_B}{4(U_A + U_B)} T_{\alpha\beta} T_{\gamma\delta} \bar{\alpha}^A \delta_{\alpha\gamma} \bar{\alpha}^B \delta_{\beta\delta} \tag{0.71} \\
 &= - \frac{3U_A U_B}{2(U_A + U_B)} \frac{\bar{\alpha}^A \bar{\alpha}^B}{R^6},
 \end{aligned}$$

with

$$T_{\alpha\beta} T_{\gamma\delta} = \frac{(3R_\alpha R_\beta - R^2 \delta_{\alpha\beta})(3R_\gamma R_\delta - R^2 \delta_{\gamma\delta})}{R^{10}}. \tag{0.72}$$

A more sophisticated way has been introduced by Casimir and Polder ¹⁵⁶ which led together with other works ¹⁵⁷⁻¹⁵⁹ to the pairwise dispersion energy formula including dynamic polarizabilities at imaginary frequencies

$$\begin{aligned}
 E_{\text{DISP}}^{(6)} &= - \frac{2}{\pi} T_{\alpha\beta} T_{\gamma\delta} \int_0^\infty d\omega \underbrace{\sum_m' \frac{\langle 0_A | \hat{\mu}_\alpha^A | m_A \rangle \langle m_A | \hat{\mu}_\gamma^A | 0_A \rangle \nu_m^A}{(\nu_m^A)^2 + \omega^2}}_{\alpha_{\alpha\gamma}^A(i\omega)} \\
 &\quad \times \underbrace{\sum_n' \frac{\nu_n^B \langle 0_B | \hat{\mu}_\beta^B | n_B \rangle \langle n_B | \hat{\mu}_\delta^B | 0_B \rangle}{(\nu_n^B)^2 + \omega^2}}_{\alpha_{\beta\delta}^B(i\omega)}. \tag{0.73}
 \end{aligned}$$

Equation 0.73 reduces to the pairwise term after substituting the tensor elements

given in equation 0.72

$$\bar{E}_{\text{DISP}}^{(6)} = -\frac{3}{\pi} \int_0^{\infty} d\omega \frac{\bar{\alpha}^A(i\omega)\bar{\alpha}^B(i\omega)}{R^6} = -\frac{C_6}{R^6}. \quad (0.74)$$

The pairwise dispersion energy of a system can thus be calculated on the basis of dynamic polarizabilities resulting in pairwise dispersion coefficients C_6 .

Apart from PT, density-density response functions can be used to calculate the dynamic correlation energy. This approach exploits the *Adiabatic Connection Fluctuation Dissipation* (ACFD) theorem¹⁶⁰ which captures effects of an external Coulomb perturbation (interaction scaled by λ) acting on the electron density.

$$E_{\text{corr}}^{\text{ACFD}} = -\frac{1}{2} \int_0^1 d\lambda \int d^3r d^3r' \frac{1}{|\mathbf{r} - \mathbf{r}'|} \int_0^{\infty} d\omega [\chi_{\lambda}(\mathbf{r}, \mathbf{r}', i\omega) - \chi_0(\mathbf{r}, \mathbf{r}', i\omega)] \quad (0.75)$$

The induced density and the external potential are related through a position- and frequency-dependent charge density susceptibility

$$\chi_0(\mathbf{r}, \mathbf{r}', i\omega) = -4 \sum_{\mathbf{i}} \sum_{\mathbf{a}} \frac{\omega_{\mathbf{a}\mathbf{i}}}{\omega_{\mathbf{a}\mathbf{i}}^2 + \omega^2} \phi_{\mathbf{i}}(\mathbf{r}) \phi_{\mathbf{a}}(\mathbf{r}) \phi_{\mathbf{a}}(\mathbf{r}') \phi_{\mathbf{i}}(\mathbf{r}'). \quad (0.76)$$

Unfortunately, most systems can not be treated exactly due to increasing computational costs with increasing system size. In order to circumvent this obstacle, semi-classical methods are used to enable the computation of LD interactions^{161,162} even for large system sizes. A deeper discussion of such semi-classical LD correction schemes is given in the next chapter.

0.5. Semi-Classical London Dispersion Corrections

Many semi-classical correction schemes are inspired by perturbation theory. Instead of solving the complicated many-body problem, they reduce the complexity to local dynamical properties of individual fragments, *e. g.*, to polarizabilities at imaginary frequencies. Such polarizabilities can be used for the calculation of dispersion coefficients between any fragments. If the dispersion coefficients for the fragments are known, the pairwise dispersion energy is easily amenable. However, in general dispersion coefficients are unknown for arbitrary fragments which is furthermore complicated by defining the fragments themselves. A straightforward and elegant way is the fragmentation into atomic contributions¹⁶³ which allows the formulation of methods that are more or less applicable to any system as long as the pairwise dispersion coefficients are known. Since dynamic polarizabilities are second-order properties, their calculation is time-intensive, which prohibits their

0. Theoretical Background

system-specific calculation in order to deduce pairwise dispersion energies. However, approximations enable the efficient calculation of system-specific dynamic polarizabilities. One method that realizes an efficient scheme to calculate such polarizabilities for systems of most sizes is the DFT-D3 method.^{17,46} This semi-classical scheme requires only the geometry as input to calculate the inter- and intramolecular dispersion energy based on pre-calculated TD-DFT^{164,165} data. The D3 method expands the Coulomb operator into multipoles. A coarse-grain partitioning to atomic polarizabilities enables the calculation of dipole-dipole dispersion coefficients as introduced by Casimir and Polder.¹⁵⁶

$$C_6^{AB} = \frac{3}{\pi} \int_0^{\infty} d\omega \alpha^A(i\omega) \alpha^B(i\omega). \quad (0.77)$$

In 2010 Grimme and co-workers proposed this approach that includes the molecular environment explicitly by the empirical concept of CNs. This concept represents hybridization conditions for each element that is in agreement with chemical intuition. The molecular geometry and, therefore, the CNs define the chemical environment. DFT-D3 uses pre-calculated TD-DFT reference polarizabilities obtained with a PBE0-like hybrid functional ($a_X = 37.5\%$) in a nearly complete basis set. A modified Casimir–Polder equation uses those pre-calculated reference polarizabilities to derive atom pairwise dispersion coefficients $C_{6,\text{ref}}^{AB}(\text{CN}^A, \text{CN}^B)$ for atoms A and B in these reference systems.

$$C_{6,\text{ref}}^{AB}(\text{CN}^A, \text{CN}^B) = \frac{3}{\pi} \int_0^{\infty} d\omega \frac{1}{m} \left[\alpha^{A_m H_n}(i\omega) - \frac{n}{2} \alpha^{H_2}(i\omega) \right] \times \frac{1}{k} \left[\alpha^{B_k H_l}(i\omega) - \frac{l}{2} \alpha^{H_2}(i\omega) \right] \quad (0.78)$$

Here, $A_m H_n$ and $B_k H_l$ are the reference systems for A and B with the corresponding coordination number CN^A and CN^B . These reference systems describe different bonding situations and are distinguished by their CNs. An interpolation over the reference coefficients enables the calculation of system-specific dispersion coefficients

$$C_6^{AB} = \frac{\sum_i^{N_A} \sum_j^{N_B} C_{6,\text{ref}}^{AB} L_{ij}}{\sum_i^{N_A} \sum_j^{N_B} L_{ij}} \quad (0.79)$$

with

$$L_{ij} = \exp \left(-4 \left[(\text{CN}^A - \text{CN}_i^A)^2 + (\text{CN}^B - \text{CN}_j^B)^2 \right] \right). \quad (0.80)$$

0.5. Semi-Classical London Dispersion Corrections

The CN-interpolation ensures an efficient calculation of system-specific dispersion coefficients only by geometrical mean. The D3 method uses recursion relations to obtain C_8^{AB} coefficients from the dipole-dipole ones which enables the calculation of dipole-quadrupole interactions $E_{DISP}^{(8)}$. By default DFT-D3 neglects higher-order terms of the dispersion energy (e. g., triple-dipole or quadrupole-quadrupole interactions). The atom pairwise dispersion energy is calculated as follows

$$E_{DISP}^{D3} = -\frac{1}{2} \sum_{AB} \sum_{n=6,8} s_n \frac{C_n^{AB}}{R^{n}} f_{damp}^{(n)}(R_0^{AB}). \quad (0.81)$$

Different approaches are available for choosing $f_{damp}^{(n)}(R^{AB})$ where R^{AB} is an inter-atomic distance for atom pair AB. However, the rational Becke-Johnson damping function is the default¹⁶⁶ as given by

$$f_{damp,BJ}^{(n)}(R_0^{AB}) = \frac{R_{AB}^{(n)}}{R_{AB}^{(n)} + (\alpha_1 R_0^{AB} + \alpha_2)^{(n)}}. \quad (0.82)$$

The scheme incorporates functional-specific parameter α_1 and α_2 as well as the radii $R_0^{AB} = \sqrt{C_8^{AB}/C_6^{AB}}$. *Axilrod–Teller–Muto* (ATM) define the leading order non-additive dispersion contribution^{167,168} as

$$E_{ABC} = \frac{C_9^{ABC} (3 \cos \theta_a \cos \theta_b \cos \theta_c + 1)}{(R_{AB} R_{BC} R_{CA})^3}. \quad (0.83)$$

Here, θ_a , θ_b , and θ_c are the internal angles of the triangle formed by R_{AB} , R_{BC} , and R_{CA} while C_9^{ABC} is the triple-dipole constant defined by

$$C_9^{ABC} = \frac{3}{\pi} \int_0^{\infty} d\omega \alpha^A(i\omega) \alpha^B(i\omega) \alpha^C(i\omega). \quad (0.84)$$

Their contribution to the total dispersion energy are, however, rather small ($\approx 5-10\%$). An established approximation uses the geometric mean of dipole-dipole dispersion coefficients to obtain triple-dipole dispersion coefficients.⁴⁶

$$C_9^{ABC} \approx -\sqrt{C_6^{AB} C_6^{BC} C_6^{CA}} \quad (0.85)$$

The triple-dipole dispersion energy expression contribution is as follows

$$E_{DISP}^{(9)} = \sum_{ABC} E_{ABC} f_{damp,(9)}(\bar{R}_{ABC}), \quad (0.86)$$

0. Theoretical Background

where the sum is over all atom triples in the system applied with a zero-damping scheme as proposed by Chai and Head-Gordon¹²²

$$f_{\text{damp,(9)}}(\bar{R}_{\text{ABC}}) = \frac{1}{1 + 6 \left(\bar{R}_{\text{ABC}} / \left(4/3 \bar{R}_0^{\text{ABC}} \right) \right)^{-16}}. \quad (0.87)$$

Equation 0.87 uses the geometrically averaged inter-atomic distances \bar{R}_{ABC} as well as the cutoff radii \bar{R}_0^{ABC} . In densely packed systems the correction is in general repulsive. Attractive contributions are only found for linear arrangements. As demonstrated by a database of 1225 inter-molecular C_6^{AB} coefficients, the semi-classical D3 schemes yields highly accurate results competitive to approaches that directly use electronic structure information to scale tabulated atomic references.³⁸ Since its publication, several groups successfully applied the DFT-D3 method in works including, *e. g.*, the description of cohesive energies and lattice parameter of molecular crystals,¹⁶⁹ the treatment of adsorption processes (small molecules on surfaces,¹⁷⁰ methane on carbon models,¹⁷¹ amino acids on graphene¹⁷²), the description of thermochemistry and intramolecular LD effects in conformers,¹⁷³ the determination of structural and energetic properties of TiO_2 modifications,¹⁷⁴ the application of DFT-D3 noncovalent interactions with DFT methods applied with small AO basis sets,¹⁷⁵ the D3 contribution to interatomic force constants,¹⁷⁶ the determination of anharmonic vibrational frequency calculation of nucleobases and their dimers,¹⁷⁷ and the lithium migration process in lithium-graphite intercalation compounds.¹⁷⁸ Of course, this is only a limited selection of works that applied the D3 correction. Nevertheless, when listing the different works, the general applicability of the DFT-D3 method can quickly be seen.

Aside from the pure geometrical DFT-D3 dispersion model, several electron density-dependent approaches exist. Examples are the *Tkatchenko–Scheffler* (TS)⁴⁹ model with its *Many-Body Dispersion* (MBD@scsTS)¹⁷⁹ analogon, the *Exchange Dipole Moment* (XDM)^{47,48,180} model of Becke and Johnson, or the *Local-Response Dispersion* (LRD)^{181,182} model by Sato and Nakai. Other approaches include non-local density information in the design of their XC functional. Established examples are the family of *van der Waals Density Functionals* (vdw-DF)^{183–187} as well as the VV10 method.^{51,52}

In the following Part of this work the theoretical framework of the DFT-D4 method is introduced.

Part I.

Development of the DFT-D4 London Dispersion Correction

As introduced in Chapter 0.5, the DFT-D3 method belongs to the class of semi-classical LD corrections. This method uses pre-calculated reference dispersion coefficients in combination with CNs representing the atomic hybridization. All CNs are used within an interpolation scheme between the references to obtain hybridization-specific dispersion coefficients. The reference dispersion coefficients are obtained from AIM partitioned molecular TD-DFT polarizabilities. One drawback of this approach is the fixed electronic structure of the reference polarizabilities. A more detailed description would consider the electronic structure of the atom inside its chemical environment to modulate the particular atomic reference polarizability, *i.e.*, scale the polarizabilities of cations to lower and the ones of anions to higher values compared to the polarizabilities of neutral atoms.

In Part I, the semi-classical DFT-D4 dispersion correction scheme is introduced, which adds charge-flexibility to the D3 reference polarizabilities using a scaling ansatz. This approach uses a multiplicative scaling function that modifies each reference polarizability with respect to relative atomic charge changes. The next three chapters introduce the theoretical foundations of this method including details about the development and proper validation with respect to literature-known benchmark sets. As its predecessor, this correction scheme can in principle be coupled to all mean-field electronic structure methods, however, in the following only the coupling to density functional approximations is described in detail.

Chapter 1 describes the general idea how element-specific scaling functions are used. Here, the concept of effective nuclear charges is introduced rendering the calculation of charge-dependent polarizabilities possible. Atomic partial charges used within the scaling functions are obtained from the GFN-xTB¹⁸⁸ method. The charge-scaling effect is verified by testing several properties: First, molecular pairwise dispersion coefficients for small molecules and AIM polarizabilities for large systems are discussed. Second, molecular dispersion coefficients are calculated for an electronically complicated dissociating lithium-cation benzene complex. Hereafter, noncovalent interaction energies are examined for three common benchmark sets, which mainly consist of noncovalently bound complexes.

Chapter 2 generalizes the scaling functions to a global one that incorporates elemental properties, as the chemical hardness, to calculate scaling factors based on relative effective charge changes. Contrary to the method described in Chapter 1, atomic partial charges are obtained from an electronegativity equilibration model, which enables the robust and efficient calculation of atomic charges at a high quality. Furthermore, a many-body dispersion model based on a coupling of atomic polarizabilities in terms of quantum harmonic oscillators is introduced. The DFT-D4 default method is defined and the use of alternative partial charges is investigated. This default method is verified by means of several literature-

known benchmark sets including properties like molecular dispersion coefficients, noncovalent and conformational energies, thermochemistry, as well as covalent and noncovalent structures.

Physically reasonable atomic polarizabilities are the foundation of any DFT-D-like LD correction. So-called Dobson type-A many-body effects¹⁸⁹ reduce the polarizability of an atom when its coordination number is increased. Such environmental effects predicate that it is not sensible to utilize polarizabilities derived from free isolated atoms to describe the ones in molecules. This conclusion holds when a condensed phase is created from molecules, where the decrease of atomic polarizabilities is even more enhanced. Particularly in very densely packed solids like in alkaline halides, the atomic polarizability decrease is significant. Chapter 3 discusses the calculation of new reference polarizabilities for densely packed periodic model systems using TD-DFT. A new procedure enables their efficient calculation using a pseudo-periodic scheme, splitting the solid into three regions, of which only the innermost region is described quantum-mechanically. This QM region is surrounded by a layer of effective core potentials to overcome additional polarization effects. The outer region of the cluster is described by a simple point charge model, that imitates Coulomb interactions of the perfect crystal. The extension of the DFT-D4 reference set of polarizabilities with those for densely packed periodic systems enables the consideration of additional periodic type-A nonadditive effects. Following this approach, new reference polarizabilities are calculated for alkaline metals, earth alkaline metals, and early *d*-metals of group 3-5.

Compared to experimental solid-state polarizabilities, DFT-D4 outperforms its predecessor DFT-D3 and other density-dependent dispersion corrections. An organic polymer database is used to measure the quality of refractive indices. Here, theoretical reference values are used for a comparison, showing that DFT-D4 is able to accurately calculate refractive indices. Furthermore, other correction schemes are compared, including the TS method and MBD@scsTS. Important solid-state quantities as, *e.g.*, lattice energies and cell volumes of various molecular crystals, are discussed. Additionally, this chapter compares theoretically obtained adsorption energies for three surface-adsorbate combinations to experimental or theoretical reference data. Computational timings for the self-consistent field calculation of the cyclohexadione crystal demonstrate the computational efficiency of different dispersion correction models.

1. Extension of the D3 Dispersion Coefficient Model

Eike Caldeweyher*, Christoph Bannwarth*, and Stefan Grimme*

Received 22nd of June 2017, Published online 21st of July 2017

Reprinted (adapted) with permission from^{††}

Caldeweyher, E. and Bannwarth, C. and Grimme, S. *J. Chem. Phys.* **2017**, *147*, 034112.

— Copyright © 2017 American Institute of Physics.

DOI [10.1063/1.4993215](https://doi.org/10.1063/1.4993215)

Own manuscript contribution

- Development, parametrization, and implementation of the DFT-D4 model (2017 version)
- Calculation of all results
- Interpretation of the results and writing the manuscript

*Mulliken Center for Theoretical Chemistry, Institut für Physikalische und Theoretische Chemie, Rheinische Friedrich-Wilhelms-Universität Bonn, Berlingstraße 4, 53115 Bonn, Germany

^{††}Permission requests to reuse material from this chapter should be directed to the American Institute of Physics.

Abstract A new model, termed D4, for the efficient computation of molecular dipole-dipole dispersion coefficients is presented. As in the related, well established D3 scheme, these are obtained as a sum of atom-in-molecule dispersion coefficients over atom pairs. Both models make use of dynamic polarizabilities obtained from first-principles time-dependent density functional theory calculations for atoms in different chemical environments employing fractional atomic coordination numbers for interpolation. Different from the D3 model, the coefficients are obtained on-the-fly by numerical Casimir–Polder integration of the dynamic, atomic polarizabilities $\alpha(i\omega)$. Most importantly, electronic density information is now incorporated via atomic partial charges computed at a semi-empirical quantum mechanical tight-binding level, which is used to scale the polarizabilities. Extended statistical measures show that errors for dispersion coefficients with the proposed D4 method are significantly lower than with D3 and other, computationally more involved schemes. Alongside, accurate isotropic charge and hybridization dependent, atom-in-molecule static polarizabilities are obtained with an unprecedented efficiency. Damping function parameters are provided for three standard density functionals, i.e., TPSS, PBE0, and B3LYP, allowing evaluation of the new DFT-D4 model for common noncovalent interaction energy benchmark sets.

1.1. Introduction

Due to its excellent accuracy-cost ratio, Kohn–Sham density functional theory (KS-DFT, or DFT in the following)^{190,191} is the workhorse of modern electronic structure calculations. Especially for the chemistry or physics of large or condensed-phase systems, the inclusion of long-range electron correlation interactions is indispensable in order to reach the so-called chemical accuracy (≈ 1 kcal mol⁻¹) in theoretical simulations. Semi-local or hybrid density functional approximations (DFAs) do not describe such correlation effects,¹⁷ hence they cannot account for the important London dispersion interactions.¹⁶¹ In order to correct for this shortcoming, semi-classical methods were developed to enable the computation of the long-range (London) dispersion energy in molecules and solids. The computationally efficient atom pairwise D3(BJ) scheme¹⁶⁶ requires only the molecular geometry as input to calculate the inter- and intramolecular dispersion energy based on pre-computed linear-response time-dependent DFT (TD-DFT) data. Aside from this geometrical dispersion model, electron density dependent approaches like the Tkatchenko–Scheffler (TS) model,⁴⁹ the exchange dipole moment (XDM) model of Becke and Johnson,^{47,48,180} or the local-response dispersion (LRD) model by Sato and Nakai exist.^{181,192} Conceptually somewhat different are the nonlocal density functional based dispersion corrections for which the family of van der Waals density functionals^{183–187} (vdW-DFs) and VV10^{51,52} are noteworthy examples.

I. Development of the DFT-D4 London Dispersion Correction

While the D3 approach is by far the fastest dispersion correction, one disadvantage of this geometrical scheme is that changes in the underlying electron density are not reflected in the dispersion coefficients. Whenever the density around an atom in a molecule or solid is significantly different from the one present in the reference compound, larger errors can occur.^{170,193} This is in particular relevant for applications involving metal centers (ions), which often change their effective electron number (atomic charge) and corresponding dipole-dipole dispersion coefficients (C_6). Density dependent approaches are, however, computationally more expensive compared to the D3 model and often neglect atomic hybridization effects (for respective modification of the hybridization devoid TS model, see Ref. 194). With this in mind, an extension of the well established and widely used D3 method is proposed here.

1.2. Theory

1.2.1. General

The new model introduced here, termed D4, calculates charge dependent dispersion coefficients efficiently and in a black box manner by incorporation of molecular input coordinates [for coordination numbers (CNs)] and also by semi-empirical quantum mechanical (QM) tight-binding (TB) computation (for atomic charges). The Mulliken charges¹⁹⁵ from a (partially polarized) minimal basis tight-binding scheme were shown to agree rather well with DFT Hirshfeld charges.¹⁹⁶ By using the same (semi-empirical) QM method (GFN-xTB¹⁸⁸) throughout to obtain the charges for our new model, we avoid complications arising solely from the fact that various functionals (e.g., hybrid vs. GGA) yield different charges. This choice furthermore reduces the number of necessary fit procedures and facilitates interfacing the model to existing QM codes. A related atom pairwise dispersion correction, denoted as dDMC,¹⁹⁷ also incorporated TB based Mulliken charges from the self-consistent charge density functional tight-binding (SCC-DFTB^{198,199}) method. The general applicability of TB charge based dispersion models depends on the availability of parameters for different elements. Since all elements up to $Z = 86$ are parameterized for GFN-xTB, the new D4 method has practically no limitations regarding the applicability to various chemical problems. Starting from the D3 scheme, conceptually minimal changes are applied such that for neutral (non-polar) molecules only small differences (mostly small improvements) between D3 and D4 are found. The new model is intended to be combined with various, predominantly mean-field electronic structure methods¹⁷ similar to D3 (for a recent successful use of D3 dispersion in SAPT, see Ref. 200). The D4 dispersion coefficients and static dipole polarizabilities are already used in a newly developed

I. Development of the DFT-D4 London Dispersion Correction

intermolecular force-field (FF).²⁰¹

1.2.2. Dispersion Coefficients

The calculated Mulliken charges serve as descriptors to scale pre-computed reference TD-DFT polarizabilities at imaginary frequencies $\alpha(i\omega)$. These are then used to obtain charge and coordination number (see below) dependent C_6^{AB} coefficients via numerical on-the-fly Casimir–Polder integration¹⁵⁶

$$C_6^{AB} = \sum_{A,\text{ref}=1}^{N^{A,\text{ref}}} \sum_{B,\text{ref}=1}^{N^{B,\text{ref}}} \frac{3}{\pi} \int_0^{\infty} d\omega \alpha^{A,\text{ref}}(i\omega, z^A) W_A^{A,\text{ref}} \alpha^{B,\text{ref}}(i\omega, z^B) W_B^{B,\text{ref}} \quad (1.1)$$

with

$$\alpha^A(i\omega, z^A) = \frac{1}{m} \left[\alpha^{A_m H_n}(i\omega) - \frac{n}{2} \alpha^{H_2}(i\omega) \zeta(z^{H_A}) \right] \zeta(z^A, z^{A,\text{ref}}) \quad (1.2)$$

and

$$\zeta(z^A, z^{A,\text{ref}}) = b a^{[1.47 \exp(z^A/z^{A,\text{ref}}) \log_{10}(z^{A,\text{ref}}/z^A)]}. \quad (1.3)$$

The reference polarizabilities $\alpha^{A_m H_n}$, describing the molecular polarizabilities of the symmetric hydride systems $A_m H_n$ (i.e., containing m chemically equivalent atoms A), incorporate hybridization in the D3 model (e.g., for carbon, the reference system with $CN^C = 2$ is C_2H_2). Polarizabilities were calculated at the same level of theory as for D3 (hybrid TD-DFT with augmented quadruple- ζ AO basis set).⁴⁶ In equation 1.1, $W_{A/B}^{A,\text{ref}/B,\text{ref}}$, are weighting factors to determine the contributions of all element specific reference systems $N^{A,\text{ref}/B,\text{ref}}$ (for further details see Appendix A1). In equation 1.2, z^{H_A} describes the effective charge of hydrogen bound to atom A in the particular reference system $A_m H_n$ while z^{H_2} describes the effective charge of hydrogen in the H_2 molecule. The effective charge z^A of an atom A within a molecule equals the sum of its nuclear charge Z^A and its self-consistently derived Mulliken charge q^A ,

$$z^A = Z^A + q^A. \quad (1.4)$$

Thus, a negatively charged atom is treated as having an effectively smaller nuclear charge. Equation 1.3 introduces the atom specific charge-function ζ . Here, the parameter b has been parameterized first to match the TD-DFT derived molecular dispersion coefficients of the reference systems (i.e., $z^A = z^{A,\text{ref}}$). Then parameter a is parameterized to match cationic static polarizabilities ($z^A \neq z^{A,\text{ref}}$) for all elements with $Z = 2 - 86$. The whole training set is given within Appendix A1. In principle, the atomic charges could also be provided individually by the underlying

I. Development of the DFT-D4 London Dispersion Correction

ing DFT calculation. This, however, would introduce many empirical parameters (one set for each DFA) and would furthermore complicate interfacing the method with existing computer codes (in particular for nuclear gradients) and charge devoid methods like force-fields. We thus continue the successful D3 strategy to provide only a single, well-defined and general “set” of dispersion coefficients. For the very rare case of GFN-xTB not providing a reasonable electronic structure, we provide a fall-back option to resort to PBE0/TZVP Hirshfeld charges. Figure 1.1 illustrates the effect of the introduced scaling function for hydrogen in two extreme bonding situations.

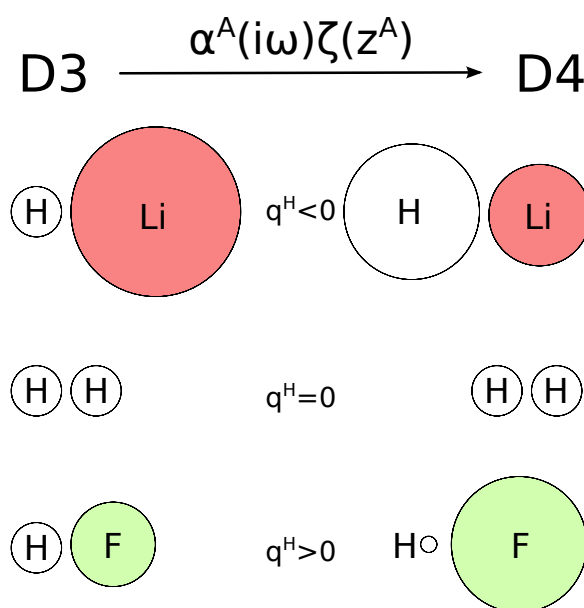


Figure 1.1.: Schematic representation of the ζ -functionality which rescales atomic polarizabilities based on input Mulliken charges q . The left side shows the standard partitioning of atomic polarizabilities in D3. On the right side, the scaled atomic polarizabilities are shown. The depicted radii of the atoms directly correspond to the calculated atomic C_6^{AA} coefficients.

The radii of the atoms directly correspond to the calculated homoatomic C_6^{AA} dispersion coefficients derived with D3 (left side) and D4 (right side). Fractional coordination numbers of all atoms are calculated to obtain atomic polarizabilities by weighting over all element specific reference systems A_mH_n with respect to those CNs. In D3, a two-dimensional interpolation scheme for different atoms A and B is used to compute C_6^{AB} , while in D4 this function is four-dimensional, i.e., two atomic charges and two CN values. The use of CNs is in accordance with chemical intuition regarding different hybridization situations for each atom within the molecule. Compared to D3, the calculation of the CN has been slightly modified. The atomic electronegativities of the two atoms enter the calculation in order to distinguish between covalent and ionic bonding. The CNs are ad-

I. Development of the DFT-D4 London Dispersion Correction

justed to approximately match Wiberg bond orders²⁰² of single bonds. Therefore, additional reference systems are included in the D4 Gaussian interpolation of polarizabilities describing nonpolar (e.g., fluorine with $CN^{F_2} = 0.96$) as well as polar (e.g., hydrogen fluoride with $CN^{HF} = 0.74$) cases resulting in a better description of the individual bonding and hybridization situation. For details of the determination of the few relevant model parameters, see Appendix A1. Furthermore, we changed the Gaussian weighting from interpolating precalculated C_6^{AB} dispersion coefficients between atoms having different CNs to a scheme which interpolates reference polarizabilities between atoms having different CNs and different charges instead (i.e., each polarizability is a two-dimensional function).

1.2.3. Dispersion Energy

The D4 dispersion coefficients are used to compute the atom pairwise dispersion energy in complete analogy to DFT-D3(BJ) by coupling to a damping scheme to be used with standard density functionals. The DFT-D4 dispersion energy is given by

$$E_{\text{DISP}}^{\text{D4}} = - \sum_{AB} \sum_{n=6,8} s_n \frac{C_6^{AB(n)}}{R^n} f_{\text{damp}}^{(n)}(R) \quad (1.5)$$

where R is an interatomic distance for atom pair AB , and $f_{\text{damp}}^{(n)}$ denotes the standard Becke–Johnson damping function¹⁶⁶ (denoted BJ-damping or simply damping in the following). The factors s_n scale the individual multipolar contributions. Due to its physically reasonable behavior at short interatomic distances, the BJ-damping function given by

$$f_{\text{damp}}^{(n)}(R) = \frac{R^{(n)}}{R^{(n)} + (\alpha_1 R_0 + \alpha_2)^{(n)}}, \quad (1.6)$$

has become the default already in D3¹⁶⁶. It incorporates functional-specific parameters α_1 and α_2 as well as the radii $R_0 = \sqrt{C_8^{AB}/C_6^{AB}}$. The atom pair-wise dipole-quadrupole contribution $E_{\text{DISP}}^{(8)}$ is included with the respective C_8^{AB} dispersion coefficient, which is computed recursively as in D3 from the dipole-dipole dispersion coefficient

$$C_8^{AB} = 3C_6^{AB} \sqrt{Q_A Q_B} \quad (1.7)$$

with

$$Q_A = \sqrt{Z^A} \frac{\langle r_A^4 \rangle}{\langle r_A^2 \rangle}. \quad (1.8)$$

Here, $\langle r_A^4 \rangle$ and $\langle r_A^2 \rangle$ are multipole-type expectation values derived from atomic densities and Z^A equals the nuclear charge of atom A . For more details, see Ref. 46.

1.2.4. Technical Details

We have coupled three established semi-local DFAs to the new D4 dispersion model (meta-GGA: TPSS¹⁰⁵, hybrid: B3LYP^{117,118} and PBE0¹¹⁶) as usual by fitting to common interaction energy benchmark sets, namely S66x8²⁰³, S22x5²⁰⁴, and NCIBLIND10⁸. We used the TURBOMOLE suite of programs^{143,205,206} (version 7.0.2) to conduct all ground-state DFT calculations. Within the DFT calculations, we applied standard exchange-correlation functional integration grids (*m4*) and typical self-consistent field (SCF) convergence criteria ($10^{-7}E_h$) as well as the resolution of the identity integral approximation^{207–209}. Ahlrich's type quadruple-zeta basis sets (def2-QZVP) are used for all single-point calculations. The density functional specific damping parameters are obtained by least-squares Levenberg–Marquardt minimization to the reference interaction energies in the three investigated benchmark sets.

1.3. Results

1.3.1. Molecular C_6 Coefficients

Experimentally, molecular C_6 coefficients are accessible from dipole oscillator strength distributions (DOSDs). Figure 1.2 displays computed molecular dispersion coefficients in comparison to experimental values and data from related theoretical methods (D3, TS, LRD). The respective statistical evaluation over all

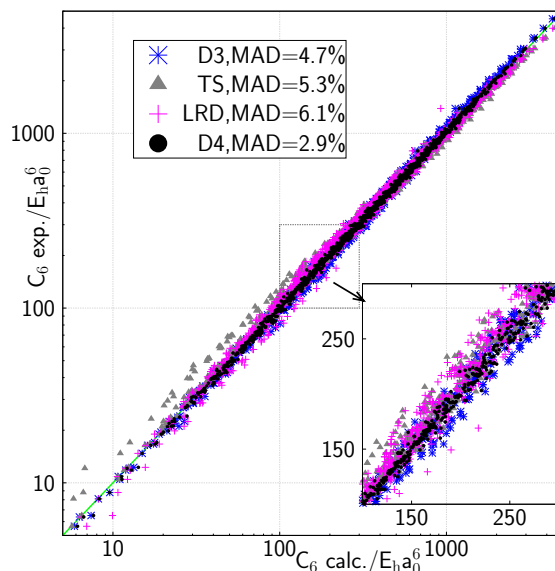


Figure 1.2.: Comparison of experimentally derived molecular dispersion coefficients (from dipole oscillator strength distributions) with calculated ones (1225 cases, compilation by A. Tkatchenko). Note the logarithmic scale and variation of the coefficients over three orders of magnitude. The test set contains small to medium-sized, inorganic and organic molecules ($H_2 - C_8H_{18}$).

I. Development of the DFT-D4 London Dispersion Correction

calculated dispersion coefficients in Figure 1.2 is given in Table 1.1, presenting the mean absolute deviation (MAD), mean deviation (MD), standard deviation (SD), and the absolute maximum (AMAX) error. The deviations are always taken as relative values (in %).

Table 1.1.: Statistical measures for the relative deviations (in %) of calculated molecular C_6 dispersion coefficients from different approaches with respect to experimental values for the molecular benchmark set in Figure 1.2. All calculated values are given in the Supporting Information of Ref. 210.

Method	MAD	MD	SD	AMAX
D3	4.7	-2.4	5.2	23.9
TS	5.3	-2.7	7.3	44.0
LRD	6.1	-2.5	7.7	52.9
D4	2.8	-0.6	3.6	17.5

It is noteworthy that already the calculation of dispersion coefficients for “normal”, medium-sized inorganic and organic molecules is substantially improved upon the accurate D3 model which has an MAD of 4.7%³⁸ for this benchmark set compiled by A. Tkatchenko. The D4 MAD value of 2.9% is remarkable and is well within the accuracy limits of the underlying hybrid TD-DFT quantum chemistry method. To the best of our knowledge, the new D4 model yields the best cost-accuracy ratio for calculating isotropic C_6 dispersion coefficients for arbitrary systems compared to other approaches.^{43,47-50,53,180-182,211-217}

1.3.2. Atoms-in-Molecules Polarizabilities

As a by-product of the D4 procedure, accurate atomic polarizabilities are obtained which may have a widespread application in classical force-fields (see our parallel work on a GFN-xTB based intermolecular FF²⁰¹). As an example for a possible large target system, the dispersion coefficients and atomic polarizabilities of the green fluorescent protein²¹⁸ (GFP, PDB entry 1GFL, with 3601 atoms and a total molecular charge of -6) were calculated within 30 minutes on a single desktop computer. Figure 1.3 shows the charge and coordination dependency of homoatomic C_6^{AA} dispersion coefficients in the chromophore of the GFP exemplifying the relatively big changes between D3 and D4 for very polar bonding situations. Because of the presence of charged side-chains, we used an implicit generalized Born solvation model²¹⁹ augmented with a solvent accessible surface term for water [GBSA(H₂O), GBSA in the following] in this calculation, while the default D4 procedure employs gas phase Mulliken partial charges. However, GFN-xTB/GBSA provides higher stability in the self-consistent charge procedure

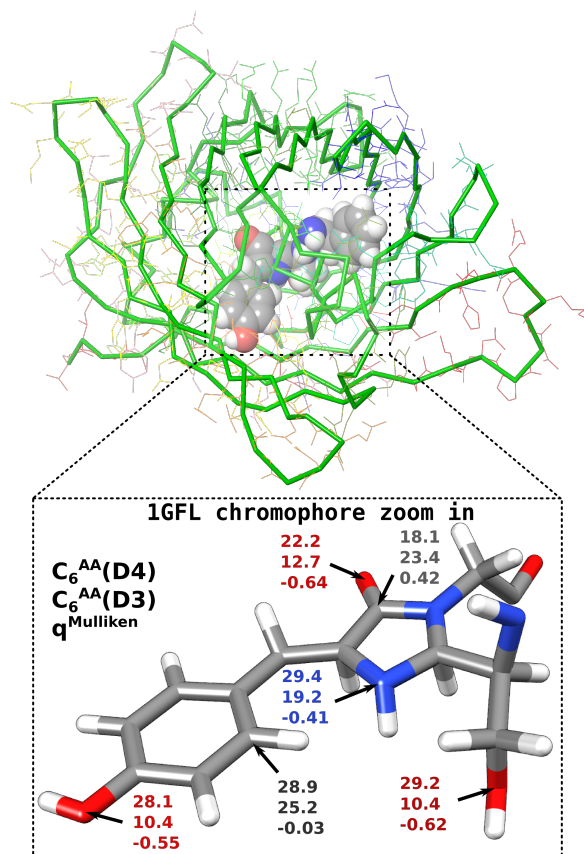


Figure 1.3.: Chain A of the green fluorescent protein as well as an enlarged display of the chromophore (PHE64, SER65, and TYR66). All homoatomic C_6^{AA} dispersion coefficients were calculated for the whole protein at the D4 and the D3 level of theory.

for highly charged molecular systems so that we recommend its use in such calculations. The quality of the calculated atomic polarizabilities is estimated by exploiting their additivity property¹⁵³ to compute molecular polarizabilities that are directly comparable to calculated hybrid TD-DFT molecular polarizabilities. For an organic molecule benchmark set (ROT34²²⁰), this results in a small deviation of only 2.5% similar to the one obtained for the molecular C_6 coefficients (see Table 1.1).

1.3.3. Li^+ -benzene: An Electronically Complicated Example System

As a cross-check and an example for a more difficult case involving a charged, organometallic system, the cation- π dissociation of a lithium cation and benzene (Bz) is considered. Figure 1.4 depicts the dissociation curve of the complex.

I. Development of the DFT-D4 London Dispersion Correction

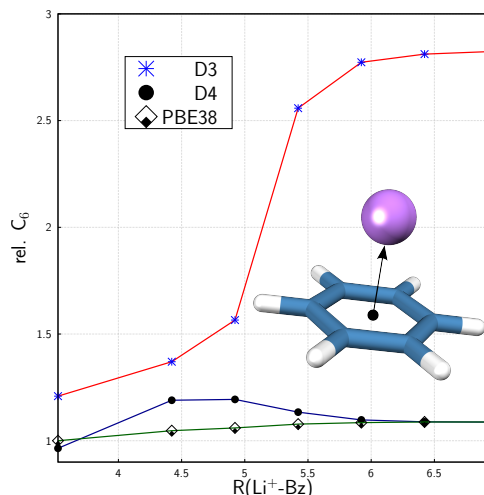


Figure 1.4.: Molecular dispersion coefficient C_6^{mol} for the dissociating lithium cation-benzene complex. The initial structure is optimized at the PBE0-D3(BJ)/def2-QZVP level of theory. All values are divided by the calculated TD-DFT molecular dispersion coefficient for the optimized minimum structure $C_6^{\text{mol,ref}}$. The reference TD-DFT curve is plotted in green while D3 and D4 data are shown in red and blue, respectively. The black arrow corresponds to the distance of the lithium cation to the center-of-mass of the benzene molecule denoted $R(\text{Li}^+-\text{Bz})$.

The calculated molecular dispersion coefficient is plotted against the center-of-mass distance $R(\text{Li}^+-\text{Bz})$ (shown as a black arrow in the inset). With increasing $R(\text{Li}^+-\text{Bz})$, the coordination number of the lithium cation CN^{Li^+} is decreasing to zero in the asymptotic region. This leads to an overestimation of the C_6 coefficient in D3, which essentially coincides with the huge dispersion coefficient of the free lithium atom. A charge dependent method like D4 is able to correct this deficiency by considering the electronic structure. The implemented charge function scales neutral reference polarizabilities to values that agree well with the ones in cationic or anionic situations. An MAD of 5% is calculated with D4 for the entire dissociation curve with respect to TD-DFT reference molecular dispersion coefficients. The maximum deviation is found at $\text{CN}^{\text{Li}^+} \approx 0.5$, with an error of 12.1%. Upon ionization, the static polarizability ($\alpha_{\text{ref}}^{\text{Li}}(0) = 149.6 \text{ Hartree Bohr}^6$) is decreased of a lithium atom by three orders of magnitude compared to the value of the free cation ($\alpha_{\text{ref}}^{\text{Li}^+}(0) = 0.2 \text{ Hartree Bohr}^6$). Thus the residual error is comparably small in this extreme case. The direct comparison to D3 demonstrates the major improvement and shows that the description of charged and neutral systems is more consistent in D4. This is important for many organometallic systems in chemistry (see Ref. 193, for example). For atomic dispersion coefficients calculated by the XDM method for related systems, see Ref. 221.

1.3.4. Noncovalent Interaction Energies

In Table 1.2, we directly compare DFT-D4 and DFT-D3(BJ) derived interaction energies for three density functionals.

Table 1.2.: Interaction energies calculated with three dispersion corrected DFAs (meta-GGA: TPSS,¹⁰⁵ hybrid: B3LYP^{117,118} and PBE0¹¹⁶) and Ahlrich’s type def2-QZVP basis set (not counter-poise corrected). All statistical measures are given in kcal mol⁻¹ relative to the reference energies. The best result for each measure is highlighted in bold-face.

S66x8						
Measure	TPSS		B3LYP		PBE0	
	D3	D4	D3	D4	D3	D4
MAD	0.29	0.26	0.20	0.22	0.33	0.30
MD	0.07	-0.03	-0.14	-0.10	-0.17	-0.15
SD	0.37	0.33	0.26	0.27	0.42	0.39
AMAX	1.06	1.00	0.99	0.82	1.61	1.52
S22x5						
MAD	0.32	0.29	0.28	0.26	0.42	0.37
MD	-0.11	-0.21	-0.14	-0.14	-0.23	-0.27
SD	0.51	0.41	0.46	0.42	0.67	0.56
AMAX	2.54	1.95	2.39	1.66	3.04	2.70
NCIBLIND10						
MAD	0.90	0.56	0.22	0.20	0.28	0.24
MD	0.72	0.28	0.06	-0.04	-0.04	-0.08
SD	1.98	1.10	0.47	0.32	0.54	0.42
AMAX	9.40	4.77	2.23	1.55	2.10	1.69

Here, the DFT-D3(BJ) damping parameters are re-fitted by the same procedure on the same benchmark sets for a fair comparison between both models. As can be seen from the table, the DFT interaction energies are mostly improved by using D4, even for neutral systems. This is noteworthy because the DFT-D3(BJ) model is usually considered as being already rather accurate. It furthermore indicates that a part of the residual DFT-D3(BJ) interaction energy error is rooted in the dispersion coefficients although the DFT part is also significant at this accuracy level.

1.4. Summary and Conclusion

We have presented an atomic charge and coordination number dependent scheme, termed D4, to compute C_6 dispersion coefficients, which can be coupled to stan-

I. Development of the DFT-D4 London Dispersion Correction

standard density functional approximations in a DFT-D4 sense. Atomic Mulliken charges are taken from a recently published semiempirical tight-binding method (GFN-xTB),¹⁸⁸ which is available for all elements with $Z = 1-86$. The dispersion model is based on the well-established D3 scheme and, by incorporating the atomic charge information, basically corrects for some failures for polar, organo-metallic, and ionic systems. The accuracy of the dispersion coefficients is slightly improved for the “normal” cases which were already good with D3. Importantly, the general black-box philosophy of the approach and the coupling of a single dispersion coefficient model to various standard DFAs is equivalent to the one of D3, which allows a broad application to quantum chemical problems. Compared to the purely geometrical D3 model, the computational cost of D4 is increased due to the semi-empirical tight-binding procedure. Since the entire D4 procedure is orders of magnitude faster compared to a Hartree–Fock or DFT treatment, the cost of D4 is negligible in a DFT-D4 scheme. Preliminary DFT-D4 interaction energy benchmarks for noncovalently bound systems (S66x8, S22x5, NCIBLIND10) show small but consistent improvements for the TPSS, PBE0, and B3LYP DFAs. Prospective works will couple D4 to more contemporary DFAs leading to a general and widely applicable DFT-D4 approach. Current work is devoted to an efficient implementation of analytical D4 nuclear gradients, which are necessary for geometry optimizations. Furthermore, a periodic implementation of GFN-xTB will be developed to treat dispersion interactions of bulk materials and surfaces under periodic boundary conditions. In the current form, the D4 dispersion energy program can be downloaded from the authors’ website and used in a single-point energy mode for checking results of other pairwise dispersion corrections and due to its high accuracy even approximate wave function theory calculations.

1.5. Acknowledgments

This work was supported by the DFG in the framework of the priority Program No. SPP 1807, “Control of Dispersion Interactions in Chemistry.”

1.6. Appendix A1

See Appendix A1 for further details about the D4 model, parametrization details of the charge function, and BJ-damping parameters for TPSS, B3LYP, and PBE0.

2. A Generally Applicable Atomic-Charge Dependent London Dispersion Correction

Eike Caldeweyher*, Sebastian Ehlert*, Andreas Hansen*, Hagen Neugebauer*, Sebastian Spicher*, Christoph Bannwarth[†], and Stefan Grimme*

Received 21st of March 2019, Published online 19th of April 2019

Reprinted (adapted) with permission from^{††}

Caldeweyher, E. and Ehlert, S. and Hansen, A. and Neugebauer, N. and Spicher, S. and Bannwarth, C. and Grimme, S. *J. Chem. Phys.* **2019**, *150*, 154122.

— Copyright © 2017 American Institute of Physics.

DOI [10.1063/1.5090222](https://doi.org/10.1063/1.5090222)

Own manuscript contribution

- Development and implementation of the DFT-D4 model with great help of S. Ehlert
- Interpretation of the results and writing the manuscript
- Contribution of co-authors:
 - GMTKN55, MOR41 (S. Ehlert)
 - DLPNO-CCSD(T) energies for $[[\text{Rh}(\text{CNPh})_4]_2]_2^+$ dication (A. Hansen)
 - EEQ parametrization (S. Spicher)
 - TOMC6 benchmark (H. Neugebauer)

*Mulliken Center for Theoretical Chemistry, Institut für Physikalische und Theoretische Chemie, Rheinische Friedrich-Wilhelms-Universität Bonn, Berlingstraße 4, 53115 Bonn, Germany

[†]Department of Chemistry, Stanford University, Stanford, California 94305, USA

^{††}Permission requests to reuse material from this chapter should be directed to the American Institute of Physics.

Abstract The so-called D4 model is presented for the accurate computation of London dispersion interactions in density functional theory approximations (DFT-D4) and generally for atomistic modeling methods. In this successor to the DFT-D3 model, the atomic coordination-dependent dipole polarizabilities are scaled based on atomic partial charges which can be taken from various sources. For this purpose, a new charge-dependent parameter-economic scaling function is designed. Classical charges are obtained from an atomic electronegativity equilibration procedure for which efficient analytical derivatives with respect to nuclear positions are developed. A numerical Casimir–Polder integration of the atom-in-molecule dynamic polarizabilities then yields charge- and geometry-dependent dipole-dipole dispersion coefficients. Similar to the D3 model, the dynamic polarizabilities are precomputed by time-dependent DFT and all elements up to radon ($Z = 86$) are covered. The two-body dispersion energy expression has the usual sum-over-atom-pairs form and includes dipole-dipole as well as dipole-quadrupole interactions. For a benchmark set of 1225 molecular dipole-dipole dispersion coefficients, the D4 model achieves an unprecedented accuracy with a mean relative deviation of 3.8% compared to 4.7% for D3. In addition to the two-body part, three-body effects are described by an Axilrod–Teller–Muto term. A common many-body dispersion expansion was extensively tested, and an energy correction based on D4 polarizabilities is found to be advantageous for larger systems. Becke–Johnson-type damping parameters for DFT-D4 are determined for more than 60 common density functionals. For various standard energy benchmark sets, DFT-D4 slightly but consistently outperforms DFT-D3. Especially for metal containing systems, the introduced charge dependence of the dispersion coefficients improves thermochemical properties. We suggest (DFT-)D4 as a physically improved and more sophisticated dispersion model in place of DFT-D3 for DFT calculations as well as other low-cost approaches like semi-empirical models.

2.1. Introduction

Many computational studies have shown that dispersion-corrected Kohn–Sham density functional theory (abbreviated as DFT in the following) is currently the method of choice for the routine computation of the electronic and geometric structure of large systems,^{95,190} e.g., in the fields of supramolecular chemistry,^{4,5,222} catalysis,^{223,224} or in materials science.^{6,225,226} In contrast to more elaborate wave function theory (WFT) based methods, most density functional approximations (DFAs) are not able to describe long-ranged electron correlation effects.^{34,36,227,228} Their treatment is, however, important to compute energetic properties with high accuracy (approximately 1 kcal mol^{-1}), particularly for non-covalently bonded or condensed phase systems. Therefore, various correction

I. Development of the DFT-D4 London Dispersion Correction

schemes have been developed to describe so-called London dispersion interactions in a DFT framework.¹⁷ The most commonly used method for molecular applications is the so-called DFT-D3 scheme,⁴⁶ which calculates the inter- and intramolecular dispersion interactions only by employing the given system coordinates (and atomic numbers). Similar atom pairwise models, which additionally include information from the electron density, have been reviewed recently¹⁷ and are only mentioned briefly here. Among them are the exchange hole dipole moment^{47,48,228,229} (XDM) model and the Tkatchenko–Scheffler (TS)⁴⁹ model both employing Hirshfeld partitioning. It is also possible to directly develop nonlocal density functionals, which are inherently capable of describing London dispersion interactions. This way, atomic partitioning, which always involves some arbitrariness, is avoided. Here, the family of van der Waals density functionals is to be mentioned, which are based on the fundamental adiabatic connection theory and offer a rigorous basis for the design of dispersion-inclusive exchange-correlation functionals.^{183,187} A simplified construction scheme for the nonlocal correlation part has been introduced by Vydrov and Van Voorhis.^{51,52} The computational costs of incorporating dispersion corrections into a standard DFT treatment are very method dependent but generally smaller compared to the actual DFT calculation. Consequently, it is reasonable to include them by default, and it has been demonstrated that the accuracy of dispersion-corrected DFAs for thermochemical properties on average follows Jacob’s ladder⁵⁷ classification. Note that for very low-cost atomistic models such as semi-empirical molecular orbital or force-field methods, only nondensity dependent schemes like DFT-D3 (and here proposed D4) are computationally feasible. The current work describes the further development of the widely used semi-classical DFT-D3 approach. Recently, it was shown that this “geometry-only” model can be further improved by addition of atomic charge information.²¹⁰ Therein, we showed that computed atom-in-molecule dynamic polarizabilities can be scaled by means of an element specific function with Mulliken-type atomic charges as input. Here, we want to report on the final version of the D4 model and provide it in a usable form for a large number of density functionals as DFT-D4. In general, we retained the general idea and strong points of the well established D3 scheme and introduced the charge dependence as well as some less important, mostly, technical improvements. Compared to the scaling scheme in Ref. 210, a less empirical function is used (see below) and the Mulliken partial charges are replaced by default with classical electronegativity equilibration (EEQ) partial charges as recently described by Goedecker *et al.*²³⁰. The D4 scheme is, however, general in a sense that any type of atomic charges in addition to the geometric structure of the can be used as input. Previous studies have revealed that many-body dispersion (MBD) interactions beyond a pairwise picture are important, e.g., in supramolecular,^{231,232} in cluster,^{233,234}

I. Development of the DFT-D4 London Dispersion Correction

and in condensed-phase systems^{235–239} where so-called Dobson type B effects¹⁸⁹ play an important role. The use of a coupled-dipole based many-body dispersion (MBD) correction (cf. the MBD method in Refs. 50 and 179) in our implementation does not yield systematic improvements compared to the simple third-order Axilrod–Teller–Muto^{167,168} (ATM) term. However, the MBD correction proves to be useful for large systems (see noncovalent benchmarks in section 2.3), for which we recommend its application in terms of an energy correction. The theory and technical details of the D4 method are described in section 2.2. Subsequently, in section 2.3, results for dispersion coefficients with D4 as well as for energies and structures obtained with DFT-D4 are compared directly to those of other established dispersion correction schemes for the same underlying DFA. Finally, a summary and an outlook on possible future work will be given.

2.2. Theory

Atomic units are used throughout in this work. The DFT-D4 workflow is simplified for an example molecule in Figure 2.1.

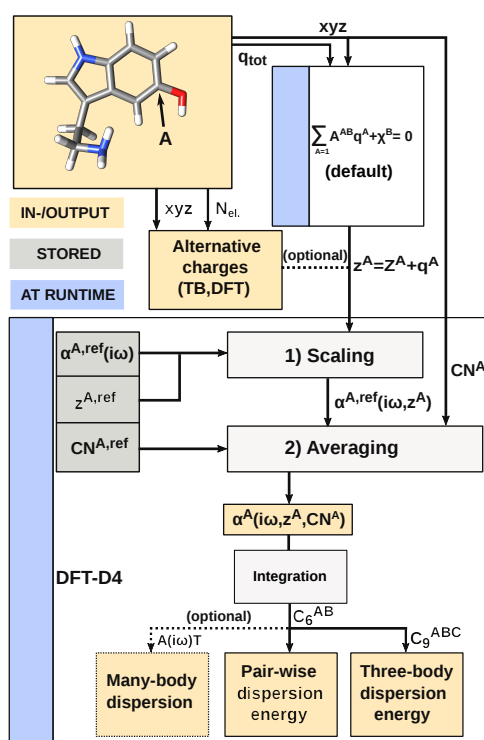


Figure 2.1.: Schematic workflow of the D4 program for an example molecule (all definitions and steps are explained in detail in the text).

The pairwise dipole-dipole dispersion coefficients in D4 are calculated by numerical

I. Development of the DFT-D4 London Dispersion Correction

integration via the well-known Casimir–Polder relation

$$C_6^{AB} = \frac{3}{\pi} \int_0^{\infty} d\omega \alpha^A(i\omega) \alpha^B(i\omega). \quad (2.1)$$

At runtime, the isotropically averaged atomic dynamic polarizabilities at imaginary frequency $\alpha(i\omega)$ in equation 2.1 are obtained in two steps: The first step incorporates an atomic partial charge dependent scaling of atomic reference polarizabilities. For this purpose, a new charge-scaling function ζ has been designed in this work given by

$$\zeta(z^A, z^{A,\text{ref}}) = \exp \left[\beta_1 \left\{ 1 - \exp \left[\gamma^A \left(1 - \frac{z^{A,\text{ref}}}{z^A} \right) \right] \right\} \right], \quad (2.2)$$

which is sketched exemplarily in Figure 2.2.

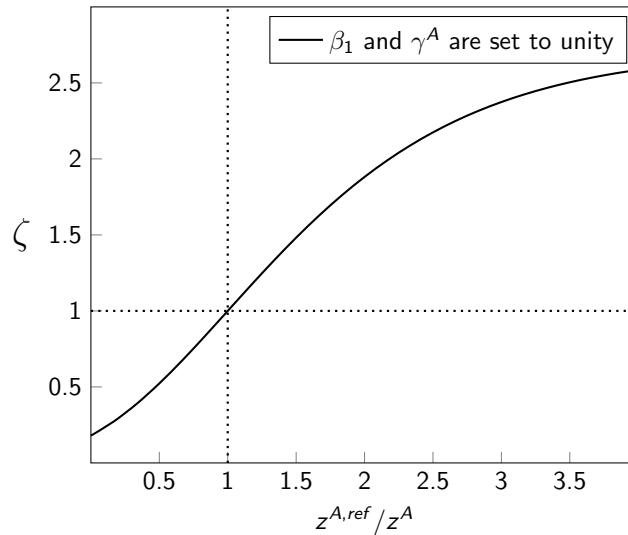


Figure 2.2.: The ζ -function is shown, which scales the time-dependent density functional theory (TD-DFT) computed dynamic polarizabilities $\alpha(i\omega)$ depending on the calculated effective nuclear charge z^A . The scaling depends on the quotient of the latter and the precalculated charge $z^{A,\text{ref}}$ of the atom in the reference system for which the dynamic polarizability has been computed. If both effective charges are equal, no scaling is performed (the crossing point of dotted lines) and the reference polarizability is taken.

In equation 2.2, the chemical hardness γ^A is taken from Ref. 240 and serves as a nonfitted element-specific parameter to control the steepness of the scaling function. The value of the global parameter $\beta_1 = 3$ was determined by inspection. The empirical charge-dependent scaling in D4 is intended to increase the magnitude of the atomic dynamic dipole polarizabilities $\alpha(i\omega)$ for larger number of electrons in proximity to the considered atom. Independent from the actual

I. Development of the DFT-D4 London Dispersion Correction

DFA which is to be corrected, environment dependent atomic partial charges are taken as input. The advantage is that such external partial charges can be (independently from the actual calculation) made accurate and robust and that the D4 dispersion coefficients remain functional independent. By default, classical EEQ type partial charges are used as descriptor for the electron density change (see section 2.2.1). Other common options for the choice of the charges are discussed below. In equation 2.2, we follow the definition of the effective nuclear charge z^A , used also in Ref. 210, as the sum of the nuclear charge of atom A and the atomic partial charge q^A

$$z^A = Z^A + q^A, \quad (2.3)$$

and introduce effective nuclear charges for element specific reference systems $z^{A,\text{ref}}$. For all elements beyond krypton, we consistently employ modified nuclear charges Z' , as defined in Table 2.1, due to the use of effective core potentials (ECPs) in the computation of the dynamic polarizability reference values.

Table 2.1.: Effective nuclear charges Z' used in the D4 charge scaling function for elements beyond krypton. The subtracted number corresponds to the number of core electrons absorbed in the ECP used (default def2-ECPs in TURBO-MOLE ^{143,205,206}).

Element	Z'
Rb-Xe	$Z - 18$
Cs-La	$Z - 46$
Ce-Lu	$Z - 28$
Hf-Rn	$Z - 60$

In comparison to the initially proposed charge-scaling function presented in Ref. 210, the two element-specific parameters could be discarded resulting in a global scaling function with only one empirical parameter. The charge-dependent atomic dynamic polarizability for a single reference system of atom A is given by the product of $\alpha^{A,\text{ref}}(i\omega)$ and its scaling function as

$$\alpha^{A,\text{ref}}(i\omega, z^A) = \alpha^{A,\text{ref}}(i\omega) \zeta(z^A, z^{A,\text{ref}}). \quad (2.4)$$

In equation 2.4, atom-in-molecule dynamic polarizabilities of element specific reference systems $\alpha^{A,\text{ref}}(i\omega)$ are utilized. Since such atom-in-molecule dynamic polarizabilities cannot be calculated directly, molecular dynamic polarizabilities of the reference systems $A_m X_n$ (having m chemically equivalent atoms A and n chemically equivalent X atoms) are used in the present model. From these

I. Development of the DFT-D4 London Dispersion Correction

molecular dynamic polarizabilities $\alpha^{A_m X_n}(i\omega)$, the contribution of the nX atoms is subtracted to obtain atom-in-molecule dynamic polarizabilities $\alpha^{A,ref}(i\omega)$ for atom A in different chemical environments. Here, the approximate additivity of polarizabilities²⁴¹ is exploited to generate atom-in-molecule dynamic polarizabilities according to the following partitioning scheme:

$$\alpha^{A,ref}(i\omega) = \frac{1}{m} \left[\alpha^{A_m X_n}(i\omega) - \frac{n}{l} \alpha^{X_l}(i\omega) \zeta(z^X, z^{X,ref}) \right]. \quad (2.5)$$

Equation 2.5 directly considers the charge scaling of all X atoms in the respective reference system. l is a stoichiometric factor specific to the reference molecule of element X . The effective nuclear charges $z^{X,ref}$ entering equation 2.5 are constant values determined once for the respective reference system. By subtracting charge-scaled polarizabilities of the atoms X , the partitioning of molecular polarizabilities into atomic contributions changes—with respect to D3—depending on the charge of the atoms X within each reference system. In D4, the polarizability of atom A is either increased (positive partial charge at X , subtract lower amount from A) or decreased (negative partial charge at X , subtract higher amount from A) when comparing with polarizabilities obtained by subtracting neutral X atoms. The second step in the D4 procedure is the geometry-based interpolation over the charge-scaled element specific reference systems. In order to enable a geometric interpolation of all $\alpha^{A,ref}(i\omega, z^A)$ of atom A , a weighting procedure similar to the fractional coordination number (CN) based scheme in D3 is used. As already described in Ref. 210, the CN used within D4 is, however, slightly modified and includes an electronegativity difference dependence for the respective element-pair, i.e.,

$$\begin{aligned} \text{CN}^A &= \sum_A \sum_{B \neq A} \frac{\delta_{AB}^{\text{EN}}}{2} \left(1 + \text{erf} \left(-k_0 \left(\frac{R_{AB} - R_{AB}^{\text{cov}}}{R_{AB}^{\text{cov}}} \right) \right) \right) \\ \delta_{AB}^{\text{EN}} &= \left(k_1 \exp(|\text{EN}_A - \text{EN}_B| + k_2)^2 \right) / k_3. \end{aligned} \quad (2.6)$$

In equation 2.6, Pauling²⁴² electronegativities (EN), the internuclear distance R_{AB} of pair AB , and the covalent atomic radii²⁴³ ($R_{AB}^{\text{cov}} = R_A^{\text{cov}} + R_B^{\text{cov}}$) are used. The parameters in equation 2.6 ($k_0 = 7.5$, $k_1 = 4.1$, $k_2 = 19.09$, and $k_3 = 254.56$) were obtained by fitting CN values to GFN2-xTB²⁴⁴ derived Wiberg bond orders²⁰² of singly bonded diatomic molecules. The exponential used in D3 is replaced here by an error function to avoid a divergence behavior of the CN in applications for dense systems under periodic boundary conditions.²⁴⁵ A graphical comparison of CN values is shown for D4 and D3 in Figure 2.3 for a catalyst frequently used in organometallic synthesis as an example.

I. Development of the DFT-D4 London Dispersion Correction

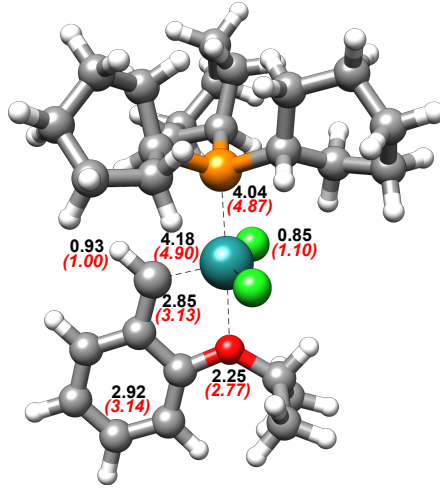


Figure 2.3.: Coordination numbers of selected atoms for the first generation Hoveyda-Grubbs catalyst^{246,247} given as an example. Black/red (brackets) values show CN values for D4/D3.

All reference coordination numbers, termed $CN^{A,ref}$, are precalculated and stored in the code such that a Gaussian weighting function $W_A^{A,ref}$ can efficiently be used to generate system-specific charge- and geometry-dependent atom-in-molecule polarizabilities for atom A abbreviated as $\alpha^A(i\omega)$ for clarity

$$\alpha^A(i\omega) \equiv \alpha^{A,ref}(i\omega, z^A, CN^A) = \sum_{A,ref=1}^{N^{A,ref}} \alpha^{A,ref}(i\omega, z^A) W_A^{A,ref}. \quad (2.7)$$

The contribution of each reference value $\alpha^{A,ref}(i\omega, z^A)$ to the final atom-in-molecule polarizability of atom A is given by

$$W_A^{A,ref}(CN^A, CN^{A,ref}) = \frac{\sum_{j=1}^{N^s} \exp(-\beta_2 \times j (CN^A - CN^{A,ref})^2)}{\sum_{A,ref=1}^{N^{A,ref}} \sum_{j=1}^{N^s} \exp(-\beta_2 \times j (CN^A - CN^{A,ref})^2)}, \quad (2.8)$$

for $N^{A,ref}$ reference systems per element A (note that $\sum_{A,ref=1}^{N^{A,ref}} W_A^{A,ref} = 1$). The parameter $\beta_2 = 6$ is adjusted manually to guarantee a smooth weighting function. In contrast to D3, the Gaussian weighting is changed, such that several Gaussian functions can be used for single reference systems as shown in equation 2.8. Generally the number of Gaussian functions N^s is obtained once for every reference system and used at runtime as described in equation 2.8. The procedure of setting N^s – for different reference systems – is exemplified in Figure 2.4 to explain the

I. Development of the DFT-D4 London Dispersion Correction

principle of the weighting scheme.

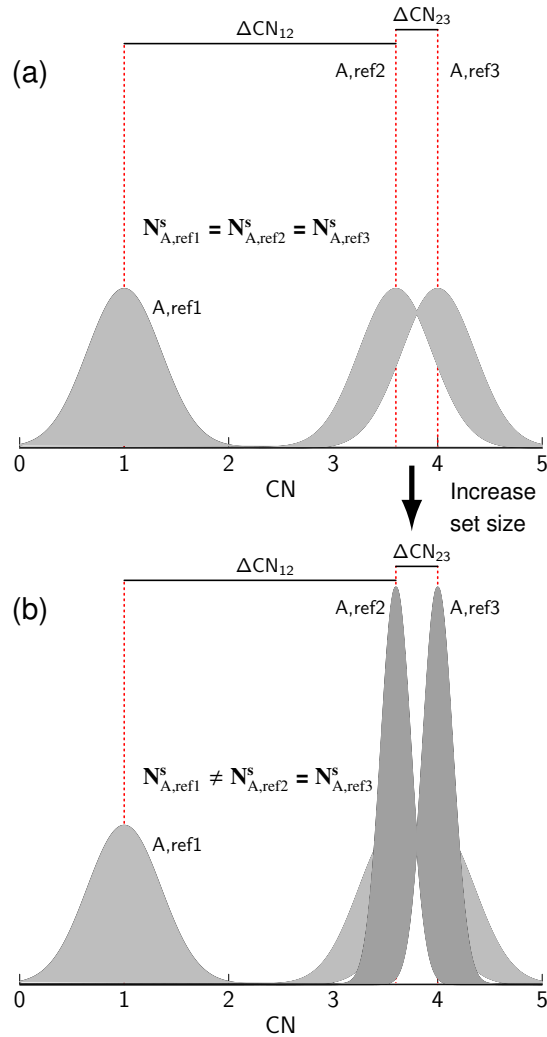


Figure 2.4.: Example for setting N^s for different reference systems. The CN difference between systems $A, \text{ref1}$ and $A, \text{ref2}$ is denoted as ΔCN_{12} . $A, \text{ref1}$ and $A, \text{ref2}$ are easily distinguishable within the Gaussian weighting procedure of equation 2.8 with $N^s = 1$, while $A, \text{ref2}$ and $A, \text{ref3}$ are not as could be seen in part (a) of the figure. To circumvent this behavior, the set of Gaussian functions is enlarged for $A, \text{ref2}$ and $A, \text{ref3}$ as it is shown in part (b) by varying the N^s value in equation 2.8 dynamically.

Differences between CN values of reference systems are used to indicate when another more compact Gaussian is necessary. As indicated in Figure 2.4(a), reference systems with a sufficiently large CN difference can easily be distinguished from each other within the Gaussian weighting procedure in equation 2.8 for $N^s = 1$. This is no longer the case if the reference CN difference between two systems approaches smaller values as present between reference system $A, \text{ref2}$ and $A, \text{ref3}$

I. Development of the DFT-D4 London Dispersion Correction

(denoted as ΔCN_{23} in Figure 2.4). The overlap between the Gaussian functions placed on A, ref2 and A, ref3 – shown in white – makes it considerably more difficult to differentiate between both reference systems. For this reason, the set of Gaussian functions is enlarged – by increasing N^s – for these near lying reference systems, as shown in Figure 2.4(b). This way, less overlapping functions are added, which makes both reference systems distinguishable within the Gaussian weighting procedure. By following this strategy it is possible to generate a smooth weighting scheme without any discontinuities. The final charge- and coordination-dependent atom-in-molecule polarizabilities, as obtained from equation 2.7, hence include the dependence of $\alpha(i\omega)$ on the spatially closest binding partners (i.e., so-called Dobson type A effects¹⁸⁹). They are used to calculate pairwise dispersion coefficients *via* a numerical Casimir–Polder integration over a fixed number of 23 points (between $i\omega_{\min} = 10^{-6}i$ and $i\omega_{\max} = 10.0i$ given in Hartree).

$$C_6^{AB} \equiv C_6^{AB}(CN^A, z^A, CN^B, z^B)$$

$$= \frac{3}{2\pi} \sum_{j=1}^{22} (\omega_{j+1} - \omega_j) \times (\alpha^A(i\omega_{j+1})\alpha^B(i\omega_{j+1}) + \alpha^A(i\omega_j)\alpha^B(i\omega_j)).$$
(2.9)

The effect of charge scaling and Gaussian weighting on the $\alpha^A(0)$ values with variations in the partial charge (leading to different effective nuclear charges z) and in the coordination number is visualized for carbon and hydrogen in Figure 2.5.

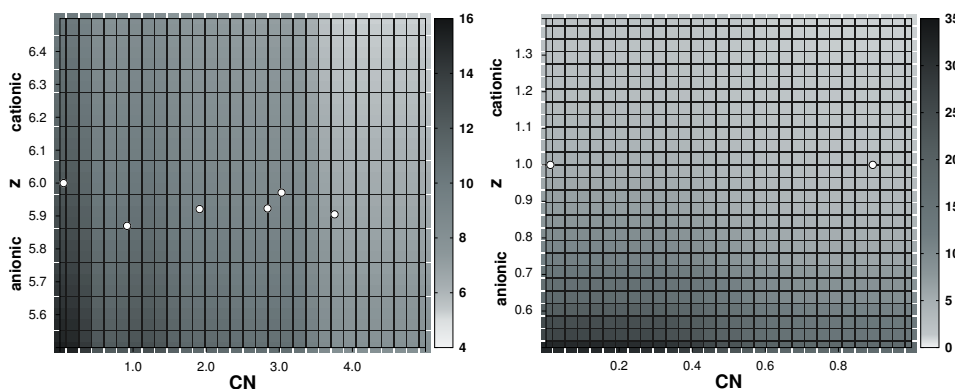


Figure 2.5.: Visualization of the two-dimensional dependence of static polarizabilities $\alpha(0)$ (in Bohr³) on the charge and coordination state in the D4 model for (left) carbon and for (right) hydrogen. White circles represent $\alpha^A(0)$ values for the reference systems.

Furthermore, Figure 2.6 shows static atom-in-molecule polarizabilities for carbon atoms in different hybridization states for the (3Z)-hexen-1-yne molecule.

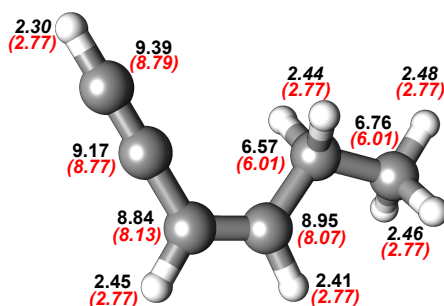


Figure 2.6.: Example molecule with depicted static atom-in-molecule polarizabilities $\alpha(0)$ (in Bohr³) from D4 (black) according to equation 2.5 and for D3 (red in brackets). Values for carbon/hydrogen are given in bold/italic font.

Here, we follow the definition in equation 2.5 for D4 and the definition given in Ref. 46 for D3 to obtain those polarizabilities. As atomic partitioning schemes generally introduce some arbitrariness, the individual atom-in-molecule polarizabilities from D3 and D4 also differ (by about 10%). However, the physical observable, i.e., the total molecular dispersion coefficient, is similar with the two methods for this rather nonpolar compound ($C_{6,\text{mol}}^{\text{AA}}(\text{TD-PBE38/daug-def2-QZVP})=2103.1$, $C_{6,\text{mol}}^{\text{AA}}(\text{D4})=1949.5$, and $C_{6,\text{mol}}^{\text{AA}}(\text{D3})=1893.0$ – all given in Hartree Bohr⁶). Here, the additivity of pairwise dispersion coefficients in molecules P (atoms $p \in P$) and Q (atoms $q \in Q$) has been used

$$C_{6,\text{mol}}^{\text{PQ}} = \sum_p \sum_q C_6^{\text{pq}}. \quad (2.10)$$

2.2.1. Classical Environment Dependent Partial Charges

For the scaling of atom-in-molecule polarizabilities, an established classical charge model based on electronegativity equilibration of Gaussian type charge densities is used.²³⁰ It allows the electronic charge to distribute itself in an optimal way over the whole system, includes penetration effects, and thus can describe both neutral and charged systems. Unlike environmental dependent partial charges that are determined by neural networks,²⁴⁸ the adapted method determines the total charge (as sum of all atomic charges) of the system exactly. For this purpose, atomic charge densities are used within an isotropic electrostatics (IES) energy expression where elements of the \mathbf{X} vector and elements of the \mathbf{A} matrix are given by

$$X^A = -\chi^A \quad \text{and} \quad A^{AB} = \begin{cases} J^{AA} + \frac{\sqrt{2}\gamma^{AA}}{\sqrt{\pi}} & A = B \\ \frac{\text{erf}(\gamma^{AB}R_{AB})}{R_{AB}} & \text{otherwise} \end{cases} \quad (2.11)$$

I. Development of the DFT-D4 London Dispersion Correction

The EEQ model presented here contains as atomic radii α^A , which are used in the expression $\gamma^{AB} = ((\alpha^A)^2 + (\alpha^B)^2)^{-1/2}$, as well as element dependent atomic hardnesses J^{AA} , and the right-hand side (RHS) χ^A . The RHS consists of the atomic electronegativity EN^A which is scaled by the square-root of the error function modified D3 coordination number (termed mCN) that incorporates the environment dependency into the model including an element specific scaling parameter κ^A

$$\chi^A = EN^A - \kappa^A \sqrt{\text{mCN}^A}. \quad (2.12)$$

The mCN is given for atom A as

$$\text{mCN}^A = \frac{1}{2} \sum_{\substack{B=1 \\ B \neq A}} \left(1 + \text{erf} \left(-k \left(\frac{R_{AB}}{R_{AB}^{\text{cov}}} - 1 \right) \right) \right) \quad (2.13)$$

similar to equation 2.6 with $R_{AB}^{\text{cov}} = R_A^{\text{cov}} + R_B^{\text{cov}}$. Geometry-only dependent partial charges are obtained by solving a set of linear equations under the constraint that the atomic charges sum up to the correct overall charge

$$L = E_{\text{IES}} + \lambda \left(\sum_{\Lambda=1} q^\Lambda - q_{\text{tot}} \right), \quad (2.14)$$

with $\partial L / \partial \mathbf{q} = 0$ and $\partial L / \partial \lambda = \sum_{i=1}^N q_i - q_{\text{tot}}$. Adding this constraint in terms of an Lagrange multiplier leads to the modified linear system of equations

$$\begin{pmatrix} \mathbf{A} & \mathbf{1} \\ \mathbf{1}^T & 0 \end{pmatrix} \begin{pmatrix} \mathbf{q} \\ \lambda \end{pmatrix} = \begin{pmatrix} \mathbf{X} \\ q_{\text{tot}} \end{pmatrix}. \quad (2.15)$$

This classical charge model requires five empirical parameters (J^{AA} , α^A , EN^A , κ^A , and R_{cov}^A) per element and achieves for molecules across the entire periodic table of elements an average deviation of about 0.04 e⁻ (0.03 e⁻ for organic molecules) from PBE0 based Hirshfeld charges (see Appendix A2). The main motivation to propose a classical charge model as default instead of a quantum chemistry based one is the higher robustness in electronically complicated cases for which simple tight-binding or DFT methods may fail to converge properly (see Appendix A2 for discussion). Furthermore, it enables the use of D4 in combination with fast approaches. For the construction of the analytical gradient of the D4 dispersion energy, the derivatives of the charges with respect to nuclear displacements are required. The partial derivative of the Lagrangian is derived with respect to inter-nuclear distances in complete analogy to, e.g., coupled-perturbed SCF equations, and the analytical partial charge derivatives were developed in this work for the first time as given in Appendix A2. Computer timings for the

I. Development of the DFT-D4 London Dispersion Correction

calculation of the charges and their derivatives are given in Table 2.2 for different protein structures. The formal scaling of the procedure is $\mathcal{O}(N^3)$ with number of atoms N and hence the same as for the dispersion energy in D3-ATM and D4 (for a two-body only approach – abbreviated by 2B – the formal scaling reduces to $\mathcal{O}(N^2)$).

Table 2.2.: Computer timings in seconds for the calculation of energies (E), energies and analytical gradients (E+g), and analytical charge derivatives ($\partial\mathbf{q}/\partial\mathbf{R}_j$) for differently sized protein structures with their protein database (PDB) entry. All calculations have been conducted at four cores (each CPU: Intel(R) Core(TM) i7-7700K CPU@4.20GHz) with DFT-D4-2B, DFT-D4-ATM, or DFT-D4-MBD. Timings for D4-MBD are excluded for proteins with more than 1500 atoms.

PDB (atoms)	E(D4)			E+g(D4)	
	2B	ATM	MBD	ATM	$\partial\mathbf{q}/\partial\mathbf{R}_j$
2BEG(373)	0.07	0.20	2.11	0.25	0.01
1R0I(782)	0.22	1.32	37.08	2.18	0.04
1MOL(1562)	1.13	9.75	401.00	13.28	0.40
2ZOH(1929)	1.80	18.21	...	24.85	1.29
1YMB(2489)	3.45	38.70	...	48.26	2.24
1JS8(5988)	47.07	528.45	...	570.45	24.47

By using the definition of the Lagrangian given in equation 2.14, the analytical charge gradients are derived as

$$\begin{pmatrix} \frac{\partial\mathbf{q}}{\partial\mathbf{R}_j} \\ \frac{\partial\lambda}{\partial\mathbf{R}_j} \end{pmatrix} = \begin{pmatrix} \mathbf{A} & \mathbf{1} \\ \mathbf{1}^\top & 0 \end{pmatrix}^{-1} \times \left[- \begin{pmatrix} \frac{\partial\mathbf{A}}{\partial\mathbf{R}_j} & \mathbf{0} \\ \mathbf{0}^\top & 0 \end{pmatrix} \begin{pmatrix} \mathbf{q} \\ \lambda \end{pmatrix} + \begin{pmatrix} \frac{\partial\mathbf{X}}{\partial\mathbf{R}_j} \\ 0 \end{pmatrix} \right] \quad (2.16)$$

where the inverse of the indefinite $(N+1)$ matrix has been obtained by a Bunch-Kaufman factorization²⁴⁹ and inversion.

2.2.2. Two-body Dispersion Energy

The pairwise dispersion coefficients are then used to compute the corresponding dispersion energy in complete analogy to DFT-D3 by multiplying with a short-range damping function in order to apply the model in combination with standard DFAs. The DFT-D4 pairwise dispersion energy is given by

$$E_{\text{DISP}}^{(6,8)} = - \sum_{AB} \sum_{n=6,8} s_n \frac{C_{AB}^{(n)}}{R_{AB}^{(n)}} f_{\text{damp}}^{(n)}(R_{AB}), \quad (2.17)$$

I. Development of the DFT-D4 London Dispersion Correction

where s_n scales the individual multi-polar contributions (s_6 and s_8 for the dipole-dipole and dipole-quadrupole term, respectively), and $f_{\text{damp}}^{(n)}$ denotes the rational Becke–Johnson (BJ) damping function (denoted as BJ-damping (BJD) in the following).

$$f_{\text{BJD}}^{(n)}(R_{AB}) = \frac{R_{AB}^{(n)}}{R_{AB}^{(n)} + (\alpha_1 R_0^{AB} + \alpha_2)^{(n)}} \quad (2.18)$$

has become already the default in DFT-D3. For alternatives, see Ref. 122 and for a general discussion of damping functions in dispersion corrected DFT models, see Ref. 166. Equation 2.18 incorporates the functional-specific parameters α_1 and α_2 and the cutoff-radii defined as

$$R_0^{AB} = \sqrt{\frac{C_8^{AB}}{C_6^{AB}}}, \quad (2.19)$$

where the recursive relation between dipole-dipole and dipole-quadrupole dispersion coefficients is used as in DFT-D3⁴⁶.

$$R_{0,\text{BJ}}^{AB} = (\alpha_1 R_0^{AB} + \alpha_2). \quad (2.20)$$

Furthermore, we define the following expression for the rational damping term

$$R_{0,\text{BJ}}^{AB} = (\alpha_1 R_0^{AB} + \alpha_2). \quad (2.21)$$

2.2.3. Three-body Dispersion and Efficient Geometry Optimizations

The simplest way to include three-body effects is to use the well-known ATM term

$$E^{ABC} = \frac{C_9^{ABC} (3 \cos \theta_a \cos \theta_b \cos \theta_c + 1)}{(R_{AB} R_{BC} R_{CA})^3}. \quad (2.22)$$

Here, θ_a , θ_b , and θ_c are the internal angles of the triangle formed by R_{AB} , R_{BC} , and R_{CA} , while C_9^{ABC} is the triple-dipole constant given by

$$C_9^{ABC} = \frac{3}{\pi} \int_0^\infty d\omega \alpha^A(i\omega) \alpha^B(i\omega) \alpha^C(i\omega). \quad (2.23)$$

The numerical integration of the triple-dipole dispersion coefficient is possible using D4 polarizabilities, but due to the fact that the three-body energy contribution is rather small (at most 5-10% of E_{DISP}), the coefficients can be reasonably approximated as in the D3-ATM model by a geometric mean of dipole-dipole

I. Development of the DFT-D4 London Dispersion Correction

dispersion coefficients, i.e.,

$$C_9^{ABC} \approx \sqrt{C_6^{AB} C_6^{BC} C_6^{CA}}. \quad (2.24)$$

This approximation was already tested within the DFT-D3-ATM scheme for different element combinations and a typically small deviation of about 10–20% to the exact expression has been found⁴⁶. In the D4 model, the C_6 coefficients used to obtain the C_9^{ABC} are obtained from charge-neutral atomic polarizabilities (i.e., neutral atoms with $z^A = Z^A$). The finally used three-body dispersion energy expression is then given as

$$E_{\text{DISP}}^{(9),\text{ATM}} = \sum_{ABC} E^{ABC} f_{\text{damp}}^{(9)}(\bar{R}_{ABC}), \quad (2.25)$$

where the sum is over all atom triples ABC applied with a zero-damping scheme proposed by Chai and Head-Gordon¹²²

$$f_{\text{damp}}^{(9)}(\bar{R}_{ABC}) = \frac{1}{1 + 6(\bar{R}_{ABC})^{-16}}. \quad (2.26)$$

Equation 2.26 includes the averaged inter-atomic distance

$$\bar{R}_{ABC} = \left(R_{AB} R_{BC} R_{CA} / R_{0,BJ}^{AB} R_{0,BJ}^{BC} R_{0,BJ}^{CA} \right)^{1/3}, \quad (2.27)$$

which incorporates $R_{0,BJ}^{AB/BC/CA}$ (cf. equation 2.21). The final energy expression used is therefore given as

$$E_{\text{DISP}}^{\text{D4}} = E_{\text{DISP}}^{(6,8)} + E_{\text{DISP}}^{(9),\text{ATM}}. \quad (2.28)$$

Analytical gradients are available for this energy expression within the D4 implementation as tested against numerical derivatives.

2.2.4. Many-body Dispersion Energy

Depending on the size and the geometrical arrangement of the atoms, higher-order dispersion contributions (larger than three-body) can be of similar magnitude as three-body contributions and hence, for consistency, terms up to infinite order should be included to achieve a consistent description of all dipole-dipole interaction orders¹⁸⁹. Here, a conceptually simple but robust approach introduced originally by Cao and Berne²⁵⁰ is adapted, which has been made popular by Tkatchenko *et al.*²³⁹. Physically it is based on a coupling of atomic dipole polarizabilities in terms of quantum harmonic oscillators (QHOs). The coupled dipole model of QHOs serves as an approximation to describe the density-density

I. Development of the DFT-D4 London Dispersion Correction

response functions, which would otherwise be calculated, e.g., via the random phase approximation (RPA). The atomic response functions in a coupled dipole model allow a considerable reduction in the degrees of freedom (i.e., three QHOs per atom) and the computational costs. With this in mind, an alternative energy expression is proposed which consists of two parts. The first is to compose the two-body dipole-dipole and dipole-quadrupole interaction. The second part includes all dipole-dipole interactions up to infinite order, $E_{\text{DISP}}^{(n),\text{MBD}}$ ($n = 6, 9, 12, 15, \dots, \infty$). To avoid double counting of the two-body dipole-dipole energy, it is removed explicitly from the MBD energy according to

$$E_{\text{DISP}}^{\text{D4-MBD}} = E_{\text{DISP}}^{(6,8)} + \left(E_{\text{DISP}}^{(n),\text{MBD}} - E_{\text{DISP}}^{(6),\text{MBD}} \right). \quad (2.29)$$

Here we have exploited that $E_{\text{DISP}}^{(6)} = E_{\text{DISP}}^{(6),\text{MBD}}$ (see Appendix A2 for the complete derivation), which is the case in our consistent damping formulation for the two-body dispersion energy. It should be noted that this mutual consistency does not exist in the TS and MBD schemes of Tkatchenko and coworkers, which unfortunately, has obfuscated the scientific discussion about the relevance of many-body dispersion beyond two- and three-body interactions. Furthermore, rearranging to $E_{\text{DISP}}^{\text{D4-MBD}} = E_{\text{DISP}}^{(n),\text{MBD}} + E_{\text{DISP}}^{(8)}$ is not possible in the general case, as for double hybrid density functionals (abbreviated as DHDF) $s_6 \neq 1$, whereas this scaling cannot be applied to an individual term in the infinite-order MBD energy.

2.2.5. Definition of the D4 Default Model and Use of Alternative Charges

At first, it should be emphasized that the D4 model only turns into a DFT-D4 method when used in combination with a specific density functional. If just polarizabilities or dispersion coefficients are calculated, the results are functional independent. The D4 default setting uses classical EEQ partial charges to scale atom-in-molecule polarizabilities due to their characteristics of being robust and efficient. The quality of the used charges is important but not essential for the finally obtained accuracy. The D4 model also works well with other charges, e.g., with partial charges obtained by the recently developed GFN2-xTB tight-binding method. This indicates its robustness and that under almost all circumstances D4 is similar or better than D3 but never worse (by construction). Generally, the use of three types of reference charges is currently implemented in the model: EEQ gas phase charges q (default), Mulliken-type partial charges q^{TB} from the GFN2-xTB tight-binding method²⁴⁴, and DFT Hirshfeld charges q^{DFT} (PBE0¹¹⁶/def2-TZVP²⁵¹ level). Hirshfeld partial charges at the PBE0/def2-TZVP level of theory were also used to parameterize the EEQ model. If DFT charges should be used they must be calculated separately such that they can be fed into the model.

I. Development of the DFT-D4 London Dispersion Correction

For a given type of charges (classical or TB or DFT) different reference effective nuclear charges $z^{A,\text{ref}}$, as introduced in equation 2.4, are stored and accordingly used in the D4 program. The DFT-D4 default model always includes an ATM term as described in section 2.2.3 (see equation 2.28 for the total energy expression). Nevertheless we offer the possibility to use DFT-D4 including MBD effects (termed DFT-D4-MBD) in terms of an energy correction. The rational BJ-damping function is always applied. The use of other damping functions is not supported since we obtained in many test calculations the overall best results always with the BJ-damping for several DFA classes. When using this so-defined method, it should be abbreviated as “method-D4” (where “method” represents either a DFA or Hartree-Fock), which allows simple and clear referencing in future publications. If charges other than the default are used, this could be indicated by adding e.g. “(TB)” or “(PBE0/def2-TZVP)”. Unfortunately, the previous DFT-D3 method has partly lost a clear abbreviation over the years, since additional parameterizations or extensions to the method have been assigned with various nomenclatures (see, e.g., DFT-D3(0)⁴⁶, DFT-D3(BJ)¹⁶⁶, DFT-D3(CSO)^{73,252}, DFT-D3(op)⁷⁵, DFT-D3M⁷⁴). In the next sections, the technical details of the calculations are given first, followed by benchmarking of this finalized D4/DFT-D4 method for dispersion coefficients, interaction energies, conformational energies, as well as in general thermochemical applications. Last, optimized covalent as well as noncovalent geometries are discussed.

2.2.6. Technical Details

All ground state DFT calculations were performed with either TURBOMOLE 7.0.2, and TURBOMOLE 7.2.1 (for all SCAN^{114,253} calculations) or ORCA 4.0.1^{58,145}. Standard exchange-correlation energy integration grids (TURBOMOLE: *m4*, ORCA: *grid4*, *finalgrid5*) and usual convergence criteria for the self-consistent field convergence (10^{-7} Hartree) were used. The resolution of the identity (RI) approximation^{207–209} was applied in all calculations for the electronic Coulomb energy contribution. Ahlrich’s type quadruple-zeta basis sets (def2-QZVP²⁵⁴) were used throughout if not stated otherwise.

BJ-damping function parameterization The functional specific parameters of the BJ-damping function have been determined using a Levenberg–Marquardt least-squares minimization to reference interaction energies of established noncovalent interaction benchmark sets (S66x8²⁰³, S22x5²⁰⁴, NCIBLIND10⁸). In total, 98 dissociation curves with 718 reference data points of high accuracy were used for regression. The use of this new fitting set enabled parameterizations of such DFAs for which BJ-damping parameters could not be obtained successfully in earlier works due to over-binding tendencies (e.g., Minnesota functionals, see Ref.

57).

Molecular Dispersion Coefficients All molecular dynamic dipole polarizabilities $\alpha(i\omega)$ were calculated using TD-DFT^{164,165}. As in D3, a variant of the PBE0 hybrid functional was used, with a Fock-exchange admixture of 37.5% (dubbed PBE38). This method has already proved its accuracy and robustness in previous works^{46,210}. The atomic orbital (AO) basis sets used in the TD-DFT calculations are of doubly augmented def2-QZVP quality very closely representing the complete basis set (CBS) limit for this property. Here, for the respective systems, each hydrogen has been augmented with additional (2s/2p), each main group element with additional (2s/2p/1d), and each transition metal with additional (2s/2p/1d/1f) Gaussian primitive functions. The exponent-extrapolation of the additional primitives was done with the subprogram `DEFINE` from TURBOMOLE 7.0.2. The following def2-ECPs are used: ECP-28 covering 28 core electrons (for Rb, Sr, Y-Cd, In-Sb, Te-Xe, Ce-Lu), ECP-46 covering 46 core electrons (for Cs, Ba, La), and ECP-60 covering 60 core electrons (for Hf-Hg, Tl-Bi, Po-Rn) as defined in Ref. 251. Comparative calculations with the XDM model were conducted with the `POSTG`²⁵⁵ program based on TURBOMOLE generated wave function *wfn*-files. Unfortunately, `POSTG` only supports a limited number of basis sets, since each basis set has its own parameterization linked to the applied density functional. Therefore, all `POSTG` input files were calculated with the PBE¹⁰²/def2-TZVP setup. Furthermore, calculations were also carried out with the TS based MBD method of Tkatchenko et al. using the corresponding standalone code²⁵⁶. The required relative Hirshfeld volumes were taken from `POSTG` calculations performed at the PBE/def2-TZVP level. All geometries of the TD-DFT derived organometallic molecular C_6 coefficient benchmark set (abbreviated as TOMC6 benchmark set) were obtained on the TPSS¹⁰⁵-D3(BJ)-ATM/def2-TZVP level of theory and molecular reference dispersion coefficients are shared in Appendix A2.

Noncovalent Reference Interaction Energies for L7 and S30L Benchmark Sets We use recently published reference values (see Supplementary Material of Ref. 257) for the L7²⁵⁸ and the S30L²⁵⁹ benchmark sets. They were obtained from local CCSD(T) calculations together with a special purpose CBS estimation scheme including the geometry deformation energy and Boys/Bernardi counter-poise (CP) correction²⁶⁰ (DLPNO-CCSD(T)^{261,262} in its sparse matrix implementation²² employing the CBS* protocol as described in reference²⁶³).

Reference Energies for Thermochemical Benchmarks The reference conformational energies and structures of SCONF²⁶⁴, PCONF21^{265,266}, ICONF⁵⁷,

and UPU23²⁶³ subsets were extracted from the GMTKN55 database (see Ref. 57 for further information and our homepage²⁶⁷ for the entire database). For each benchmark set, the respective reference data with the accompanying level of theory are listed in Appendix A2. The reference energies and structures for the MOR41 transition metal reaction benchmark set were taken from previous work (see Ref. 268 and our homepage²⁶⁹ for the entire database).

Tetrakis(isonitrile)rhodium(I) Dimer and Monomer Calculations For the generation of reference association energies of the tetrakis(isonitrile)rhodium(I) complex, CP-corrected DLPNO-CCSD(T) calculations with tight thresholds and extended basis sets (def2-TZVPP(VeryTightPNO²⁷⁰) / def2-QZVPP(TightPNO²⁷⁰)) were conducted using ORCA 4.0.1. A basis set extrapolation was performed using optimized exponents proposed by Neese and Valeev²⁷¹. The deformation energy of the monomers (0.42 kcal mol⁻¹) was also taken into account. The error bar of the calculated interaction energy is estimated to about ± 0.5 kcal mol⁻¹. Geometries have been obtained at the PBEh-3c²⁷² level of theory and verified as minimum structures by frequency calculations.

2.3. Results

2.3.1. Molecular Dispersion Coefficients

We have taken reference molecular dispersion coefficients which were determined experimentally from dipole oscillator strength distributions (DOSD) as described in previous works by Meath and co-workers^{273,274}. From this data, a benchmark set has been compiled in Ref. 49 consisting of 1225 molecular dispersion coefficients for systems ranging from di-hydrogen to octane and other nonorganic molecules such as SF₆ or O₂. The respective statistical evaluation for D3³⁸, D4, D4(TB), the local response dispersion method (LRD)¹⁸², and TS⁴⁹ for all systems in the DOSD benchmark set are given in Table 2.3.

I. Development of the DFT-D4 London Dispersion Correction

Table 2.3.: Top (entries labeled for DOSD set): Statistical measures for the relative deviation (in %) of calculated molecular C_6 dispersion coefficients for different approaches with respect to experimental values for a molecular benchmark set consisting of 50 molecules. For D3, LRD, and TS values are taken from Refs. 38,49,182. Bottom (entries labeled for TOMC6 set): Statistical measures for the relative deviation (in %) of calculated homo-molecular C_6 dispersion coefficients for different approaches with respect to theoretical TD-DFT values for a transition metal benchmark set of 25 complexes for the complete set and 15 complexes for the subset. The best values are highlighted in bold font.

		Measure	D4	D4(TB)	D3	LRD	TS
DOSD		MAD	3.8	3.9	4.7	6.1	5.3
		MD	-0.1	0.3	-2.4	-2.5	-2.7
		SD	5.1	5.3	5.2	7.7	7.3
		AMAX	29.1	34.7	23.9	52.9	44.0
			D4	D4(TB)	D3	XDM	MBD
TOMC6	Subset	MAD	8.7	8.9	20.5	9.4	13.7
		MD	-1.7	-2.3	-9.6	1.4	13.7
		SD	11.2	11.4	28.1	13.3	6.1
		AMAX	29.7	25.1	80.8	36.6	26.2
		Measure	D4	D4(TB)	D3		
Complete	MAD	7.0	7.9	12.0			
	MD	-2.2	-3.6	-5.5			
	SD	9.3	9.4	15.7			
	AMAX	29.7	25.1	56.1			

For medium-sized organic and inorganic molecules, D4/D4(TB) further improves upon the already accurate D3 model (mean absolute deviation, MAD, of 3.8% and 3.9% vs. 4.7%). Other statistical measures for D4/D4(TB) are also lowered in comparison to values for the competitors which indicates a robust and consistent improvement in the description of pairwise dispersion coefficients for such systems. In the authors' opinion, the achieved MAD of 3.8% closely approaches the inherent accuracy of the underlying TD-DFT calculations and is thus difficult to improve further. For comparison, an assessment of the XDM method yielded an MAD of 10.0% for a similar small-molecule database²²⁹, while a number of vdW density functionals yield even larger deviations for asymptotic molecular C_6 coefficients²⁷⁵. Note that the resulting DFT-D4 interaction energy errors in the asymptotic regime of about 4.0% are comparable or even smaller than, e.g., residual errors in WFT energy calculations employing large but finite triple- or quadruple-zeta basis sets. Since the DOSD set excludes the important class of transition metal complexes, we have created a corresponding benchmark

I. Development of the DFT-D4 London Dispersion Correction

set consisting of computed molecular dipole-dipole dispersion coefficients derived from TD-DFT dynamic reference polarizabilities at the PBE38/daug-def2-QZVP level of theory. This benchmark set consists of 25 organometallic complexes (see left side of Figure 2.7 for example structures) and is dubbed as TOMC6 which stands for TD-DFT derived organometallic molecular C_6 coefficient benchmark set.

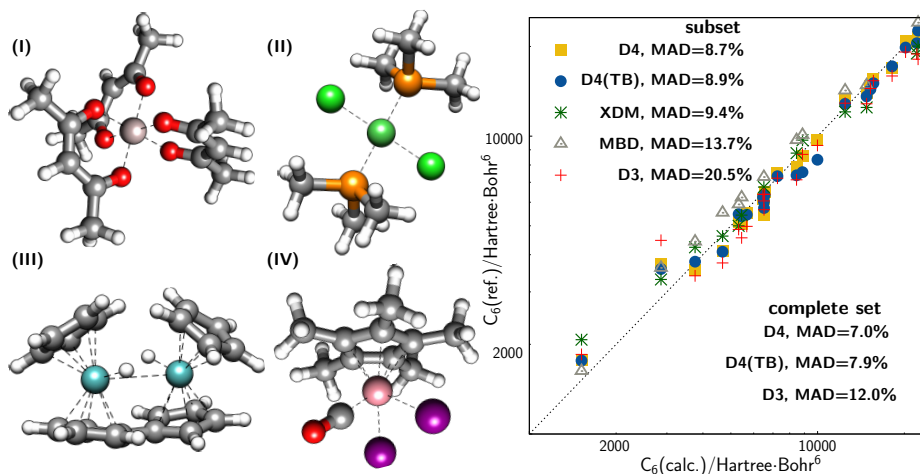


Figure 2.7.: (left) Example complexes from the TOMC6 set including (I) aluminium, (II) nickel, (III) molybdenum, and (IV) cobalt to demonstrate the diversity of the benchmark set. Structures and reference molecular dispersion coefficients are listed in Appendix A2. (right) Correlation plot between reference molecular dispersion coefficients of transition metal complexes obtained by hybrid TD-DFT (numerically integrated from molecular $\alpha(i\omega)$ values according to equation 2.9) and molecular ones derived from pairwise dispersion coefficients with D3, D4, D4(TB), XDM, and MBD models.

Results for the D3, D4, D4(TB), XDM, and MBD schemes are given on the right side of Figure 2.7 together with their statistical evaluation listed in Table 2.3. Here, the TOMC6 set was divided into two parts because several systems could not be treated with XDM and MBD for technical reasons. The resulting smaller set for which also XDM and MBD data are available is termed “subset” in the following. In accordance with the previously discussed DOSD benchmark set, the use of scaled polarizabilities in D4/D4(TB) improves upon the accuracy of the D3 method. For this set only XDM is able to achieve a comparable accuracy, however, at a substantially larger computational effort because a properly converged DFT electron density is required in XDM. Furthermore, XDM energies need to be integrated numerically over a fine grid to avoid numerical noise. The MBD model achieves a result which is in between of D4/D4(TB) and D3 (here the molecular dispersion coefficient changes for different range-separation parameters – we used $\beta^{\text{PBE}} = 0.83$ – and, therefore, for different DFAs within MBD). Notably, all methods yield larger errors for the electronically more complicated systems in the

I. Development of the DFT-D4 London Dispersion Correction

TOMC6 (sub)set than for the DOSD molecules. Nevertheless, the asymptotic D4 error of about 7.0% is still smaller than typical errors of DFAs for other correlation energy effects. This will be further discussed below for the thermochemistry of transition metal complexes. The application of Hirshfeld partial charges at the PBE0/def2-TZVP level of theory slightly worsen upon the D4(TB) result with an MAD of 9.5% for the complete set. The fact that calculated D4 molecular dispersion coefficients have the smallest errors with respect to reference values when applying the EEQ charges additionally motivates their use as default (as already defined in section 2.2.5). An explicit discussion of the effect of using different charges is avoided, whereby DFT-D4 results with GFN2-xTB charges are shared in Appendix A2 for interaction energies and structures.

2.3.2. Noncovalent Interactions and Conformational Energies

As shown in the section 2.3.1, the pairwise dispersion coefficients for organic/i-norganic molecules and transition metal complexes are improved with the D4 method. In general, it is assumed that improved dispersion coefficients in DFT-D type methods are associated with improved noncovalent interaction energies. This assumption is to be verified in this section for various small to large molecule benchmark sets. Reference interaction energies refer to the CCSD(T) or DLPNO-CCSD(T) level of theory with tight threshold settings and CBS extrapolation mostly taken from Ref. 257.

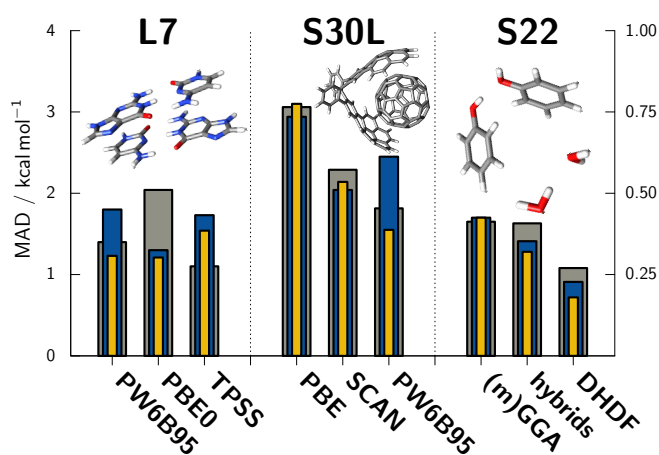


Figure 2.8.: Comparison of MAD values for three typical noncovalent interaction benchmark sets (L7, S30L, S22) and various standard DFAs. Density functionals corrected by D3(BJ)-ATM are shown in gray (bar width 1.0), DFT-D4 results are shown in blue (bar width 0.4), and DFT-D4-MBD results are shown in yellow (bar width 0.2). For the S22 benchmark set the scaling of the MAD axis was adjusted accordingly and values were obtained by averaging over several typical DFAs (eight meta-GGAs, nine hybrids, and three DHDFs).

Figure 2.8 shows interaction energies in benchmark sets of increasing molecule size

I. Development of the DFT-D4 London Dispersion Correction

which are mainly stabilized by London dispersion: S22²⁷⁶, L7²⁵⁸, and S30L²⁵⁹. Various typical noncovalent interaction motifs like hydrogen and halogen bonding, π - π stacking, nonpolar dispersion, CH- π , and cation-dipolar interactions are represented. The description of noncovalent interactions in the larger systems is slightly (S30L) to largely (L7) improved at the DFT-D4-MBD level compared to the already well performing DFT-D3(BJ)-ATM method. The only exception is the TPSS-D4-MBD treatment for the L7 set which is worse than the D3(BJ)-ATM corrected values. Note that residual MAD values of about 1 kcal mol⁻¹ for L7 and 1-2 kcal mol⁻¹ for S30L are not far from the accuracy of the reference data. For the S30L benchmark the MAD values increase when the ATM term is neglected, i.e., for DFT-D3 (DFA/MAD(DFA-D3(BJ)))/MAD(DFA-D3(BJ)-ATM), in kcal mol⁻¹): PW6B95/3.4/2.4, TPSS/4.1/3.6, B3LYP/5.9/4.1, PBE/2.3/2.8. For the S22 set, we use averaged MAD values for different DFA classes arranged according to Jacob's ladder. Data for eight (meta) generalized gradient approximation DFAs, abbreviated as (m)GGA, (namely BLYP^{103,104}, BP86²⁷⁷, M06L^{106,278}, O-LYP^{279,280}, PBE, revPBE²⁸¹, RPBE²⁸², and SCAN), nine hybrid DFAs (M06²⁸³, B3LYP^{117,118}, B3LYP, M062X, O3LYP, PBE0, PW6B95²⁸⁴, TPSS0, and TPSSh), and three DHDF (DSD-BLYP²⁸⁵, DSD-PBEB95²⁸⁶, and PWPB95²⁸⁶) are used to obtain averaged MAD values for S22. For this important and prototypical noncovalent interaction (NCI) benchmark, D4 outperforms D3(BJ)-ATM especially for hybrids and DHDFs.

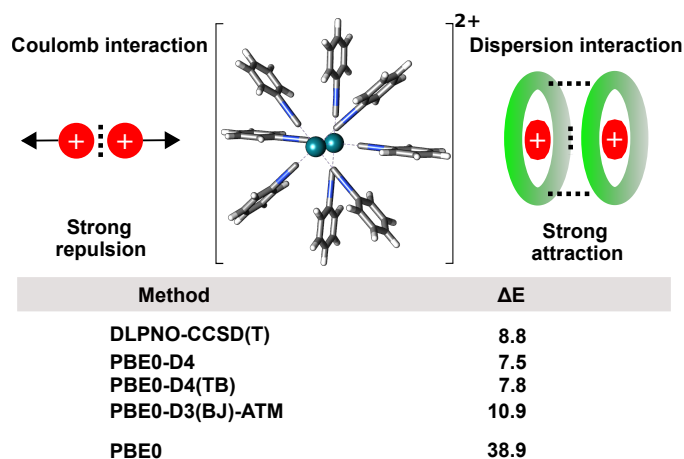


Figure 2.9.: Shown is a cationic dirhodium complex with the respective association energy ΔE in the gas phase where the repulsive cation-cation interaction is almost compensated by attractive London dispersion interactions schematic adapted from Ref. 287.

Figure 2.9 shows an interesting example for strong London dispersion interactions in a doubly positively charged organometallic dirhodium complex. Here, the dominant Coulomb repulsion can almost be compensated by dispersion interactions²⁸⁷

I. Development of the DFT-D4 London Dispersion Correction

in the gas phase (compare the association energy $\Delta E(\text{PBE0})$ in Figure 2.9 with its corresponding dispersion corrected values). This and related complexes have been studied intensively and the property of oligomer formation in solution has been an “open case” for many years^{288–290}. Quantum chemical calculations have been able to assign the main binding motif of this highly charged system to be the London dispersion thus making it an ideal test case for the DFT-D4 method. The theoretical reference association energy was calculated with an accurate local coupled-cluster protocol (see technical details section) and is compared to the dispersion and Boys-Bernardi CP-corrected PBE0/def2-QZVPP values.

Counterintuitively, the D4 corrected gas phase interaction is more favorable (less positive association energy) than the corresponding D3 value. This is initially surprising, since cationic compared to neutral complexes should feature smaller dispersion coefficients as accounted for in D4 but not in D3. According to a detailed analysis, the observed increased dispersion interaction in DFT-D4 is based on new reference systems that have been added to some elements within the D4 model (e.g., RhH_5 , $\text{CN}^{\text{Rh}} = 4.70$ and C_6H_6 , $\text{CN}^{\text{C}} = 2.92$), increasing the homo-atomic dispersion coefficient for those elements (e.g., for rhodium atoms within the complex the difference between D3 ($C_6^{\text{AA}}(\text{D3})=244.7$ Hartree Bohr⁶) and D4 ($C_6^{\text{AA}}(\text{D4})=294.9$ Hartree Bohr⁶) is significant). Furthermore, the molecular charge is distributed over all atoms in the molecule and is not centered on the rhodium atoms. Thus, the partial charges of the rhodium atoms are only marginally changed when the neutral dimer complex is turned into the dication (the change in q^{Rh} is less than 0.1). In summary, the stronger binding in D4 which is in better agreement with the localized CCSD(T) reference value (for both types of partial charges – EEQ or TB) can be explained by larger atomic dispersion coefficients in combination with only a small decrease of atomic polarizabilities due to small partial charges on the central rhodium atoms. DFT-D4 also yields comparable or higher accuracies for (bio)chemically important conformational energies in various test systems. Figure 2.10 exemplifies this for sugar conformers (SCONF) as well as for tri- and tetra-peptide conformers (PCONF21) both taken from the GMTKN55 database.

I. Development of the DFT-D4 London Dispersion Correction

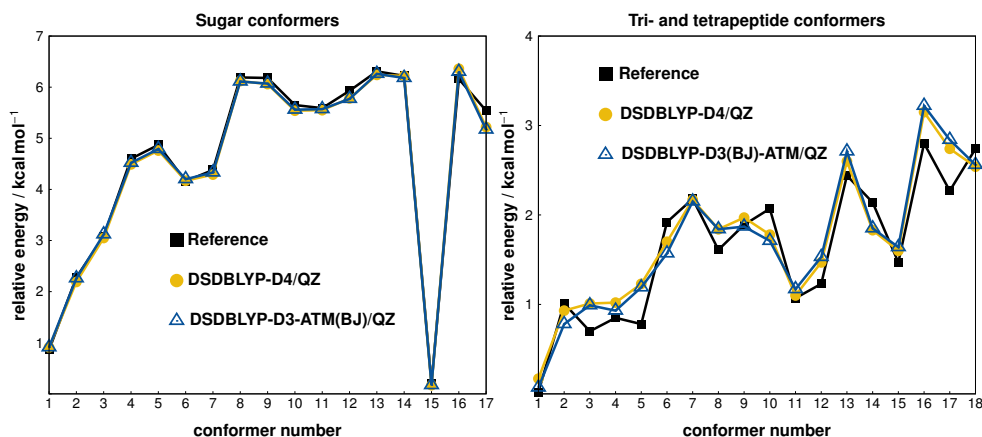


Figure 2.10.: Conformational energies for two benchmark sets SCNF (left) and PCONF21 (right) in comparison to accurate reference values at the DLPNO-CCSD(T)/TightPNO/CBS level of theory⁵⁷. For all calculations a def2-QZVP basis set (abbreviated as QZ) has been applied.

Additionally, results for conformational energies of inorganic molecules (ICONF), as well as for RNA backbone conformers (UPU23) are given in Table 2.4.

Note that in contrast to DFT-D3, the DFT-D4 training set used for the determination of the BJ-damping parameters does not contain conformational energies. In Figure 2.10 we show DSD-BLYP based results as an example and provide statistical evaluations for other selected DFAs (PBE, B3LYP, and PW6B95) in Table 2.4. Overall, the conformational energies are generally improved for PBE, B3LYP, and PW6B95 by applying DFT-D4/DFT-D4(TB) compared to DFT-D3(BJ)-ATM. The reduction of the MAD is often noticeable (about 0.1 kcal mol⁻¹) but sometimes significant, e.g., 0.20–0.25 kcal mol⁻¹ for peptides and RNA structures with PBE or B3LYP. Especially for the peptide set the improvement is large when compared to the small averaged absolute relative energy of only 1.62 kcal mol⁻¹.

2.3.3. Thermochemistry

As discussed in section 2.3.1, the D4 model is particularly good for systems in which atomic partial charges show significant deviations from the reference systems used in the Gaussian weighting procedure (cf. equation 2.8). Typical examples are transition metal complexes, which contain d-block elements in varying oxidation states. We have discussed the improved description of pair-wise dispersion coefficients for transition metal complexes for the TOMC6 set (see section 2.3.1). In the following, the thermochemistry of transition metal compounds is investigated employing the recently composed MOR41 set consisting of 41 closed-shell transition metal reactions of uncharged molecules. The estimated maximum error of the reference reaction energies is about 2 kcal mol⁻¹ (see Ref. 268 for further information). The reactions in this set typically occur in homogeneous catalysis,

I. Development of the DFT-D4 London Dispersion Correction

Table 2.4.: Conformational energies calculated with three widely used dispersion corrected DFAs (PBE, B3LYP, and PW6B95) with the def2-QZVP basis set. All statistical measures are given in kcal mol⁻¹ relative to the reference energies. The best result for each measure is highlighted in bold, DFT-D3(BJ)-ATM is abbreviated by D3, DFT-D4 is abbreviated by D4, and DFT-D4(TB) by D4(TB). The average reference energy over all entries in the set $\overline{|\Delta E|}$ are taken from Ref. 57.

Sugar conformers (SCONF, $\overline{ \Delta E } = 4.60$)									
Measure	PBE			B3LYP			PW6B95		
	D3	D4	D4(TB)	D3	D4	D4(TB)	D3	D4	D4(TB)
MAD	0.78	0.88	0.77	0.29	0.33	0.23	0.24	0.28	0.20
MD	0.28	0.34	0.29	-0.14	-0.07	-0.14	-0.01	0.04	-0.02
SD	0.98	1.09	0.94	0.48	0.58	0.42	0.38	0.43	0.36
AMAX	2.73	2.96	2.67	1.73	2.07	1.64	1.21	1.33	1.12
Tri- and tetrapeptides (PCONF21, $\overline{ \Delta E } = 1.62$)									
MAD	1.20	0.99	1.04	0.53	0.35	0.30	0.48	0.49	0.49
MD	-0.54	-0.51	-0.53	-0.04	0.03	0.01	0.34	0.36	0.38
SD	1.44	1.24	1.18	0.60	0.41	0.37	0.58	0.60	0.46
AMAX	2.51	2.31	2.36	1.11	0.90	0.88	1.05	0.98	0.98
Inorganic conformers (ICONF, $\overline{ \Delta E } = 3.27$)									
MAD	0.31	0.31	0.31	0.28	0.28	0.27	0.22	0.22	0.22
MD	0.09	0.09	0.10	-0.06	-0.08	-0.07	0.04	0.02	0.02
SD	0.38	0.40	0.40	0.39	0.42	0.39	0.33	0.33	0.34
AMAX	0.84	1.12	1.11	0.99	1.15	0.98	0.90	0.83	0.85
RNA backbone conformers (UPU23, $\overline{ \Delta E } = 5.72$)									
MAD	0.57	0.51	0.48	0.68	0.60	0.54	0.66	0.63	0.59
MD	0.36	0.27	0.20	0.55	0.42	0.31	0.52	0.49	0.42
SD	0.71	0.63	0.58	0.80	0.70	0.57	0.80	0.76	0.58
AMAX	1.67	1.62	1.50	1.57	1.50	1.33	1.65	1.55	1.44

i.e., complexation reactions, oxidative additions, and ligand exchange reactions. For the MOR41 set, the D4 model outperforms D3(BJ)-ATM for all tested DFAs (the only exception is PW6B95-D4). This is particularly noticeable for the well performing double hybrid DFAs DOD-PBE²⁹¹, and DSD-PBE²⁹¹ or hybrid DFAs (especially for PBE0) for which it is now possible to almost reach the estimated error level of the reference method. Hence, the combination of such DFAs with D4 represents an efficient route to obtain reaction energies in transition metal thermochemistry applications. During the D4 parameterization process, damping parameters for some DFAs could also be “repaired”. The RPBE functional is given as example, where the published parameters were apparently not optimal (see Supplementary Material of Ref. 57 for original values). A recently published work shows furthermore that DFT-D4 is particularly suitable for the description of noncovalent interactions in organometallic complexes²⁹². For main group ele-

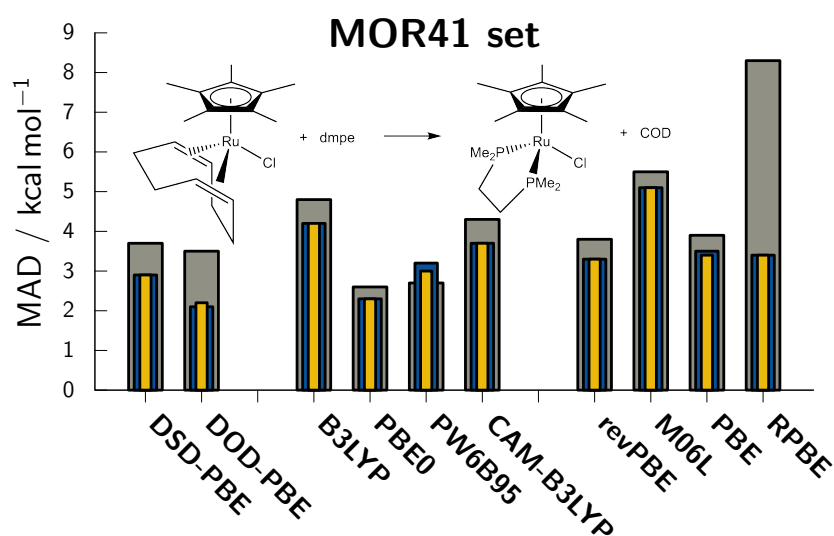


Figure 2.11.: Comparison of MAD values for MOR41 reaction energies. The inset shows one example reaction (reaction 28 in the set). Various density functionals from different rungs of Jacob's ladder are investigated. Shown are deviations of D3(BJ)-ATM corrected (gray, bar width 1.0), D4 corrected (blue, bar width 0.4), and D4-MBD corrected (yellow, bar width 0.2) DFT computed reaction energies to reference values with an estimated uncertainty of $\approx 2 \text{ kcal mol}^{-1}$.

ments, the general performance of DFT-D4 for thermochemistry and kinetics is assessed using the large GMTKN55 database. This database allows an evaluation for a wide variety of chemical problems and provides a large number of 2462 systems resulting in 1505 relative energies.

Figure 2.12 shows results for several dispersion-corrected DFAs grouped according to Jacob's ladder plotted with their weighted mean total absolute deviations (WTMAD-2, see Ref. 57 for the exact definition). The figure is divided into two parts describing the performance for the entire GMTKN55 database (termed as GMTKN55 full) and for all its NCI subsets (shown inverted and termed as GMTKN55 NCIs). Overall for this typical selection of DFAs, DFT-D4 represents a retention or small improvement over DFT-D3(BJ)-ATM for general thermochemistry. No single outlier in the huge number of systems in GMTKN55 was detected. The improvement obtained with DFT-D4 is more pronounced in the NCI subsets than for the entire database because in the former the dispersion contributions are relatively larger than for most "normal" chemical reactions. A direct comparison between DFT-D4 (ATM, MBD either with EEQ or TB charges) and nonlocally corrected DFT (DFT-NL) for this NCI subsets shows a clear improvement when applying D4 (see Table 2.5).

I. Development of the DFT-D4 London Dispersion Correction

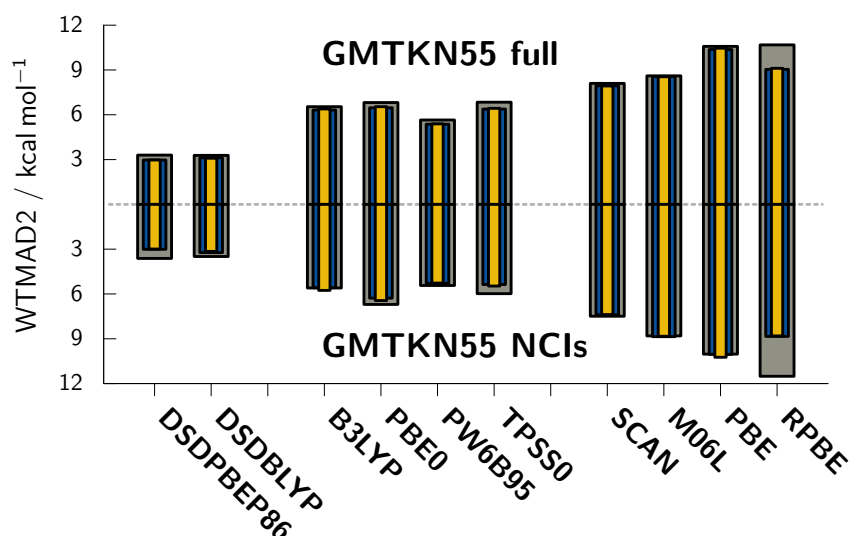


Figure 2.12.: Comparison of weighted mean deviations (WTMAD-2 values) for the entire GMTKN55 set and its noncovalent interaction subsets. Shown are deviations of DFT-D3(BJ)-ATM (gray), DFT-D4 (blue), and DFT-D4-MBD (yellow) values to reference data (see technical details section for further information).

Table 2.5.: WTMAD-2 values over all NCI subsets of the GMTKN55 benchmark database given in kcal mol^{-1} for DFT-D4 ((EEQ/TB)-ATM, (EEQ/TB)-MBD) or DFT-NL which were extracted from Ref. 293.

DFA	EEQ		TB		
	ATM	MBD	ATM	MBD	DFT-NL
B3LYP	5.58	5.76	6.29	6.36	6.03
PW6B95	5.29	5.27	5.38	5.50	5.87
DSD-BLYP	3.23	3.15	3.09	3.12	3.18

Importantly, the remaining MAD of $2.0 \text{ kcal mol}^{-1}$ for the MOR41 set and the WTMAD-2 of $2.0\text{--}3.0 \text{ kcal mol}^{-1}$ for GMTKN55 with the best functionals is not far from the accuracy of the underlying reference methods. The s_6 damping parameters for the double hybrid DFAs (which is unity for all lower-rung DFAs) has been constrained in the fitting according to the procedure of Ref. 46, i.e., we have not followed the construction scheme of Martin and co-workers²⁹¹ for its determination. This constraint, however, does not affect their accuracy which is actually significantly increased with DFT-D4 compared to the already very accurate DFT-D3 versions. Overall, the performance of D4 and D4-MBD is very

similar for the whole GMTKN55 benchmark database which shows that an ATM treatment is sufficient, if the damping function is chosen in a consistent manner (see Secs. 2.2.2 and 2.2.4).

2.3.4. Covalent and Noncovalent Structures

In order to investigate the DFT-D4 accuracy more closely, various standard benchmark sets for bond distances in equilibrium geometries are discussed here. This is of particular importance because structure determination is a common application area of DFT methods. First, covalent bond lengths are to be investigated, whereby noncovalent distances, and entire equilibrium structures are also examined in this section. All geometries discussed here are fully optimized employing an Ahlrich's type quadruple-zeta AO basis set (def2-QZVP²⁵⁴). The sets used for testing covalent bond lengths consist of molecules formed by the first or second row main group elements of the periodic table (LMGB35), molecules which are composed of main group elements of the third or higher rows (HMGB11), and 3d-transition metal complexes with a total of 50 analyzed bond lengths as compiled by Bühl and Kabrede²⁹⁴ (TMC32). For a detailed description of the former benchmark sets see Ref. 272. These sets are ideally suited also for "cross-checking", since many of the here treated elements were not part of the D4 parameterization process (only the elements H, C, N, and O are present in the BJ-damping function fit), which was furthermore based solely on energies. Figure 2.13 shows mean absolute deviations from reference values for three typical D3(BJ)-ATM and D4 dispersion-corrected DFAs and a statistical evaluation of all three benchmark sets is given in Appendix A2.

Inspection of Figure 2.13 shows only marginal differences between DFT-D4 and DFT-D3(BJ)-ATM for bond lengths which is expected because dispersion corrections mostly affect the noncovalent distance regime which is not really covered in these relatively small molecules tested. The tiny worsening observed for HMGB11 and for the TMC32 benchmark (the MAD increases by less than 0.1 pm) are practically irrelevant. Small differences between DFT-D4 and DFT-D3(BJ)-ATM are found for equilibrium rotational constants B_e while larger differences occur for intermolecular distances in the S66²⁹⁵ noncovalent equilibrium complex benchmark (as derived from data for the S66x8 benchmark set²⁰³). The B_e values can be considered as a measure for the quality of a complete molecular structure. Its accurate computation requires a consistently good description of covalent bond lengths as well as of nonbonded distances and small changes of internal rotational degrees of freedom may result in rather large deviations of a few percent for B_e . As already discussed in the literature, dispersion corrections to DFT typically increase B_e values (shrink molecular size) significantly by about 0.5-1.5%²⁹⁶, thereby in

I. Development of the DFT-D4 London Dispersion Correction

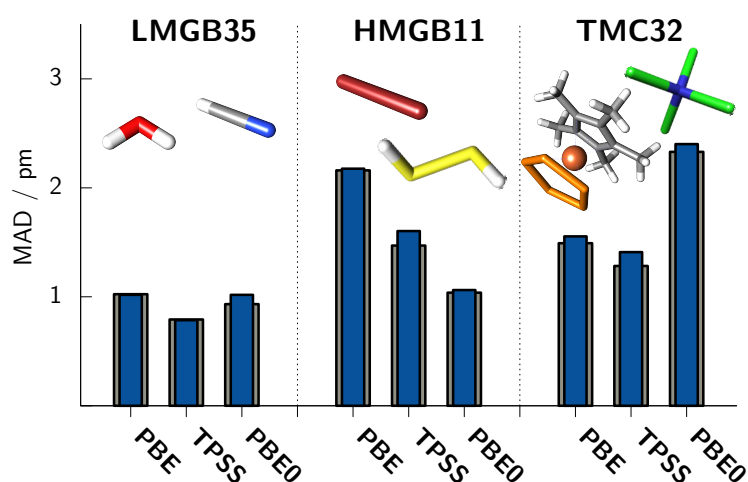


Figure 2.13.: Mean absolute deviations from reference values for covalent bond lengths for the LMGB35, HMGB11, and TMC32 benchmark sets with three DFAs. Gray bars: DFT-D3(BJ)-ATM (bar width 1.0), and blue bars: DFT-D4 (bar width 0.4).

general improving the agreement with the reference data.

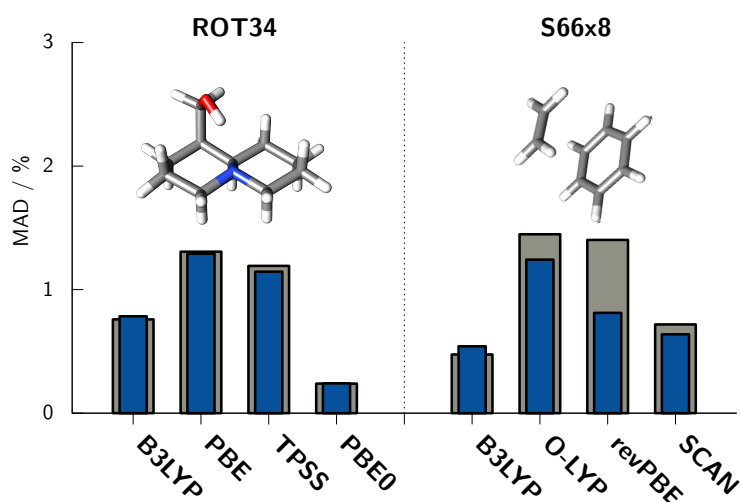


Figure 2.14.: Mean relative deviations from reference values for two benchmark sets representing the quality of entire equilibrium structures (rotational constants, ROT34) and noncovalent center-of-mass equilibrium distances (derived from S66x8) for seven DFAs. Gray bars: DFT-D3(BJ)-ATM (bar width 1.0), blue bars: DFT-D4 (bar width 0.4).

Figure 2.14 shows the relative MAD in % of computed equilibrium rotational constants compared to back-corrected experimental values for the ROT34 benchmark set²²⁰. Here, dispersion corrected PBE0 yields accurate molecular structures within the uncertainty of the reference data while dispersion corrected TPSS and

I. Development of the DFT-D4 London Dispersion Correction

PBE on average overestimate molecular size (see the statistical evaluation in Appendix A2). Dispersion corrected B3LYP provides slightly enlarged molecular structures where both, the D4 and the D3(BJ)-ATM correction, perform equally well. All in all, the high quality of covalent equilibrium geometries obtained with DFT-D3(BJ)-ATM is retained with DFT-D4. Noncovalent equilibrium geometries are considered in Figure 2.14. Reference coupled-cluster interaction energies taken from Ref. 203 for eight different shifted center-of-mass (CMA) distances were interpolated to obtain reference CMA distances for all complexes in the S66 set. The DFT computed CMA distances were obtained in the same way to allow a direct comparison to the reference values. As can be seen from this plot, the D4 model yields a slight (O-LYP and SCAN) to enormous improvement (revPBE) compared to the already very accurate DFT-D3(BJ)-ATM geometries. For the standard DFAs PBE, TPSS, and PBE0 shown in Figure 2.13, D4 performs slightly better or equally well than D3-ATM. Note, that the relative error for calculated CMA distances without dispersion correction is about one order of magnitude larger and that the very small residual relative deviations of 1.0% or less are similar for mostly covalent (ROT34) and noncovalent (S66) sets, respectively.

2.4. Summary and Conclusions

We presented the theory and main features of the final D4 method, in which charge-scaled atom-in-molecule dipole polarizabilities are interpolated by means of an atomic coordination number within a Gaussian weighting procedure to generate charge- and geometry-dependent atom-in-molecule polarizabilities $\alpha(i\omega)$. The partial charges used in the polarizability scaling are obtained by default with a classical electronegativity equilibration (EEQ) model. As fall-back levels, TB based Mulliken-type partial charges q^{TB} (GFN2-xTB) or DFT based Hirshfeld partial charges q^{DFT} (PBE0/def2-TZVP) are proposed. The polarizabilities are then numerically integrated at runtime of the D4 code to obtain system-dependent dipole-dipole dispersion coefficients C_6^{AB} . For two benchmark sets they are more accurate than the charge-independent ones from the predecessor D3 scheme, and particularly, better coefficients are obtained for transition metal compounds. The two-body dispersion energy is computed in the commonly applied form as a sum over pair interactions including dipole-dipole and approximate dipole-quadrupole terms. A well-known many-body dispersion model based on coupled harmonic oscillators is used for the determination of all higher-order dipole terms using the charge- and geometry-dependent $\alpha(i\omega)$ values. Exact analytical gradients including derivatives of the EEQ charges are available for the simplified default energy expression where the higher-order dipole-dipole interactions are truncated to the ATM term for computational efficiency. The final DFT-D4 default model

I. Development of the DFT-D4 London Dispersion Correction

uses the two-body and the ATM energy expression (cf. equation 2.28) in structure optimizations. In addition, a single-point MBD correction is recommended as a sanity check for larger systems (cf. equation 2.29). The degree of empiricism in the *ad hoc* more physical D4 is slightly higher than in D3 with the same number of functional-dependent damping parameters (three) and a few additional global parameters for the charge dependency and coordination numbers.

The accuracy of the D4 method has been extensively verified using various benchmark sets including dispersion coefficients (organic and organometallic systems) and with various standard density functionals as DFT-D4 for interaction energies (intramolecular dispersion, and host-guest systems of medium to large size), conformational energies (sugars, tri- and tetrapeptides, inorganic systems, and RNA backbone models), covalent bond lengths (light main group elements, heavy main group elements, and 3d-transition metal elements), organic equilibrium structures (rotational constants), noncovalent equilibrium structures, and reaction energies of main group chemistry (extended GMTKN55 database) and transition metal complexes occurring in homogeneous catalysis (MOR41).

DFT-D4 in general improves slightly upon the already accurate and well-established DFT-D3(BJ)-ATM method and the new D4 model seems to be the most accurate and general molecular dispersion correction available. This mainly results from the inclusion of atomic charge effects into the atomic polarizabilities, the balanced treatment of higher-order dipole-dipole interactions, and most importantly the high accuracy of the underlying TD-DFT dispersion coefficients. In particular, systems involving large atomic charges or respective charge changes in chemical processes (e.g., oxidation/reduction) benefit from a DFT-D4 treatment compared to DFT-D3. Moreover, it should be emphasized that the generally good description of dispersion interactions in nonpolar main group or organic molecules is retained compared to DFT-D3(BJ)-ATM, i.e., DFT-D4 represents a safe replacement of a widely used and well tested method. In the current form, the D4 method appears to have reached a plateau level within the DFT-D methodology in terms of physical sophistication and cost-accuracy ratio. Further improvements would most likely lead to significantly increased computational costs and moreover would require concomitant improvements of the applied DFAs or damping schemes. Importantly, the general black-box philosophy of the DFT-D4 approach and the coupling of a single dispersion model to various standard DFAs is analogous to DFT-D3. This and the availability for most of the periodic table (elements up to atomic number $Z = 86$) enables broad application to a wide variety of quantum chemical problems. A list of all 67 currently parameterized DFAs together with their BJ-damping parameters is given in Appendix A2 (for different atomic partial charges in combination with an ATM or an MBD treatment).

The proposal of D4 with a robust and reasonably accurate classical charge model as

basis allows its application not only in the DFT context. Simplified semi-empirical orbital models, sophisticated force-fields²⁰¹ or neural network potentials can easily be coupled with the D4 model simply because no electron density is required and the whole procedure including nuclear gradients still runs at “force-field speed”. This opens a route for an efficient, physically sound, and basically nonempirical treatment of noncovalent interactions in large systems with thousands of atoms. Ongoing work focuses on the implementation of the D4 model for periodic systems, which requires a cost-efficient determination of partial charges under periodic boundary conditions. The here presented final molecular (nonperiodic) version can be downloaded in coded form from the authors’ website free of charge²⁹⁷. Furthermore, the DFT-D4 method is available in the upcoming release of TURBOMOLE 7.3 software^{143,205,206}, the next release of ORCA 4.1.0¹⁴⁵, and within an update of MOLPRO⁶⁸.

2.5. Acknowledgments

This work was supported by the DFG in the framework of the priority Program No. SPP 1807, “Control of Dispersion Interactions in Chemistry”. EC thanks Philipp Pracht for the preparation of $\partial q/\partial R$ timings and Jakob Seibert for sharing several PDB structures. Furthermore, EC thanks Markus Bursch and Dr. Jan Gerit Brandenburg for fruitful discussions.

2.6. Appendix A2

In Appendix A2 the classical charge model is defined in more detail including an energy expression and analytical gradients. The theoretical foundations of the many-body dispersion correction used within the DFT-D4-MBD method is discussed in detail. The derivation of the two-body dispersion potential which is included into the GFN2-xTB Hamiltonian matrix is given. The definitions of the double hybrid density functionals used are given. The BJ-damping parameters are given for 67 DFAs and for Hartree-Fock. We compare timings (single-point energies and gradients) between DFT-D4 and DFT-D3(BJ)-ATM for the tetrakis(isonitrile)rhodium(I) dimer with 106 atoms and for a diamond chunk with 430 atoms. Furthermore, all statistical quantities are defined and listed as used in the evaluation of the calculated data. Statistical evaluations of the following benchmark systems are given with all reference and computed data for S30L, L7, MOR41, SCONF, PCONF21, ICONF, UPU23, ROT34, LMGB35, HMGB11, and TMC32. Structures of the tetrakis(isonitrile)rhodium(I) monomer and dimer are attached, whereas the TOMC6 benchmark set (structures and reference molecular C_6 coefficients) is given as a tarball. Furthermore, we share the fitting set

I. Development of the DFT-D4 London Dispersion Correction

used for determination of damping parameters, to ensure that new DFAs can be parameterized consistently.

3. Extension and Evaluation of the D4 London Dispersion Model for Periodic Systems

Eike Caldeweyher*, Jan-Michael Mewes*, Sebastian Ehlert*, and Stefan Grimme*

Caldeweyher, E. and Mewes, J.-M. and Ehlert, S. and Grimme, S. *ChemRxiv. Preprint*, DOI:10.26434/chemrxiv.10299428.v1 2019

Own manuscript contribution

- Development and implementation of the periodic DFT-D4 model
- Derive the pseudo-periodic model and calculate periodic reference polarizabilities
- Interpretation of the results and writing large parts of the manuscript
- Contribution of co-authors:
 - Dispersion stress tensor (S. Ehlert)
 - DMC8, adsorption energies (J.-M. Mewes)

*Mulliken Center for Theoretical Chemistry, Institut für Physikalische und Theoretische Chemie, Rheinische Friedrich-Wilhelms-Universität Bonn, Berlingstraße 4, 53115 Bonn, Germany

Abstract We present an extension of the DFT-D4 model [*J. Chem. Phys.*, 2019, **150**, 154122] for periodic systems. The main new ingredient are additional reference polarizabilities for highly-coordinated group 1-5 elements derived from periodic electrostatically-embedded cluster calculations. To demonstrate the performance of the improved scheme, several test cases are considered, for which we compare D4 results to those of its predecessor D3(BJ) as well as to several other dispersion corrected methods. The largest improvements are observed for solid state polarizabilities of 16 inorganic salts, where the new D4 model achieves an unprecedented accuracy, surpassing its predecessor as well as other, computationally much more demanding approaches. For cell volumes and lattice energies of two sets of chemically diverse molecular crystals, the accuracy gain is less pronounced compared to the already excellently performing D3(BJ) method. For the challenging adsorption energies of small organic molecules on metallic as well as on ionic surfaces, DFT-D4 provides values in good agreement with experimental and/or high-level references. These results suggest the standard application of the proposed periodic D4 model as a physically improved yet computationally efficient dispersion correction for standard DFT calculations as well as low-cost approaches like semi-empirical or even force-field models.

3.1. Introduction

The efficiency of modern Kohn–Sham density functional theory^{190,191} (DFT) enables its routine application to very large molecules with thousands of atoms, as well as the systematic screening of huge numbers of smaller compounds.²⁹⁸ However, DFT as approximate mean-field electronic structure method can fail dramatically for certain types of interactions. The two most prominent and relevant problems are (i) the absence or severe underestimation of long-range electronic-correlation effects, which give rise to London dispersion interactions,¹⁷ and (ii) the so-called self-interaction error (SIE).^{281,299} The SIE problem will not be further discussed in this work, as the focus of the present study is the extension of a correction scheme which attempts to solve the first mentioned London dispersion problem.

An accurate account of dispersion interactions is mandatory for most reasonable description of chemically relevant molecules and even more so for condensed-phase systems. Accordingly, it has shown, that dispersion-corrections systematically improve the accuracy of density functionals on all rungs of Jacob's ladder.⁵⁷ The development of dispersion correction schemes is a very active field of research which has spawned several different approaches. The unifying idea of all these approaches is to reintroduce the in principle well understood physics of London dispersion to the DFT framework. The existing approaches may be organized

I. Development of the DFT-D4 London Dispersion Correction

in two categories. On the one hand, there are self-consistent schemes in which dispersion is directly included in the functional, *e.g.*, *via* a response function and/or non-local dispersion kernels, and on the other with additive post-SCF-type corrections which model dispersion based on atomic polarizabilities. The latter may be subdivided in corrections which explicitly take into account the electron density, and semi-classical approaches that are electron density independent.

Most approaches incorporate the electron density into their theoretical apparatus. These include the exchange-hole dipole moment (XDM) approach of Becke and Johnson,^{47,48} as well as the Tkatchenko–Scheffler (TS) model,⁴⁹ and its many-body dispersion (MBD) successor.^{50,300} All those methods employ a Hirshfeld-type atomic partitioning of the electron density, either to rescale the polarizabilities of the neutral atoms (TS, MBD), or to density-weight the approximated expectation value of the squared total multipole operator for each atom within the molecule (XDM). For the TS related approaches, Bučko and co-workers^{217,301} showed that an iterative Hirshfeld partitioning, in which the fractionally charged atomic reference state is determined self-consistently, can improve the description of dispersion interactions.

Approaches of the first category, which self-consistently include dispersion in the density functional circumvent the somewhat arbitrary atomic partitioning of the electron density. However, this comes at the cost of a reduced flexibility — coupling to any method is hardly possible — and increased computational costs. Approaches of this class are, *e.g.*, the van der Waals density functionals^{302–307} (vdW-DF), which are based on the fundamental adiabatic connection theory. A simplified construction scheme for the non-local correlation part has been introduced by Vydrov and Van Voorhis (rVV10).^{51,52}

Topic of this work are the semi-classical DFT-D methods of the last category.^{17,153} Testing representatives from each of these categories, including TS(TS/HI), MBD(MBD/HI,MBD/FI), opt-vdw-DF2, rVV10, and DFT-D, we find that they are all equally able to accurately account for dispersion interactions in various scenarios within a DFT framework. However, the associated computational costs of these methods can differ significantly. The overarching principle for the cost of any such correction should be that the computational efficiency of the underlying DFT method must be retained. While this is in general the case for all of these methods in combination with hybrid functionals employing large Gaussian basis sets, the correction can become the bottleneck in low-cost GGA DFT calculations, as will be shown and discussed later in this article. For even lower-cost atomistic models such as semi-empirical molecular orbital or force-field methods, only the fastest approaches remain viable. An important point concerning the computational efficiency of additive dispersion-correction schemes is their account of the chemical environment. While it appears as a logical step to derive and/or scale

I. Development of the DFT-D4 London Dispersion Correction

the atomic polarizabilities based on the electron density, this also introduces a computationally demanding step, which typically slows down the calculation.

The DFT-D3 model^{46,166} avoids the electron density partitioning by interpolating between atomic reference polarizabilities based on fractional coordination numbers (CNs). The recently introduced successor DFT-D4 further improves this model by making the atomic reference polarizabilities charge-dependent.^{210,308} However, to retain the computational efficiency, the charge-information is not derived from the electron density, but provided by a classical and thus efficient electronegativity equilibration (EEQ) model calculation. While this charge-scaling improves the description for most molecular applications, in particular for transition metals,²⁹² there are still issues with certain metal-ions in highly polar and periodic environments, such as Na^+ in crystalline NaCl. In bulk systems, the D3/D4 method sometimes lacks an accurate description due to the absence of suitable reference systems. In the solid state, the coordination number of alkaline, alkaline-earth and early transition metals can approach values far beyond those for which reference polarizabilities are available from molecular treatments, causing the otherwise accurate interpolation to become an unreliable extrapolation.

The present work addresses this problem by widening the scope of the references. Polarizabilities for new, highly coordinated systems are included based on pseudo-periodic model calculations with the periodic electrostatic embedded cluster method (PEECM). This includes new polarizabilities for alkaline, alkaline-earth, and early transition metal elements. Herein theoretically observed solid state polarizabilities are evaluated against experimentally determined ones. We benchmark the quality for properties such as organic polymer refractive indices which are directly dependent on polarizabilities. Lattice energies and cell volumes of molecular crystals are evaluated using different literature known London dispersion correction schemes in comparison to the new approach. Furthermore, interfaces between organic molecules and inorganic surfaces are treated for which new properties can emerge.^{309–311} Noncovalent London dispersion effects are essential for structural properties, but also for the quantification of the stability of such systems.^{312–314} For this purpose we discuss adsorption energies of organic molecules on non-polar and ionic surfaces which either exhibit partly covalent or partly electrostatically driven binding motifs penetrating the particular description of noncovalent interactions (NCIs) between adsorbate and surface.

The next section shortly introduces the DFT-D4 theory, which defines the method under periodic boundary conditions. A detailed description of the methodologies—especially the generation of periodic EEQ partial charges and the periodic dispersion energy expression—is given in Appendix A3. A special focus shall be put on a scheme to calculate periodic reference polarizabilities. Afterwards the results for the above mentioned tests will be discussed. Finally, a summary and an outlook

are given presenting the quality of the method on solid state properties and discuss possible future applications.

3.2. Theory

The theoretical framework of this work was presented in detail in Ref. 308 describing the basics of the molecular DFT-D4 model. For the calculation of periodic CNs, charge and geometry dependent dynamic polarizabilities $\alpha(i\omega)$, as well as for pair and triple-wise dispersion energies see the detailed theoretical description given in Appendix A3. A periodic EEQ model is developed within the present work for the efficient calculation of partial charges used in the ζ -scaling for atom-in-molecules polarizabilities. For this purpose, a cyclic cluster model is used to capture periodic boundary conditions. Since dispersion interactions are much faster decaying (leading order term is proportional to R^{-6}) than, *e.g.*, Coulomb interactions, we employ for this energy contribution a real-space cutoff within the periodic implementation. Analytical gradients (nuclear forces and stress tensor) are available for the dispersion energy expression including pairwise and triple wise London dispersion interactions.

3.2.1. Dynamic Polarizabilities from Cluster Extrapolation

A major problem for D3/D4 calculations of dense periodic systems has been the absence of suitable molecular reference systems. Consider for example the alkaline (earth) metals, for which there are only singly or doubly coordinated molecular references (KH, MgH₂), but no references with CNs close to the ones realized, *e.g.*, in salts (KCl, MgCl₂, etc.). This problem persisted up to group 5, and causes too large polarizabilities to be used in these situations and in turn an over-stabilization of such systems. In order to eliminate this shortcoming, it is desirable to augment the database of references. For this purpose, the polarizability per crystal unit cell and eventually that of the anions and cations has to be calculated, which can in principle be accomplished in two ways: (i) the calculation of polarizability per volume from the dielectric function of the solid (using, *e.g.*, the Clausius–Mosotti equation³¹⁵ in the limit of ideal ionic crystals), and (ii) the calculation of polarizability per atom from a cluster extrapolation. Zhang *et al.* have shown that a cluster extrapolation gives satisfactory results for obtaining atomic polarizabilities within the solid state (maximum deviation of about 2% for the polarizability of silicon³¹⁶). Since this latter approach is moreover more similar with the method used to obtain molecular reference polarizabilities, it is suitable for our purpose. To simulate periodic boundary conditions of the crystal we apply the PEECM.³¹⁷ Within this approach the entire periodic system is divided into three parts: the

I. Development of the DFT-D4 London Dispersion Correction

inner part covering the cluster (I), an optional shell (II) which is build from effective core potentials (ECPs), and the outer part (III) which describes its environment. Part (I) is treated quantum mechanically (QM), whereby in part of (II) ions are replaced by ECPs. Such an isolating ECP shell—surrounding the actual QM part—is necessary in order to prevent artificial polarization of the electron density by ions which would otherwise be in direct contact with the QM boundary. The outer part (III) is described by a periodic array of point charges, representing cationic and anionic sites of the perfect ionic crystal. The effect of the additional ECP shell is briefly shown in Table 3.1 where a simple point charge embedding (PCE) model describes the cluster without additional ECPs.

Table 3.1.: Static polarizabilities (given in Bohr³) and homoatomic dispersion coefficients (given in HartreeBohr⁶) as obtained by a cluster extrapolation for lithium inside the lithium chloride crystal. Here the effect of an ECP shell on the absolute size of the particular property within the crystal is investigated starting from a Li₄Cl₄ cluster. Furthermore, the point charges (termed q^{PC}) creating the outer part are given.

Embedding	q ^{PC}	α ^{Li(0)}	C ₆ ^{Li-Li}
None	0.0	37.2	129.7
PCE	±0.3	8.0	15.4
PCE	±1.0	<0.1	0.1
PEECM	±1.0	5.0	7.6

The polarizability of lithium as part of an isolated Li₄Cl₄ cluster (*i. e.*, no embedding) decreases significantly in PBC. Furthermore, when applying a PCE model, it is crucial to use adjusted point charges, since properties such as polarizabilities are strongly influenced by the present Coulomb field. The effect of unadjusted point charges within a PCE model (q^{PC} = ±1) results in artificially low polarizabilities and thus small dispersion coefficients. However, this can be overcome by means of an ECP shell, without having to manually adjust the point charge in advance (see “PEECM” embedding in Table 3.1). Thus, it is advisable to embed the QM region into ECPs to get the right answer for the right reason. The electronic Coulomb energy term arising from the periodic field of point charges surrounding the cluster has the following form

$$J = \sum_{\mu\nu} \sum_{\mathbf{k}}^{N \in \text{UC}} \sum_{\mathbf{T} \in \mathbf{O}}^{\infty} D_{\mu\nu} q_{\mathbf{k}} \int d\mathbf{r} \frac{\mu(\mathbf{r})\nu(\mathbf{r})}{|\mathbf{r} - \mathbf{R}_{\mathbf{k}} - \mathbf{T}|}, \quad (3.1)$$

where UC denotes the unit cell of point charges, D_{μν} are elements of the density matrix, μ and ν are basis functions, q_k and **R**_k denote charges and positions of point charges, and **T** denotes the direct lattice vector of the outer part III. The

I. Development of the DFT-D4 London Dispersion Correction

energy term is evaluated using the periodic fast multipole method³¹⁸ (PFMM) which—unlike the Ewald method—defines the lattice sums entirely in the direct space. Figure 3.1 schematically shows the distribution of the cluster into three parts.

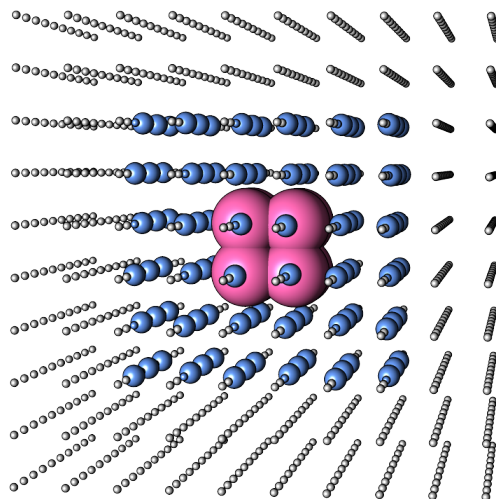


Figure 3.1.: The schematic construction of a cluster within the periodic electrostatic embedded cluster method. Part (I) consists out of the QM part (pink spheres) embedded into part (II) which is build from ECPs (blue atoms). Part (III) is embedding part (II) by periodic point charges (small gray atoms) representing cationic and anionic sites as in the perfect ionic crystal.

The correct representation of polarities for atoms inside solids without using QM information still remains a challenge. For the geometry dependent D3 method this is hardly possible, because only the CN is used to weight reference systems accordingly. This disadvantage was partly overcome with the development of the D4 method by including information from the electronic structure (atomic partial charges) in the calculation of the atomic dipole polarizabilities. Nevertheless, periodic dipole polarizabilities are significantly smaller than those present in molecules which rises the need of reference systems that are especially designed for representing solid state properties. Addition of such references is easily feasible in the D4 method. Here, only dynamic polarizabilities of the new references are required. We obtain pairwise dipole-dipole C_6 coefficients during the calculation by means of numerical Casimir–Polder integration. Figure 3.2 highlights the elements which are broadened with new periodic reference polarizabilities. In particular, the elements of group 1–5 were supplemented with new references.

I. Development of the DFT-D4 London Dispersion Correction

1 H						
3 Li	4 Be					
11 Na	12 Mg					
19 K	20 Ca	21 Sc	22 Ti	23 V	24 Cr	...
37 Rb	38 Sr	39 Y	40 Zr	41 Nb	42 Mo	...
55 Cs	56 Ba		72 Hf	73 Ta	74 W	...

Figure 3.2.: The yellow highlighted elements received new periodic reference polarizabilities at the PEECM level. All these elements exposed relatively high polarizabilities for molecular reference systems.

3.3. Results

3.3.1. Polarizabilities and Refractive Indices

Accurate polarizabilities are the foundation of many London-dispersion correction schemes. As demonstrated in previous works,^{46,210,308} there is a direct correlation between the description of molecular polarizabilities and the accurate description of NCI energies. Therefore, this section will briefly discuss the quality of the new reference polarizabilities. For this, ionic polarizabilities are shown representing the polarizabilities of cations and anions inside the crystal. In general, cations have a lower electron density and thus a lower local (atomic) polarizability and *vice versa*. The last part of this section covers the calculation of refractive indices of several optical organic polymers to validate the quality of polarizabilities in “organic” crystals where the new reference polarizabilities are supposed to have a small effect.

I. Development of the DFT-D4 London Dispersion Correction

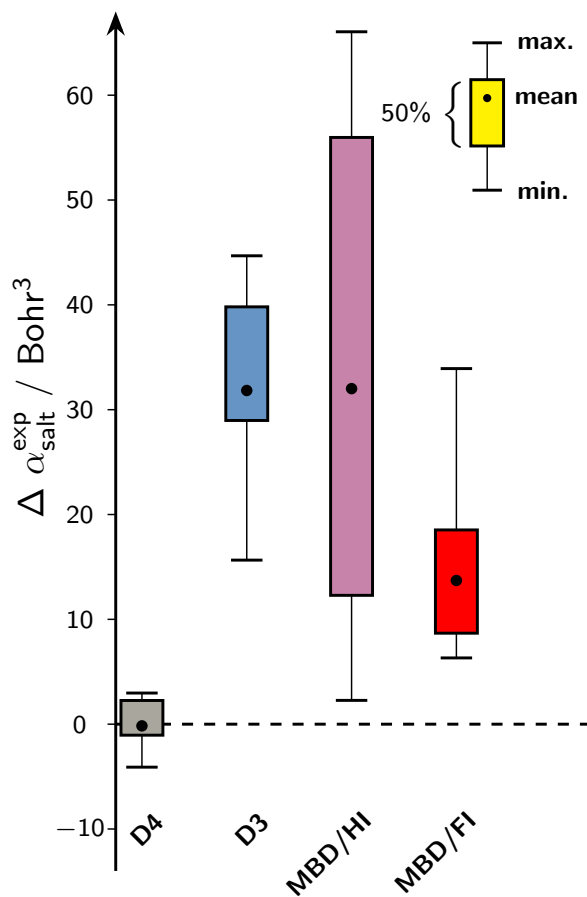


Figure 3.3.: Given are periodic static polarizabilities as obtained by experimental measurements (molecular polarizabilities are extracted from Ref. 315).

The experimental literature data were obtained by measuring the refractive index n (RI) at several wavelengths λ . In Ref. 315 all RIs are extrapolated to $\lambda = \infty$ (obtaining n_∞) and used within the Lorentz expression to calculate the particular experimental salt polarizability

$$\alpha_{\text{salt}}^{\text{exp}} = \frac{3V_{\text{m}}}{4\pi} \frac{n_\infty^2 - 1}{n_\infty^2 + 2}, \quad (3.2)$$

where V_{m} is the volume of the crystal divided by the number of molecules inside the crystal. All V_{m} values are taken from X-ray data³¹⁹ and all theoretical salt polarizabilities are obtained as the sum of the cationic and the anionic polarizability

$$\alpha_{\text{salt}}^{\text{calc}} = \alpha_{\text{salt}}^{\text{cation}} + \alpha_{\text{salt}}^{\text{anion}}. \quad (3.3)$$

For D3, atomic polarizabilities are calculated as introduced in Ref. 46, hence we do not approximate polarizabilities as introduced in the empirical relationship for determining polarizabilities from homoatomic dispersion coefficients^{320,321}. Fur-

I. Development of the DFT-D4 London Dispersion Correction

thermore, the Tkatchenko-Scheffler⁴⁹ method with iterative Hirshfeld (HI) partitioning^{217,301} (termed TS/HI) as well as its many-body dispersion analogon^{50,300} (termed MBD/HI) are listed for the sake of completeness^{217,301,322}. Here an HI analysis is indispensable, since the TS and MBD variants calculate cationic polarizabilities that are too high in their absolute value (similar to neutral atomic polarizabilities) leading to artificially high salt polarizabilities. Furthermore, the MBD/FI (fractionally ionic) variant is used, which was developed by Gould *et al.*³²³ This method promises in particular a drastic improvement for the calculation of polarizabilities in ionic systems. In Figure 3.3 the quality of salt polarizabilities are given for two DFT-D methods (DFT-D3 and DFT-D4) as well as for two MBD methods (MBD/HI and MBD/FI).

Extended statistical evaluations are given for the mean deviation (MD), the mean absolute deviation (MAD), the root mean squared deviation (RMSD), and the absolute maximum error (AMAX) and are given in Bohr³ if not stated otherwise. The experimentally determined polarizabilities are reproduced with high accuracy by the DFT-D4 method (MD = -0.2, MAD = 1.7, RMSD = 2.1, AMAX = 4.1). MBD is not able to calculate reasonable polarizabilities for seven out of 16 different salts due to non-physical negative values after its screening procedure. Note that these problems are already literature-known.³²³ MBD/HI calculates polarizabilities for all salts without such problems, however, this method gives only poor results (MD = 32.0, MAD = 32.0, RMSD = 21.4, AMAX = 66.1). This is slightly improved at the density-independent DFT-D3 level (MD = 31.8, MAD = 31.8, RMSD = 9.5, AMAX = 44.7). Compared to DFT-D3, further improvements are obtained when using the MBD/FI method where the fractional ionic reference systems are beneficial for describing salt polarizabilities (MD = 14.6, MAD = 14.6, RMSD = 8.4, AMAX = 40.6). TS and TS/HI show overall the largest deviations. Here even the iterative Hirshfeld partitioning cannot lower the absolute values of the neutral TS atomic polarizabilities enough to produce reasonable salt polarizabilities (TS: MD = 192.0, MAD = 192.0, RMSD = 199.0, AMAX = 256.3, and TS/HI: MD = 114.1, MAD = 114.1, RMSD = 118.4, AMAX = 158.2).

To check for ionic polarizabilities themselves, we use experimental ionic polarizabilities that have been created by partitioning salt polarizabilities to the contributions of their cations and anions using a least-squares fitting procedure.³¹⁵ Those experimental ionic polarizabilities are compared to theoretically derived polarizabilities representing the cation and the anion inside the crystal.

I. Development of the DFT-D4 London Dispersion Correction

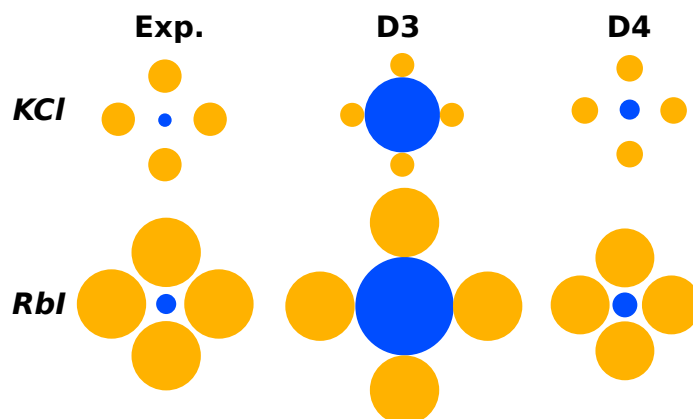


Figure 3.4.: Schematic 2D-representation for anionic (yellow) and cationic (blue) polarizabilities within the KCl (top) and RbI (bottom) solid state. Given are the experimentally derived ion polarizabilities (left) as computed by Tessman and coworkers,³¹⁵ the calculated atomic D4 polarizabilities (right), and the D3 polarizabilities (center). The radii of the spheres correspond to the absolute value of the polarizability.

Figure 3.4 schematically highlights how D4 and D3 obtain ionic polarizabilities for K^+ and Cl^- in KCl and for Rb^+ and I^- in RbI (both space group $\text{Fm}\bar{3}\text{m}$) compared to experimental ionic polarizabilities. Here, the absolute value of polarizabilities are expressed in sphere-radii, where large radii correspond to large polarizabilities and *vice versa*. Furthermore, cationic polarizabilities are represented in blue and anionic polarizabilities in yellow. The agreement to experimental ionic polarizabilities is significantly improved by adding periodic reference polarizabilities in combination with a charge scaling procedure (*i.e.*, $\alpha_{\text{exp}}^{\text{Rb}\in\text{RbI}}/\alpha_{\text{exp}}^{\text{I}\in\text{RbI}} = 0.3$ versus $\alpha_{\text{D4}}^{\text{Rb}\in\text{RbI}}/\alpha_{\text{D4}}^{\text{I}\in\text{RbI}} = 0.4$, and $\alpha_{\text{D3}}^{\text{Rb}\in\text{RbI}}/\alpha_{\text{D3}}^{\text{I}\in\text{RbI}} = 1.8$). A comparison with the TS and the MBD model shows that the scaling of neutral atomic polarizabilities using Hirshfeld volumes is insufficient for the accurate calculation of ionic polarizabilities within RbI ($\alpha_{\text{TS}}^{\text{Rb}\in\text{RbI}}/\alpha_{\text{TS}}^{\text{I}\in\text{RbI}} = 8.0$ and $\alpha_{\text{MBD}}^{\text{Rb}\in\text{RbI}}/\alpha_{\text{MBD}}^{\text{I}\in\text{RbI}} = 13.1$). TS/Hi and MBD/Hi perform better in determining ionic polarizabilities within RbI compared to their non-iterative analogues ($\alpha_{\text{TS/Hi}}^{\text{Rb}\in\text{RbI}}/\alpha_{\text{TS/Hi}}^{\text{I}\in\text{RbI}} = 4.5$ and $\alpha_{\text{MBD/Hi}}^{\text{Rb}\in\text{RbI}}/\alpha_{\text{MBD/Hi}}^{\text{I}\in\text{RbI}} = 1.3$). The MBD/FI method significantly improves here ($\alpha_{\text{MBD/FI}}^{\text{Rb}\in\text{RbI}}/\alpha_{\text{MBD/FI}}^{\text{I}\in\text{RbI}} = 0.1$) whereby the cationic polarizability of Rb^+ is obtained somewhat too small and the anionic polarizability of I^- too large within this salt. In general it is assumed that improved ionic polarizabilities also yield improved interaction energies for ionic systems (*e.g.*, adsorption processes on ionic surfaces) which will be discussed in more detail in section 3.3.3.

Another test case is the calculation of RI values for optical organic polymers, which is based on the work of Hachmann and co-workers.³²⁴ In their work, polymer polarizabilities of organic compounds were calculated using hybrid TD-DFT (TD-PBE0/def2-TZVP) and RIs were obtained using the Lorentz equation. We calculate RIs from molecular polarizabilities of the monomer units of each polymer

I. Development of the DFT-D4 London Dispersion Correction

obtained by approximated methods (DFT-D, TS, or MBD). This approximation, however, is accompanied by a lack of many-body effects, so that the RIs to be calculated are known to be too large in absolute value. Furthermore, monomer structures are used, since the explicit polymer growth (including conformational analysis for each polymer) is beyond the scope of this work. However, this is intended to be covered in more detail in future works, *e.g.*, by interfacing the supramolecular toolkit of Jelfs and co-workers³²⁵ to explicitly build polymer structures. Overall 73 monomer units of polymer structures have been extracted from Ref. 324 and re-optimized at the PBEh-3c²⁷² level of theory after searching for minimum conformers using the conformer-rotamer ensemble sampling tool³²⁶ for each monomer unit. We calculate RI values as follows

$$n_{\infty} = \sqrt{\frac{3V_m + 8\pi \cdot \alpha}{3V_m - 4\pi \cdot \alpha}}, \quad (3.4)$$

where V_m values are taken from Ref. 324 assuming a constant packing fraction of the bulk polymer. Figure 3.5 shows the relative deviation of RIs from exper-

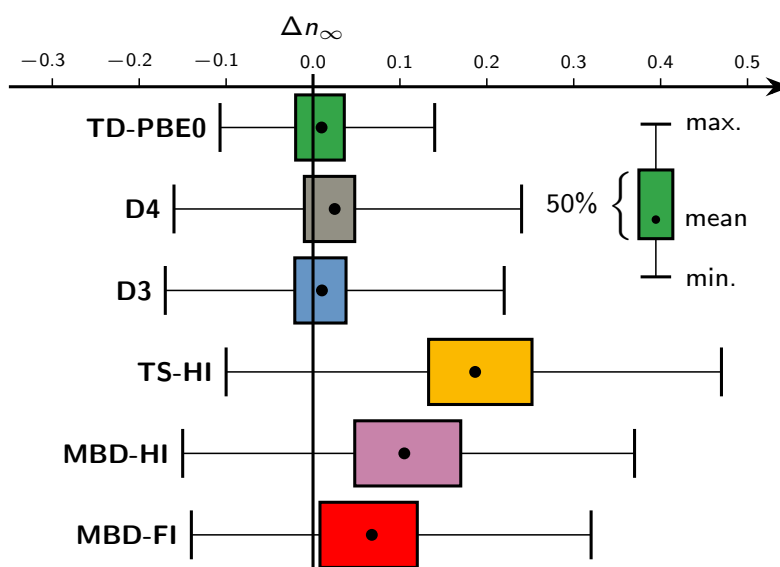


Figure 3.5.: Error ranges (relative to experimental data) for calculated refractive indices at different theoretical levels of theory (D4, D3, MBD/HI, MBD/FI, and TS/HI) for an organic polymer database.

imental values³²⁴ (the MAD of TD-DFT RIs from experimental RIs is 2.3% its RMSD 3.0%). As can be seen from the graph, all methods generally calculate too large RI values, which is partly due to the approximation of using molecular polarizabilities α in equation 3.4. However, since this approximation is applied to all methods, they can be directly compared with each other. The smallest MD and RMSD values are obtained from the D3 and D4 methods, which are able to determine RI values with good accuracy. The slightly better performance

of D3 compared to D4 is within statistical uncertainty and expected, as D3 already provides highly accurate polarizabilities for organic molecules and molecular crystals. Subsequently, the MBD/FI method from Gould and co-workers achieves adequate accuracy. The least suitable method for predicting RIs is the TS/HI method, which achieves improvements through additional many-body dispersion effects within the MBD/HI method.

3.3.2. Molecular Crystals

Lattice Energies

Molecular crystals are relevant in pharmaceutical chemistry.^{327,328} An important property is the lattice energy E_{lat} , which reflects how much energy is released per molecule upon resublimation. It is defined as

$$E_{\text{lat}} = \frac{1}{Z} E_{\text{crystal}} - E_{\text{gas}}, \quad (3.5)$$

where E_{crystal} is the energy of the crystal including overall Z molecules within the primitive cell and E_{gas} is the energy of the isolated molecule in the lowest energy conformation.

Recently, a set of eight highly accurate reference energies for molecular crystals have been published based on diffusion Monte-Carlo (DMC) calculations.²⁷ These reference systems include various binding motifs like, e. g., hydrogen bonding in ice, electrostatic interactions in CO_2 , as well as London-dispersion dominated unsaturated hydrocarbons. The statistical deviation (RMSD) of these high-level results from experimental data is small (0.004 eV). To provide a framework for the following discussion of the DFT results, it is useful to consider previous applications of this data set, which has been used to benchmark RPA and MP2.^{329–331} With a computational cost between the DMC benchmark calculations and DFT-based methods, RPA and MP2 afford RMSDs of 0.08 eV and 0.06 eV, respectively. Moreover, by systematically studying the deviations from the reference, it was possible to devise an efficient GW-type singles correction to RPA (GWSE), which provides a much improved RMSD of only 0.01 eV.

In the following, we will explore the performance of DFT-D4 and D3(BJ) in combination with various functionals (PW91,³³² SCAN,^{114,253} PBE,¹⁰² rPBE,³³³ revPBE,²⁸¹ TPSS,¹⁰⁵ B3LYP,^{118,334} and PBE0¹¹⁶), and moreover compare D4 to other dispersion-corrected DFT methods. We include dispersion-corrected method implemented in the latest version of the prominent VASP program package, namely the methods of Tkatchenko/Scheffler (TS and MBD with fixed and iterative atomic charges)^{49,50,217,217,300,301,301,323}, Landgreth/Lundquist (original vdW-optPBE^{302–307} and revised rev-vdW-DF2)³³⁵ and Vydrov/Van Voorhis (re-

I. Development of the DFT-D4 London Dispersion Correction

vised VV10)^{51,52}.

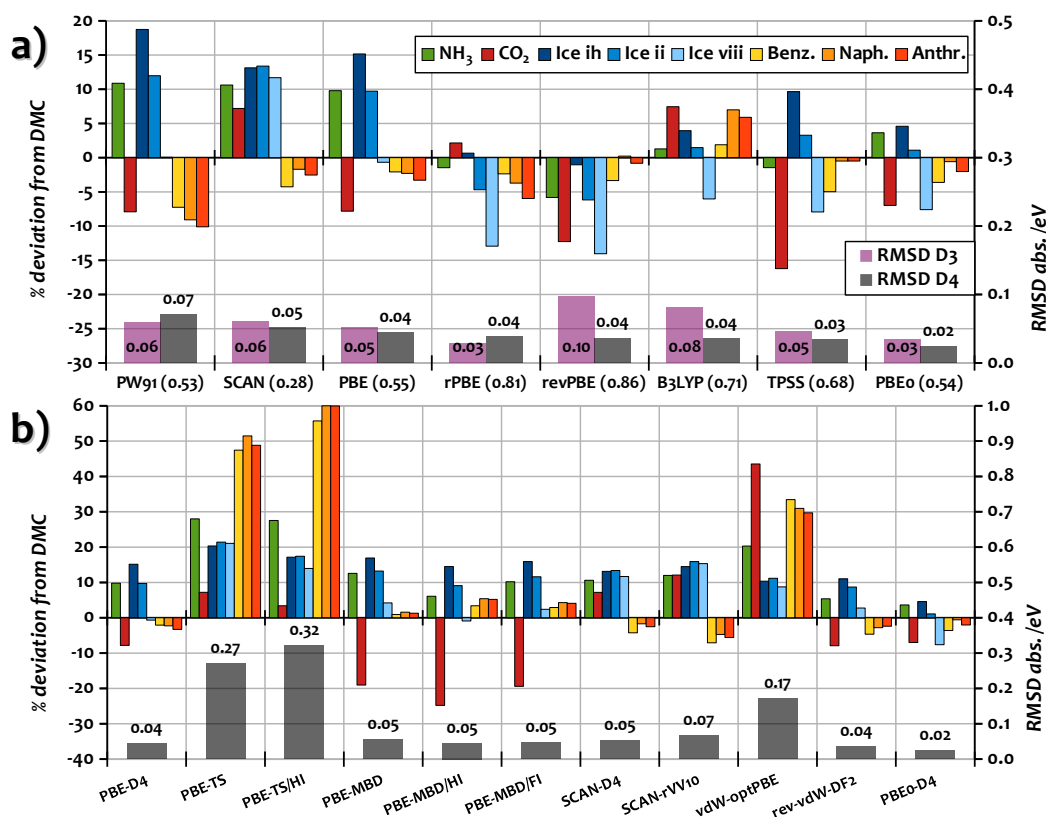


Figure 3.6.: **a)** Benchmark of DFT-D4 with several prominent DFs for the computation of lattice energies of eight molecular crystals (subset of the ICE10³³⁶ and X23^{337,338} benchmark set), for which high-level fixed node diffusion Monte-Carlo (FN-DMC) references are available.²⁷ The RMSD of the uncorrected DFs is given in parenthesis (x-axis). **b)** PBE-D4 compared to other dispersion corrected approaches, including the original two-body TS correction,⁴⁹ TS/Hi with iterative Hirschfeld charges,^{217,301} TS/MBD with many-body effects,^{50,300} the combination of MBD with HI,^{217,301} as well as yet another revision that includes ionic references (MBD/FI).³²³ Also shown are results obtained with SCAN-D4 compared to SCAN-rVV10,^{51,52} as well as with the original variant of vdW-DF,^{302–307} and a more recent revised variant. The colored bars depict the relative (%) deviation from the reference, whereas the transparent bars at the bottom show the absolute root-mean square deviation (RMSD) from the reference including its numerical value. All calculations were conducted with VASP and employ the hardest PAW-PBE (GW) potentials available in the VASP library, an energy cut-off of 1000 eV and fine k-spacing. See Supplementary Material for more details.

We begin the discussion with the performance of D4 and D3(BJ) in combination with different functionals, which is depicted in Figure3.6a. In almost all cases, the error without dispersion correction is well above 0.5 eV, whereas the worst performance including the dispersion correction is 0.1 eV (revPBE-D3). Only the uncorrected SCAN functional achieves an RMSD below 0.3 eV, indicating that it

I. Development of the DFT-D4 London Dispersion Correction

includes medium-range correlation effects to some extent, which is in agreement with previous reports.^{114,253,339} The best overall performance is provided by PBE0-D4 with an RMSD of 0.02 eV, which is well below that of much more demanding MP2 and RPA approaches. Considering also the MDs of 0.08 eV, 0.06 eV and 0.01 eV for RPA, MP2 and PBE0-D4 shows that the error of PBE0-D4 is less systematic. The computationally even more efficient (no exact exchange) rPBE-D3(BJ) approach is almost as accurate as PBE0-D4, and closely followed by TPSS-D4, B3LYP-D3 and revPBE-D3, which all provide an RMSD ≤ 0.04 eV in the range of chemical accuracy (about 1 kcal mol⁻¹). For perspective, these DFT calculations take only hours for hybrid density functional approximations (DFAs) to minutes for generalized gradient approximations (GGAs) on a compute node with 16 CPUs.

Comparing D3(BJ) and D4, the agreement with the reference improves significantly in some cases for D4 (*cf.*, revPBE and B3LYP), while for most DFAs it is only slightly more accurate, and in some cases slightly worse (*cf.*, PW91 and rPBE).

The results shown in Figure 3.6b for the two-body models TS and TS/HI indicate a systematic under-binding. In particular for the crystals of the aromatics, one of the most common structural motif in organic chemistry, the deviations are as large as 50% of the total lattice energy. This is cured by the inclusion many-body effects in the MBD approaches, which has an accuracy comparable to that of D3(BJ) and D4. Note, that D3(BJ) as employed here achieves this good result without including many-body effects. While the vdW-optPBE functional based on the original approach is not able to accurately describe the different interaction motifs, the revised variant rev-vdW-DF2 does a much better job, approaching the accuracy of PBE-D4. SCAN-D4 and SCAN-rVV10 perform very similar. Although they are slightly worse than PBE-D4 regarding their RMSD, the deviation within a given chemical compound class as indicated by similar colors in Figure 3.6 is consistent. They provide by far the best relative energies of the ice (blue) and NH₃ forms.

In conclusion, these results suggest PBE0-D4 as the most accurate approach for studies on molecular crystals. At the computationally much more efficient (meta)GGA level, rPBE-D3 and TPSS-D4 are the next best options, providing only slightly worse lattice energies at much lower computational cost. Rev-vdW-DF2 and the MBD based approaches provide very similar accuracy. However, for MBD/HI and MBD/FI the computation of the dispersion-correction takes much longer than the GGA calculation itself (*cf.* timings below), limiting their applicability. If the variation in investigated chemical structures is small and the relative energies are more important than absolute energies, SCAN-D4 and similarly also SCAN-rVV10 can be recommended. However, due to the increased cost of the

I. Development of the DFT-D4 London Dispersion Correction

SCAN functional, also these approaches are computationally more demanding than GGA+D3/D4.

Geometries from Experimental Measurements

The packing of organic molecules into crystals is highly sensitive to an accurate treatment of NCIs and dispersion effects in particular. In 2012, Johnson and co-workers compiled a set of organic crystals from available low temperature X-ray structures (termed C21 benchmark³³⁷) which was refined and extended by Reilly and Tkatchenko resulting in the X23 benchmark set.³³⁸ Various groups already used this benchmark set to test electronic structure methods.^{340,341} In their work Johnson *et al.* applied an artificial pressure to include volume expansion due to vibrational effects in the optimization procedure. However, as discussed in earlier works²⁷² the zero point vibrational energy (ZPVE) and thermal contributions of the unit cell volume can be estimated and used to transform the experimental volume V_0 into back-corrected reference equilibrium volumes V_e which are directly comparable to optimizations on the electronic energy surface.

Here we have calculated unit cell volumes using PBE-D3(BJ), PBE-D4, PBE-TS, PBE-TS/HI, PBE-MBD, PBE-MBD/HI, PBE-MBD/FI, and pure PBE for the X23 systems. Figure 3.7 shows deviations from reference volumes per molecule for the 23 crystal structures. Uncorrected PBE only achieves a poor description by generally overestimating the cell volumes for these molecular crystals (black bar in Figure 3.7, MD = 14.7%, MAD = 14.7%, and RMSD = 5.2%). Coupling PBE to any dispersion correction improves the description significantly but the respective methods perform differently well. PBE-TS performs worst which, however, can be improved by using an iterative Hirshfeld partitioning.

Including many-body dispersion effects or adding an iterative Hirshfeld partitioning further improves the accuracy. Additional reference systems with fractional ionic character do not further increase the quality of the MBD results which is expected, since the considered molecular crystals have almost no ionic character. PBE-D3(BJ) volumes are comparable to those calculated with the TS/HI method. For the 23 tested molecular crystals, MBD gives a more accurate description compared to D3(BJ). However, PBE-D4 also improves upon PBE-D3(BJ) and furthermore is *on par* with the computationally more demanding MBD method in terms of all statistical evaluations (MD, MAD, and RMSD).

As another test, the D4 and MBD models are tested for their capability of reproducing strong hydrogen networks within different ice polymorphs. This important binding motif is under-represented in the X23 benchmark set, so that the ICE10 benchmark³³⁶ set is to be used for this purpose. A detailed description of crystallized water requires an accurate description of NCIs especially for reproducing structural properties. Overall, we investigate eight experimentally studied ice

I. Development of the DFT-D4 London Dispersion Correction

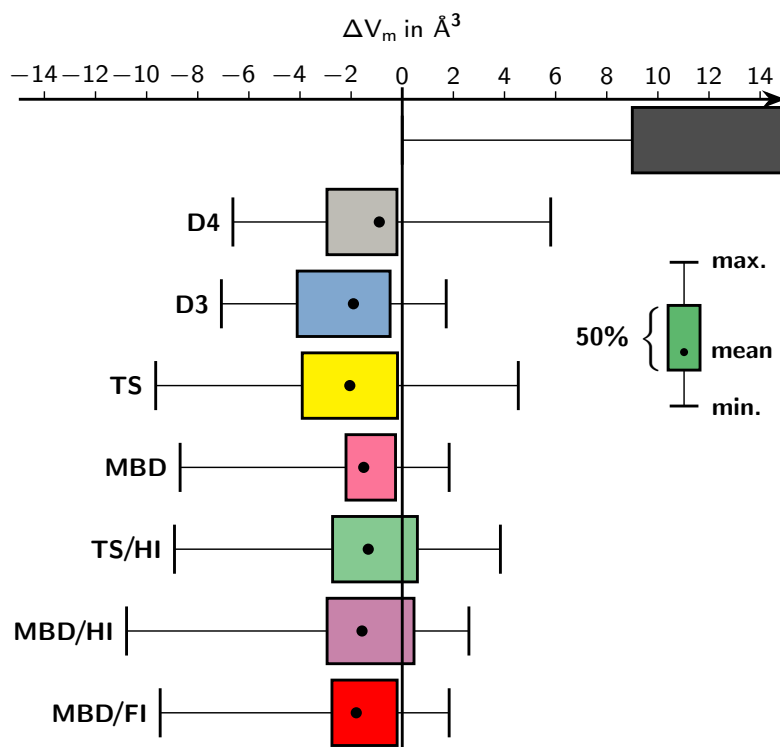


Figure 3.7.: Error ranges (relative to experimental data) for calculated cell volumes divided by the number of molecules inside the cell for 23 molecular crystal structures (X23 benchmark set). Shown are data for pure PBE (black) and PBE coupled to D4, D3(BJ), TS, MBD, TS/Hi, MBD/Hi, and MBD/FI. For all PAW calculations an 800 eV plane-wave energy cutoff is applied to minimize Pulay stress.

polymorphs. The measurements have been conducted at low temperatures (up to 100 K) where the thermal contribution to the ice density has been assumed to be rather small assuming that measured structures can be treated as equilibrium structures.³³⁶ In the original ICE10 publication the ZPVE is estimated on each unit cell volume by correcting for thermal effects using the HF-3c³⁴² method applied with an ATM many-body dispersion treatment. In the present work we apply the quasi-harmonic approximation (QHA, see Supplementary Material for details) to eight out of ten ICE10 polymorphs to obtain back-corrected equilibrium volumes that are listed in Table 3.2. For this purpose HSE-3c³⁴³ calculations are performed within CRYSTAL17⁷¹ to revise parts of this benchmark set. This composite DFT method has already proven its accuracy with respect to the reproducibility of volumes of molecular crystals³⁴³ and is ideally suited for such computational intensive calculations.¹⁸

I. Development of the DFT-D4 London Dispersion Correction

Table 3.2.: Refinement of the ICE10 benchmark set³³⁶ (excluding polymorph II and XIII) with a correction of equilibrium volumes V_e to free-energy volumes V_0 due to ZPVE and thermal energies calculated at the HSE-3c level of theory³⁴³ using a quasi-harmonic approximation. Structures and experimental temperatures are taken from Ref. 336. For all PAW calculations an 800 eV plane-wave energy cutoff is applied to minimize Pulay stress. All volumes are given in \AA^3 .

Polymorph	HSE-3c			Experiment ^a		$\Delta V / \%$		
	V_0	V_e	$\Delta V/V_0$ (%)	V_0	V_e^{ref}	PBE	-D4	-MBD
Ih	29.19	28.11	3.7	32.05	30.86	-3.0	-5.8	-6.5
III	25.11	23.69	5.7	25.69	24.23	7.3	0.9	-0.5
VI	23.36	21.44	8.2	22.84	20.97	5.0	0.5	-0.7
VII	23.03	21.32	7.4	20.26	18.76	7.4	1.8	0.8
VIII	23.03	21.38	7.2	20.09	18.64	8.2	2.7	2.2
IX	24.88	23.76	4.5	25.63	24.48	5.8	-1.0	-2.8
XIV	23.65	21.75	8.0	23.12	21.27	6.4	1.4	0.1
XV	23.45	21.60	7.9	22.45	20.68	7.2	1.8	5.0

^aExperimental V_e estimated as $V_e^{\text{ref}} = V_0^{\text{ref}} \left(1 + \frac{V_e^{\text{HSE-3c}} - V_0^{\text{HSE-3c}}}{V_0^{\text{HSE-3c}}} \right)$.

The direct comparison of PBE-D4 and PBE-MBD shows that both methods are well suited to describe equilibrium volumes of ice polymorphs. For the IX system, both methods calculate volumes that are too small, while for the VI and III systems D4 yields a too large volume while MBD does the opposite. The only ‘‘outlier’’ can be seen in the hexagonal ice Ih, where both methods drastically underestimate the equilibrium volume. The effect of the underlying density functional should be considered as well, since PBE is known to overbind hydrogen bonds³⁴⁴. For the Ih polymorph earlier studies already showed that PBE drastically underestimates the equilibrium volume³⁴⁵ which could be corrected by explicitly including many-body correlation effects in terms of diagrammatic perturbation theory. However, this is beyond the scope of this work and will be neglected. The data of Table 3.2 show that PBE-D4 is suitable to generate accurate volumes for ice polymorphs (MD = 0.3%, MAD = 2.0%, RMSD = 2.7%) when comparing to MBD corrected PBE (MD = -0.3%, MAD = 2.3%, RMSD = 3.4%). In general, pure PBE drastically overestimates all equilibrium volumes (PBE: MD = 5.6%, MAD = 6.3%, RMSD = 3.6%) indicating that use of an appropriate London dispersion correction is indispensable even in systems that are dominated by hydrogen bonding.

3.3.3. Adsorption on Surfaces

To evaluate the performance of the D4 and related approaches for the calculation of adsorption energies, three chemically diverse model systems dominated by NCIs are considered.³⁴⁶ These include the adsorption of non-polar benzene on gold (sparse), polar CO on polar MgO (saturated), as well as non-polar C₂H₂ on ionic NaCl (also saturated). For all of these, accurate experimental and/or high-level computational references are available. The respective adsorption models are shown in Figure 3.8. In addition to D4, we consider its predecessors D3(BJ), D2, as well as other established methods, namely MBD (including variants), TS (including variants) and the vdw-DF2 and rVV10 dispersion functionals. All DFT-D and TS/MBD calculations are conducted in combination with the PBE functional. This is done for the sake of comparability and in spite of experience showing related GGAs and meta-GGA like RPBE, revPBE and TPSS are often more accurate for the investigation of adsorption. The adsorption energies are calculated using

$$\Delta E_{\text{ads}} = (E_{\text{total}} - E_{\text{slab}} - nE_{\text{molecule}}) / n, \quad (3.6)$$

where n is the number of adsorbed molecules per unit cell, E_{slab} the energy of the vacant surface, E_{total} the energy of the adsorbed molecule on the surface, and E_{molecule} the energy of the isolated molecule. To circumvent computationally expensive structure optimizations at each level, and yet avoid a bias by using one of the tested dispersion-correction schemes to conduct the optimizations, all calculations refer to single-point energies (cut-off 800 eV) on geometries obtained at the plain DFT/SCAN level (cut-off 500 eV). In these optimizations, the molecules as well as the first (complete) layer of the surfaces is relaxed, while the lower layers were kept fixed at default values provided by the atomic simulation environment (ASE).³⁴⁷ SCAN has been chosen for this purpose because it provides reasonable agreement for all systems without any dispersion correction, and moreover accurate structural parameters for bulk *fcc* gold.³³⁹ In general, the impact of the geometric relaxation from the ASE default structures is small but not negligible with the adsorption energy changing by about 0.01-0.02 eV in case of the polar surfaces and 0.05 eV for benzene on gold (calculated at the PBE-D3(BJ) and SCAN levels of theory)

Figure 3.8 shows the deviation from reference values for all considered methods. Before we begin the discussion, it should be pointed out that there is a systematic bias when comparing calculated adsorption energies to experimental enthalpy values. The problem being that no straightforward approach exists to account for zero-point and thermal contributions in these types of calculations. However, since both of these contributions reduce the interaction strength, an overestimation of the theoretical adsorption energy compared to the reference values is preferable

I. Development of the DFT-D4 London Dispersion Correction

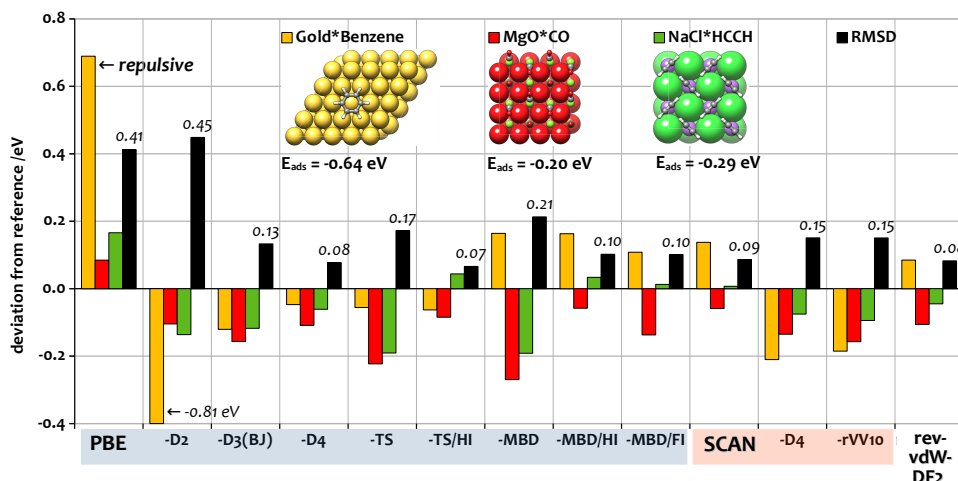


Figure 3.8.: Comparison and benchmark of DFT-D4 and related approaches for the adsorption of small organic molecules at metallic and ionic surfaces.

to an underestimation. To provide an estimate for the magnitude of these contributions, we estimate the thermal contributions and neglect zero-point vibrational contributions. The latter are typically small in the case of adsorption since the bond formed between surface and adsorbate is rather weak. Assuming a classical picture and moreover that adsorption freezes out all translations and rotations of the adsorbate in the gas phase, this provides a correction of $5/2kT = 0.065$ eV for the linear CO and acetylene molecules and $3kT = 0.078$ eV for benzene at 300 K. These will be taken into account in the discussion.

Benzene on gold—The adsorption of aromatic molecules on transition metal surfaces is of particular interest in materials science because the catalytic conversion of aromatic substances is a key reaction in many petrochemical processes.³⁴⁸ Our model is based on the common adsorption mode with benzene flat on the (111) surface of *fcc* Au as is shown in Figure 3.8, and corresponds to coverage of $\theta = 1/25$.³⁴⁹ Since gold provides one of the most inert surfaces, the adsorption is almost exclusively driven by London dispersion. The experimental estimate of the adsorption energy is -0.64 eV at a sub-monolayer coverage.³⁵⁰ Plain PBE provides a qualitatively wrong, repulsive energy of (0.49 eV). While the old D2 model clearly over-corrects this failure of PBE with an adsorption energy of -1.4 eV, the newer D3(BJ) model provides a much improved energy of -0.76 eV, which can be considered in agreement with the experiment given the absence of zero-point and thermo-chemical corrections in the calculated values. The D4 model presented here is even closer to the experimental result with -0.69 eV. The original TS model performs very similar to D4 (-0.70 eV) irrespective if fixed or iterative Hirshfeld charges are used. Including many-body effects via the MBD approach significantly worsens the agreement, providing too small adsorption energies (-0.48 eV). Plain

I. Development of the DFT-D4 London Dispersion Correction

SCAN finds, in contrast to PBE, an attractive interaction between adsorbate and surface. However, with -0.50 eV it is slightly below the experimental value. This confirms that SCAN describes parts of medium-range correlation effects intrinsically. However, as already seen for the molecular crystals, this can lead to double counting in combination with dispersion corrections. Accordingly, both SCAN-rVV10 and SCAN-D4 slightly over-bind the system with adsorption energies of -0.83 eV and -0.85 eV, respectively. Also the rev-vdw-DF2 functional correctly recovers the (attractive) interaction between adsorbate and surface, but slightly underestimates it with an adsorption energy of -0.56 eV.

Carbon monoxide on magnesium oxide—The adsorption of carbon monoxide on MgO(001) surfaces has been extensively studied both experimentally^{351–353} and theoretically.^{354–357} Experimental studies provided adsorption energies ranging from about -0.13 eV^{352,358} up to -0.20 eV,³⁵⁹ and showed that CO adsorbs in a C-down configuration on top of five-fold coordinated Mg atoms.³⁵² This is reflected in our model system with a coverage of 75%, which has been taken from Ref. 170 and is shown in Figure 3.8. While previous DFT-based studies predict a wide range of adsorption energies from -0.10 eV to -0.56 eV,³⁵⁵ coupled-cluster based approaches provide values in better agreement with the experiment of -0.15 eV³⁵⁷ to -0.17 eV³⁶⁰. Considering the absence of zero-point and thermo-chemical corrections in our calculations, we selected the lowest experimental value of -0.20 eV to be used as reference. Already plain PBE is with a computed adsorption energy of -0.12 eV in qualitative agreement with the reference value. As noted previously, the D2 model over-binds CO with an adsorption energy of -0.30 eV. Surprisingly, this becomes even worse with D3(BJ) (-0.36 eV), and even D4 does not improve the result with -0.31 eV. In fact, all employed methods except plain PBE predict much too large adsorption energies for this system, which range from the worst value of -0.47 eV (MBD) to the best of -0.26 eV (SCAN, MBD/HI). This may be seen as a hint towards a more fundamental problem of DFT for this system, or a problem with the model system. In face of this general over-binding of dispersion-corrected DFT for this system, it is not surprising that SCAN and MBD/HI provide the best agreement, as these are also the approaches that provide the over-all smallest adsorption energies, and accordingly the only ones besides plain PBE with a positive mean average deviation.

Acetylene on sodium chloride—The adsorption of acetylene on sodium chloride has been studied by several groups experimentally and theoretically. Experimental adsorption energies^{361,362} range from -0.25 to -0.31 eV corresponding to full and half coverage, respectively. Previous studies employing periodic DFT provide values ranging from -0.32 eV to -0.44 eV.¹⁷⁰ We employ the same model system, which corresponds to full coverage with the C₂H₂ molecules ordered in

I. Development of the DFT-D4 London Dispersion Correction

a T-shaped formation (*cf.* Figure 3.8). We use a reference value of -0.29 eV, which is between the experimental estimates for full and half coverage. Plain PBE affords an attractive yet too small interaction between adsorbate and surface, as evident from the adsorption energy of -0.12 eV. Again, D2 significantly over-corrects to an adsorption energy of (-0.42 eV). This improves slightly with D3(BJ) providing -0.40 eV, and more significantly with the latest D4 approach to -0.35 eV. Most certainly, this improvement is related to the superior ionic polarizabilities of the D4 approach compared to D3(BJ). Also the results of the other methods demonstrate the necessity for accurate ionic polarizabilities. While the TS and MBD approaches with their fixed atomic charges both over-stabilize this system even more than D2 with an adsorption energies of -0.48 eV, the iterative schemes TS/Hi and MBD/Hi yield much better agreement with -0.24 eV and -0.25 eV. Adding ionic references in the MBD/Hi schemes further improves this agreement, leading to an adsorption energy closer to both D4 and the reference with -0.27 eV. Also plain SCAN provides a good description, yielding an adsorption energy of -0.28 eV, which increases slightly when the functional is combined with a dispersion correction (SCAN-D4 -0.36 eV, SCAN-rVV10 -0.38 eV). Also the rev-vdW-DF2 functional performs well with a value of -0.33 eV.

In particular this last system nicely demonstrates the necessity to include charge and/or density information in the dispersion correction, as evident from the superiority of D4 over D3(BJ), as well as the charge-iterative Hirshfeld schemes over the standard models. Regarding the over-all statistical agreement, the data indicate that PBE-D4, PBE-TS/Hi, SCAN and rev-vdW-DF2 are the most accurate approaches with an RMSD below 0.1 eV. Of these, in particular PBE-D4 stands out with the most consistent deviation in the form of a slight over-binding of the adsorbates. As pointed out earlier, this is preferable to an under-binding and would be corrected by including zero-point and thermo-chemical contributions in the calculations. The perhaps most surprising result from this benchmark is the excellent performance of the uncorrected SCAN functional. However, this also comes at an increased computational cost, as will be discussed in detail in the next section.

3.3.4. Timings

In this section, we compare the computational cost of different dispersion-corrected DFT methods using the cyclohexanedione crystal structure as a test case. For this purpose, single-point energy calculations are conducted with VASP with settings for high numerical precision (cut-off of 800 eV, fine k -point grid) on a 16 core Intel(R) Xeon(R) CPU (E5-2660 v4 @ 2.00 GHz). With this set-up, the DFT/PBE single-point takes about 7.5 minutes walltime. Figure 3.9 provides the total wall-

I. Development of the DFT-D4 London Dispersion Correction

time of the calculation, as well as (if possible) the timing for the dispersion-correction only, which is determined as the difference between the DFT/PBE calculation with and without the respective correction.

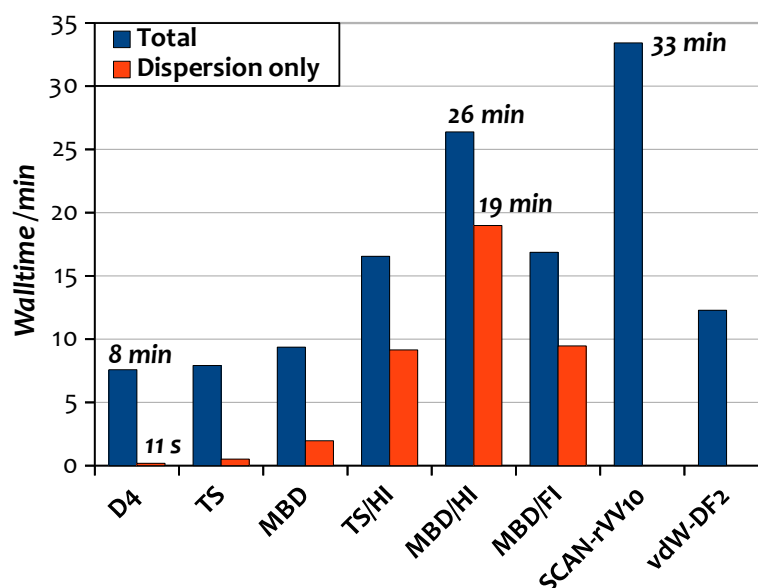


Figure 3.9.: Total wall-clock time of a single-point calculation for the cyclohexanedione crystal with DFT/PBE and various dispersion-correction schemes, SCAN-rVV10 and rev-vdW-DF2 (blue bars). Time spent on the dispersion correction alone is shown in orange (not available for the self-consistent approaches). While cost of D4, TS (and MBD) is almost negligible compared to the DFT calculation (7.4 minutes), the charge-iterative TS and MBD schemes are much slower (MBD/Hi over 100 times slower than D4) and become the bottleneck of the calculation.

Regarding the total walltime, DFT-D4, -TS and -MBD (the latter with fixed charges) are comparable with timings just under 10 minutes, followed by rev-vdW-DF2 just above 10 minutes. The charge-iterative schemes are significantly more expensive taking just above 15 (TS/Hi, MBD/FI) up to almost 30 minutes (MBD/Hi). Only the SCAN-rVV10 calculation takes even longer with 33 minutes, but this is mostly due to the increased computational cost of the SCAN functional. Removing the overhead of the DFT calculation and focusing only on the timing of the dispersion-correction, D4 turns out as the fastest method by far with 11 s, followed by fixed-charge TS and MBD with 31 s and 118 s, respectively. All of these are in stark contrast to the charge-iterative schemes, which are orders of magnitude slower taking as long (9 min for TS/Hi and MBD/FI), or twice as long (19 min for MBD/Hi) as the underlying DFT/PBE calculation. As a result, the dispersion-correction becomes the bottleneck of the calculation, in spite of the high numerical precision settings for the DFT calculation. In combination with semi-empirical and/or tight-binding approaches, or just more sloppy DFT settings and a good initial guess – as is the typical scenario for DFT molecular-dynamics

simulations – the charge-iterative schemes are impractical and only the fastest schemes (D4, TS) remain useful.

3.4. Summary and Conclusions

We presented an extension of the molecular DFT-D4 model for describing dense condensed-phase systems under periodic boundary conditions. For this purpose, new periodic reference polarizabilities for alkaline, for alkaline-earth, and for early *d*-metals (group 3-5) were calculated using a pseudo-periodic electrostatic embedded cluster model.

The utility of the additional reference polarizabilities was demonstrated by calculating solid state polarizabilities of different salts and comparing them to experimental data. Here, the new references lead to a dramatic improvement for cationic and anionic polarizabilities, which now exhibit the correct ordering compared to the experiment and also show better quantitative agreement. For the same test set, related methods like MBD, MBD/HI and even MBD/FI exhibited much larger deviations. This is despite the explicit inclusion of ionic reference systems in the MBD/FI approach, which improves the description compared to MBH/HI, but does not approach the accuracy of the D4 model.

Eventually, the performance of the periodic DFT-D4 model was tested and compared to its predecessors and related approaches in three real-world application scenarios. These include (i) the calculation of lattice energies of molecular crystals, (ii) the determination of cell volumes of molecular crystals, as well as (iii) the modeling of the adsorption of chemically diverse substrates on non-polar, polar and ionic surfaces. For lattice energies of molecular crystals, various D3 and D4 corrected DFAs showed excellent agreement to high-level references. Especially “repulsive” density functionals (*e.g.*, revPBE, TPSS, and PBE0) turned out to provide an accurate account for NCIs, whereas density functionals that already include mid-range correlation to some extent (SCAN) appear to suffer from possible double-counting issues. Other approaches showed to be competitive to D4 for describing such lattice energies like MBD/HI corrected DFAs or the rev-vdw-DF2 functional. The quality of geometries was investigated using cell volumes of 23 molecular crystals and eight different ice polymorphs. For those systems, DFT-D4 yielded accurate cell volumes with a deviation very similar to related approaches. In general, all tested approaches show a tendency to calculate slightly too small volumes. Regarding the calculation of adsorption energies for organic molecules, a direct comparison between DFT-D4 and electron density dependent (TS;TS/HI, MBD;MBD/HI;MBD/FI, vdw-DF2, rVV10) and independent (DFT-D3(BJ) and DFT-D2) models showed DFT-D4, TS/HI and rev-vdW-DF2 to provide the best agreement, followed by SCAN (without any vdW correction) and the iterative

MBD schemes. Of these, D4 stands out as the approach provides the most systematic deviation in the form of a slight over binding.

Ultimately, an analysis of computational timings shows that DFT-D4 is orders of magnitude faster than the iterative MBD schemes which offer similar accuracy, and thus provides the best balance between cost and accuracy. With the development of the periodic DFT-D4 model it is routinely possible to describe chemically diverse molecular, periodic solids or surfaces accurately with a low computational effort.

3.5. Acknowledgments

EC thanks T. Bredow for valuable discussions. Furthermore, the authors thank J. G. Brandenburg for sharing molecular crystal structure benchmark sets of the DMC8 benchmark set and T. Bučko for help with the MBD calculations.

3.6. Appendix A3

Within Appendix A3, first the periodic DFT-D4 methodologies are introduced followed by the theoretical definition of the quasi-harmonic approximation. Afterwards, the technical details for the calculation of reference polarizabilities are shown. Finally, the computational details of all applications are given in detail.

Part II.

**Applications of London
Dispersion Corrections in
Molecular Systems**

The use of large, sterically overcrowded substituents is common practice for many synthetic works in organic chemistry. As frequently proposed, the primary purpose of substituents is to prevent their central atom from initiating reactions that could lead to decomposition or transformation of the compounds. Substituents cause stabilization by occupying space around a reactive centre^{363,364} preventing access to it, or by shielding this space by the use of bowl-shaped or concave ligands.³⁶⁵ Examples of such ligands are, e. g., tertphenyls^{366–368} or *N-heterocyclic Carbenes* (NHCs)^{369,370}. The bulk effects of such ligands base upon EXR that originates from one or more hydrocarbon-substituted groups. Formerly, scientists typically assumed that the attractions caused by LD are individually weak and virtually negligible. This misunderstanding roots in the validity of the assumption when applied to a single pair of atoms. In larger molecules, however, LD effects have considerable significance inducing stabilization in the order of dozens of kilocalories per mole. Such attractive effects can thus compete with the EXR and realize special binding situations. One famous example is the instability of the hexaphenyl ethane ($\text{Ph}_3\text{C}-\text{CPh}_3$), which only exists as persistent radicals ($\text{Ph}_3\text{C}\cdot$) as first reported by Gomberg.^{371,372} These trityl radicals do not dimerize to the expected hexaphenyl ethane. By contrast, the sterically more crowded tris(3,5-di-tert-butylphenyl)methyl radical dimerizes,^{373,374} forming a stable colourless, crystalline solid with an elongated C-C bond of 1.67(3) Å (see system **2** in figure 4.1). A computational study³⁷⁵ revealed that the tremendous stabilizing energy arises from LD effects between the *meta tert*-butyl groups.

As the importance of LD is well-known, e. g., in protein research,³⁷⁶ supramolecular,³⁷⁷ and theoretical chemistry,^{17,239,378} the next two chapters highlight some organic and organometallic compounds where these forces play a crucial role. Chapter 4 investigates another unique binding situation in the tris(3,5-di-tert-butylphenyl)methane (TPM) molecular crystal. This compound crystallizes in C_3 -symmetric head-to-head dimers, each revealing an intermolecular $\text{H}\cdots\text{H}$ contact of only 1.566(5) Å. This binding motif is rationalized by the HSE-3c composite scheme, and an energy decomposition scheme verifies the importance of LD effects for the molecular TPM-dimer complex. The dissociation energy of the TPM dimer and the unsubstituted symmetric triphenyl-methane dimer shows the substantial overall stabilizing effect of the *meta tert*-butyl groups.

One of the first publications that describe the structural distortion of an organometallic complex utilizing LD effects concerned the transition metal and lanthanide amido derivatives $\text{M}[\text{N}(\text{SiMe}_3)]$ ($\text{M} = \text{Sc}$ and Eu). Those three-coordinated compounds display a pyramidalized rather than a planar metal coordination.³⁷⁹ Studies suggested that the planarity distortion arises in the formation of the crystalline phase, in which the metal ion is pushed out of the coordination plane by a sym-

metrical contraction resulting from intramolecular-interligand van der Waals attractions. Recently, the number of publications concerning LD effects controlling the stability, structure and reactivity of various transition metals increased rapidly. Examples are found for Pd(PPh₃)₄,³⁸⁰ Pd(P^tBu₃)₂,³⁸¹ Os(Cl)₂(H₂)(PⁱPr₃)₂,³⁸² or the Grubbs' catalysts.³⁸³ The theoretical understanding and quantification of LD within such organometallic complexes are of crucial importance when it comes to reaction planning of future synthesis. Chapter 5 deals with LD effects in such organometallic complexes. The theoretical foundations of long-range correlation are shortly recapped. Afterwards, the necessity of including a dispersion correction in DFT is highlighted by the calculation of high-quality structures and high-quality relative energies. The latter is verified by comparing against literature-known benchmark sets. A comparison to experimental data validates the theoretically obtained molecular geometries. Furthermore, absolute DFT-D3 and DFT-D4 dispersion energy values are discussed for HF and several DFAs and compared to high-level coupled-cluster values obtained in a local energy decomposition.

4. London Dispersion Enables the Shortest Intermolecular Hydrocarbon H · · · H Contact

Sören Rösel*, Hendrick Quanz*, Jonathan Becker†, Estelle Mossou‡ §, Laura Cañadillas-Delgado¶‡, Eike Caldeweyher||, Stefan Grimme||, Peter R. Schreiner*

Received 28th of February 2017, Published online 13th of May 2017

Reprinted (adapted) with permission from††

Rösel, Sören and Quanz, Hendrick and Logemann, Christian and Becker, Jonathan and Mossou, Estelle and Cañadillas-Delgado, Laura and Caldeweyher, Eike and Grimme, Stefan *J. Am. Chem. Soc.* **2017**, *139*, 7428–7431.

— Copyright © 2017 American Chemical Society.

DOI [10.1021/jacs.7b01879](https://doi.org/10.1021/jacs.7b01879)

Own manuscript contribution

- Periodic (HSE-3c) and molecular (B3LYP-D3(BJ)-ATM/def2-TZVPP) geometries as well as frequency calculations with PBEh-3c (including deuterium derivate of [Bis(tri(3,5-di-tert-butylphenyl)-methane)])
- Solvation free energies with COSMO-RS and Gibbs free energies
- Energy decomposition analysis with B3LYP-D3(BJ)-ATM/def2-TZVPP
- Interpretation of the results and writing theoretical part of the manuscript

*Institute of Organic Chemistry, Justus-Liebig University, Heinrich-Buff-Ring 17, 35392 Giessen, Germany

†Institut für Anorganische und Analytische Chemie, Justus-Liebig Universität, Heinrich-Buff-Ring 17, 35392 Giessen, Germany

‡Institute Laue-Langevin, Rue Jules Horowitz 6, BP 156, 38042 Grenoble Cedex 9, France

§Faculty of Natural Sciences, Keele University, Staffordshire ST5 5BG, United Kingdom

¶Centro Universitario de la Defensa de Zaragoza, Ctra Huesca s/n, 50090 Zaragoza, Spain

||Mulliken Center for Theoretical Chemistry, Institute of Physical and Theoretical Chemistry, University Bonn, Berlingstraße 4, 53115 Bonn, Germany

††Permission requests to reuse material from this chapter should be directed to the American Chemical Society.

II. Applications of London Dispersion Corrections

Abstract Neutron diffraction of tri(3,5-tert-butylphenyl)methane at 20 K reveals an intermolecular C-H...H-C distance of only 1.566(5) Å, which is the shortest reported to date. The compound crystallizes as a C₃-symmetric dimer in an unusual head-to-head fashion. Quantum chemical computations of the solid state at the HSE-3c level of theory reproduce the structure and the close contact well (1.555 Å at 0 K) and emphasize the significance of packing effects; the gas-phase dimer structure at the same level shows a 1.634 Å C-H...H-C distance. Intermolecular London dispersion interactions between contacting tert-butyl substituents surrounding the central contact deliver the decisive energetic contributions to enable this remarkable bonding situation.

Continuously probing the limits of chemical bonding helps improve our current understanding of molecular structure theories. Many are enthralled by the notion of going beyond carbon-carbon triple bonds,³⁸⁴ inorganic quadruple and higher bond orders,^{385,386} twisted double bonds,^{387–389} compressed^{390,391} and stretched covalent bonds^{392–394} and noncovalent interactions such as extremely short C...C contacts,^{395,396} and many more. To the best of our knowledge, we report here the shortest intermolecular H...H contact in a hydrocarbon as evident from the exceptional congruence of both neutron and X-ray diffraction experimental data with quantum chemical crystal structure computations. Impressive examples for very short intramolecular C-H...H-C contacts are some bowl-like structures such as exo,exo-tetracyclo[6.2.1.1.^{386,389}0^{385,390}]dodecane **3** derivatives with R_{H...H} down to 1.713(3) Å³⁹⁷ (neutron diffraction data, NRD) and the famous current record holder “half-cage” pentachloro-pentacyclododecane **4** with a short H...H contact of 1.617(3) Å (NRD), thereby significantly undercutting the sum of the van der Waals (vdW) radii of 2.40 Å³⁹⁸ by $\Delta R_{\text{vdW}} = -0.78$ Å (Figure 4.1).⁷⁷ Such compressions are not uncommon in heteroatomic polycycles, with Pascal’s record holder **5** that displays an intramolecular Si-H...H-Si contact of roughly 1.56 Å, as judged from quantum chemical computations and the Si...Si distance of 4.433(2) Å derived from X-ray single crystal diffraction (XRD) data; unfortunately, no NRD study of **5** has been published.^{399,400}

II. Applications of London Dispersion Corrections

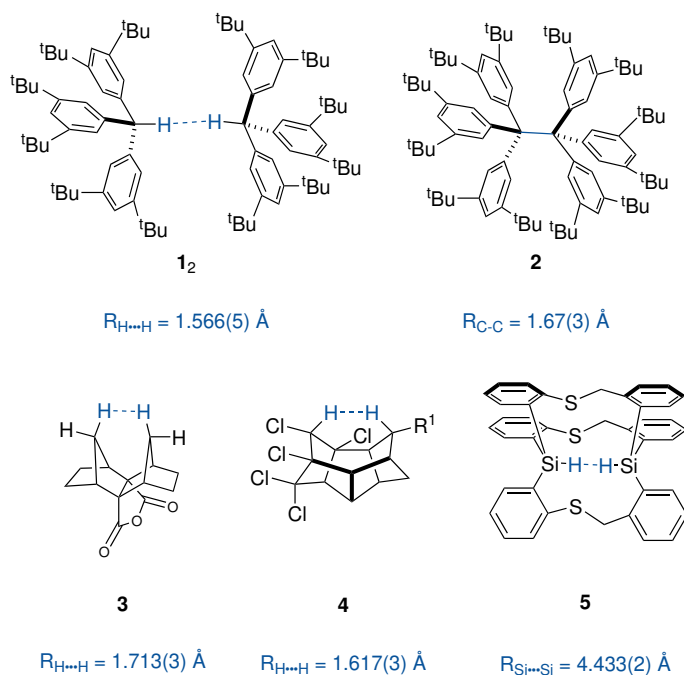


Figure 4.1.: Short intermolecular H...H contact in all-meta ^tBu-triphenyl-methane dimer **1₂** and the long R_{C-C} in LD stabilized all-meta ^tBu-hexaphenylethane **2**. Polycyclic structures with short intramolecular H...H contacts: *exo,exo*-tetracyclododecane **3** (NRD), "half-cage" **4** (NRD) and *in,in*-bis(hydrosilane) **5** (XRD; $R_{H...H} \approx 1.56$ Å by computations and 1.531(8) Å by NRD⁴⁰⁰).

Structures **3-5** share tight transannular H...H contacts within a sterically confined environment, and at first glance such short contacts would not be expected intermolecularly because of the energetic penalty associated with bringing atoms much within their comfortable vdW-radii.⁴⁰¹⁻⁴⁰⁴ Here we demonstrate not only that this energetic drawback can be overcome in an intermolecular bonding situation via highly attractive London dispersion^{161,162,405} (LD) interactions, but also that such short nonbonding distances can be compressed even more than in the shortest published intramolecular case. In molecular design, large alkyl groups are used to introduce bulk and sterically shield reactive moieties. The fact bulky groups are highly polarizable, thereby increasing their ability to engage in non-negligible, stabilizing LD interactions, is often disregarded. Such groups are appropriately termed "dispersion energy donors", DEDs.⁴⁰⁶ This thermodynamic stabilization can be utilized to isolate otherwise highly reactive molecular entities within an LD shell,⁴⁰⁷ as demonstrated for bulky NHC coordinated main group compounds⁴⁰⁸ and the exceedingly crowded hexaphenylethane derivatives such as all-meta ^tBu-hexaphenylethane (**2**).^{375,409} Although hexaphenylethane is experimentally unknown, sterically much more crowded **2** is isolable and was characterized via XRD³⁷⁴ and NMR spectroscopy.⁴¹⁰ The origin of the stabilization

II. Applications of London Dispersion Corrections

was traced back to LD interactions between the ^tBu-groups, which are deemed excellent DEDs.^{375,409} The otherwise delicate organic peroxide functionality⁴¹¹ is also highly stabilized when embedded in the all-meta ^tBu-trityl motive leading to a m.p. (decomp.) of 253 °C in bis(tri(3,5-di-tert-butylphenyl)methyl) peroxide.⁴¹² These peripheral LD interactions also give rise to an all-meta ^tBu-triphenylmethane dimer **1**₂ [Bis(tri(3,5-di-tert-butylphenyl)-methane)], featuring the shortest C-H···H-C contact reported to date (Figure 4.2)

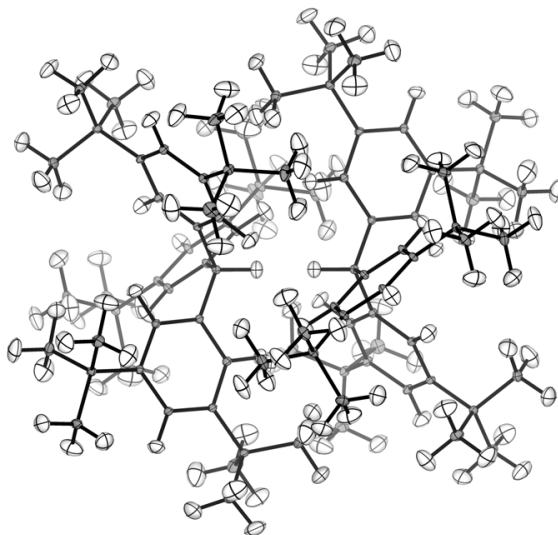


Figure 4.2.: ORTEP representation of **1**₂ derived from neutron diffraction data with ellipsoids drawn at 50% probability.

Hydrocarbon **1** crystallizes in the cubic space group $Pa\bar{3}$ as determined by XRD at 100 K. The asymmetric unit consists of one 3,5-di-^tBu-phenyl group attached to the central C_α - H_α moiety. Application of the S_6 symmetry operation present in $Pa\bar{3}$ along the C_α - H_α axis results in dimer **1**₂ with a $R_{C_\alpha \dots C_\alpha}$ of 3.780(7) Å. As the XRD C-H bond length of $R_{C-H} = 1.00(4)$ Å already revealed a remarkably short C-H···H-C distance of 1.77(7) Å, we reckoned the true distance must be significantly shorter because of the well-known underestimation of XRD C-H bond distances. Using NRD at the lowest achievable temperature of 20 K utilizing a large crystal with 2 mm edges, we determined the cubic, yet less symmetric space group $P2_13$.⁴¹³ The new asymmetric unit consists of two distinguishable fragments, lowering the symmetry in the dimer to C_3 . Although the C_α - H_α bond lengths are ordinary⁴¹⁴ (Table 4.1) with 1.088(5) Å and 1.098(5) Å, the extremely short intermolecular $H_\alpha \dots H'_\alpha$ contact of only 1.566(5) Å is the shortest reported to date.

II. Applications of London Dispersion Corrections

Table 4.1.: Structural Data of $\mathbf{1}_2$ Determined by NRD and DFT Computations.

	NRD			HSE-3c ^b	
T [K] (state)	20	100	200	0 (s)	0 (g)
R-value	0.031	0.054	0.096		
Volume [\AA^3]	7833.1(4)	7901.4(4)	8040.4(4)	7676.9	
$H_\alpha \cdots H'_\alpha$	1.566(5)	1.577(6)	1.594(9)	1.555	1.634
$C_\alpha \cdots H_\alpha$	1.093(5) ^{c,d}	1.093(3)	1.091(5)	1.088	1.092
Ave. $C_{\text{alk}}\text{-H}$	1.090(7)	1.078(29)	1.068(45)	1.091	1.091
Ave. $C_{\text{arom}}\text{-H}$	1.085(6)	1.085(2)	1.076(4)	1.082	1.082
$C_\alpha\text{-}C_i$	1.515(1) ^c	1.515(1)	1.515(2)	1.509	1.513
$H_\alpha\text{-}C_\alpha\text{-}C_i$	106.0(1) ^c	106.0(1)	105.9(1)	105.9	104.8
$C_i\text{-}C_\alpha\text{-}C_i$	112.7(1) ^c	112.7(1)	112.8(1)	112.8	113.7
$H_\alpha\text{-}C_\alpha\text{-}C_i\text{-}C_o$	39.8	39.8	40.1	39.8	45.3
$H_o \cdots Ph^a$	3.632	3.639	3.654	3.613	3.637
$H_o \cdots C'_o$	2.927(1)	2.958(1)	2.978(1)	2.917	3.062
^t Bu $\cdots Ph^a$	5.192	5.136	5.140	5.025	4.982
^t Bu \cdots ^t Bu ^a	6.166	6.115	6.113	6.037	5.889

^aGroup centroid distances.

^bBasis set: def2-mSVP.

^cAve. of both molecules in $\mathbf{1}_2$ (cf. supporting information of Ref. 409).

^d $C'_\alpha\text{-}H'_\alpha = 1.098(5)$ \AA .

To allow such short contacts well below their vdW radii,^{398,415} the overall stabilization must derive from other parts of the molecule, which, based on the measured NRD data, do not suffer from significant deformations: The sp^3 angles around the central carbon C_α amount to 106.0° ($H_\alpha\text{-}C_\alpha\text{-}C_i$) and 112.7° ($C_i\text{-}C_\alpha\text{-}C'_i$); the C-C bonds are ordinary.⁴¹⁴ More importantly, there are 33 contacts within the attractive vdW-range below the sum of the atom radii (3.08 \AA)⁴¹⁶ down to 2.39 \AA . NRD measurements at higher temperatures (Table 4.1) reveal the expected structural temperature dependence resulting in an $H \cdots H$ distance change of $\Delta R_{H \cdots H} (20 \rightarrow 200 \text{ K}) = 0.03 \text{ \AA}$; linear extrapolation leads to a minimum $R_{H \cdots H}$ of 1.563 \AA at 0 K. To rationalize the structural peculiarities of $\mathbf{1}_2$, we employed DFT computations within the CRYSTAL14 software suite⁷¹ utilizing the developed screened Fock exchange density functional composite scheme termed HSE-3c.³⁴³ This efficient method includes the D3 correction⁴⁶ and a geometrical counterpoise correction scheme¹⁵⁰ accounting for the basis set superposition error (BSSE) and improving the description of LD interactions. The primitive cell starting from the 20 K NRD data ($P2_13$) was fully optimized featuring relaxation

II. Applications of London Dispersion Corrections

of all atom positions as well as cell parameters. Because of the high symmetry of the molecular crystal, we were able to reduce the atom count within the primitive cell from 856 reducible to 74 irreducible atoms. The HSE-3c computed solid state structure is in agreement with the NRD structure of **1**₂ (Table 4.1). The H···H distance of 1.555 Å at 0 K reproduces the NRD extrapolated value within the error bounds. The volume of the primitive cell is 2% smaller than observed experimentally. This equals a thermal density gradient of $\approx 1 \text{ mg cm}^{-3} \text{ K}^{-1}$ (cf. supporting information of Ref. 409), which deviates from the experimental value ($0.1 \text{ mg cm}^{-3} \text{ K}^{-1}$) but is in the typical range for organic crystals.⁴¹⁷ To estimate packing effects, **1**₂ was computed in the gas phase at the same level of theory. This elongates the central H···H contact to 1.634 Å. Crystal packing thus provides some non-negligible stabilization to the tight H···H contact. Note that the often employed approximation of using molecularly (non-periodic) optimized structures as substitute for periodic crystal data is insufficient in our case and would lead to inconsistencies between theory and experiment of about 0.07 Å. Closely related unsubstituted triphenylmethane **6**⁴¹⁸ and the all-meta methyl derivative **7** (cf. supporting information of Ref. 409) crystallize in space groups different from **1**₂, namely in $Pna2_1$ and $P\bar{1}$, respectively, and no linear head-to-head dimers can be discerned. An energy decomposition analysis (EDA, Figure 4.3 and cf. Appendix A4)⁴¹⁹ of **1**₂ at the B3LYP-D3(BJ)-ATM/def2-TZVPP level is instructive in understanding the roles of the various (arguably somewhat arbitrary) energy contributions to the overall stability of **1**₂; the trends are mirrored by an SAPT(0) analysis (Figure 4.3).

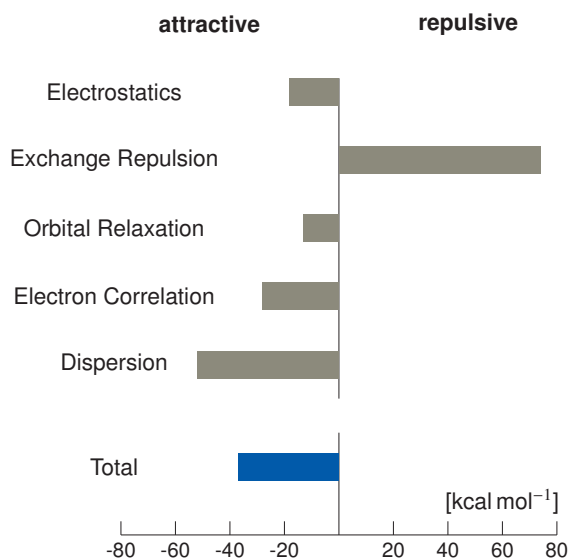


Figure 4.3.: Energy decomposition analysis of **1**₂ at B3LYP-D3(BJ)-ATM/def2-TZVPP.

Of course, the steric bulk of the ^tBu-groups increase the overall Pauli exchange

II. Applications of London Dispersion Corrections

repulsion between the monomers significantly. However, all other contributions including electrostatics stabilize the dimer interactions, with the dispersion component being by far the most important. To estimate overall stabilizing energy contributions of the ^tBu groups, the dissociation energy of **1**₂ was computed by optimization at B3LYP-D3(BJ)-ATM/def2-TZVPP including thermostistical corrections at PBEh-3c and compared to the unsubstituted symmetric triphenylmethane dimer **6**₂. Structure **1**₂ is bound by 48.9 kcal mol⁻¹ of LD; dissociation therefore is unfavored by $\Delta G_{\text{d}}^{298} = 7.7$ kcal mol⁻¹.¹⁶⁷ By omitting the ^tBu moieties, the head-to-head arrangement of **6**₂ becomes unstable and about 77% of LD interaction is lost resulting in $\Delta G_{\text{d}}^{298} = -8.5$ kcal mol⁻¹. Solvation free energy contributions computed with BP86-COSMO-RS⁴²⁰⁻⁴²² for CHCl₃ destabilize the dimerization of **1**₂ by $\Delta\Delta G^{298} = -8.1$ kcal mol⁻¹. In addition, we note a relatively large contribution of the (often repulsive) three-body Axilrod-Teller-Muto (ATM) dispersion terms^{17,167,168} that enlarge the H···H distance by about 0.01 to 0.02 Å while decreasing the *D_e* from 30.9 to 27.7 kcal mol⁻¹. Dimer **1**₂ is formally the hydrogenation product of **2**. Upon dissociation of **2**, a second, local minimum was predicted to occur along the intrinsic reaction coordinate.³⁷⁵ Such radical “van der Waals complexes”, better termed LD-complexes, are related to the “cage-effect”.⁴²³ The bis(all-meta ^tBu-triphenylmethyl radical) LD-complex **8**₂ with a C···C distance of 5.28 Å can be taken as a hydrocarbon analogue of structures with frustrated Lewis pairs (FLPs),⁴²⁴ where the split central C-C bond corresponds to the unsaturated dative D→A bond. This analogy was recognized in the very first appearance of FLPs, where the authors depicted HPE derivatives as structures analogous to FLPs.⁴²⁵ As FLPs are able to split H₂,⁴²⁶ it seemed plausible that **8**₂ may be able to split H₂ with **1**₂ being the formal product. Unfortunately, all attempts to split dihydrogen with the corresponding radical **8**• were unsuccessful, as solutions of **8**• eventually hydrolyze over a period of one month to all-meta ^tBu-triphenylmethanol and all-meta ^tBu-triphenyl-methane **1** when pressurized with H₂ or D₂ (for ease of identification by NMR, for details see supporting information of Ref. 409). We attributed this to the fact that the barrier for H₂ cleavage is the highest when there is no polarization as is the case for **8**•. From a different viewpoint, **1**₂ may also be viewed as a “frozen early transition state” because of the very close contact of the H_α's. Indeed, our computational analysis of the contact between the close hydrogens using the quantum theory of atoms in molecules (QTAIM)⁴²⁷ reveals a bond critical point and the noncovalent interaction (NCI) plot⁴²⁸ displays a strongly attractive region. Such computed attractions in tight H···H contacts were also found in a study of **5**.⁴²⁹ As such arrangements are far off equilibrium, an interpretation of the analysis of the density gradient is delicate and might lead to contradictory results. A bonding interaction between the H_α's should weaken the respective C_α-H_α bond, measur-

II. Applications of London Dispersion Corrections

able by a red-shifted C-H bond stretching frequency. However, experimentally the stretching vibration frequency of, e.g., **5** increases.⁷⁷ Unfortunately, the central C-H IR absorptions are buried under other vibrational bands for **1₂**. Deuteration at the central methine carbon red-shifts the corresponding C-²H bond stretching frequency into the uncongested region around 2100 to 2300 cm⁻¹ but we did not observe additional absorptions. The PBEh-3c computed central asymmetric (IR active) $\nu(\text{C}_\alpha\text{-H}\cdots\text{H-C}_\alpha)$ is about 56 cm⁻¹ blue-shifted as compared to $\nu(\text{C}_\alpha\text{-H})$ of the monomer, similar to what was found for **5** (Table 4.2).

Table 4.2.: B3LYP-D3(BJ)-ATM/def2-TZVPP Computations of the Dimeric Structures of Unsubstituted Triphenylmethane **6** and All-meta ^tBu-Substituted **1^a**

Measure	1₂	6₂
D _e	27.8	8.2
ΔH _d ²⁹⁸	26.6	8.7
TΔS _d ²⁹⁸	18.9	17.2
ΔG _d ²⁹⁸	7.7	-8.5 ^c
ΔG _{d,solv} ²⁹⁸	-0.4 ^d	-8.3 ^d
E _{DISP}	48.9	11.3
ΔR _{C-H} ^b	-0.007	-0.005
R _{CH...HC}	1.601	1.717

^aDistances in Å, energies in kcal mol⁻¹.

Thermostatistical corrections to free energy using PBEh-3c structures and vibrational frequencies.

^bDifference to monomer.

^c ΔG<0 means dissociation.

^dAfter solvent correction [BP86-COSMO-RS:CHCl₃].

In summary, we have identified the shortest intermolecular H···H contact (1.566(5) Å) reported to date in the crystal structure of the all-meta ^tBu-triphenylmethane dimer **1₂**, as analyzed by NRD at temperatures as low as 20 K. Solid state DFT computations reveal crystal packing does affect this distance but is not chiefly responsible for this short H···H contact. Rather, large LD interactions exerted via the ^tBu-groups surrounding the compressed H···H contact stabilize **1₂**. The ^tBu-groups act as DEDs and counter the otherwise energetically unfavorable head-to-head arrangement of H_α's.

4.1. Acknowledgments

This work was supported by the Priority Program *Dispersion* of the Deutsche Forschungsgemeinschaft.

4.2. Appendix A4

See Appendix A4 for further information about the applied computational setup. This includes coordinates of the previously introduced structures. Furthermore, values for the dissociation energies of the dimers to two monomers are given. Finally, values are given for the applied energy decomposition analysis for the TPM dimer structure.

5. Understanding and Quantifying London Dispersion Effects in Organometallic Complexes

Eike Caldeweyher*[†], Markus Bursch*[†], Andreas Hansen*, Hagen Neugebauer*, Sebastian Ehlert*, and Stefan Grimme*.

Received 3rd of October 2018, Published online 26th of December 2018

Reprinted (adapted) with permission from^{††}

Bursch, Markus and Caldeweyher, Eike and Hansen, Andreas and Neugebauer, Hagen and Ehlert, Sebastian and Grimme, Stefan *Acc. Chem. Res.* **2019**, *52*, 258–266.

— Copyright © 2017 American Chemical Society.

DOI [10.1021/acs.accounts.8b00505](https://doi.org/10.1021/acs.accounts.8b00505)

Own manuscript contribution

- Writing large parts of the manuscript (conspectus, introduction, and theory)
- Calculating $[[\text{Rh}(\text{CNPh})_4]_2]^{2+}$ dication structure and CPU timings
- Contributions of co-authors:
 - MOR41, WCCR10, HEAVY28 (S. Ehlert)
 - Grubs II, NCplots, sumanene complexes, indenyl complexes (M. Bursch)
 - LED analysis (H. Neugebauer)

*Mulliken Center for Theoretical Chemistry, Institute of Physical and Theoretical Chemistry, University Bonn, Berlingstraße 4, 53115 Bonn, Germany

[†]M.B. and E.C. contributed equally.

^{††}Permission requests to reuse material from this chapter should be directed to the American Chemical Society.

II. Applications of London Dispersion Corrections

CONSPECTUS Quantum chemical methods are nowadays able to determine properties of larger chemical systems with high accuracy and Kohn-Sham density functional theory (DFT) in particular has proven to be robust and suitable for everyday applications of electronic structure theory. A clear disadvantage of many established standard density functional approximations like B3LYP is their inability to describe long-range electron correlation effects. The inclusion of such effects, also termed London dispersion, into DFT has been extensively researched in recent years, resulting in some efficient and routinely used correction schemes. The well-established D3 method has demonstrated its efficiency and accuracy in numerous applications since 2010. Recently, it was improved by developing the successor (termed D4) which additionally includes atomic partial charge information for the generation of pairwise dispersion coefficients. These coefficients determine the leading-order (two-body) and higher-order (three- or many-body) terms of the D4 dispersion energy which is simply added to a standard DFT energy. With its excellent accuracy-to-cost ratio, the DFT-D4 method is well suited for the determination of structures and chemical properties for molecules of most kinds. While dispersion effects in organic molecules are nowadays well studied, much less is known for organometallic complexes. For such systems, there has been a growing interest in designing dispersion-controlled reactions especially in the field of homogeneous catalysis. Here, efficient electronic structure methods are necessary for screening of promising model complexes and quantifying dispersion effects. In this Account, we describe the quality of calculated structural and thermodynamic properties in gas-phase obtained with DFT-D4 corrected methods, specifically for organometallic complexes. The physical effects leading to London dispersion interactions are briefly discussed in the picture of second-order perturbation theory. Subsequently, basic theoretical aspects of the D4 method are introduced followed by selected case studies. Several chemical examples are presented starting with the analysis of transition metal thermochemistry and noncovalent interactions for small, heavy element containing main group compounds. Computed reaction energies can only match highly accurate reference values when all energy contributions are included in the DFT treatment, thus highlighting the major role of dispersion interactions for the accurate description of thermochemistry in gas-phase. Furthermore, the correlation between structural and catalytic properties is emphasized where the accessibility of high quality structures is essential for reaction planning and catalyst design. We present calculations for aggregates of organometallic systems with intrinsically large repulsive electrostatic interactions which can be stabilized by London dispersion effects. The newly introduced inclusion of atomic charge information in the DFT-D4 model robustly leads to quantitatively improved dispersion energies in particular for metallic systems. By construction it yields results which are easily understandable due to a clear separation into hybridization

II. Applications of London Dispersion Corrections

shows an asymptotic R^{-6} behavior, with R being the interfragment distance, and is thus classified to belong to the long-range electron correlation energy regime. Nowadays, state-of-the-art wave function theory (WFT) methods exist which are able to determine such long-range correlations with high accuracy. However, these methods are often not computationally feasible for calculating large or many smaller molecules due to the involved high computational effort. Hence, the development of simplified methods is of great importance that provide a reasonable compromise between accuracy and efficiency. Specifically, Kohn-Sham density functional theory (abbreviated as DFT in the following) has developed into a robust electronic structure method within modern electron structure theory in recent years. One disadvantage of DFT is its inability to describe long-range correlations sufficiently. However, such interactions are indispensable to obtain interaction energies with errors less than the common chemical accuracy of 1 kcal mol^{-1} , particularly for noncovalently bonded systems. Therefore, semiclassical dispersion corrections to DFT have been developed in the past years and are meanwhile used routinely in many quantum chemistry codes.^{17,46,47,179,210,432,433} Some of these correction schemes accurately incorporate LD into DFT at very small computational costs. The low-cost composite DFT schemes¹⁸ PBEh-3c²⁷² and B97-3c²⁵⁷ as well as the corrected Hartree-Fock (HF) method HF-3c³⁴² and the extended tight-binding methods GFN- and GFN2-xTB^{188,244} are examples for the inclusion of such correction schemes into functional and method design. Here we focus on the very recent D4 method as successor of the widely applied D3 correction^{46,166} and concentrate on the application to DFT leading to DFT-D4 methods. The D4 scheme employs charge-scaled atomic reference polarizabilities $\alpha(i\omega)$ as well as a geometry-based interpolation scheme to obtain charge- and geometry-dependent pairwise dispersion coefficients C_6^{AB} .²¹⁰ It should be particularly useful for metallic systems. Figure 5.2 shows small organic molecules to medium-sized organometallic complexes that contain a d-block element in varying oxidation states with some exemplary homoatomic atoms-in-molecules dispersion coefficients C_6^{AA} .

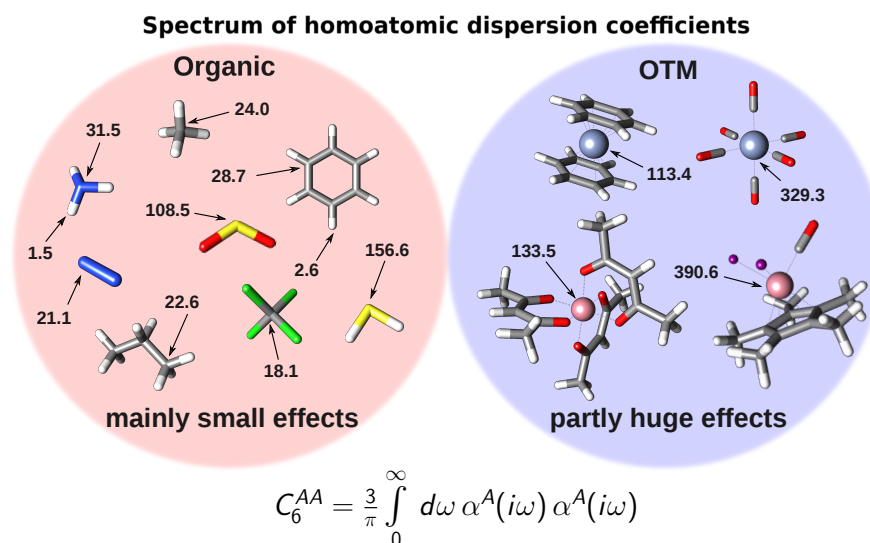


Figure 5.2.: Homoatomic dispersion coefficients C_6^{AA} are shown for small organic molecules and organotransitionmetallic (OTM) complexes. Dispersion coefficients are given in atomic units (1 au equals 1 Hartree Bohr⁶). Gray = C; white = H; blue = N; red = O; yellow = S; green = Cl; purple = I; pink = Co; gray-blue = Cr.

These coefficients mainly determine the strength of LD and can vary over several orders of magnitude. For carbon atoms in typical organic compounds, the absolute values for homoatomic dispersion coefficients are in a relatively narrow range. For example, coefficients between 18.1 au for the more positively charged carbon atom in CCl₄ compared to 28.0 au for carbon in C₆H₆ are obtained. This picture is different for organometallic complexes where dispersion coefficients can vary significantly depending on the complex geometry and oxidation state. For example, the coefficient for chromium (gray-blue, right side of Figure 5.2) drops by more than 50% between the Cr(C₆H₆)₂ sandwich complex and the Cr(CO)₆ molecule. Dispersion-corrected DFT methods are adopted in contemporary research and in chemical industry, e.g., in polymer chemistry, catalyst design, adhesive studies, or colloid stability evaluation, where accurate interaction energies for larger systems (200-300 atoms) are essential for, e.g., verifying reaction mechanisms or screening purposes. Here, the cooperation between experiment and theory is important for optimizing chemical processes and verifying new synthetic routes. Especially organometallic complexes play an important role, because metal specific chemical properties allow a conceivable range of chemical transformations, which are chemically interesting but challenging for theory because of their diverse, often complicated electronic structure. In this Account, we briefly describe the theoretical foundations that lead to long-range electron correlation effects and LD and how to treat those in the framework of DFT. Subsequently, theoretical results for

II. Applications of London Dispersion Corrections

structural and thermodynamical properties obtained at typical dispersion-corrected DFT levels are discussed in comparison to high-level WFT reference data or experimental results. This includes energy decomposition analysis to understand the interactions as well as comparison to noncorrected DFT results. Finally, a short comment on computational efficiency, a summary, and an outlook on possible future work will be given.

5.2. Theory and Methods

Figure 5.1 depicts the Coulomb and exchange interactions between two coupled single excitations which occur spontaneously and simultaneously through quantized electronic fluctuations. Such coupled excitations describe electron correlation, which is an attractive contribution to the total energy of the system. In second order perturbation theory (PT2), the energy of such coupled excitations can be expressed as

$$E_{\text{corr}}^{(\text{PT2})} = - \sum_{ij}^{n_{\text{occ.}}} \sum_{ab}^{n_{\text{virt.}}} \frac{\{(\text{ia}|\text{jb}) - (\text{ib}|\text{ja})\}^2}{\omega_{\text{ai}} + \omega_{\text{bj}}} \quad (5.1)$$

Here, the Coulomb $(\text{ia}|\text{jb}) = J$ and exchange $(\text{ib}|\text{ja}) = K$ integrals together with the energies ω of the single excitations determine the magnitude of the correlation energy. Since the electron density decreases exponentially, the exchange contribution K between separated fragments vanishes in the asymptotic region, such that only the long-range Coulomb interaction remains. Expanding this Coulomb interaction into multipoles, the first nonvanishing term describes the fragment (or atom) pairwise dipole-dipole interaction, which can be represented by averaged and integrated, isotropic dynamic dipole-dipole polarizabilities of the two fragments A and B leading to the Casimir-Polder and London formulas, respectively, for the dispersion energy E_{DISP}

$$E_{\text{DISP}}^{(6)} = -\frac{3}{\pi R^6} \int_0^{\infty} d\omega \alpha^A(i\omega) \alpha^B(i\omega) = -C_6^{AB}/R^6 \quad (5.2)$$

The above equations form the basis for very many dispersion energy correction schemes. Semilocal density functional approximations (DFAs) include short- to mid-ranged electron correlation effects through the exchange-correlation functional. In order to avoid double counting of interactions, the atom-pairwise dispersion energy $-C_6^{AB}/R^6$ is usually damped at short-range using internuclear distance (R_{AB}) dependent damping functions as, e.g., multiplied by the rational function

II. Applications of London Dispersion Corrections

proposed by Becke and Johnson^{432,433} (abbreviated as BJ in the following)

$$f_{\text{BJ}}^{(n)}(R_{\text{AB}}) = \frac{R_{\text{AB}}^{(n)}}{R_{\text{AB}}^{(n)} + (\alpha_1 R_0^{\text{AB}} + \alpha_2)^{(n)}} \quad (5.3)$$

The D4 dispersion correction used within this work incorporates both two-body and three-body dispersion interactions.³⁰⁸ Three-body effects are captured by inclusion of an Axilrod-Teller-Muto (ATM) term^{167,168} as known from earlier DFT-D methods⁴⁶ which contributes normally less than about 5%. The total dispersion energy is given by the following formula

$$E_{\text{DISP}}^{\text{D4}} = - \sum_{\text{AB}} \sum_{n=6,8} s_n \frac{C_{\text{AB}}^{(n)}}{R_{\text{AB}}^{(n)}} f_{\text{BJ}}^{(n)}(R_{\text{AB}}) + E_{\text{DISP}}^{(9),\text{ATM}} \quad (5.4)$$

In addition to the two-body C_6 and three-body C_9 terms, less long-ranged dipole-quadrupole pairwise terms ($n = 8$) are included as well. Atomic polarizabilities for atoms-in-molecules are obtained from element specific reference molecule polarizabilities that are scaled with respect to relative charge differences between the target and the reference molecule. Importantly, all fundamental polarizabilities in the model are obtained nonempirically at the time-dependent DFT level.⁴³⁴ Those scaled reference polarizabilities are interpolated based on a geometrical measure of the hybridization state (coordination number, CN) to produce charge- and geometry-dependent atomic polarizabilities as depicted in Figure 5.3.

Those polarizabilities are used to calculate pairwise dispersion coefficients from which dipole-quadrupole and triple-dipole dispersion coefficients are available via recursion in analogy to earlier works.⁴⁶ As can be seen from Figure 5.3, generally the polarizability and the dispersion coefficients increase with decreasing CN (lower saturation) and decreasing positive charge. The latter effect is more pronounced for metals where the D4 method (which includes charges) is beneficial compared to the older D3 scheme. Note that computationally more involved density dependent dispersion correction schemes like vdW-DF¹⁸⁷ or VV10^{51,52} automatically include this oxidation state dependence. Those methods, however, are less accurate for dispersion coefficients¹⁷ and do not allow simple analysis which is available in D4 through the atomic partitioning. The charges in the D4 approach can be computed by DFT, simple tight-binding methods or even classically by electronegativity equilibration depending on the degree of sophistication of the basic theoretical method which is dispersion corrected.

II. Applications of London Dispersion Corrections

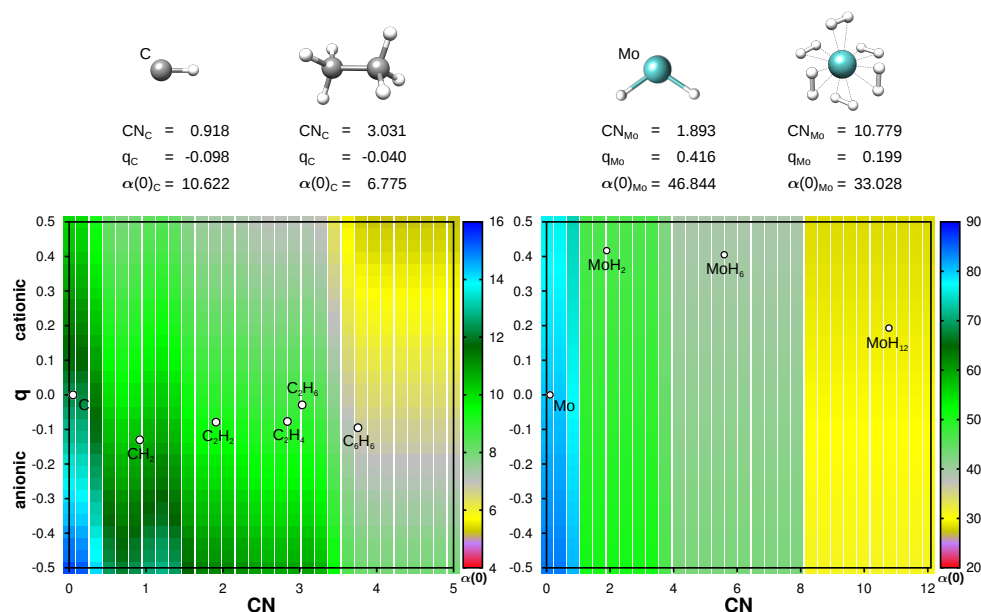


Figure 5.3.: Charge- and geometry-dependent static atomic polarizabilities $\alpha(0)$ for carbon (left) and molybdenum (right) from averaging element specific reference polarizabilities. Positive (negative) partial charges decrease (increase) the polarizabilities magnitude.

5.3. Applications

Although consideration of LD is an accepted standard in computational organic chemistry, the awareness for the importance of LD in organometallic chemistry was not widespread. Recently, a resurgent interest in LD effects on organometallic chemistry is noted.^{193,365,430,435,436} Two major aspects, emerging from the interface between theoretical and experimental chemistry are the influence of LD on (a) structural properties and (b) reaction thermodynamics. Both are closely connected to reactivity prediction and catalyst design.⁴³⁵ In this context, the applicability and accuracy of methods varies significantly throughout the zoo of theoretical approaches ranging from force-fields over semiempirical approaches to DFT and WFT based methods. Approaching highest accuracy at smallest possible cost represents an inevitable compromise with growing system size and complexity. Therefore, careful assessment of quantum chemical (QC) methods remains essential. With a growing focus on organometallic chemistry, new benchmark sets had to be developed to verify the strengths of DFT known from computational organic chemistry and to identify its weaknesses with respect to the exigencies of organometallic chemistry. In the following we present selected benchmark studies and examples of how further developed methods like D4 substantially improve the accuracy of state-of-the-art DFT for geometries and thermochemistry. We first discuss benchmark studies for closed-shell transition metal thermo-

II. Applications of London Dispersion Corrections

chemistry (gas-phase reaction energies) like the MOR41²⁶⁸ and WCCR10^{437,438} sets as well as the HEAVY28⁴⁶ benchmark set for intermolecular noncovalent interactions of small, heavy main group element containing compounds (*cf.* Figure 5.4). In all cases the inclusion of dispersion corrections proved crucial to

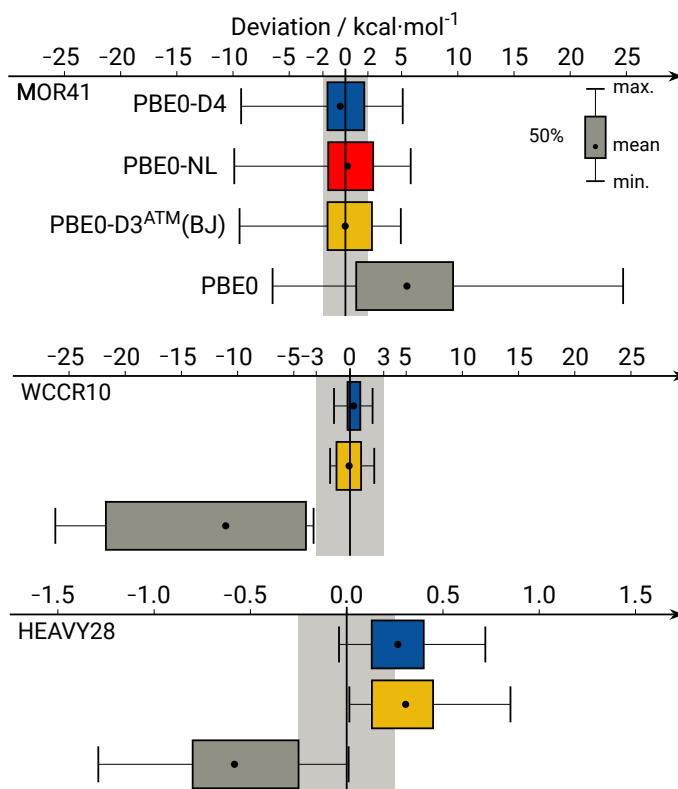


Figure 5.4.: Influence of different dispersion corrections to DFT for describing metallic thermochemistry in the MOR41, WCCR10, and HEAVY28 benchmark sets. All values are obtained at the PBE0/def2-QZVPP level.

obtain high accuracy compared to WFT references. For MOR41, consisting of 41 realistic transitionmetal complex reactions, plain DFT yields a large mean absolute deviation (MAD) of 6.6 kcal mol⁻¹ and a standard deviation (SD) of 6.9 kcal mol⁻¹ for the robust PBE0¹¹⁶ functional with a large def2-QZVPP²⁵¹ atomic orbital (AO) basis set. Application of either D3(BJ)-ATM (further abbreviated as D3) or the nonlocal (NL) VV10^{51,52} dispersion corrections improve the results significantly with MAD of 2.6 kcal mol⁻¹ for D3 and 2.4 kcal mol⁻¹ for the density-dependent NL correction. The D4 model further improves the results, yielding a MAD of 2.1 kcal mol⁻¹. An exemplary reaction with large dispersion effects is the association of PCy₃ to benzyliden[1,3-bis(2,4,6-trimethylphenyl)-2-imidazolidinylidene]dichlororuthenium forming the Grubbs II catalyst (*cf.* Figure 5.5). Here, plain PBE0 yields a deviation of 24.7 kcal mol⁻¹ for the reaction energy. Including the D4 correction reduces this deviation to only 0.5 kcal mol⁻¹.

II. Applications of London Dispersion Corrections

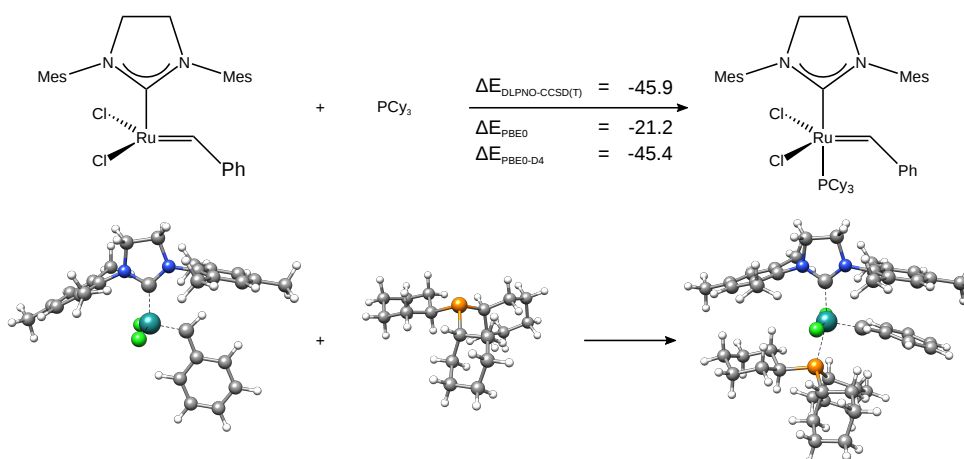


Figure 5.5.: Reaction energies for the association of PCy₃ to benzylidene[1,3-bis(2,4,6-trimethylphenyl)-2-imidazolidinylidene]dichlororuthenium forming the Grubbs II catalyst (kcal mol⁻¹). All DFT energies are calculated with the def2-QZVPP basis with reference to DLPNO-CCSD(T)/ TightPNO/CBS(def2-TZVPP/def2-QZVPP) level results.

Similar trends are observed for the WCCR10 and the HEAVY28 benchmark sets where the application of the D4 model decreases the MD by one order of magnitude (WCCR10) and by about 50% (HEAVY28) as depicted in Figure 5.4. While these studies highlight the importance of dispersion corrections to standard DFT functionals for thermochemistry, the systematic influence of LD on structural features of organometallic systems is far less systematically studied. A well established benchmark set of small first to third row transition metal compounds by Bühl and co-workers^{294,439,440} is available. However, as only small molecules (<20 atoms) are included, the influence of the dispersion correction schemes is small and not representative for most realistically sized organometallic complexes. The latter often have extensive ligand spheres with large inter- and intramolecular dispersion interactions. In the following we present selected examples of significant dispersion interaction influenced organometallic geometries. A strong correlation between structural and catalytic properties has been studied by Bickelhaupt and co-workers in 2015.⁴⁴¹ They investigated the influence of sterically attractive LD on the bite-angle flexibility and the metal-mediated C-H bond activation of bis-phosphane palladium catalysts. It was shown that significantly bent minimum structures of the PdR₂ catalysts with R = PiPr₃, PCy₃, and PPh₃ are favored with increasing ligand size. These observations were predominantly attributed to interligand dispersion interactions (*cf.* Figure 5.6). The resulting increased bite-angle flexibility decreases the catalyst activation strain leading to comparably small activation barriers for the oxidative addition of methane (about 8.6 kcal mol⁻¹ smaller) for Pd(PPh₃)₂ with respect to Pd(PH₃)₂. Concluding, Bick-

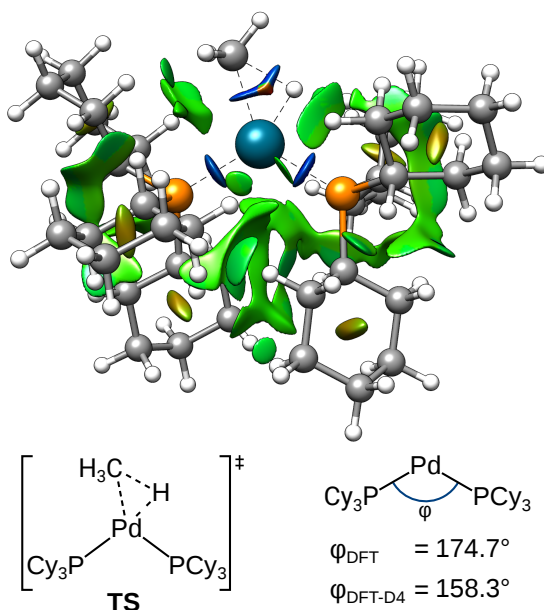


Figure 5.6.: NCIplot^{428,442} of the transition state of the oxidative addition of methane to $\text{Pd}(\text{PCy}_3)_2$. A blue color indicates strongly attractive, red repulsive regions, and green regions are dispersion dominated. Note the large effect of the D4 correction on the calculated bite angle in the equilibrium structure of about 16° .

elhaupt and co-workers pointed out the importance of dispersion interactions for modern concepts of catalyst design reconsidering sterically controlled mechanisms for enhancing catalyst properties. Another example of significant dispersion induced structural features are heavy group 14 carbene analogues carrying large terphenyl ligands.^{443,444} Power *et al.* synthesized a series of bis-terphenyl tetrylenes of the formula $\text{E}\{\text{C}_6\text{H}_3\text{-}2,6\text{-(C}_6\text{H}_2\text{-}2,4,6\text{-iPr}_3)_2\}_2$ ($\text{E} = \text{Ge}, \text{Sn}$ or Pb) with systematically increased ligand size.⁴⁴³ Surprisingly these compounds show a counter-intuitive trend of decreased $\text{C}_{\text{ipso}}\text{-E-C}_{\text{ipso}}$ angles with increased steric demand of the terphenyl ligands $\text{Ar}^{\text{Mes}} < \text{Ar}^{\text{Diipp}} < \text{Ar}^{\text{Tripp}}$. The dovetailing of both ligands (*cf.* Figure 5.7) favors intramolecular dispersion interactions thus decreasing the $\text{C}_{\text{ipso}}\text{-E-C}_{\text{ipso}}$ angle. Uncorrected DFT yields systematically too large $\text{C}_{\text{ipso}}\text{-E-C}_{\text{ipso}}$ angles. Specifically for the largest system $\text{Pb}(\text{Ar}^{\text{Tripp}})_2$ the deviation of 9.3° from the experimentally observed angle (108.1°) is substantial (*cf.* Figure 5.7). Here, already the DFT-D3 optimization yields equilibrium geometries in good accordance with the experimental structure. The significant angle compression with increased steric demand is reproduced well. The $\text{C}_{\text{ipso}}\text{-E-C}_{\text{ipso}}$ angle is 107.3° at the DFT-D4 level, only deviating 0.8° from the experiment ($\phi_{\text{DFT-D3}} = 107.5^\circ$). These results further emphasize the indispensability of dispersion corrections to DFT for describing complex molecular systems. In particular for compounds in-

II. Applications of London Dispersion Corrections

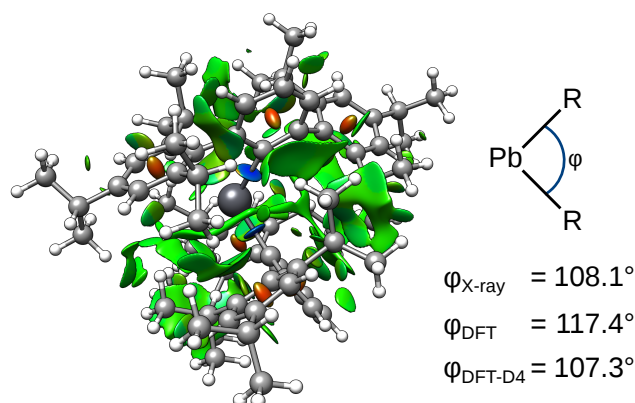


Figure 5.7.: NCIplot of a sterically crowded heavy carbene analogue $\text{Pb}\{\text{C}_6\text{H}_2\text{-}2,4,6\text{-iPr}_3\}_2$ and its experimental and calculated $\text{C}_{\text{ipso}}\text{-Pb-C}_{\text{ipso}}$ angles in degrees.

cluding heavy elements that often involve flexible bonding, attractive interligand interactions play an important role on key structural features. Furthermore, the stabilization of unprecedented organometallic complex structures due to dispersion interactions were investigated by Merino and co-workers for cationic group 8 sumanene complexes of the formula $\text{CpM}(\eta^6\text{-sumanene})^+$ (with $\text{M} = \text{Fe}, \text{Ru}, \text{Os}$).⁴⁴⁵ From sterical considerations the bonding motif of the domed sumanene ligand should be dominated by a convex (B) bound structure, minimizing the steric repulsion between the CpM and the sumanene fragment (*cf.* Figure 5.8). Counterintuitively, a concave (A) bonding is observed experimentally. Merino and

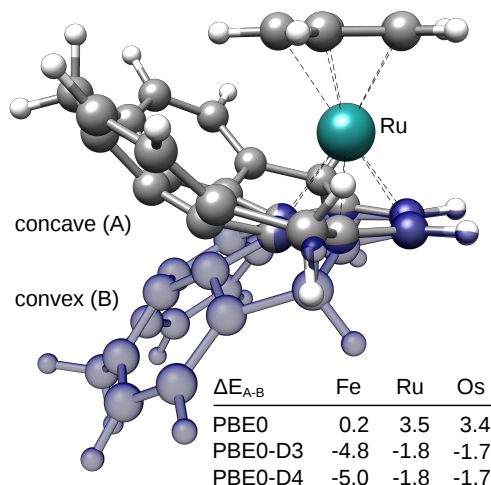


Figure 5.8.: Overlay of a concave and a convex bound sumanene structure plots. The convex coordinated structure motif is depicted in blue. Relative energies with the def2-QZVPP basis sets are given in kcal mol^{-1} .

co-workers showed that several dispersion-free DFT approaches fail to qualitatively reproduce this observation. Upon inclusion of the D3 correction most presented

II. Applications of London Dispersion Corrections

DFT functionals provide qualitatively correct relative energies. This indicates a significant stabilization of the concave structures by attractive intramolecular dispersion interactions of up to 5 kcal mol⁻¹. Even though dispersion effects in large organometallic systems are often dominated by ligand-ligand interactions, various examples show clear indications for important metal-metal dispersion interactions as well. A prominent example are bimetallic indenyl bridged complexes (*cf.* Figure 5.9).

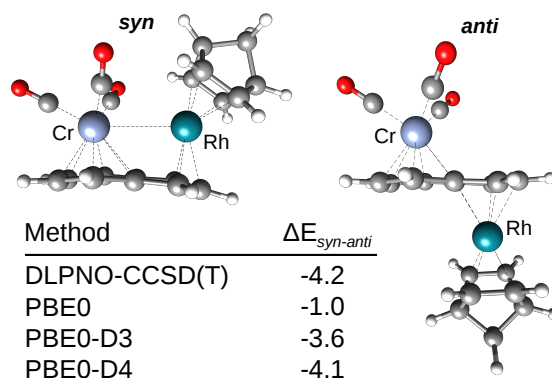


Figure 5.9.: Isomers of a bimetallic indenyl complex optimized at the PBE0-D4/def2-QZVP level. Energies calculated with the def2-QZVPP basis set with reference to DLPNO-CCSD(T)/CBS(def2-TZVPP/VeryTightPNO/def2-QZVPP/TightPNO) values (in kcal mol⁻¹).

Several representative compounds were investigated, focusing on the relative stabilities of their *syn*- and *anti*-isomers. Moreover, the role of noncovalent metal-metal interactions⁴⁴⁶ was studied. The stabilizing metal-metal interaction was shown to be of purely noncovalent nature and intramolecular dispersion interactions were identified to play a crucial role in stabilizing the *syn*-isomer. This stabilization stands in contrast to expected steric repulsion between the bridged transition metal fragments. Inclusion of dispersion interactions in DFT is crucial for the correct reproduction of the relative energies and structures of the investigated indenyl complexes. The plain PBE0 functional with the large def2-QZVPP basis set is not able to reproduce the DLPNO-CCSD(T)/CBS(def2-TZVPP/VeryTightPNO/def2-QZVPP/TightPNO)²⁶¹ reference values, yielding too stable *anti*-isomers (for details see Appendix A5). Inclusion of the D4 correction improves the DFT relative energy, reproducing the reference value well. For all four indenyl systems PBE0-D4/def2-QZVPP yields small MAD (0.45 kcal mol⁻¹) and MD (-0.1 kcal mol⁻¹) values. Furthermore, organometallic aggregates with intrinsically large repulsive electrostatic interactions can be stabilized by dispersion effects.²⁸⁷ The DLPNO-CCSD(T)/TightPNO/def2-QZVPP interaction energy of a cationic tetrakis(isonitrile)-rhodium(I) dimer was analyzed by applying the Local

II. Applications of London Dispersion Corrections

Energy Decomposition (LED) method⁴⁴⁷ (cf. Figure 5.10).

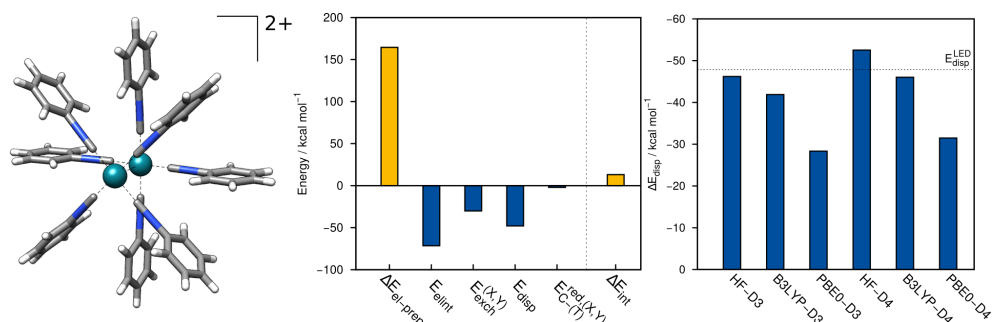


Figure 5.10.: LED analysis of the $[[\text{Rh}(\text{CNPh})_4]_2]^+$ dication obtained at the DLPNO-CCSD(T)/def2-QZVPP level.

The DFT-D dispersion models are therefore applicable even to huge systems consisting of several thousands of atoms thereby without significant overhead increasing the accuracy of the obtained results significantly. Overall, neglecting dispersion corrections in state-of-the-art DFT-based computational chemistry is mostly unjustifiable. As already mentioned, the D3 (and D4 with classical charges) schemes are even sufficiently fast in order to be applied in the framework of very fast semiempirical DFT approximations^{188,244} or force-fields.

5.4. Summary and Perspective

The progressive understanding of London dispersion interactions has led to an increased interest in the application of dispersion correction schemes to organometallic systems. By comparison to WFT results, it was shown that dispersion-corrected DFT performs excellently in terms of accuracy and speed for a variety of organometallic complexes. The accurate prediction of thermochemical and structural properties is routinely facilitated by applying combinations of well understood and robust DFT functionals like PBE0 and an efficient and accurate dispersion correction like the newly developed D4 model. It generally improves results by keeping established and extremely well tested D3 components with an additional inclusion of charge-dependent atomic polarizabilities. This improvement was largely inspired by the requirements immanent to organometallic complexes with respect to versatile charge characteristics. In addition to accurate total energy calculations, a quantification and dissection of dispersion effects is possible. It was shown that for some dispersion-corrected density functionals (e.g., B3LYP) absolute dispersion energies agree well with localized coupled-cluster values obtained by an energy decomposition scheme. With these possibilities at hand, routine application of the efficient D4 model to organometallic systems enables close on time cooper-

ation of experimentalists and computational chemists. Specifically, challenges like rational organometallic catalyst design will profit from easily accessible improvements to DFT. The neglect of dispersion interactions in modern computational chemistry proved negligent and unjustifiable as robust and efficient dispersion correction schemes are available. Residual errors in DFT based computational chemistry treatments are mostly caused by partially remaining (and persistent) deficiencies like inaccurate treatment of solvation (which partially quenches dispersion effects),⁴⁴⁸ thermal effects (entropy), as well as inherent problems of the underlying exchange-correlation functionals (mainly caused by the self-interaction error).³⁰ It remains to be seen how modern density functionals^{449,450} which try to tackle such problems will evolve and influence the field of organometallic chemistry in the future.

5.5. Appendix A5

See Appendix A5 for further information about the applied density functional calculations, the applied DFT-D methods, the applied DLPNO-CCSD(T) setup as well as information about the Tetrakis(isonitrile)rhodium(I) dimer structure. This is followed by benchmark data including data for the MOR41 benchmark, the WCCR10 benchmark set, and the HEAVY28 benchmark set. Afterwards, the local energy decomposition is compared against dispersion-corrected DFT which is followed by a discussions about computational timings. Finally, structures of the indenyl complexes are given

Final Summary and Conclusion

KS-DFT emerged as the method of choice when describing the electronic structure of molecular or periodic systems. Practical DFAs are commonly used for the routine calculation of structures and physical properties of systems with hundreds of atoms. However, DFAs are unable to account for dynamic long-range correlation effects. Although methods exist to determine LD correlation effects accurately, *e. g.*, TD-DFT or correlated WFT, they usually exceed the computational effort of the underlying electronic structure method. To cure this deficit, several cost-effective LD correction models have been developed. Considering their exploited approximations, Klimeš classified dispersion corrections in different groups introducing his “stairway to heaven”.³⁷⁸ In analogy to Jacob’s ladder, each group is placed on a different rung with increasing use of environment information leading to higher overall accuracy when climbing this ladder. Since the majority of this dissertation deals with DFT-D methods, the basic idea of the “stairway to heaven” is adapted, but only related to DFT-D methods.

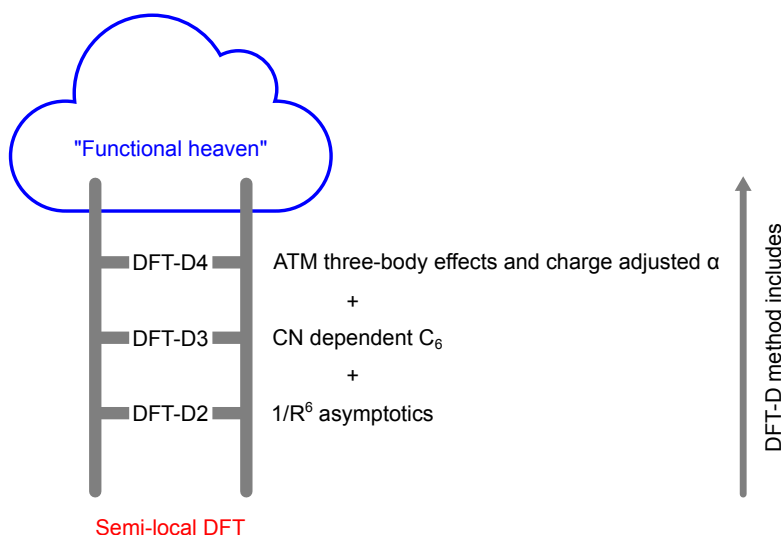


Figure 6.1.: DFT-D version of Klimeš’ “stairway to heaven”.³⁷⁸

Starting at a semi-local DFT level, the accuracy is improved for each rung approaching the best result within the “Functional Heaven”. As with Jacob’s ladder, higher rungs do not correlate with higher accuracies for a particular problem. Instead, the overall statistical performance is improved. The DFT-D2 method on the first rung incorporates the right $-C_6/R^6$ asymptotic behavior for the interaction of two atoms being separated by their distance R with their pairwise dispersion coefficient C_6 . This is achieved by including constant dispersion coefficients to each element irrespective of its oxidation or hybridization state. The errors introduced by this rough approximation can be huge, *e. g.*, dispersion coefficients of carbon atoms in sp and sp^3 hybridized states can differ by up to 35%.⁴³ The DFT-D3 method on rung two corrects for this drawback through the inclusion of hybridiza-

tion dependent pairwise dispersion coefficients (Dobson type-A nonadditivity¹⁸⁹) in terms of fractional coordination numbers.

Despite the widespread reliability and versatility of DFT-D dispersion corrections, intensive research is ongoing to enhance their universality, robustness, and accuracy further. This dissertation presented the extension of the DFT-D3 model from rung two by considering oxidation-state information and many-body effects with the aim to diversify the application areas while simultaneously improving the accuracy. An important constraint is that the extension does not deteriorate the computational efficiency of DFT-D3.

Chapter 1 introduced a simple ansatz to incorporate oxidation-state information in the hybridization-dependent reference D3-polarizabilities. The presented approach rescales D3-polarizabilities regardless of the DFT electron density but rather by empirical functions. Initially, DFT-D4 was designed using element specific charge-scaling functions (three parameter per element) with partial charges calculated at the GFN-xTB tight-binding level of theory. This charge-scaling procedure enabled the modeling of cationic and anionic polarizabilities.

The subsequent development of one global charge-scaling function resulted in the reduction of the number of empirical parameters (two global parameters). In the final DFT-D4 (Chapter 2), the calculation of partial charges is replaced by a classical electronegativity equilibration charge model, which introduced a high efficiency while maintaining the accuracy. The application of the final DFT-D4 model shows excellent accuracy for diverse properties like molecular dispersion coefficients, noncovalent interaction energies, conformational energies, thermochemical applications, as well as covalent and noncovalent geometries.

The development of the periodic DFT-D4 model was the topic of Chapter 3. This chapter examined the influence of additional Dobson type-A effects for dynamic polarizabilities and their influence on interaction energies. The addition of periodic reference polarizabilities to the pool of existing D4-references enables the accurate calculation of polarizabilities that match experimental data, *e. g.*, of alkaline halides. It was shown that lattice energies and cell volumes of molecular crystals are slightly improved when comparing to its predecessor DFT-D3. Larger improvements are found for obtaining adsorption energies of small organic molecules on several (non-)polar surfaces.

The general importance of LD effects to verify experimental data was highlighted in Chapter 4 and 5. Here, long-range correlation effects led to a unique binding motif with the shortest intermolecular hydrogen-hydrogen contact reported to date. Low-temperature single-crystal neutron diffraction measurements of crystalline TPM have been reported showing an intermolecular H...H distance of 1.566(5) Å. This unusual binding motif originates from a LD driven crystal packing effect as verified by the HSE-3c composite scheme. To strengthen this hypothesis,

an energy decomposition analysis was performed showing that LD interactions are the dominant binding motif leading to the overall stability of the TPM dimer. Also, the effect of LD on structural and reaction thermodynamic properties was analyzed for organometallic complexes. For transition metal complexes, the absolute size of homoatomic dispersion coefficients is highly dependent on the geometry and oxidation state of the complex. For example, the coefficient for chromium drops by more than 50% between the $\text{Cr}(\text{CO})_6$ molecule and the $\text{Cr}(\text{C}_6\text{H}_6)_2$ sandwich complex. DFT-D4 generally improves for such complexes by keeping the established and extremely well tested D3-components and including flexibility in terms of charge-dependent atomic polarizabilities.

Additional computational costs associated with the physical improvements of DFT-D4 are negligible when coupling with standard semi-local DFAs. Figure 6.2 compares the computational timings of single point and gradient calculations of DFT-D methods with the ones of PBE in two different basis set expansions for a saturated diamond chunk.

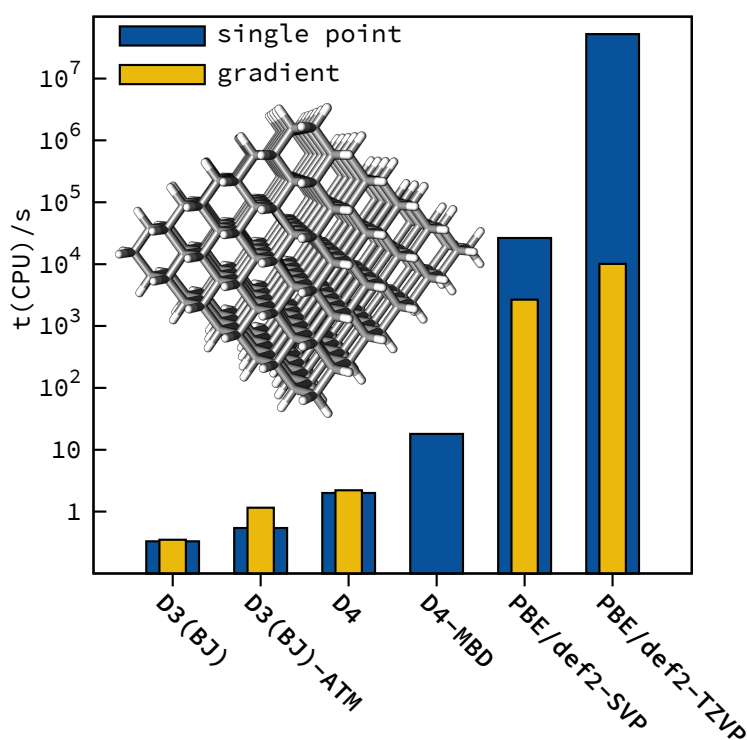


Figure 6.2.: Timings analysis of different DFT-D methods compared to PBE calculations applied with different basis sets. For the MBD-D4 method no gradients are available.

The presented PBE calculations are computationally orders of magnitudes more demanding than all applied DFT-D methods, which verifies that the computational costs do not increase by incorporating additional LD corrections schemes in

terms of DFT-D methods. However, among the DFT-D methods, the presented DFT-D4 method is slightly more costly than its predecessor method DFT-D3. The additional costs occurring in DFT-D4 can be traced back to the calculated electronegativity equilibration partial charges. An exception is DFT-D4-MBD, which is only recommended for the subsequent correction of interaction energies for large intramolecular complexes as recommended in Ref. 308.

To conclude, this dissertation presented the development of the DFT-D4 London dispersion correction. The comparison to several standard energy benchmark sets showed that the DFT-D4 method typically outperforms its predecessor DFT-D3. Due to the fact that many-body dispersion effects are incorporated up to third-order by default, the DFT-D “stairway to heaven” is complemented with DFT-D4 on the highest rung. Thus, it is indeed possible to develop an improved DFT-D3 scheme while maintaining its computational efficiency within a DFT-based framework. The errors arising due to the approximation in modern LD corrections are typically smaller compared to errors in the semi-local DFAs treatment. Continuous development of short-range XC functionals seems necessary to advance dispersion-corrected DFT methods further.

The competitors to dispersion-corrected DFT methods are correlated WFT methods like the coupled-cluster “gold-standard” CCSD(T), its various localized versions, and quantum Monte-Carlo methods. While these methods are basically more accurate and general, in practice they are still limited by the slow convergence with respect to the basis set size, the associated large BSSE, and their (technical) inability to efficiently provide nuclear gradients. Those disadvantages are also present in modern DFT-based methods, which try to describe dispersion interactions seamlessly (*e. g.*, RPA,¹²⁹ *ab initio* DFT,⁴⁵¹ double-hybrid functionals,¹²⁸ or range-separated hybrids with long-range components from WFT⁴⁵²). These methods are often less empirical than dispersion-corrected DFT methods, more generally applicable, and may address other deficiencies of standard DFT such as self-interaction errors or static correlation problems. However, their correlation functionals depend on virtual orbitals, which results in considerably higher computational costs and thus limits the applicability of these methods. Therefore, dispersion-corrected DFT methods will be indispensable in the near future. Especially the presented cost-effective and highly accurate DFT-D4 London dispersion correction is intended to be used as an “everyday”-tool for standard computational applications like structure generation and molecular dynamics simulations.

Currently, the best approach for an accurate and efficient electronic structure theory is a multi-level ansatz. This ansatz combines the structure generation using dispersion-corrected DFT with high-accuracy WFT single-point calculations. However, the latter is still time demanding and generally the bottleneck of this

ansatz. With the development of the DFT-D4 dispersion correction, double hybrid DFAs can replace the WFT part of this ansatz. D4-corrected double hybrid DFAs achieve high accuracies as shown for general main group thermochemistry, kinetics, noncovalent interactions, and for realistic metal organic reactions.³⁰⁸

In future works, this DFT multi-level ansatz is promising to obtain the best cost-accuracy ratio and thus paves the way for the precise description of larger molecular and condensed phase systems.

Bibliography

- [1] Houk, K. N.; Liu, F. *Acc. Chem. Res.* **2017**, *50*, 539–543.
- [2] Thiel, W. *Angew. Chem. Int. Ed.* **2011**, *50*, 9216–9217; *Angew. Chem.* **2011**, *123*, 9382–9384.
- [3] Cavalleri, M. *Int. J. Quantum Chem.* **2013**, *113*, 1.
- [4] Sure, R.; Antony, J.; Grimme, S. *J. Phys. Chem. B* **2014**, *118*, 3431–3440.
- [5] Yin, J.; Henriksen, N. M.; Slochower, D. R.; Shirts, M. R.; Chiu, M. W.; Mobley, D. L.; Gilson, M. K. *J. Comput. Aided Mol. Des.* **2017**, *31*, 1–19.
- [6] Bardwell, D. A. et al. *Acta Cryst. B* **2011**, *67*, 535–551.
- [7] Reilly, A. M.; et al., *Acta Cryst. B* **2016**, *72*, 439–459.
- [8] Taylor, D. E.; Ángyán, J. G.; Galli, G.; Zhang, C.; Gygi, F.; Hirao, K.; Song, J. W.; Rahul, K.; Anatole von Lilienfeld, O.; Podeszwa, R. t. *J. Chem. Phys.* **2016**, *145*, 124105.
- [9] Curtarolo, S.; Hart, G. L. W.; Nardelli, M. B.; Mingo, N.; Sanvito, S.; Levy, O. *Nat. Mater.* **2013**, *12*, 191.
- [10] de Pablo, J. J.; Jackson, N. E.; Webb, M. A.; Chen, L. Q.; Moore, J. E.; Morgan, D.; Jacobs, R.; Pollock, T.; Schlom, D. G.; Toberer, E. S.; et al., *Npj Comput. Mater.* **2019**, *5*, 41.
- [11] Hao, S.; Dravid, V. P.; Kanatzidis, M. G.; Wolverton, C. *Npj Comput. Mater.* **2019**, *5*, 58.
- [12] Jain, A.; Shin, Y.; Persson, K. A. *Nat. Rev. Mater.* **2016**, *1*, 15004.
- [13] Cernak, T. A.; Gleason, J. L. *J. Org. Chem.* **2008**, *73*, 102–110.
- [14] Garbuzynskiy, S. O.; Melnik, B. S.; Lobanov, M. Y.; Finkelstein, A. V.; Galzitskaya, O. V. *Proteins* **2005**, *60*, 139–147.
- [15] Szalewicz, K. *WIREs Comput. Mol. Sci.* **2012**, *2*, 254–272.
- [16] Jansen, G. *WIREs Comput. Mol. Sci.* **2014**, *4*, 127–144.
- [17] Grimme, S.; Hansen, A.; Brandenburg, J. G.; Bannwarth, C. *Chem. Rev.* **2016**, *116*, 5105–5154.
- [18] Caldeweyher, E.; Brandenburg, J. G. *J. Phys.: Condens. Matt.* **2018**, *30*, 213001.

Bibliography

- [19] Bygrave, P. J.; Allan, N. L.; Manby, F. R. *J. Chem. Phys.* **2012**, *137*, 164102.
- [20] Beran, G. J. O.; Wen, S.; Nanda, K.; Huang, Y.; Heit, Y. *Prediction and Calculation of Crystal Structures*; 2013; pp 59–93.
- [21] Masur, O.; Schütz, M.; Maschio, L.; Usvyat, D. *J. Chem. Theory Comput.* **2016**, *12*, 5145–5156.
- [22] Riplinger, C.; Pinski, P.; Becker, U.; Valeev, E. F.; Neese, F. *J. Chem. Phys.* **2016**, *144*, 024109.
- [23] Maurer, S. A.; Lambrecht, D. S.; Kussmann, J.; Ochsenfeld, C. *J. Chem. Phys.* **2013**, *138*, 014101.
- [24] Schütz, M.; Masur, O.; Usvyat, D. *J. Chem. Phys.* **2014**, *140*, 244107.
- [25] Beran, G. J. O. *Chem. Rev.* **2016**, *116*, 5567–5613.
- [26] Yang, J.; Hu, W.; Usvyat, D.; Matthews, D.; Schütz, M.; Chan, G. K.-L. *Science* **2014**, *345*, 640–643.
- [27] Zen, A.; Brandenburg, J. G.; Klimeš, J.; Tkatchenko, A.; Alfè, D.; Michaelides, A. *Proc. Natl. Acad. Sci.* **2018**, *115*, 1724–1729.
- [28] Ren, X.; Rinke, P.; Joas, C.; Scheffler, M. *J. Mater. Sci.* **2012**, *47*, 7447–7471.
- [29] Waldrop, M. M. *Nature* **2016**, *530*, 144–147.
- [30] Grimme, S.; Schreiner, P. R. *Angew. Chem. Int. Ed.* **2018**, *57*, 4170–4176.
- [31] Lemonick, S. *C&EN* **2019**, *97*, 16–18.
- [32] Engel, E.; Dreizler, R. M. *Density functional theory*; Springer, 2013.
- [33] Hohenberg, P.; Kohn, W. *Phys. Rev. B* **1964**, *136*, 864–871.
- [34] Kristyán, S.; Pulay, P. *Chem. Phys. Lett.* **1994**, *229*, 175–180.
- [35] Hobza, P.; Šponer, J.; Reschel, T. *J. Comput. Chem.* **1995**, *16*, 1315–1325.
- [36] Pérez-Jordá, J. M.; Becke, A. D. *Chem. Phys. Lett.* **1995**, *233*, 134–137.
- [37] Pérez-Jordá, J. M.; San-Fabián, E.; Pérez-Jiménez, A. J. *J. Chem. Phys.* **1999**, *110*, 1916–1920.
- [38] Grimme, S. *WIREs Comput. Mol. Sci.* **2011**, *1*, 211–228.
- [39] Kurita, N.; Sekino, H. *Chem. Phys. Lett.* **2001**, *348*, 139–146.
- [40] Seponer, J.; Leszczynski, J.; Hobza, P. *J. Comput. Chem.* **1996**, *17*, 841–850.
- [41] Couronne, O.; Ellinger, Y. *Chem. Phys. Lett.* **1999**, *306*, 71–77.
- [42] Cohen, J. S.; Pack, R. T. *J. Chem. Phys.* **1974**, *61*, 2372–2382.

- [43] Wu, Q.; Yang, W. *J. Chem. Phys.* **2002**, *116*, 515–524.
- [44] Elstner, M.; Hobza, P.; Frauenheim, T.; Suhai, S.; Kaxiras, E. *J. Chem. Phys.* **2001**, *114*, 5149–5155.
- [45] Wu, X.; Vargas, M. C.; Nayak, S.; Lotrich, V.; Scoles, G. *J. Chem. Phys.* **2001**, *115*, 8748–8757.
- [46] Grimme, S.; Antony, J.; Ehrlich, S.; Krieg, H. *J. Chem. Phys.* **2010**, *132*, 154104.
- [47] Becke, A. D.; Johnson, E. R. *J. Chem. Phys.* **2005**, *123*, 154101.
- [48] Becke, A. D.; Johnson, E. R. *J. Chem. Phys.* **2005**, *122*, 154104.
- [49] Tkatchenko, A.; Scheffler, M. *Phys. Rev. Lett.* **2009**, *102*, 073005.
- [50] Tkatchenko, A.; DiStasio, R. A.; Car, R.; Scheffler, M. *Phys. Rev. Lett.* **2012**, *108*, 236402.
- [51] Vydrov, O. A.; Van Voorhis, T. *J. Chem. Phys.* **2009**, *130*, 104105.
- [52] Vydrov, O. A.; Van Voorhis, T. *Phys. Rev. Lett.* **2009**, *103*, 063004.
- [53] Grimme, S. *J. Comput. Chem.* **2004**, *25*, 1463–1473.
- [54] Grimme, S. *J. Comput. Chem.* **2006**, *27*, 1787–1799.
- [55] Hepburn, J.; Scoles, G.; Penco, R. *Chem. Phys. Lett.* **1975**, *36*, 451–456.
- [56] Ahlrichs, R.; Penco, R.; Scoles, G. *Chem. Phys.* **1977**, *19*, 119–130.
- [57] Goerigk, L.; Hansen, A.; Bauer, C.; Ehrlich, S.; Najibi, A.; Grimme, S. *Phys. Chem. Chem. Phys.* **2017**, *19*, 32184–32215.
- [58] Neese, F. *WIREs Comput. Mol. Sci.* **2018**, *8*.
- [59] TURBOMOLE V7.3 2018 ;University of Karlsruhe and Forschungszentrum Karlsruhe GmbH , TURBOMOLE GmbH: Karlsruhe, Germany, 2007; available from <http://www.turbomole.com>.
- [60] Frisch, M. J. et al. Gaussian 09 Revision D.01. Gaussian Inc. Wallingford CT 2009.
- [61] Frisch, M. J. et al. Gaussian~16 Revision A.03. 2016; Gaussian Inc. Wallingford CT.
- [62] Kresse, G.; Hafner, J. *Phys. Rev. B* **1993**, *47*, 558.
- [63] Kresse, G.; Hafner, J. *J. Phys.: Condens. Matt.* **1994**, *6*, 8245.
- [64] Kresse, G.; Furthmüller, J. *Phys. Rev. B* **1996**, *54*, 11169.
- [65] Kresse, G.; Furthmüller, J. *J. Comp. Mat. Sci.* **1996**, *6*, 15.
- [66] Kresse, G.; Joubert, J. *Phys. Rev. B* **1999**, *59*, 1758.

Bibliography

- [67] Turney, J. M.; Simmonett, A. C.; Parrish, R. M.; Hohenstein, E. G.; Evangelista, F. A.; Fermann, J. T.; Mintz, B. J.; Burns, L. A.; Wilke, J. J.; Abrams, M. L. e. a. *WIREs Comput. Mol. Sci.* **2012**, *2*, 556–565.
- [68] Werner, H. J.; Knowles, P. J.; Knizia, G.; Manby, F. R.; Schütz, M. *WIREs Comput. Mol. Sci.* **2012**, *2*, 242–253.
- [69] Baerends, E. J. et al. ADF2019, SCM, Theoretical Chemistry, Vrije Universiteit, Amsterdam, The Netherlands, <https://www.scm.com>. 2019.
- [70] Shao, Y.; Gan, Z.; Epifanovsky, E.; Gilbert, A. T.; Wormit, M.; Kussmann, J.; Lange, A. W.; Behn, A.; Deng, J.; Feng, X.; et al., *Mol. Phys.* **2015**, *113*, 184–215.
- [71] Dovesi, R.; Orlando, R.; Erba, A.; Zicovich-Wilson, C. M.; Civalieri, B.; Casassa, S.; Maschio, L.; Ferrabone, M.; De La Pierre, M.; D’Arco, P.; Noël, Y.; Causà, M.; Rérat, M.; Kirtman, B. *Int. J. Quantum Chem.* **2014**, *114*, 1287–1317.
- [72] Hutter, J.; Iannuzzi, M.; Schiffmann, F.; VandeVondele, J. *WIREs Comput. Mol. Sci.* **2014**, *4*, 15–25.
- [73] Schröder, H.; Creon, A.; Schwabe, T. *J. Chem. Theory Comput.* **2015**, *11*, 3163–3170.
- [74] Smith, D. G. A.; Burns, L. A.; Patkowski, K.; Sherrill, C. D. *J. Phys. Chem. Lett.* **2016**, *7*, 2197–2203.
- [75] Witte, J.; Mardirossian, N.; Neaton, J. B.; Head-Gordon, M. *J. Chem. Theory Comput.* **2017**, *13*, 2043–2052.
- [76] Rösel, S.; Quanz, H.; Logemann, C.; Becker, J.; Mossou, E.; Canadillas-Delgado, L.; Caldeweyher, E.; Grimme, S.; Schreiner, P. R. *J. Am. Chem. Soc.* **2017**, *139*, 7428–7431.
- [77] Ermer, O.; Mason, S. A.; Anet, F. A.; Miura, S. S. *J. Am. Chem. Soc.* **1985**, *107*, 2330–2334.
- [78] Helgaker, T.; Jorgensen, P.; Olsen, J. *Molecular electronic-structure theory*; John Wiley & Sons, 2014.
- [79] Born, M.; Oppenheimer, R. *Ann. Phys* **1927**, *84*, 457–484.
- [80] Szabo, A.; Ostlund, N. S. *Modern Quantum Chemistry*; Dover Publications: New York, 1996.
- [81] Fulde, P. *Electron correlations in molecules and solids*; Springer Science & Business Media, 2012; Vol. 100.
- [82] Van Loan, C. *Computational frameworks for the fast Fourier transform*; Siam, 1992; Vol. 10.

- [83] Hackbusch, W. *Multi-grid methods and applications*; Springer Science & Business Media, 2013; Vol. 4.
- [84] Martinsson, P.-G. In *Encyclopedia of Applied and Computational Mathematics*; Engquist, B., Ed.; Springer Berlin Heidelberg, 2015; pp 498–508.
- [85] Roothaan, C. C. J. *Rev. Mod. Phys.* **1951**, *23*, 69–89.
- [86] Hall, G. G. *Proc. R. Soc. Lond. A* **1951**, *205*, 541–552.
- [87] Johnson, B. G.; Gill, P. M.; Pople, J. A. *J. Chem. Phys.* **1992**, *97*, 7846–7848.
- [88] Furche, F. *J. Chem. Phys.* **2008**, *129*, 114105.
- [89] Runge, E.; Gross, E. K. U. *Phys. Rev. Lett.* **1984**, *52*, 997–1000.
- [90] Zangwill, A. *Phys. today* **2015**, *68*, 34.
- [91] Jensen, F. *Introduction to Computational Chemistry*; Wiley: Chichester, 207; Vol. 2.
- [92] Kohn, W.; Sham, L. J. *Phys. Rev.* **1965**, *140*, A1133–A1138.
- [93] Becke, A. D. *J. Chem. Phys.* **1993**, *98*, 1372–1377.
- [94] Peverati, R.; Truhlar, D. G. *J. Chem. Theory Comput.* **2012**, *8*, 2310–2319.
- [95] Becke, A. D. *J. Chem. Phys.* **2014**, *140*, 18A301.
- [96] Sousa, S. F.; Fernandes, P. A.; Ramos, M. J. *J. Phys. Chem. A* **2007**, *111*, 10439–10452.
- [97] Goerigk, L.; Grimme, S. *Phys. Chem. Chem. Phys.* **2011**, *13*, 6670–6688.
- [98] Perdew, J. P.; Schmidt, K. Jacob's ladder of density functional approximations for the exchange–correlation energy. AIP Conference Proceedings. 2001; pp 1–20.
- [99] Perdew, J. P.; Ruzsinszky, A.; Tao, J.; Staroverov, V. N.; Scuseria, G. E.; Csonka, G. I. *J. Chem. Phys.* **2005**, *123*, 062201.
- [100] von Barth, U.; Hedin, L. *J. Phys. C* **1972**, *5*, 1629.
- [101] Trickey, S. B. *Phys. Rev. Lett.* **1986**, *56*, 881.
- [102] Perdew, J. P.; Burke, K.; Ernzerhof, M. *Phys. Rev. Lett.* **1996**, *77*, 3865–3868; erratum: *Phys. Rev. Lett.* **1997**, *78*, 1396.
- [103] Becke, A. D. *Phys. Rev. A* **1988**, *38*, 3098.
- [104] Lee, C.; Yang, W.; Parr, R. G. *Phys. Rev. B* **1988**, *37*, 785–789.
- [105] Tao, J.; Perdew, J. P.; Staroverov, V. N.; Scuseria, G. E. *Phys. Rev. Lett.* **2003**, *91*, 146401.

Bibliography

- [106] Zhao, Y.; Truhlar, D. G. *J. Chem. Phys.* **2006**, *125*, 194101.
- [107] Peverati, R.; Truhlar, D. G. *J. Phys. Chem. Lett.* **2011**, *3*, 117.
- [108] Peverati, R.; Truhlar, D. G. *Phys. Chem. Chem. Phys.* **2012**, *14*, 13171–13174.
- [109] Mardirossian, N.; Head-Gordon, M. *J. Chem. Phys.* **2015**, *142*, 074111.
- [110] del Campo, J. M.; Gázquez, J. L.; Trickey, S.; Vela, A. *Chem. Phys. Lett.* **2012**, *543*, 179–183.
- [111] Sun, J.; Xiao, B.; Ruzsinszky, A. *J. Chem. Phys.* **2012**, *137*, 051101.
- [112] Sun, J.; Haunschild, R.; Xiao, B.; Bulik, I. W.; Scuseria, G. E.; Perdew, J. P. *J. Chem. Phys.* **2013**, *138*, 044113.
- [113] Sun, J.; Perdew, J. P.; Ruzsinszky, A. *Proc. Natl. Acad. Sci. U.S.A.* **2015**, *112*, 685–689.
- [114] Sun, J.; Ruzsinszky, A.; Perdew, J. P. *Phys. Rev. Lett.* **2015**, *115*, 036402.
- [115] Perdew, J. P.; Parr, R. G.; Levy, M.; Balduz Jr, J. L. *Phys. Rev. Lett.* **1982**, *49*, 1691.
- [116] Adamo, C.; Barone, V. *J. Chem. Phys.* **1999**, *110*, 6158–6170.
- [117] Becke, A. D. *J. Chem. Phys.* **1993**, *98*, 5648–5652.
- [118] Stephens, P. J.; Devlin, F. J.; Chabalowski, C. F.; Frisch, M. J. *J. Phys. Chem.* **1994**, *98*, 11623–11627.
- [119] Heyd, J.; Scuseria, G. E.; Ernzerhof, M. *J. Chem. Phys.* **2003**, *118*, 8207–8215.
- [120] Baerends, E.; Gritsenko, O.; Van Meer, R. *Phys. Chem. Chem. Phys.* **2013**, *15*, 16408–16425.
- [121] Yanai, T.; Tew, D. P.; Handy, N. C. *Chem. Phys. Lett.* **2004**, *393*, 51–57.
- [122] Chai, J.-D.; Head-Gordon, M. *Phys. Chem. Chem. Phys.* **2008**, *10*, 6615–6620.
- [123] Mardirossian, N.; Head-Gordon, M. *Phys. Chem. Chem. Phys.* **2014**, *16*, 9904–9924.
- [124] Görling, A.; Levy, M. *Phys. Rev. B* **1993**, *47*, 13105–13113.
- [125] Facco Bonetti, A.; Engel, E.; Schmid, R. N.; Dreizler, R. M. *Phys. Rev. Lett.* **2001**, *86*, 2241–2244.
- [126] Mori-Sánchez, P.; Wu, Q.; Yang, W. *J. Chem. Phys.* **2005**, *123*, 062204.
- [127] Brémond, E.; Ciofini, I.; Sancho-García, J. C.; Adamo, C. *Acc. Chem. Res.* **2016**, *49*, 1503–1513.
- [128] Goerigk, L.; Grimme, S. *WIREs Comput. Mol. Sci.* **2014**, *4*, 576–600.

- [129] Eshuis, H.; Bates, J. E.; Furche, F. *Theor. Chem. Acc.* **2012**, *131*, 1084.
- [130] Langreth, D. C.; Perdew, J. P. *Phys. Rev. B* **1977**, *15*, 2884–2901.
- [131] Kurth, S.; Perdew, J. P. *Phys. Rev. B* **1999**, *59*, 10461.
- [132] Toulouse, J.; Gerber, I. C.; Jansen, G.; Savin, A.; Angyán, J. G. *Phys. Rev. Lett.* **2009**, *102*, 096404.
- [133] Paier, J.; Janesko, B. G.; Henderson, T. M.; Scuseria, G. E.; Grüneis, A.; Kresse, G. *J. Chem. Phys.* **2010**, *132*, 094103.
- [134] Grimme, S.; Steinmetz, M. *Phys. Chem. Chem. Phys.* **2016**, *18*, 20926–20937.
- [135] Slater, J. C. *The self-consistent field for molecules and solids*; McGraw-Hill, 1974; Vol. 4.
- [136] Chadi, D.; Cohen, M. L. *Phys. Rev. B* **1973**, *8*, 5747.
- [137] Monkhorst, H. J.; Pack, J. D. *Phys. Rev. B* **1976**, *13*, 5188.
- [138] Andrade, X.; et al., *Phys. Chem. Chem. Phys.* **2015**, *17*, 31371–31396.
- [139] Blum, V.; Gehrke, R.; Hanke, F.; Havu, P.; Havu, V.; Ren, X.; Reuter, K.; Scheffler, M. *Comput. Phys. Commun.* **2009**, *180*, 2175 – 2196.
- [140] Gonze, X.; et al., *Comput. Mater. Sci.* **2002**, *25*, 478–492.
- [141] Te Velde, G. t.; Bickelhaupt, F. M.; Baerends, E. J.; Fonseca Guerra, C.; van Gisbergen, S. J.; Snijders, J. G.; Ziegler, T. *J. Comput. Chem.* **2001**, *22*, 931–967.
- [142] Fernández Rico, J.; López, R.; Aguado, A.; Ema, I.; Ramírez, G. *Int. J. Quantum Chem.* **2001**, *81*, 148–153.
- [143] Furche, F.; Ahlrichs, R.; Hättig, C.; Klopper, W.; Sierka, M.; Weigend, F. *WIREs Comput. Mol. Sci.* **2014**, *4*, 91–100.
- [144] ORCA An Ab Initio, Density Functional and Semiempirical Program Package, V. 4.0 (Rev. 1); F. Neese, Max-Planck Institut für Kohlenforschung, Mülheim a.d. Ruhr (Germany), 2017.
- [145] Neese, F. *WIREs Comput. Mol. Sci.* **2012**, *2*, 73–78.
- [146] Mortensen, J. J.; Hansen, L. B.; Jacobsen, K. W. *Phys. Rev. B* **2005**, *71*, 035109.
- [147] Blöchl, P. E. *Phys. Rev. B* **1994**, *50*, 17953.
- [148] Furthmüller, J.; Käckell, P.; Bechstedt, F.; Kresse, G. *Phys. Rev. B* **2000**, *61*, 4576–4587.
- [149] Brandenburg, J. G.; Grimme, S.; Jones, P. G.; Markopoulos, G.; Hopf, H.; Cyran-ski, M. K.; Kuck, D. *Chem. Eur. J.* **2013**, *19*, 9930–9938.
- [150] Kruse, H.; Grimme, S. *J. Chem. Phys.* **2012**, *136*, 154101.

Bibliography

- [151] Brandenburg, J. G.; Alessio, M.; Civalleri, B.; Peintinger, M. F.; Bredow, T.; Grimme, S. *J. Phys. Chem. A* **2013**, *117*, 9282–9292.
- [152] Hirschfelder, J. O. *Chem. Phys. Lett.* **1967**, *1*, 325–329.
- [153] Stone, A. J. *The Theory of Intermolecular Forces: Second Edition*; Oxford University Press: Oxford, 2013.
- [154] London, F. *Z. Phys. Chem. Abt* **1930**, 222–251.
- [155] Unsöld, A. *Z. Physik* **1927**, *43*, 563–574.
- [156] Casimir, H. B. G.; Polder, D. *Phys. Rev.* **1948**, *73*, 360–372.
- [157] Linder, B. *J. Chem. Phys.* **1962**, *37*, 963–966.
- [158] Mavroyannis, C.; Stephen, M. *Mol. Phys.* **1962**, *5*, 629–638.
- [159] McLachlan, A. *Proc. Roy. Soc. A* **1963**, *271*, 387–401.
- [160] Zangwill, A.; Soven, P. *Phys. Rev. A* **1980**, *21*, 1561.
- [161] Eisenschitz, R.; London, F. *Z. Phys.* **1930**, *60*, 491–527.
- [162] London, F. *Z. Phys.* **1930**, *63*, 245–279.
- [163] Tkatchenko, A.; Ambrosetti, A.; DiStasio Jr, R. A. *J. Chem. Phys.* **2013**, *138*, 074106.
- [164] van Gisbergen, S. J. A.; Snijders, J. G.; Baerends, E. J. *J. Chem. Phys.* **1995**, *103*, 9347–9354.
- [165] Osinga, V. P.; van Gisbergen, S. J. A.; Snijders, J. G.; Baerends, E. J. *J. Chem. Phys.* **1997**, *106*, 5091–5101.
- [166] Grimme, S.; Ehrlich, S.; Goerigk, L. *J. Comput. Chem.* **2011**, *32*, 1456–1465.
- [167] Axilrod, B. M.; Teller, E. *J. Chem. Phys.* **1943**, *11*, 299–300.
- [168] Muto, Y. *Proc. Phys. Soc. Jpn.* **1943**, *17*, 629.
- [169] Moellmann, J.; Grimme, S. *J. Phys. Chem. C* **2014**, *118*, 7615–7621.
- [170] Ehrlich, S.; Moellmann, J.; Reckien, W.; Bredow, T.; Grimme, S. *ChemPhysChem* **2011**, *12*, 3414–3420.
- [171] Qiu, N.-X.; Xue, Y.; Guo, Y.; Sun, W.-J.; Chu, W. *Comput. Theor. Chem.* **2012**, *992*, 37–47.
- [172] Zhiani, R. *Appl. Surf. Sci.* **2017**, *409*, 35–44.
- [173] Goerigk, L. *J. Chem. Theory Comput.* **2014**, *10*, 968–980.
- [174] Moellmann, J.; Ehrlich, S.; Tonner, R.; Grimme, S. *J. Phys.: Condens. Matt.* **2012**, *24*, 424206.

- [175] Hostas, J.; Rezac, J. *J. Chem. Theory Comput.* **2017**, *13*, 3575–3585.
- [176] Van Troeye, B.; Torrent, M.; Gonze, X. *Phys. Rev. B* **2016**, *93*, 144304.
- [177] Fornaro, T.; Biczysko, M.; Monti, S.; Barone, V. *Phys. Chem. Chem. Phys.* **2014**, *16*, 10112–10128.
- [178] Thinius, S.; Islam, M. M.; Heitjans, P.; Bredow, T. *J. Phys. Chem. C* **2014**, *118*, 2273–2280.
- [179] DiStasio, R. A.; Gobre, V. V.; Tkatchenko, A. *J. Phys.: Condens. Matter* **2014**, *26*, 213202.
- [180] Becke, A. D.; Johnson, E. R. *J. Chem. Phys.* **2006**, *124*, 014104.
- [181] Sato, T.; Nakai, H. *J. Chem. Phys.* **2009**, *131*, 224104.
- [182] Sato, T.; Nakai, H. *J. Chem. Phys.* **2010**, *133*, 194101.
- [183] Dion, M.; Rydberg, H.; Schröder, E.; Langreth, D. C.; Lundqvist, B. I. *Phys. Rev. Lett.* **2004**, *92*, 246401.
- [184] Dion, M.; Rydberg, H.; Schröder, E.; Langreth, D. C.; Lundqvist, B. I. *Phys. Rev. Lett.* **2005**, *95*, 109902.
- [185] Berland, K.; Hyldgaard, P. *Phys. Rev. B* **2014**, *89*, 035412.
- [186] Langreth, D.; Lundqvist, B. I.; Chakarova-Käck, S. D.; Cooper, V.; Dion, M.; Hyldgaard, P.; Kelkkanen, A.; Kleis, J.; Kong, L.; Li, S. *J. Phys.: Condens. Matter* **2009**, *21*, 084203.
- [187] Berland, K.; Cooper, V. R.; Lee, K.; Schröder, E.; Thonhauser, T.; Hyldgaard, P.; Lundqvist, B. I. *Rep. Prog. Phys.* **2015**, *78*, 066501.
- [188] Grimme, S.; Bannwarth, C.; Shushkov, P. *J. Chem. Theory Comput.* **2017**, *13*, 1989–2009.
- [189] Dobson, J. F. *Int. J. Quant. Chem.* **2014**, *114*, 1157–1161.
- [190] Parr, R. G.; Weitao, Y. *Density-functional theory of atoms and molecules*. 1989.
- [191] Kohn, W. *Rev. Mod. Phys.* **1999**, *71*, 1253.
- [192] Sato, T.; Tsuneda, T.; Hirao, K. *J. Chem. Phys.* **2005**, *123*, 104307.
- [193] Hansen, A.; Bannwarth, C.; Grimme, S.; Petrović, P.; Werlé, C.; Djukic, J.-P. *ChemistryOpen* **2014**, *3*, 177–189.
- [194] Stöhr, M.; Michelitsch, G. S.; Tully, J. C.; Reuter, K.; Maurer, R. J. *J. Chem. Phys.* **2016**, *144*, 151101.
- [195] Mulliken, R. S. *J. Chem. Phys.* **1955**, *23*, 1841–1846.
- [196] Grimme, S.; Bannwarth, C. *J. Chem. Phys.* **2016**, *145*, 054103.

Bibliography

- [197] Petraglia, R.; Steinmann, S. N.; Corminboeuf, C. *Int. J. Quantum Chem.* **2015**, *115*, 1265–1272.
- [198] Elstner, M.; Porezag, D.; Jungnickel, G.; Elsner, J.; Haugk, M.; Frauenheim, T.; Suhai, S.; Seifert, G. *Phys. Rev. B* **1998**, *58*, 7260–7268.
- [199] Yang, Y.; Yu, H.; York, D.; Cui, Q.; Elstner, M. *J. Phys. Chem. A* **2007**, *111*, 10861–10873.
- [200] Sedlak, R.; Řezáč, J. *J. Chem. Theory Comput.* **2017**, *13*, 1638–1646.
- [201] Grimme, S.; Bannwarth, C.; Caldeweyher, E.; Pisarek, J.; Hansen, A. *J. Chem. Phys.* **2017**, *147*, 161708.
- [202] Wiberg, K. B. *Tetrahedron* **1968**, *24*, 1083–1096.
- [203] Brauer, B.; Kesharwani, M. K.; Kozuch, S.; Martin, J. M. L. *Phys. Chem. Chem. Phys.* **2016**, *18*, 20905–20925.
- [204] Gráfová, L.; Pitonak, M.; Řezáč, J.; Hobza, P. *J. Chem. Theory Comput.* **2010**, *6*, 2365–2376.
- [205] TURBOMOLE V7.0 2017 ;University of Karlsruhe and Forschungszentrum Karlsruhe GmbH , TURBOMOLE GmbH: Karlsruhe, Germany, 2007; available from <http://www.turbomole.com>.
- [206] Ahlrichs, R.; Bär, M.; Häser, M.; Horn, H.; Kölmel, C. *Chem. Phys. Lett.* **1989**, *162*, 165–169.
- [207] Vahtras, O.; Almlöf, J.; Feyereisen, M. *Chem. Phys. Lett.* **1993**, *213*, 514–518.
- [208] Eichkorn, K.; Weigend, F.; Treutler, O.; Ahlrichs, R. *Theor. Chem. Acc.* **1997**, *97*, 119–124.
- [209] Weigend, F. *Phys. Chem. Chem. Phys.* **2006**, *8*, 1057–1065.
- [210] Caldeweyher, E.; Bannwarth, C.; Grimme, S. *J. Chem. Phys.* **2017**, *147*, 034112.
- [211] von Lilienfeld, O. A.; Tavernelli, I.; Röthlisberger, U.; Sebastiani, D. *Phys. Rev. Lett.* **2004**, *93*, 153004.
- [212] Steinmann, S. N.; Csonka, G.; Corminboeuf, C. *J. Chem. Theory Comput.* **2009**, *5*, 2950–2958.
- [213] Zimmerli, U.; Parrinello, M.; Koumoutsakos, P. *J. Chem. Phys.* **2004**, *120*, 2693–2699.
- [214] Steinmann, S. N.; Corminboeuf, C. *J. Chem. Theory Comput.* **2010**, *6*, 1990–2001.
- [215] Steinmann, S. N.; Corminboeuf, C. *J. Chem. Phys.* **2011**, *134*, 044117.
- [216] Steinmann, S. N.; Corminboeuf, C. *J. Chem. Theory Comput.* **2011**, *7*, 3567–3577.

- [217] Bučko, T.; Lebègue, S.; Hafner, J.; Ángyán, J. G. *J. Chem. Theory Comput.* **2013**, *9*, 4293–4299.
- [218] Yang, F.; Moss, L. G.; Phillips, G. N. *Nature Biotech.* **1996**, *14*, 1246–1251.
- [219] Still, W. C.; Tempczyk, A.; Hawley, R. C.; Hendrickson, T. *J. Am. Chem. Soc.* **1990**, *112*, 6127–6129.
- [220] Risthaus, T.; Steinmetz, M.; Grimme, S. *J. Comput. Chem.* **2014**, *35*, 1509–1516.
- [221] Johnson, E. R. *J. Chem. Phys.* **2011**, *135*, 234109.
- [222] Assaf, K. I.; Florea, M.; Antony, J.; Henriksen, N. M.; Yin, J.; Hansen, A.; Qu, Z. W.; Sure, R.; Klapstein, D.; Gilson, M. K.; Grimme, S.; Nau, W. M. *J. Phys. Chem. B* **2017**, *121*, 11144–11162.
- [223] Pérez, M.; Qu, Z. W.; Caputo, C. B.; Podgorny, V.; Hounjet, L. J.; Hansen, A.; Dobrovetsky, R.; Grimme, S.; Stephan, D. W. *Chem. Eur. J.* **2015**, *21*, 6491–6500.
- [224] Sperger, T.; Sanhueza, I. A.; Kalvet, I.; Schoenebeck, F. *Chem. Rev.* **2015**, *115*, 9532–9586.
- [225] Reilly, A. M. et al. *Acta Crystallogr. Sect. B* **2016**, *72*, 439–459.
- [226] Price, S. L.; Reutzel-Edens, S. M. *Drug Discov. Today* **2016**, *21*, 912–923.
- [227] Wodrich, M. D.; Corminboeuf, C.; Schleyer, P. R. *Org. Lett.* **2006**, *8*, 3631–3634.
- [228] Johnson, E. R.; DiLabio, G. A. *Chem. Phys. Lett.* **2006**, *419*, 333–339.
- [229] Otero-de-la-Roza, A.; Johnson, E. R. *J. Chem. Phys.* **2013**, *138*, 054103.
- [230] Ghasemi, S. A.; Hofstetter, A.; Saha, S.; Goedecker, S. *Phys. Rev. B* **2015**, *92*, 045131.
- [231] DiStasio, R. A.; von Lilienfeld, O. A.; Tkatchenko, A. *Proc. Natl. Acad. Sci. USA* **2012**, *109*, 14791–14795.
- [232] Ambrosetti, A.; Alfè, D.; DiStasio, R. A.; Tkatchenko, A. *J. Phys. Chem. Lett.* **2014**, *5*, 849–855.
- [233] Gatica, S. M.; Cole, M. W.; Velegol, D. *Nano Lett.* **2005**, *5*, 169–173.
- [234] Kim, H. Y.; Sofo, J. O.; Velegol, D.; Cole, M. W.; Lucas, A. A. *Langmuir* **2007**, *23*, 1735–1740.
- [235] Gobre, V. V.; Tkatchenko, A. *Nature Comm.* **2013**, *4*, 2341.
- [236] Bučko, T.; Lebègue, S.; Gould, T.; Ángyán, J. G. *J. Phys.: Condens. Matt.* **2016**, *28*, 045201.
- [237] Elrod, M. J.; Saykally, R. J. *Chem. Rev.* **1994**, *94*, 1975–1997.
- [238] Donchev, A. G. *J. Chem. Phys.* **2006**, *125*, 074713.

Bibliography

- [239] Hermann, J.; DiStasio Jr, R. A.; Tkatchenko, A. *Chem. Rev.* **2017**, *117*, 4714–4758.
- [240] Ghosh, D. C.; Islam, N. *Int. J. Quantum Chem.* **2010**, *110*, 1206–1213.
- [241] Miller, K. J. *J. Am. Chem. Soc.* **1990**, *112*, 8533–8542.
- [242] Pauling, L. *Cornell University, Press, Ithaca, New York* **1960**, 17.
- [243] Pyykkö, P.; Atsumi, M. *Chem. Eur. J.* **2009**, *15*, 186–197.
- [244] Bannwarth, C.; Ehlert, S.; Grimme, S. *J. Chem. Theory Comput.* **2019**, *15*, 1652–1671.
- [245] Reckien, W.; Janetzko, F.; Peintinger, M. F.; Bredow, T. *J. Comput. Chem.* **2012**, *33*, 2023–2031.
- [246] Trnka, T. M.; Grubbs, R. H. *Acc. Chem. Res.* **2001**, *34*, 18–29.
- [247] Van Veldhuizen, J. J.; Gillingham, D. G.; Garber, S. B.; Kataoka, O.; Hoveyda, A. H. *J. Am. Chem. Soc.* **2003**, *125*, 12502–12508.
- [248] Artrith, N.; Morawietz, T.; Behler, J. *Phys. Rev. B* **2011**, *83*, 153101.
- [249] Bunch, J. R.; Kaufman, L. *Linear Algebra Its Appl.* **1980**, *34*, 341–370.
- [250] Cao, J.; Berne, B. J. *J. Chem. Phys.* **1992**, *97*, 8628–8636.
- [251] Weigend, F.; Ahlrichs, R. *Phys. Chem. Chem. Phys.* **2005**, *7*, 3297–3305.
- [252] Schröder, H.; Hühnert, J.; Schwabe, T. *J. Chem. Phys.* **2017**, *146*, 044115.
- [253] Brandenburg, J. G.; Bates, J. E.; Sun, J.; Perdew, J. P. *Phys. Rev. B* **2016**, *94*, 115144.
- [254] Weigend, F.; Furche, F.; Ahlrichs, R. *J. Chem. Phys.* **2003**, *119*, 12753–12762.
- [255] Otero de la Roza, A.; Kannemann, F.; Johnson, E. R.; Dickson, R. M.; Schmider, H.; Becke, A. D. Exchange-Hole Dipole Moment Model standalone. <http://schooner.chem.dal.ca/wiki/Postg>, 2013; [Online; accessed 2/15/2018].
- [256] Tkatchenko, A. Many-Body Dispersion (MBD) standalone. <http://www.fhi-berlin.mpg.de/~tkatchen/MBD/>, 2014; [Online; accessed 2/15/2018].
- [257] Brandenburg, J. G.; Bannwarth, C.; Hansen, A.; Grimme, S. *J. Chem. Phys.* **2018**, *148*, 064104.
- [258] Sedlak, R.; Janowski, T.; Pitoňák, M.; Řezáč, J.; Pulay, P.; Hobza, P. *J. Chem. Theory Comput.* **2013**, *9*, 3364–3374.
- [259] Sure, R.; Grimme, S. *J. Chem. Theory Comput.* **2015**, *11*, 3785–3801.
- [260] Boys, S.; Bernardi, F. *Mol. Phys.* **1970**, *19*, 553–566.

- [261] Riplinger, C.; Sandhoefer, B.; Hansen, A.; Neese, F. *J. Chem. Phys.* **2013**, *139*, 134101.
- [262] Riplinger, C.; Neese, F. *J. Chem. Phys.* **2013**, *138*, 034106.
- [263] Kruse, H.; Mladek, A.; Gkionis, K.; Hansen, A.; Grimme, S.; Sponer, J. *J. Chem. Theory Comput.* **2015**, *11*, 4972–4991.
- [264] Csonka, G. I.; French, A. D.; Johnson, G. P.; Stortz, C. A. *J. Chem. Theory Comput.* **2009**, *5*, 679–692.
- [265] Řeha, D.; Valdès, H.; Vondrášek, J.; Hobza, P.; Abu-Riziq, A.; Crews, B.; de Vries, M. S. *Chem. Eur. J.* **2005**, *11*.
- [266] Goerigk, L.; Karton, A.; Martin, J. M. L.; Radom, L. *Phys. Chem. Chem. Phys.* **2013**, *15*, 7028–7031.
- [267] Goerigk, L.; Hansen, A.; Bauer, C. A.; Ehrlich, S.; Najibi, A.; Grimme, S. GMTKN55 Database. <https://www.chemie.uni-bonn.de/pctc/mulliken-center/software/GMTKN/gmtkn>, 2017; [Online; accessed 6/28/2018].
- [268] Dohm, S.; Hansen, A.; Steinmetz, M.; Grimme, S.; Checinski, M. P. *J. Chem. Theory Comput.* **2018**, *14*, 2596–2608.
- [269] Dohm, S.; Hansen, A.; Steinmetz, M.; Grimme, S.; Checinski, M. P. MOR41 benchmark set. <https://www.chemie.uni-bonn.de/pctc/mulliken-center/software/mor41>, 2018; [Online; accessed 6/28/2018].
- [270] Pavošević, F.; Peng, C.; Pinski, P.; Riplinger, C.; Neese, F.; Valeev, E. F. *J. Chem. Phys.* **2017**, *146*, 174108.
- [271] Neese, F.; Valeev, E. F. *J. Chem. Theory Comput.* **2010**, *7*, 33–43.
- [272] Grimme, S.; Brandenburg, J. G.; Bannwarth, C.; Hansen, A. *J. Chem. Phys.* **2015**, *143*, 054107.
- [273] Zeiss, G. D.; Meath, W. J. *Mol. Phys.* **1977**, *33*, 1155–1176.
- [274] Margoliash, D. J.; Meath, W. J. *J. Chem. Phys.* **1978**, *68*, 1426–1431.
- [275] Vydrov, O. A.; Van Voorhis, T. *Phys. Rev. A* **2010**, *81*, 062708.
- [276] Jurečka, P.; Šponer, J.; Černý, J.; Hobza, P. *Phys. Chem. Chem. Phys.* **2006**, *8*, 1985–1993.
- [277] Perdew, J. P. *Phys. Rev. B* **1986**, *33*, 8822–8824.
- [278] Zhao, Y.; Truhlar, D. G. *Acc. Chem. Res.* **2008**, *41*, 157–167.
- [279] Handy, N. C.; Tozer, D. J. *Mol. Phys.* **1998**, *94*, 707–715.
- [280] Handy, N. C.; Cohen, A. J. *Mol. Phys.* **2001**, *99*, 403–412.

Bibliography

- [281] Zhang, Y.; Yang, W. *Phys. Rev. Lett.* **1998**, *80*, 890.
- [282] Hammer, B.; Hansen, L. B.; Nørskov, J. K. *Phys. Rev. B* **1999**, *59*, 7413–7421.
- [283] Zhao, Y.; Truhlar, D. G. *Theor. Chem. Acc.* **2008**, *120*, 215–241.
- [284] Zhao, Y.; Truhlar, D. G. *J. Phys. Chem. A* **2005**, *109*, 5656–5667.
- [285] Kozuch, S.; Gruzman, D.; Martin, J. M. L. *J. Phys. Chem. C* **2010**, *114*, 20801–20808.
- [286] Karton, A.; Tarnopolsky, A.; Lamère, J. F.; Schatz, G. C.; Martin, J. M. L. *J. Phys. Chem. A* **2008**, *112*, 12868–12886.
- [287] Grimme, S.; Djukic, J. P. *Inorg. Chem.* **2011**, *50*, 2619–2628.
- [288] Olmstead, M. M.; Balch, A. L. *J. Organomet. Chem.* **1978**, *148*, C15–C18.
- [289] Endres, H.; Gottstein, N.; Keller, H. J.; Martin, R.; Rodemer, W.; Steiger, W. *Z. Naturforsch. B* **1979**, *34*, 827–833.
- [290] Tran, N. T.; Stork, J. R.; Pham, D.; Olmstead, M. M.; Fettingner, J. C.; Balch, A. L. *Chem. Comm.* **2006**, 1130–1132.
- [291] Kozuch, S.; Martin, J. M. L. *J. Comput. Chem.* **2013**, *34*, 2327–2344.
- [292] Bursch, M.; Caldeweyher, E.; Hansen, A.; Neugebauer, H.; Ehlert, S.; Grimme, S. *Acc. Chem. Res.* **2019**, *52*, 258–266.
- [293] Najibi, A.; Goerigk, L. *J. Chem. Theory Comput.* **2018**, *14*, 5725–5738.
- [294] Bühl, M.; Kabrede, H. *J. Chem. Theory Comput.* **2006**, *2*, 1282–1290.
- [295] Řezáč, J.; Riley, K. E.; Hobza, P. *J. Chem. Theory Comput.* **2011**, *7*, 2427–2438.
- [296] Grimme, S.; Steinmetz, M. *Phys. Chem. Chem. Phys.* **2013**, *15*, 16031–16042.
- [297] Caldeweyher, E.; Ehlert, S.; Grimme, S. DFT-D4 software. <https://github.com/dftd4/dftd4>, 2019; [Online; accessed 11/08/2019].
- [298] Burke, K. *J. Chem. Phys.* **2012**, *136*, 150901.
- [299] Mori-Sánchez, P.; Cohen, A. J.; Yang, W. *J. Chem. Phys.* **2006**, *125*, 201102.
- [300] DiStasio, R. A.; Gobre, V. V.; Tkatchenko, A. *J. Phys.: Condens. Matter* **2014**, *26*, 213202.
- [301] Bučko, T.; Lebègue, S.; Ángyán, J. G.; Hafner, J. *J. Chem. Phys.* **2014**, *141*, 034114.
- [302] Dion, M.; Rydberg, H.; Schröder, E.; Langreth, D. C.; Lundqvist, B. I. *Phys. Rev. Lett.* **2004**, *92*, 246401.

- [303] Dion, M.; Rydberg, H.; Schröder, E.; Langreth, D. C.; Lundqvist, B. I. *Phys. Rev. Lett.* **2005**, *95*, 109902.
- [304] Berland, K.; Hyldgaard, P. *Phys. Rev. B* **2014**, *89*, 035412.
- [305] Langreth, D. C.; Lundqvist, B. I.; Chakarova-Käck, S. D.; Cooper, V. R.; Dion, M.; Hyldgaard, P.; Kelkkanen, A.; Kleis, J.; Kong, L.; Li, S. *J. Phys.: Condens. Matter* **2009**, *21*, 084203.
- [306] Berland, K.; Cooper, V. R.; Lee, K.; Schröder, E.; Thonhauser, T.; Hyldgaard, P.; Lundqvist, B. I. *Rep. Prog. Phys.* **2015**, *78*, 066501.
- [307] DiLabio, G. A.; Otero-de-la-Roza, A. *ArXiv E-Prints* **2014**, arXiv:1405.1771v2 (accessed on 23 July 2015).
- [308] Caldeweyher, E.; Ehlert, S.; Hansen, A.; Neugebauer, H.; Spicher, S.; Banwarth, C.; Grimme, S. *J. Chem. Phys.* **2019**, *150*, 154122.
- [309] Cahen, D.; Naaman, R.; Vager, Z. *Adv. Funct. Mater.* **2005**, *15*, 1571–1578.
- [310] Kronik, L.; Koch, N. *MRS Bull.* **2010**, *35*, 417–421.
- [311] Forrest, S. R.; Thompson, M. E. *Chem. Rev.* **2007**, *107*, 923–925.
- [312] Atodiresei, N.; Caciuc, V.; Lazić, P.; Blügel, S. *Phys. Rev. Lett.* **2009**, *102*, 136809.
- [313] Mercurio, G.; McNellis, E. R.; Martin, I.; Hagen, S.; Leyssner, F.; Soubatch, S.; Meyer, J.; Wolf, M.; Tegeder, P.; Tautz, F. S.; Reuter, K. *Phys. Rev. Lett.* **2010**, *104*, 036102.
- [314] Tkatchenko, A.; Romaner, L.; Hofmann, O. T.; Zojer, E.; Ambrosch-Draxl, C.; Scheffler, M. *MRS Bull.* **2010**, *35*, 435–442.
- [315] Tessman, J. R.; Kahn, A. H.; Shockley, W. *Phys. Rev.* **1953**, *92*, 890.
- [316] Zhang, G. X.; Tkatchenko, A.; Paier, J.; Appel, H.; Scheffler, M. *Phys. Rev. Lett.* **2011**, *107*, 245501.
- [317] Burow, A. M.; Sierka, M.; Döbler, J.; Sauer, J. *J. Chem. Phys.* **2009**, *130*, 174710.
- [318] Kudin, K. N.; Scuseria, G. E. *Chem. Phys. Lett.* **1998**, *289*, 611–616.
- [319] Mayer, J. E.; Mayer, M. G. *Phys. Rev.* **1933**, *43*, 605.
- [320] Grimme, S. *J. Chem. Theory Comput.* **2014**, *10*, 4497–4514.
- [321] Schröder, H.; Schwabe, T. *J. Comput. Chem.* **2016**, *37*, 2052–2059.
- [322] Ambrosetti, A.; Reilly, A. M.; DiStasio Jr, R. A.; Tkatchenko, A. *J. Chem. Phys.* **2014**, *140*, 18A508.
- [323] Gould, T.; Lebègue, S.; Ángyán, J. G.; Bučko, T. *J. Chem. Theory Comput.* **2016**, *12*, 5920–5930.

Bibliography

- [324] Afzal, M. A. F.; Cheng, C.; Hachmann, J. *J. Chem. Phys.* **2018**, *148*, 241712.
- [325] Turciani, L.; Berardo, E.; Jelfs, K. E. *J. Comput. Chem.* **2018**, *39*, 1931–1942.
- [326] Grimme, S. *J. Chem. Theory Comput.* **2019**, *15*, 2847–2862.
- [327] Cruz-Cabeza, A. J.; Reutzel-Edens, S. M.; Bernstein, J. *Chem. Soc. Rev.* **2015**, *44*, 8619–8635.
- [328] Pulido, A.; Chen, L.; Kaczorowski, T.; Holden, D.; Little, M. A.; Chong, S. Y.; Slater, B. J.; McMahon, D. P.; Bonillo, B.; Stackhouse, C. J.; et al., *Nature* **2017**, *543*, 657.
- [329] Klimeš, J. *J. Chem. Phys.* **2016**, *145*, 094506.
- [330] Wen, S.; Beran, G. J. O. *J. Chem. Theory Comput.* **2011**, *7*, 3733–3742.
- [331] Cutini, M.; Civalleri, B.; Corno, M.; Orlando, R.; Brandenburg, J. G.; Maschio, L.; Ugliengo, P. *J. Chem. Theory Comput.* **2016**, *12*, 3340–3352.
- [332] Perdew, J. P.; Chevary, J. A.; Vosko, S. H.; Jackson, K. A.; Pederson, M. R.; Singh, D. J.; Fiolhais, C. *Phys. Rev. B* **1992**, *46*, 6671.
- [333] Hammer, B.; Hansen, L. B.; Nørskov, J. K. *Phys. Rev. B* **1999**, *59*, 7413.
- [334] Becke, A. D. *J. Chem. Phys.* **1993**, *98*, 5648–5652.
- [335] Lee, K.; Murray, É. D.; Kong, L.; Lundqvist, B. I.; Langreth, D. C. *Phys. Rev. B* **2010**, *82*, 081101.
- [336] Brandenburg, J. G.; Maas, T.; Grimme, S. *J. Chem. Phys.* **2015**, *142*, 124104.
- [337] Otero-De-La-Roza, A.; Johnson, E. R. *J. Chem. Phys.* **2012**, *137*, 054103.
- [338] Reilly, A. M.; Tkatchenko, A. *J. Chem. Phys.* **2013**, *139*, 024705.
- [339] Trombach, L.; Ehlert, S.; Grimme, S.; Schwerdtfeger, P.; Mewes, J.-M. *Phys. Chem. Chem. Phys.* **2019**,
- [340] Moellmann, J.; Grimme, S. *J. Phys. Chem. C* **2014**, *118*, 7615–7621.
- [341] Carter, D. J.; Rohl, A. L. *J. Chem. Theory Comput.* **2014**, *10*, 3423–3437.
- [342] Sure, R.; Grimme, S. *J. Comput. Chem.* **2013**, *34*, 1672–1685.
- [343] Brandenburg, J. G.; Caldeweyher, E.; Grimme, S. *Phys. Chem. Chem. Phys.* **2016**, *18*, 15519–15523.
- [344] Goerigk, L.; Kruse, H.; Grimme, S. *ChemPhysChem* **2011**, *12*, 3421–3433.
- [345] Macher, M.; Klimeš, J.; Franchini, C.; Kresse, G. *J. Chem. Phys.* **2014**, *140*, 084502.

- [346] Lazić, P.; Caciuc, V.; Atodiresei, N.; Callsen, M.; Bluegel, S. *J. Phys.: Condens. Matt.* **2014**, *26*, 263001.
- [347] Larsen, A. H.; Mortensen, J. J.; Blomqvist, J.; Castelli, I. E.; Christensen, R.; Duřak, M.; Friis, J.; Groves, M. N.; Hammer, B.; Hargus, C.; et al., *J. Phys.: Condens. Matt.* **2017**, *29*, 273002.
- [348] Stanislaus, A.; Cooper, B. H. *Catal. Rev.-Sci. Eng.* **1994**, *36*, 75–123.
- [349] Wellendorff, J.; Kelkkanen, A.; Mortensen, J. J.; Lundqvist, B. I.; Bligaard, T. *Top. Catal.* **2010**, *53*, 378–383.
- [350] Syomin, D.; Kim, J.; Koel, B. E.; Ellison, G. B. *J. Phys. Chem. B* **2001**, *105*, 8387–8394.
- [351] Heidberg, J.; Kandel, M.; Meine, D.; Wildt, U. *Surf. Sci.* **1995**, *331*, 1467–1472.
- [352] Spoto, G.; Gribov, E. N.; Ricchiardi, G.; Damin, A.; Scarano, D.; Bordiga, S.; Lamberti, C.; Zecchina, A. *Prog. Surf. Sci.* **2004**, *76*, 71–146.
- [353] Sterrer, M.; Risse, T.; Freund, H. J. *Appl. Catal. A* **2006**, *307*, 58–61.
- [354] Ugliengo, P.; Damin, A. *Chem. Phys. Lett.* **2002**, *366*, 683–690.
- [355] Valero, R.; Gomes, J. R. B.; Truhlar, D. G.; Illas, F. *J. Chem. Phys.* **2008**, *129*, 124710.
- [356] Civalleri, B.; Maschio, L.; Ugliengo, P.; Zicovich-Wilson, C. M. *Phys. Chem. Chem. Phys.* **2010**, *12*, 6382–6386.
- [357] Staemmler, V. *J. Phys. Chem. A* **2011**, *115*, 7153–7160.
- [358] Wichtendahl, R.; Rodriguez-Rodrigo, M.; Härtel, U.; Kuhlenbeck, H.; Freund, H. J. *Surf. Sci.* **1999**, *423*, 90–98.
- [359] Dohnalek, Z.; Kimmel, G. A.; Joyce, S. A.; Ayotte, P.; Smith, R. S.; Kay, B. D. *J. Phys. Chem. B* **2001**, *105*, 3747–3751.
- [360] Boese, A. D.; Sauer, J. *Phys. Chem. Chem. Phys.* **2013**, *15*, 16481–16493.
- [361] Dunn, S. K.; Ewing, G. E. *J. Phys. Chem.* **1992**, *96*, 5284–5290.
- [362] Cabello-Cartagena, A. G.; Vogt, J.; Weiss, H. *J. Chem. Phys.* **2010**, *132*, 074706.
- [363] Mosher, H. S.; Tidwell, T. T. *J. Chem. Educ.* **1990**, *67*, 9.
- [364] Taft, R.-W. *John Wiley & Sons, New York* **1956**, 556.
- [365] Liptrot, D. J.; Power, P. P. *Nat. Rev. Chem.* **2017**, *1*, 0004.
- [366] Clyburne, J. A.; McMullen, N. *Coord. Chem. Rev.* **2000**, *210*, 73–99.
- [367] Twamley, B.; Haubrich, S. T.; Power, P. P. *Advances in organometallic chemistry*; 1999; Vol. 44; pp 1–65.

Bibliography

- [368] Ni, C.; Power, P. P. *Metal-Metal Bonding*; 2010; pp 59–111.
- [369] Arduengo, A. J. *Acc. Chem. Res.* **1999**, *32*, 913–921.
- [370] Bourissou, D.; Guerret, O.; Gabbai, F. P.; Bertrand, G. *Chem. Rev.* **2000**, *100*, 39–92.
- [371] Gomberg, M. *Ber. Dtsch. Chem. Ges.* **1900**, *33*, 3150–3163.
- [372] Gomberg, M. *J. Am. Chem. Soc.* **1900**, *22*, 757–771.
- [373] Stein, M.; Winter, W.; Rieker, A. *Angew. Chem. Int. Ed.* **1978**, *17*, 692–694.
- [374] Kahr, B.; Van Engen, D.; Mislow, K. *J. Am. Chem. Soc.* **1986**, *108*, 8305–8307.
- [375] Grimme, S.; Schreiner, P. R. *Angew. Chem. Int. Ed.* **2011**, *50*, 12639–12642.
- [376] Pace, C. N.; Scholtz, J. M.; Grimsley, G. R. *FEBS letters* **2014**, *588*, 2177–2184.
- [377] Biedermann, F.; Schneider, H.-J. *Chem. Rev.* **2016**, *116*, 5216–5300.
- [378] Klimeš, J.; Michaelides, A. *J. Chem. Phys.* **2012**, *137*, 120901.
- [379] Ghotra, J. S.; Hursthouse, M. B.; Welch, A. J. *J. Chem. Soc., Chem. Comm.* **1973**, 669–670.
- [380] Ahlquist, M. S.; Norrby, P.-O. *Angew. Chem. Int. Ed.* **2011**, *50*, 11794–11797.
- [381] Lyngvi, E.; Sanhueza, I. A.; Schoenebeck, F. *Organometallics* **2014**, *34*, 805–812.
- [382] Maseras, F.; Eisenstein, O. *New J. Chem.* **1998**, *22*, 5–9.
- [383] Minenkov, Y.; Occhipinti, G.; Heyndrickx, W.; Jensen, V. R. *Eur. J. Inorg. Chem.* **2012**, *2012*, 1507–1516.
- [384] Shaik, S.; Danovich, D.; Wu, W.; Su, P.; Rzepa, H. S.; Hiberty, P. C. *Nat. Chem.* **2012**, *4*, 195.
- [385] Roos, B. O.; Borin, A. C.; Gagliardi, L. *Angew. Chem. Int. Ed.* **2007**, *46*, 1469–1472.
- [386] Nguyen, T.; Sutton, A. D.; Brynda, M.; Fettingner, J. C.; Long, G. J.; Power, P. P. *Science* **2005**, *310*, 844–847.
- [387] Molins, E.; Miravittles, C.; Espinosa, E.; Ballester, M. *J. Org. Chem.* **2002**, *67*, 7175–7178.
- [388] Lenoir, D.; Wattenbach, C.; Liebman, J. F. *Struct. Chem.* **2006**, *17*, 419–422.
- [389] Krebs, A.; Kaletta, B.; Nickel, W.-U.; Rüger, W.; Tikwe, L. *Tetrahedron* **1986**, *42*, 1693–1702.
- [390] Huntley, D. R.; Markopoulos, G.; Donovan, P. M.; Scott, L. T.; Hoffmann, R. *Angew. Chem.* **2005**, *117*, 7721–7725.

- [391] Irngartinger, H.; Lukas, K. L. *Angew. Chem. Int. Ed. Engl.* **1979**, *18*, 694–695.
- [392] Schreiner, P. R.; Chernish, L. V.; Gunchenko, P. A.; Tikhonchuk, E. Y.; Hausmann, H.; Serafin, M.; Schlecht, S.; Dahl, J. E.; Carlson, R. M.; Fokin, A. A. *Nature* **2011**, *477*, 308.
- [393] Fokin, A. A.; Chernish, L. V.; Gunchenko, P. A.; Tikhonchuk, E. Y.; Hausmann, H.; Serafin, M.; Dahl, J. E.; Carlson, R. M.; Schreiner, P. R. *J. Am. Chem. Soc.* **2012**, *134*, 13641–13650.
- [394] Bettinger, H. F.; Schleyer, P. v. R.; Schaefer III, H. F. *Chem. Comm.* **1998**, *7*, 769–770.
- [395] Adcock, J. L.; Gakh, A. A.; Pollitte, J. L.; Woods, C. *J. Am. Chem. Soc.* **1992**, *114*, 3980–3981.
- [396] Wu, W.; Gu, J.; Song, J.; Shaik, S.; Hiberty, P. C. *Angew. Chem. Int. Ed.* **2009**, *48*, 1407–1410.
- [397] Ermer, O.; Mason, S. A. *J. Chem. Soc. Chem. Commun.* **1983**, 53–54.
- [398] Alvarez, S. *Dalton Trans.* **2013**, *42*, 8617–8636.
- [399] Zong, J.; Mague, J. T.; Pascal Jr, R. A. *J. Am. Chem. Soc.* **2013**, *135*, 13235–13237.
- [400] There is an unpublished neutron diffraction study available for **5** that gives an H···H distance of 1.531(8) Å for the central head-to-head Si-H bonds. Personal communication from Robert A. Pascal, Jr., March 26, 2017.
- [401] Berstis, L.; Siegel, J. S.; Baldrige, K. K. *Phys. Chem. Chem. Phys.* **2014**, *16*, 1379–1384.
- [402] Baldrige, K. K.; Siegel, J. S. *J. Phys. Org. Chem.* **2015**, *28*, 223–225.
- [403] Firouzi, R.; Shahbazian, S. *Struct. Chem.* **2014**, *25*, 1297–1304.
- [404] Firouzi, R.; Shahbazian, S. *ChemPhysChem* **2016**, *17*, 51–54.
- [405] London, F. *Trans. Faraday Soc.* **1937**, *33*, 8–26.
- [406] Grimme, S.; Huenerbein, R.; Ehrlich, S. *ChemPhysChem* **2011**, *12*, 1258–1261.
- [407] Wagner, J. P.; Schreiner, P. R. *Angew. Chem. Int. Ed.* **2015**, *54*, 12274–12296.
- [408] Wagner, J. P.; Schreiner, P. R. *J. Chem. Theory Comput.* **2016**, *12*, 231–237.
- [409] Rösel, S.; Balestrieri, C.; Schreiner, P. R. *Chem. Sci.* **2017**, *8*, 405–410.
- [410] Yannoni, N.; Kahr, B.; Mislow, K. *J. Am. Chem. Soc.* **1988**, *110*, 6670–6672.
- [411] Lv, J.; Chen, W.; Chen, L.; Tian, Y.; Yan, J. *Thermochim. Acta* **2014**, *589*, 11–18.

Bibliography

- [412] Khuong, T.-A. V.; Zepeda, G.; Sanrame, C. N.; Dang, H.; Bartberger, M. D.; Houk, K.; Garcia-Garibay, M. A. *J. Am. Chem. Soc.* **2004**, *126*, 14778–14786.
- [413] Rösel, S. and Cañadillas-Delgado, L. and Logeman, C. and Mason, S. A.; Mossou, E. and Schreiner, P. R. “Exact determination of hydrogen positions in tris(3,5-di-tert-butyl phenyl)methane could reveal the shortest intermolecular CH···HC contact”; 10.5291/ILL-DATA.5-12-321; Institut Laue-Langevin: Grenoble, 2016.
- [414] Allen, F. H. *J. Chem. Soc. Perkin Trans* **1987**, *2*, S1.
- [415] Rowland, R. S.; Taylor, R. *J. Am. Chem. Soc.* **1996**, *100*, 7384–7391.
- [416] Rahm, M.; Hoffmann, R.; Ashcroft, N. *Chem.-Eur. J.* **2016**, *22*, 14625–14632.
- [417] Sun, C. C. *J. Pharm. Sci.* **2007**, *96*, 1043–1052.
- [418] Riche, C.; Pascard-Billy, C. *Acta Crystallographica Section B* **1974**, *30*, 1874–1876.
- [419] Su, P.; Li, H. *J. Chem. Phys.* **2009**, *131*, 014102.
- [420] Klamt, A.; Schüürmann, G. *J. Chem. Soc., Perkin Trans. 2* **1993**, 799–805.
- [421] Eckert, F.; Klamt, A. *AIChE Journal* **2002**, *48*, 369–385.
- [422] Klamt, A. *WIREs Comput. Mol. Sci.* **2011**, *1*, 699–709.
- [423] Roth, W. R.; Hunold, F. *Liebigs Ann.* **1996**, *1996*, 1917–1928.
- [424] Weicker, S. A.; Stephan, D. W. *Bull. Chem. Soc. Jpn.* **2015**, *88*, 1003–1016.
- [425] Brown, H. C.; Schlesinger, H.; Cardon, S. Z. *J. Am. Chem. Soc.* **1942**, *64*, 325–329.
- [426] Welch, G. C.; Stephan, D. W. *J. AM. Chem. Soc.* **2007**, *129*, 1880–1881.
- [427] Bader, R. F. *Acc. Chem. Res.* **1985**, *18*, 9–15.
- [428] Contreras-García, J.; Johnson, E. R.; Keinan, S.; Chaudret, R.; Piquemal, J.-P.; Beratan, D. N.; Yang, W. *J. Chem. Theory Comput.* **2011**, *7*, 625–632.
- [429] Mandal, N.; Pratik, S. M.; Datta, A. *J. Phys. Chem. B* **2017**, *121*, 825–834.
- [430] Petrović, P.; Djukic, J.-P.; Hansen, A.; Bannwarth, C.; Grimme, S. In *Non-covalent Interactions in Synthesis and Design of New Compounds*; Maharromov, A. M., Mahmudov, K. T., Kopylovich, M. N., Pombeiro, A. J. L., Eds.; John Wiley & Sons, Inc: Hoboken, New Jersey, 2016; pp 115–143.
- [431] Wagner, J. P.; Schreiner, P. R. *Angew. Chem. Int. Ed.* **2015**, *54*, 12274–12296.
- [432] Becke, A. D.; Johnson, E. R. *J. Chem. Phys.* **2007**, *127*, 154108.
- [433] Becke, A. D.; Johnson, E. R. *J. Chem. Phys.* **2007**, *127*, 124108.
- [434] Runge, E.; Gross, E. K. U. *Phys. Rev. Lett.* **1984**, *52*, 997–1000.

- [435] Poree, C.; Schoenebeck, F. *Acc. Chem. Res.* **2017**, *50*, 605–608.
- [436] Jacobsen, H.; Cavallo, L. *ChemPhysChem* **2012**, *13*, 562–569.
- [437] Weymuth, T.; Couzijn, E. P.; Chen, P.; Reiher, M. *J. Chem. Theory Comput.* **2014**, *10*, 3092–3103.
- [438] Husch, T.; Freitag, L.; Reiher, M. *J. Chem. Theory Comput.* **2018**, *14*, 2456–2468.
- [439] Waller, M. P.; Braun, H.; Hojdis, N.; Bühl, M. *J. Chem. Theory Comput.* **2007**, *3*, 2234–2242.
- [440] Bühl, M.; Reimann, C.; Pantazis, D. A.; Bredow, T.; Neese, F. *J. Chem. Theory Comput.* **2008**, *4*, 1449–1459.
- [441] Wolters, L. P.; Koekkoek, R.; Bickelhaupt, F. M. *ACS Catal.* **2015**, *5*, 5766–5775.
- [442] Johnson, E. R.; Keinan, S.; Mori-Sánchez, P.; Contreras-García, J.; Cohen, A. J.; Yang, W. *J. Am. Chem. Soc.* **2010**, *132*, 6498–6506.
- [443] McCrea-Hendrick, M. L.; Bursch, M.; Gullett, K. L.; Maurer, L. R.; Fettingner, J. C.; Grimme, S.; Power, P. P. *Organometallics* **2018**, *37*, 2075–2085.
- [444] Rekker, B. D.; Brown, T. M.; Fettingner, J. C.; Lips, F.; Tuononen, H. M.; Herber, R. H.; Power, P. P. *J. Am. Chem. Soc.* **2013**, *135*, 10134–10148.
- [445] Martinez, S. H.; Pan, S.; Cabellos, J. L.; Dzib, E.; Fernandez-Herrera, M. A.; Merino, G. *Organometallics* **2017**, *36*, 2036–2041.
- [446] Schwabe, T.; Grimme, S.; Djukic, J.-P. *J. Am. Chem. Soc.* **2009**, *131*, 14156–14157.
- [447] Schneider, W. B.; Bistoni, G.; Sparta, M.; Saitow, M.; Riplinger, C.; Auer, A. A.; Neese, F. *J. Chem. Theory Comput.* **2016**, *12*, 4778–4792.
- [448] Pollice, R.; Bot, M.; Kobylanskii, I. J.; Shenderovich, I.; Chen, P. *J. Am. Chem. Soc.* **2017**, *139*, 13126–13140.
- [449] Mardirossian, N.; Head-Gordon, M. *Mol. Phys.* **2017**, *115*, 2315–2372.
- [450] Peverati, R.; Truhlar, D. G. *Phil. Trans. R. Soc. A* **2014**, *372*, 20120476.
- [451] Schweigert, I. V.; Lotrich, V. F.; Bartlett, R. J. *J. Chem. Phys.* **2006**, *125*, 104108.
- [452] Angyán, J. G.; Gerber, I. C.; Savin, A.; Toulouse, J. *Phys. Rev. A* **2005**, *72*, 012510.
- [453] Sierka, M.; Hogeckamp, A.; Ahlrichs, R. *J. Chem. Phys.* **2003**, *118*, 9136–9148.
- [454] Gaus, M.; Cui, Q.; Elstner, M. *J. Chem. Theory Comput.* **2011**, *7*, 931–948.
- [455] Grimme, S. *J. Chem. Phys.* **2006**, *124*, 034108.
- [456] Schwabe, T.; Grimme, S. *Phys. Chem. Chem. Phys.* **2006**, *38*, 4398.

Bibliography

- [457] Goerigk, L.; Grimme, S. *J. Chem. Theory Comput.* **2011**, *7*, 291.
- [458] Chai, J.-D.; Mao, S.-P. *Chem. Phys. Lett.* **2012**, *538*, 121.
- [459] Brémond, E.; Adamo, C. *J. Chem. Phys.* **2011**, *135*, 024106.
- [460] Herzberg, G. *Molecular Spectra and Molecular Structure* **1979**, 158–169.
- [461] Ghosh, D. C.; Islam, N. *Int. J. Quantum Chem.* **2010**, *110*, 1206–1213.
- [462] Dove, M. T. *Introduction to lattice dynamics*; Cambridge university press, 1993; Vol. 4.
- [463] Erba, A. *J. Chem. Phys.* **2014**, *141*, 124115.
- [464] Erba, A.; Shahrokhi, M.; Moradian, R.; Dovesi, R. *J. Chem. Phys.* **2015**, *142*, 044114.
- [465] Erba, A.; Maul, J.; De La Pierre, M.; Dovesi, R. *J. Chem. Phys.* **2015**, *142*, 204502.
- [466] Erba, A.; Maul, J.; Itou, M.; Dovesi, R.; Sakurai, Y. *Phys. Rev. Lett.* **2015**, *115*, 117402.
- [467] Andrae, D.; Haeussermann, U.; Dolg, M.; Stoll, H.; Preuss, H. *Theor. Chim. Acta* **1990**, *77*, 123–141.
- [468] Metz, B.; Stoll, H.; Dolg, M. *J. Chem. Phys.* **2000**, *113*, 2563–2569.
- [469] Peterson, K. A.; Figgen, D.; Goll, E.; Stoll, H.; Dolg, M. *J. Chem. Phys.* **2003**, *119*, 11113–11123.
- [470] Jain, A.; Ong, S. P.; Hautier, G.; Chen, W.; Richards, W. D.; Dacek, S.; Cholia, S.; Gunter, D.; Skinner, D.; Ceder, G.; Persson, K. A. *APL Mater.* **2013**, *1*, 011002.
- [471] Furche, F.; Ahlrichs, R.; Hättig, C.; Klopper, W.; Sierka, M.; Weigend, F. *WIREs Comput. Mol. Sci.* **2014**, *4*, 91–100.
- [472] Fuentealba, P.; Von Szentpaly, L.; Preuss, H.; Stoll, H. *J. Phys. B* **1985**, *18*, 1287.
- [473] Dolg, M.; Wedig, U.; Stoll, H.; Preuss, H. *J. Chem. Phys.* **1987**, *86*, 866–872.
- [474] Andrae, D.; Haeussermann, U.; Dolg, M.; Stoll, H.; Preuss, H. *Theor. Chem. Acc.* **1990**, *77*, 123–141.
- [475] Lee, C.; Yang, W.; Parr, R. G. *Phys. Rev. B: Condens. Matter Mater. Phys* **1988**, *37*, 785.
- [476] Hellweg, A.; Hättig, C.; Höfener, S.; Klopper, W. *Theor. Chem. Acc.* **2007**, *117*, 587–597.
- [477] Hättig, C. *Phys. Chem. Chem. Phys.* **2005**, *7*, 59–66.
- [478] Liakos, D. G.; Sparta, M.; Kesharwani, M. K.; Martin, J. M.; Neese, F. *J. Chem. Theory Comput.* **2015**, *11*, 1525–1539.

Appendix

A1. Supporting Information to Chapter 1

Appendix A1 contains:

- D4 model (2017 version) methodologies
- ζ function parametrization
- Extended statistical measures
- Cation- π dissociation
- BJ-damping parameter

A1.1. Appendix: Extension of the D3 Dispersion Coefficient Model

A1.2. D4 Definition

Charge Dependence

Besides the geometrical D3 dispersion model,¹⁷ there are semi-classical density dependent approaches like the Tkatchenko-Scheffler (TS) model⁴⁹ or the exchange dipole moment (XDM) model of Becke and Johnson.^{47,47,48} In the newly presented approach, which is based on D3, electronic structure information is included via atomic partial charges as continuous descriptors. Just like D3, the new scheme relies on reference systems for which the dynamic polarizabilities are computed from first-principles time-dependent density functional theory (TD-DFT). In order to describe differently charged environments, which are not described sufficiently by using D3, charge dependencies need to be included in the reference molecules. Due to the fact that TD-DFT calculations employing a fractional electron occupation are not possible with our available codes, the nuclear charges of the atoms A and B of the reference systems are varied to effectively describe different charge situations. In equation A1.1 the element specific scaling-function ζ of the reference polarizabilities (cf., equation 1.3 in chapter 1.2.2) are expressed as functions of the charges q^A of the atoms. The effective nuclear charge of atom A within

the corresponding molecule can be defined as

$$z^A = Z^A + q_{\text{Mulliken}}. \quad (\text{A1.1})$$

Here, Z^A equals the nuclear charge of atom A whereas q_{Mulliken} is the specific calculated Mulliken¹⁹⁵ partial charge for atom A within the molecule.

$$\zeta(z^A) = b\alpha^{1.47 \exp(z^A/z^{A,\text{ref}}) \log(z^{A,\text{ref}}/z^A)} \quad (\text{A1.2})$$

Equation A1.2 introduces the element-specific parameter b which is obtained for each coordination number *via* matching hybrid TD-DFT molecular dispersion coefficients of the reference systems ($z^A = z^{A,\text{ref}}$, to parametrize b). The structures of the reference systems are optimized at the hybrid density functional PBE0¹¹⁶ level of theory employing an Ahlrichs quadruple-zeta basis set²⁵¹ (def2-QZVP). Polarizabilities at imaginary frequencies are derived on these geometries with the def2-QZVP basis set for all main group elements augmented with diffuse (2s2p1d)-functions except for hydrogen whose basis set is augmented by (2s2p)-functions. For transition metals, an additional set of diffuse (2s2p1d1f)-functions is provided. This basis set will be abbreviated as aug-def2-QZVP in the following. Time-dependent density functional theory (TD-DFT) calculations are performed to compute the electric dipole polarizabilities $\alpha(i\omega)$ with a variant of the PBE0 hybrid functional containing 37.5 % Fock exchange ($a_x = 3/8$, termed PBE38) employing the aug-def2-QZVP basis sets. Differently coordinated hydrides (A_mH_n and B_kH_l) are used as model systems for atoms A and B having specific fractional coordination numbers $CN^{A/B}$, which are directly connected to the molecular environment of the described atom A and B . This is exactly as in D3. The parameter α is adjusted for each element using cross-check systems where the calculated Mulliken charge is different from those of the reference systems ($q^{A,\text{ref}} \neq q^A$, to parametrize α). Additionally, we have calculated the cationic static polarizability for atoms with $Z = 2 - 86$ and adjusted a manually to fit those data. All reference Mulliken partial charges $q^{A,\text{ref}}$ are stored as constant values in the code. The stored reference dipole polarizabilities are then scaled by the partial charge dependent function ζ to simulate effects from a higher or lower electron density around the corresponding atom. The charge function is therefore a correction scheme for dipole polarizabilities to produce, after numerical integration, more accurate molecular dispersion coefficients.

GFN-xTB Derived Charges

Recently, a tight-binding (TB) Hamiltonian¹⁹⁶ was developed, which yields accurate Mulliken partial charges in a reasonable time frame even for systems with

A1. Supporting Information to Chapter 1

thousands of atoms. A related self-consistent charge model (GFN-xTB¹⁸⁸) is used to calculate these charges which then serve as input for the presented charge dependent dispersion model. We have tested the amount of computer time for a large system having 3601 atoms (green fluorescence protein, PDB code: 1GFL,11 charge: -6). The computation time of the self-consistent Mulliken partial charges takes about 30 minutes on a desktop computer. Compared to standard Kohn-Sham DFT calculations such a computation can be regarded as negligible. A selfconsistent TB model (i.e., GFN-xTB) is preferred due to the principally simpler computation of gradients which will be developed in future work.

The Covalent Coordination Number

In order to distinguish covalent and ionic bonding situations between atom pairs the D3 functional form for the CN is modified. The new scheme is termed the covalent coordination number (CN_{cov}^A), which is given by

$$CN_{cov}^A = \sum_{B \neq A}^{N_{atoms}} \frac{\exp(-k_1 (|EN^A - EN^B + k_2|^2))}{1 + \exp\left[-16 \left(\frac{4(R^{A,cov} + R^{B,cov})}{3R^{AB}} - 1\right)\right]}. \quad (A1.3)$$

Equation A1.3 is mostly identical to the D3 case and differs only in the numerator, which always equals one in D3. The exponential function in the numerator is adjusted to approximately match Wiberg bond orders for single bonds (computed with GFN-xTB). The variables k_1 and k_2 have the values 0.016 and 19.089. In Table A1 the geometrical coordination number from D3 (CNA) and the covalent coordination number of the new D4 model (CN_{cov}^A) are given for various diatomic molecules.

Table A1.1.: Geometrical (D3) and covalent (D4) fractional coordination numbers. Considered atoms are highlighted in bold font

System	D3 CN^A	D4 CN_{cov}^A
Li-H	0.986	0.801
Li-Li	0.941	0.923
C-H	0.987	0.918
C-F	1.000	0.785
F-H	0.998	0.740
F-F	0.979	0.961

It is noted that the geometrical coordination number is very similar for covalent

and ionic connections (cf. Li_2 and LiH in Table) while the covalent coordination number enables the distinction between such cases. Consequently, more reference systems can be considered in the Gaussian average, which cover both situations for each element. Reference systems can therefore be supplemented with homoatomic molecules like alkali or halogen dimers.

Polarizability Definitions

For clarity, all possible polarizability notations are given below to dispose any occurring confusion. We start with the molecular polarizabilities at imaginary frequencies of the symmetric hydride reference molecules A_mH_n which is denoted as $\alpha^{A_mH_n}(i\omega)$ (having m chemically equal atoms A and n equally charged hydrogen atoms). Because of the fact that we are interested in atomic polarizabilities at imaginary frequencies of atom A within the reference system A_mH_n , $\alpha^{A_mH_n}(i\omega)$ is reduced by its scaled hydrogen contribution as shown in equation A1.4

$$\alpha^{A,\text{ref}}(i\omega) = \frac{1}{m} \left[\alpha^{A_mH_n}(i\omega) - \frac{n}{2} \alpha^{H_2}(i\omega) \zeta(z^{H_{A,\text{ref}}}, z^{H_2}) \right]. \quad (\text{A1.4})$$

The charge dependent atomic polarizability of atom A is introduced by the product of $\alpha^{A,\text{ref}}(i\omega)$ and the reference specific charge function, $\zeta(z^A, z^{A,\text{ref}})$ (cf., equation A1.2), as follows

$$\alpha^{A,\text{ref}}(i\omega) = \alpha^{A,\text{ref}}(i\omega) \zeta(z^A, z^{A,\text{ref}}). \quad (\text{A1.5})$$

Equation A1.5 is solved on-the-fly for all element specific reference systems. After this, a Gaussian weighting function $W_A^{A,\text{ref}}$ is used to obtain charge dependent and hybridization weighted polarizabilities at imaginary frequencies for atom A (see section below for details):

$$\alpha^A(i\omega) \equiv \alpha^{A,\text{ref}}(i\omega, z^A, \text{CN}_{\text{cov}}^A) = \sum_{A,\text{ref}=1}^{N^{A,\text{ref}}} \alpha^{A,\text{ref}}(i\omega, z^A) W_A^{A,\text{ref}} \quad (\text{A1.6})$$

Here, we introduce a short-hand notation for the final polarizability at imaginary frequencies for atom A , $\alpha^A(i\omega)$, and declare $N^{A,\text{ref}}$ as the number of reference systems for the chemical element corresponding to atom A .

The Modified Gaussian Interpolation Scheme

The introduction of charge dependent scaling functions ζ and covalent CNs leads to a modified charge dependent Casimir-Polder formula which is given in equation 10. First, we need to introduce the contribution of the polarizability in reference system (with given $\text{CN}_{\text{cov}}^{A,\text{ref}}$) to the polarizability of atom A (with

A1. Supporting Information to Chapter 1

$\sum_{A,\text{ref}=1}^{N^{A,\text{ref}}} W_A^{A,\text{ref}} = 1$), which is given by

$$W_A^{A,\text{ref}} = \frac{\exp \left[-\Omega_A \left(\text{CN}_{\text{cov}}^A - \text{CN}_{\text{cov}}^{A,\text{ref}} \right)^2 \right]}{\sum_{A,\text{ref}=1}^{N^{A,\text{ref}}} \exp \left[-\Omega_A \left(\text{CN}_{\text{cov}}^A - \text{CN}_{\text{cov}}^{A,\text{ref}} \right)^2 \right]} \quad (\text{A1.7})$$

with

$$\Omega_A = \sum_{A,\text{ref}=1}^{N^{A,\text{ref}}} \frac{\sqrt{2\text{CN}_{\text{cov}}^{A,\text{av}}}}{\left(\sqrt{3.5 \left(\text{CN}_{\text{cov}}^A - \text{CN}_{\text{cov}}^{A,\text{ref}} \right)^2 + \varepsilon} \right)} \quad (\text{A1.8})$$

and

$$\text{CN}_{\text{cov}}^{A,\text{av}} = \frac{1}{N^{A,\text{ref}}} \sum_{A,\text{ref}=1}^{N^{A,\text{ref}}} \text{CN}_{\text{cov}}^{A,\text{ref}}. \quad (\text{A1.9})$$

The stored reference polarizabilities at imaginary frequencies are scaled by $\zeta(z^A, z^{A,\text{ref}})$ and used in a Gaussian average (over CN_{cov}^A) to obtain the $\alpha^A(i\omega, z^A, \text{CN}_{\text{cov}}^A)$ from which dispersion coefficients are numerically integrated on-the-fly. The Gaussian weighting function is designed in such a way that it matches the reference polarizabilities in case that the calculated covalent CN is equal to the reference one. Compared to the D3 Gaussian weighting function, the scaling factor of 4.0 in the exponential function is replaced with a sum over all reference systems for atom A, which includes the difference between the present and the reference covalent coordination number in the denominator (see equation A1.8). In case both coordination numbers match ($\text{CN}_{\text{cov}}^A = \text{CN}_{\text{cov}}^{A,\text{ref}}$), Ω_A becomes very large ($\varepsilon = 10^{-8}$). This way, we ensure that the contribution of the exactly matched reference system is dominant in the Gaussian average. The factor of 3.5 inside the square root of the denominator and the value of 2.0 inside the square root of the nominator were adjusted manually to smooth the weighting function between different reference systems. Equation A1.8 depends on the average reference covalent coordination number $\text{CN}_{\text{cov}}^{A,\text{av}}$ (see equation A1.9), which is necessary to counteract the divergence behavior of the polarizabilities in case of high covalent CNs. Figure 1 shows the performance of both weighting functions (D3 and D4) regarding to their ability of connecting the calculated homoatomic C_6^{AA} dispersion coefficients for the given reference coordination number.

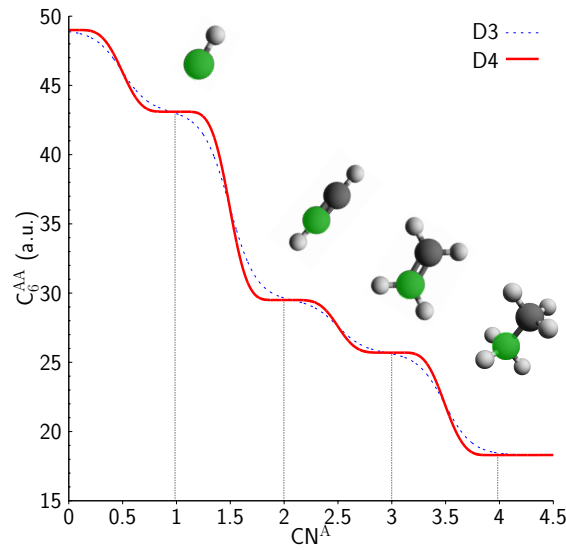


Figure A1.1.: Comparison between the D3 and the D4 Gaussian weighting function and their abilities of connecting pre-calculated homoatomic C_6^{AA} dispersion coefficients (atoms are highlighted in green) obtained from carbon reference systems as a function of the coordination number CNA (D3: CN^A ; D4: CN_{cov}^A). All reference points are highlighted via vertical lines. The blue dotted curve represents the D3 weighting function while the new scheme is represented by the red curve. It should be noted that polarizabilities are weighted in D4, while D3 weights over C_6^{AB} dispersion coefficients.

The new Gaussian weighting function (red curve) yields plateaus around the reference CNs , which demonstrates the “knock-out” criterion employed in the new function around the reference coordination (via Ω_A). This is different in D3, in which the interpolation is smoother (blue dashed curve), however, not necessarily yielding the reference value of C_6^{AA} at $CN_{cov}^A = CN_{cov}^{A,ref}$. In equation 10, the final atom pairwise dispersion coefficient in D4 is given. The polarizability of an atom A/B with effective nuclear charge z^A/z^B and covalent coordination number CN_{cov}^A/CN_{cov}^B is obtained by weighting over all ζ scaled reference systems of atom A/B . The contribution of hydrogen is scaled by $\zeta(z^{H_A}, z^{H_2})/\zeta(z^{H_B}, z^{H_2})$ (where the reference effective charge of hydrogen in dihydrogen is $z^{H_2} = 1$) and subtracted to obtain the correct polarizability of atom A/B (at $CN_{cov}^{A,ref}/CN_{cov}^{B,ref}$) from the molecular polarizability $\alpha^{A_m H_n}(i\omega)$ or $\alpha^{B_k H_l}(i\omega)$.

$$C_6^{AB} \equiv C_6^{AB}(CN_{cov}^A, z^A, CN_{cov}^B, z^B) = \frac{3}{\pi} \int_0^{\infty} d\omega \alpha^A(i\omega) \alpha^B(i\omega) \quad (A1.10)$$

Equation A1.10 uses the short-hand notation of $\alpha^{A/B}(i\omega)$ (see equation A1.6)

A1. Supporting Information to Chapter 1

and additionally introduces the short-hand notation of the weighted and charge dependent dispersion coefficients, C_6^{AB} , which is also used in chapter 1.2. In the D4 model, dispersion coefficients are directly calculated from weighted polarizabilities instead of weighting precalculated reference dispersion coefficients as it was done in D3. In comparison to the D3 model, an additional loop over the 23 imaginary frequencies is required (Simpson integration), however, the additional computational costs are negligible in a QM context. The use of polarizabilities instead of precomputed pairwise dispersion coefficients also facilitates the computation of higher-order, many-body coefficients. For example, the dispersion coefficient of the leading nonadditive term describing the three-body long-range dispersion interaction is defined, as derived from third-order perturbation theory, *via*

$$\begin{aligned} C_9^{ABC} &\equiv C_9^{ABC}(\text{CN}_{\text{cov}}^A, z^A, \text{CN}_{\text{cov}}^B, z^B, \text{CN}_{\text{cov}}^C, z^C) \\ &= -\frac{3}{\pi} \int_0^{\infty} d\omega \alpha^A(i\omega) \alpha^B(i\omega) \alpha^C(i\omega). \end{aligned} \quad (\text{A1.11})$$

In equation A1.11 we use again the short-hand notation of $\alpha^{A/B/C}(i\omega)$. The D4 model is capable of calculating equation A1.11 from the correct C_9^{ABC} expression whereas D3 approximates these coefficients. The accuracy of this approximation for C_9^{ABC} coefficients will be discussed elsewhere. In the following we summarize the procedure of D4 in a step by step scheme:

- 1 Scaling of stored reference molecule TD-DFT polarizabilities by ζ to include a charge dependence into the model.
- 2 Calculation of system specific polarizabilities at imaginary frequencies as Gaussian averages (via CN_{cov}^A) over reference polarizabilities.
- 3 Calculation of the dispersion coefficients C_6^{AB} by numerical Simpson integration from the system specific polarizabilities obtained in step (2).

The steps given above describe the working procedure of the actual program during the calculation of charge dependent pairwise C_6^{AB} dispersion coefficients for an arbitrary molecule. The additivity of these pairwise dispersion coefficients can be exploited to derive a molecular dispersion coefficient according to

$$C_6^{\text{mol}} = \sum_p^{N_{\text{atoms}}^A} \sum_q^{N_{\text{atoms}}^B} C_6^{pq}, \quad (\text{A1.12})$$

where p and q refer to atoms of the particular molecules A and B , respectively. Here, the molecular dispersion coefficient is expressed as a sum over atomic dispersion terms.¹⁵³

A1.3. Parametrization of the ζ Scaling Function

As given in chapter 1.2 the charge function is defined as

$$\zeta(z^A) = \underbrace{b}_{\text{Part B}} \alpha \underbrace{1.47 \exp(z^A/z^{A,\text{ref}})}_{\text{Part C}} \underbrace{\log(z^{A,\text{ref}}/z^A)}_{\text{Part A}}. \quad (\text{A1.13})$$

- z^A : Effective nuclear charge of atom A (see equation A1.1)
- $z^{A,\text{ref}}$: Reference effective nuclear charge of atom A in reference system $A_m H_n$

Part A The functional dependency in the exponent of the charge function is obtained from explicitly calculated polarizabilities at imaginary frequencies where the nuclear charges of the m chemically equivalent atoms within each reference system $A_m H_n$ are varied to simulate a modified fractional electron occupation.

Part B In case that both effective nuclear charges match ($z^A = z^{A,\text{ref}}$), the exponent of the charge function is equal to zero which enables the parametrization of the parameter b by recreating the explicitly calculated molecular dispersion coefficient of the particular reference system. One has to note that this parameter is reference system dependent.

Part C In case that both effective nuclear charges do not match ($z^A \neq z^{A,\text{ref}}$), the exponent of the charge function is not equal to zero. For each element molecular dispersion coefficients of different cationic cross-check systems are used to parametrize α . Additionally, the cationic static polarizabilities $\alpha(0)$ for each element of the periodic system are used to check the parametrization of the element specific α parameter. The factor $\exp(z^A/z^{A,\text{ref}})$ within the exponent of the charge function ensures the proper scaling behavior (stronger scaling for cationic systems ($z^A > z^{A,\text{ref}}$), damped scaling for anionic systems ($z^A < z^{A,\text{ref}}$). All parameter are given in the Supporting Information of Ref. 210.

A1.4. Extended Statistical Measures

As statistical measure for a set $\{x_1, \dots, x_n\}$ of data points with references $\{r_1, \dots, r_n\}$ we use

- Mean deviation (MD): $MD = \frac{1}{n} \sum_i (x_i - r_i)$
- Mean absolute deviation (MAD): $MAD = \frac{1}{n} \sum_i |x_i - r_i|$

A1. Supporting Information to Chapter 1

- Standard deviation (SD): $SD = \sqrt{\frac{1}{n-1} \sum_i (x_i - r_i - MD)^2}$
- Maximum absolute deviation (MAX): $MAX = \max\{|x_i - r_i|\}$

A1.5. Cation- π Dissociation

We have optimized the Li-Benzene cation- π -system at the PBE0-D3(BJ)/def2-QZVP level and used the optimized structure as an initial point for the dissociation process. We therefore placed the lithium cation and the center of mass (COM) of benzene along the z-axis and shifted in 0.1 Bohr intervals the benzene molecule. At each point we calculated the molecular C_6 coefficient at the D3 level of theory and compared it to the D4 one for which additionally self-consistent charges were calculated at each point using GFN-xTB. The following structure was used as initial point for the dissociation process. Coordinates are given in Bohr.

-1.00626687792760	2.43476715537044	-0.00930580305938	c
1.59615582946838	2.01486731041519	-0.05631561175738	c
2.53411243178359	-40.44913456876536	-40.05348140480449	c
0.86959342503882	-2.49318767713759	-0.00344307836595	c
-1.73282433321136	-2.07327817480661	0.04360431932939	c
-2.67078705017786	0.39072063455874	0.04059472444714	c
2.88713274098834	3.60049347821153	-0.10189959594592	h
4.55277786762725	-0.77505011564623	-0.09691768223979	h
1.59698699801968	-4.40474149652284	-0.00799365670788	h
-3.02408886260592	-3.65904634519516	0.07548875248786	h
-4.68977364596326	0.71650842369131	0.06976979632961	h
-1.73392997182037	4.34621663623828	-0.01843787662990	h
-0.00011786417452	0.00001818575674	3.42222090408594	li

Furthermore, we use some points of the dissociation process to measure the quality of the given method.

Table A1.2.: Chosen points of a dissociation curve between a lithium cation and benzene. We have calculated hybrid PBE38/aug-def2-QZVP molecular dispersion coefficients (here, denoted as TD-DFT in the following) as reference points. Distances are given in Bohr.

R(Li ⁺ -Bz)	TD-DFT	D4	D3
3.52	1628.14	1570.46	1968.13
4.42	1704.70	1936.86	2231.04
4.92	1725.67	1943.54	2548.78
5.42	1755.18	1846.32	4165.12
5.92	1766.27	1786.83	4515.05
6.42	1771.08	1772.15	4577.33
6.92	1771.02	1770.47	4596.26
	MAD	5.18	101.48
	MD	4.16	101.48
	SD	6.64	64.81
	AMAX	13.62	159.53

A1.6. BJ-Damping Parameter

Table A1.3.: Parameters for the Becke-Johnson damping function for three density functional approximations. All parameter were adjusted to match reference interaction energies of the S66x8,²⁰³ S22x5²⁰⁴, and NCIBLIND10⁸ benchmark sets.

Method	α_1	α_2	s_8
TPSS-D3	0.3352	4.4231	1.2715
TPSS-D4	0.4732	4.0794	1.3707
B3LYP-D3	0.3986	4.4236	1.9894
B3LYP-D4	0.3837	4.5261	1.7993
PBE0-D3	0.4014	4.8804	1.2664
PBE0-D4	0.0381	6.6249	1.0204

A2. Supporting Information to Chapter 2

Appendix A2 contains:

- EEQ model methodologies
- Many-body dispersion theory
- D4 dispersion potential for GFN2-xTB
- Double hybrid density functional definitions
- BJ-damping parameter sets:
DFT-D4-ATM, DFT-D4-MBD, DFT-D4(TB)-MBD, and DFT-D4(TB)-ATM
- Timings (energy and gradient)
- Extended statistical measures
- Statistical evaluations:
L7, MOR41, SCONF, PCONF21, ICONF, UPU23, ROT34, LMGB35, HMGB11, and TMC32

A2.1. Appendix: A Generally Applicable Atomic-Charge Dependent London Dispersion Correction

A2.2. Classical Partial Charges

Classical electronegativity equilibration (EEQ) partial charges are determined by minimizing the following energy expression

$$E_{\text{IES}} = \sum_{i=1}^N \left(\chi_i q_i + \frac{1}{2} \left(J_{ii} + \frac{2\gamma_{ii}}{\sqrt{\pi}} \right) q_i^2 \right) + \frac{1}{2} \sum_{i=1}^N \sum_{\substack{j=1 \\ i \neq j}}^N q_i q_j \frac{\text{erf}(\gamma_{ij} R_{ij})}{R_{ij}} \quad (\text{A2.1})$$

where γ_{ij} is given as $(\alpha_i^2 + \alpha_j^2)^{-\frac{1}{2}}$ with α_i being the van der Waals radius of atom i . For a more compact representation we rewrite the above expression in matrix notation

$$E_{\text{IES}} = \mathbf{q}^T \left(\frac{1}{2} \mathbf{A} \mathbf{q} - \mathbf{X} \right) \quad (\text{A2.2})$$

where we define the \mathbf{A} matrix and the \mathbf{X} vector by

$$\chi_i = -\chi_i \quad \text{and} \quad A_{ij} = \begin{cases} J_{ii} + \frac{\sqrt{2}\gamma_{ii}}{\sqrt{\pi}} & i = j \\ \frac{\text{erf}(\gamma_{ij}R_{ij})}{R_{ij}} & \text{otherwise} \end{cases} \quad (\text{A2.3})$$

Note that the choice of \mathbf{X} is defined according to the work of Goedecker *et al.* in 2015²³⁰, and we keep the original notation to aid comparability. To obtain EEQ partial charges from this equations, under the constraint that the partial charges conserve the total charge q_{total} of the system, the method of constrained Lagrangian optimization is used as

$$L = E_{\text{IES}} + \lambda \left(\sum_{k=1}^N q_k - q_{\text{total}} \right) \quad \text{with} \quad \frac{\partial L}{\partial \mathbf{q}} = \mathbf{0} \wedge \frac{\partial L}{\partial \lambda} = \sum_{i=1}^N q_i - q_{\text{total}} = 0 \quad (\text{A2.4})$$

which leads to the following set of $(N + 1)$ linear equations

$$\begin{pmatrix} \mathbf{A} & \mathbf{1} \\ \mathbf{1}^T & 0 \end{pmatrix} \cdot \begin{pmatrix} \mathbf{q} \\ \lambda \end{pmatrix} = \begin{pmatrix} \mathbf{X} \\ q_{\text{total}} \end{pmatrix} \quad (\text{A2.5})$$

In contrast to Goedecker's approach we determine χ_i not by a neural network but use a modified variant of the coordination number (mCN) similary as in the DFT-D3 model⁴⁶. For this EEQ charge model we suggest

$$\chi_i = EN_i - \kappa_i \sqrt{\text{mCN}_i} \quad (\text{A2.6})$$

where EN_i is the electronegativity, κ_i is a scaling factor for the geometry dependency, and mCN_i is the coordination number defined as

$$\text{mCN}_i = \sum_{\substack{j=1 \\ j \neq i}}^N \frac{1}{2} \cdot \left(1 + \text{erf} \left(-k_1 \cdot \left(\frac{R_{ij}}{R_{ij}^{\text{cov}}} - 1 \right) \right) \right) \quad (\text{A2.7})$$

where k_1 is an ad-hoc parameter which is set to 7.5 to reproduce the short range behaviour of the original DFT-D3 CN as close as possible while having a better long-range behaviour. $R_{ij}^{\text{cov}} = R_i^{\text{cov}} + R_j^{\text{cov}}$ are the covalent radii published by Pyykkö *et al.* in 2010²⁴³ which are used to be consistent with the DFT-D3 CN. As we arrived at a stationary point in the constrained optimization we can derive

A2. Supporting Information to Chapter 2

the expression needed to calculate the analytical partial charge derivative by

$$\begin{aligned} \frac{\partial L}{\partial q_k} = 0 \quad \implies \quad 0 &= \frac{d}{d\mathbf{R}_j} \frac{\partial L}{\partial q_k} = \frac{\partial^2 L}{\partial q_k \partial \mathbf{R}_j} + \frac{\partial^2 L}{\partial q_k^2} \cdot \frac{\partial q_k}{\partial \mathbf{R}_j} \\ &\iff \frac{\partial^2 L}{\partial q_k^2} \cdot \frac{\partial q_k}{\partial \mathbf{R}_j} = -\frac{\partial^2 L}{\partial q_k \partial \mathbf{R}_j} \end{aligned} \quad (\text{A2.8})$$

Plugging in the expression for L from equation A2.4 we get

$$\frac{\partial^2 L}{\partial \mathbf{q}^2} = \begin{pmatrix} \mathbf{A} & \mathbf{1} \\ \mathbf{1}^\top & 0 \end{pmatrix} \quad (\text{A2.9})$$

Plugging everything back into equation A2.8 we get

$$\begin{pmatrix} \frac{\partial \mathbf{q}}{\partial \mathbf{R}_j} \\ \frac{\partial \lambda}{\partial \mathbf{R}_j} \end{pmatrix} = \begin{pmatrix} \mathbf{A} & \mathbf{1} \\ \mathbf{1}^\top & 0 \end{pmatrix}^{-1} \cdot \left(-\begin{pmatrix} \frac{\partial \mathbf{A}}{\partial \mathbf{R}_j} & \mathbf{0} \\ \mathbf{0}^\top & 0 \end{pmatrix} \cdot \begin{pmatrix} \mathbf{q} \\ \lambda \end{pmatrix} + \begin{pmatrix} \frac{\partial \mathbf{X}}{\partial \mathbf{R}_j} \\ 0 \end{pmatrix} \right) \quad (\text{A2.10})$$

To invert the indefinite but symmetric $(N + 1)$ matrix we apply a Bunch–Kaufman factorization. Overall four parameter are fitted for each element i : EN_i , J_{ii} , κ_i , and α_i (namely the atomic electronegativity, atomic hardness terms, element specific scaling parameters, and atomic van der Waals radii).

Table A2.1.: Atomic electronegativities EN , element-dependent atomic hardness terms J , element specific scaling parameters κ , and atomic van der Waals radii α for all elements up to radon ($Z = 86$).

Atomic number	EN_i	J_{ii}	κ_i	α_i
1	1.23695041	-0.35015861	0.04916110	0.55159092
2	1.26590957	1.04121227	0.10937243	0.66205886
3	0.54341808	0.09281243	-0.12349591	0.90529132
4	0.99666991	0.09412380	-0.02665108	1.51710827
5	1.26691604	0.26629137	-0.02631658	2.86070364
6	1.40028282	0.19408787	0.06005196	1.88862966
7	1.55819364	0.05317918	0.09279548	1.32250290
8	1.56866440	0.03151644	0.11689703	1.23166285
9	1.57540015	0.32275132	0.15704746	1.77503721
10	1.15056627	1.30996037	0.07987901	1.11955204
11	0.55936220	0.24206510	-0.10002962	1.28263182
12	0.72373742	0.04147733	-0.07712863	1.22344336
13	1.12910844	0.11634126	-0.02170561	1.70936266
14	1.12306840	0.13155266	-0.04964052	1.54075036

Continued on next page

Table A2.1 – Continued from previous page

Atomic number	EN_i	J_{ii}	K_i	α_i
15	1.52672442	0.15350650	0.14250599	1.38200579
16	1.40768172	0.15250997	0.07126660	2.18849322
17	1.48154584	0.17523529	0.13682750	1.36779065
18	1.31062963	0.28774450	0.14877121	1.27039703
19	0.40374140	0.42937314	-0.10219289	1.64466502
20	0.75442607	0.01896455	-0.08979338	1.58859404
21	0.76482096	0.07179178	-0.08273597	1.65357953
22	0.98457281	-0.01121381	-0.01754829	1.50021521
23	0.96702598	-0.03093370	-0.02765460	1.30104175
24	1.05266584	0.02716319	-0.02558926	1.46301827
25	0.93274875	-0.01843812	-0.08010286	1.32928147
26	1.04025281	-0.15270393	-0.04163215	1.02766713
27	0.92738624	-0.09192645	-0.09369631	1.02291377
28	1.07419210	-0.13418723	-0.03774117	0.94343886
29	1.07900668	-0.09861139	-0.05759708	1.14881311
30	1.04712861	0.18338109	0.02431998	1.47080755
31	1.15018618	0.08299615	-0.01056270	1.76901636
32	1.15388455	0.11370033	-0.02692862	1.98724061
33	1.36313743	0.19005278	0.07657769	2.41244711
34	1.36485106	0.10980677	0.06561608	2.26739524
35	1.39801837	0.12327841	0.08006749	2.95378999
36	1.18695346	0.25345554	0.14139200	1.20807752
37	0.36273870	0.58615231	-0.05351029	1.65941046
38	0.58797255	0.16093861	-0.06701705	1.62733880
39	0.71961946	0.04548530	-0.07377246	1.61344972
40	0.96158233	-0.02478645	-0.02927768	1.63220728
41	0.89585296	0.01909943	-0.03867291	1.60899928
42	0.81360499	0.01402541	-0.06929825	1.43501286
43	1.00794665	-0.03595279	-0.04485293	1.54559205
44	0.92613682	0.01137752	-0.04800824	1.32663678
45	1.09152285	-0.03697213	-0.01484022	1.37644152
46	1.14907070	0.08009416	0.07917502	1.36051851
47	1.13508911	0.02274892	0.06619243	1.23395526
48	1.08853785	0.12801822	0.02434095	1.65734544
49	1.11005982	-0.02078702	-0.01505548	1.53895240
50	1.12452195	0.05284319	-0.03030768	1.97542736

Continued on next page

A2. Supporting Information to Chapter 2

Table A2.1 – Continued from previous page

Atomic number	EN_i	J_{ii}	κ_i	α_i
51	1.21642129	0.07581190	0.01418235	1.97636542
52	1.36507125	0.09663758	0.08953411	2.05432381
53	1.40340000	0.09547417	0.08967527	3.80138135
54	1.16653482	0.07803344	0.07277771	1.43893803
55	0.34125098	0.64913257	-0.02129476	1.75505957
56	0.58884173	0.15348654	-0.06188828	1.59815118
57	0.68441115	0.05054344	-0.06568203	1.76401732
58	0.56999999	0.11000000	-0.11000000	1.63999999
59	0.56999999	0.11000000	-0.11000000	1.63999999
60	0.56999999	0.11000000	-0.11000000	1.63999999
61	0.56999999	0.11000000	-0.11000000	1.63999999
62	0.56999999	0.11000000	-0.11000000	1.63999999
63	0.56999999	0.11000000	-0.11000000	1.63999999
64	0.56999999	0.11000000	-0.11000000	1.63999999
65	0.56999999	0.11000000	-0.11000000	1.63999999
66	0.56999999	0.11000000	-0.11000000	1.63999999
67	0.56999999	0.11000000	-0.11000000	1.63999999
68	0.56999999	0.11000000	-0.11000000	1.63999999
69	0.56999999	0.11000000	-0.11000000	1.63999999
70	0.56999999	0.11000000	-0.11000000	1.63999999
71	0.56999999	0.11000000	-0.11000000	1.63999999
72	0.87936784	-0.02786741	-0.03585873	1.47055223
73	1.02761808	0.01057858	-0.03132400	1.81127084
74	0.93297476	-0.03892226	-0.05902379	1.40189963
75	1.10172128	-0.04574364	-0.02827592	1.54015481
76	0.97350071	-0.03874080	-0.07606260	1.33721475
77	1.16695666	-0.03782372	-0.02123839	1.57165422
78	1.23997927	-0.07046855	0.03814822	1.04815857
79	1.18464453	0.09546597	0.02146834	1.78342098
80	1.14191734	0.21953269	0.01580538	2.79106396
81	1.12334192	0.02522348	-0.00894298	1.78160840
82	1.01485321	0.15263050	-0.05864876	2.47588882
83	1.12950808	0.08042611	-0.01817842	2.37670734
84	1.30804834	0.01878626	0.07721851	1.76613217
85	1.33689961	0.08715453	0.07936083	2.66172302
86	1.27465977	0.10500484	0.05849285	2.82773085

The quality of those classical partial charges can be seen in Figure A2.1 and in Figure A2.2 where we correlate PBE0/def2-TZVP Hirshfeld partial charges with classical EEQ charges and with GFN2-xTB charges.

Table A2.2.: Statistical measures calculated for the comparison between calculated partial charges and reference PBE0/def2-TZVP Hirshfeld partial charges. Deviations are given in e^- .

Measure	EEQ(Z = 1 – 86)	GFN2-xTB(Z = 1 – 86)	EEQ(Z = 1 – 17)	GFN2-xTB(Z = 1 – 17)
MAD	0.04	0.13	0.03	0.18
MD	0.00	0.00	0.00	-0.01
SD	0.06	0.36	0.05	0.65
AMAX	0.56	19.27	0.33	19.92

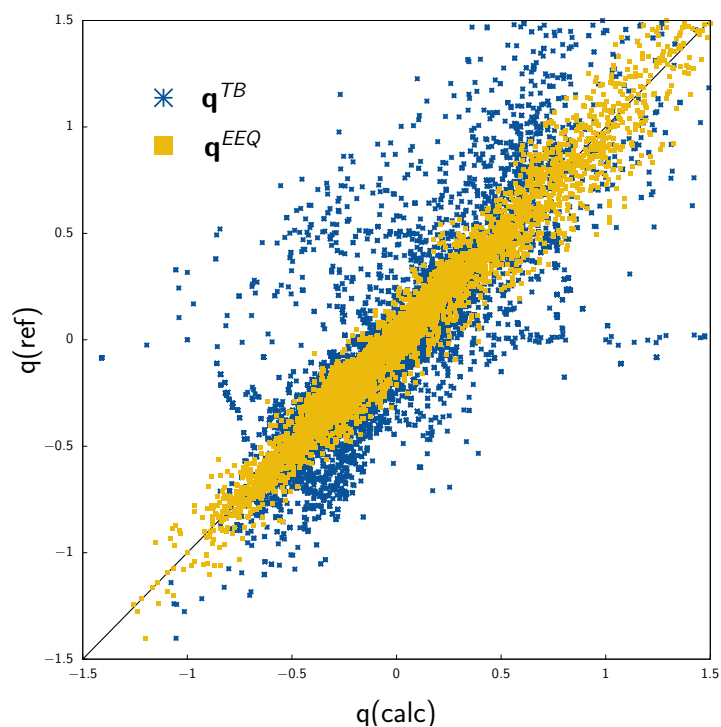


Figure A2.1.: EEQ versus GFN2-xTB partial charges in direct correlation with Hirshfeld partial charges calculated at the PBE0/def2-TZVP level of theory for all elements with $Z = 1 - 86$.

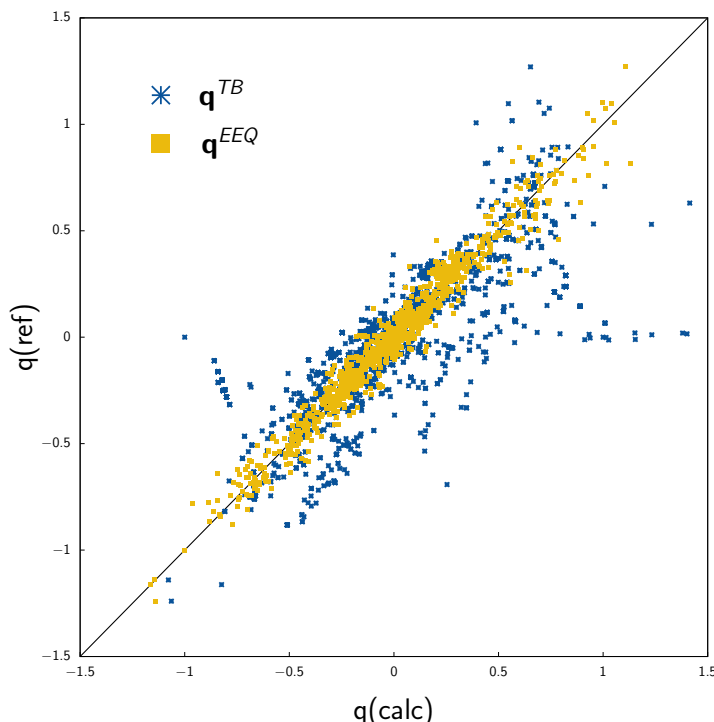


Figure A2.2.: EEQ versus GFN2-xTB partial charges in direct correlation with Hirshfeld partial charges calculated at the PBE0/def2-TZVP level of theory for all elements with $Z = 1 - 17$ (excluding helium and neon).

As can be seen from the Table A2.2, GFN2-xTB converges in some cases to the wrong electronic solution, so that huge deviations can occur (maximum deviation is $19.92 e^-$). The EEQ model on the other hand proves to be quite robust and can convince with a maximum deviation of $0.56 e^-$ on more than 20000 calculated data points for the $Z = 1 - 86$ case.

A2.3. Many-Body Dispersion Theory

Tkatchenko *et al.*¹⁶³ have shown that the dispersion energy can be written as

$$E_{\text{disp}}^{(n),\text{MBD}} = \int_0^{\infty} \frac{d\omega}{2\pi} \text{Tr}\{\ln(\mathbf{1} - \mathbf{A}(i\omega)\mathbf{T})\}, \quad (\text{A2.11})$$

when neglecting intra-oscillator interactions³²² within the matrix formulation ($\text{Tr}\{\mathbf{A}(i\omega)\mathbf{T}\} = 0$). In DFT-D4, the frequency-dependent polarizability matrix $\mathbf{A}(i\omega)$ is obtained from the previously generated atom-in-molecule dynamic polarizabilities

$$\begin{aligned} A_{\text{KP}}^{\beta\gamma}(i\omega) &= \alpha^{\text{K}}(i\omega) \delta_{\text{KP}} \delta_{\gamma\beta} \\ &= \alpha^{\text{K}}(i\omega, z^{\text{K}}, \text{CN}^{\text{K}}) \delta_{\text{KP}} \delta_{\gamma\beta}. \end{aligned} \quad (\text{A2.12})$$

In equation A2.12, K and P label atoms, and β and γ refer to the Cartesian components of their inter-nuclear distance. The use of D4 atom-in-molecule dynamic polarizabilities offers advantages. Different from the TS-based polarizabilities, the D4 polarizabilities already contain information about the molecular environment and no self-consistent screening needs to be performed, which can jeopardize the stability of the method³²³. The generation of the D4 polarizabilities is simple and robust, since only the geometry and atomic partial charges are needed and no additional information from DFT is required. \mathbf{T} is the interaction tensor describing the coupling between the oscillators. The matrix elements of the damped interaction tensor \mathbf{T} are given by

$$T_{KP}^{\beta\gamma} = \sqrt{f_{\text{BJD}}^{(6)}} \frac{\partial}{\partial R_{KP}^{\beta}} \frac{\partial}{\partial R_{KP}^{\gamma}} \left(\frac{1}{R_{KP}} \right). \quad (\text{A2.13})$$

It should be noted that the BJ-damping function is used here as well to screen the elements of the tensor. A motivation for this choice is given below. The MBD energy can be viewed as a series of n -body dipole-dipole terms, and hence, the n -body energy can be obtained directly *via* a Casimir-Polder similar integration of the coupled atom-in-molecule polarizabilities. Because the contributions of the terms in the series tend to oscillate and it converges slowly with n , the value of the limit of the series is used here as computed in equation A2.11. The astute reader will note that the evaluation of the logarithmic trace in equation A2.11 is not directly possible since the product $\mathbf{A}(i\omega)\mathbf{T}$ is a trace-less matrix. To obtain the logarithmic trace, the matrix created by subtraction $(\mathbf{1} - \mathbf{A}(i\omega)\mathbf{T})$ is diagonalized and the sum of the eigenvalues is used to calculate all many-body dispersion terms. Furthermore, splitting the diagonal polarizability matrix $\mathbf{A}(i\omega)$ into the product of its square roots, which is possible due to the invariance regarding cyclic permutation, simplifies the problem to symmetrical matrices only, which makes the calculation of eigenvalues much simpler

$$\left(\mathbf{1} - \mathbf{A}^{1/2}(i\omega)\mathbf{T}\mathbf{A}^{1/2}(i\omega) \right) \mathbf{U} = \mathbf{U}\mathbf{\Lambda}. \quad (\text{A2.14})$$

Here, $\mathbf{\Lambda}$ represents the matrix of eigenvalues with elements λ . The eigenvalues are then used analogously to equation A2.11, and hence the final expression for the MBD energy reads

$$E_{\text{disp}}^{(n),\text{MBD}} = \int_0^{\infty} \frac{d\omega}{2\pi} \ln \left(\prod_{l=1}^{3N} \lambda_l \right). \quad (\text{A2.15})$$

Semi-local DFAs already include short-ranged electron correlation within the exchange-correlation functional. Along with avoiding singularities, this is why the dispersion

A2. Supporting Information to Chapter 2

energy is always damped at short range. Likewise, the interaction tensor in the MBD model needs to be damped. Ideally, the second order term of the MBD energy should be exactly equivalent to the D4 two-body dipole-dipole energy, i.e.,

$$\begin{aligned}
E_{\text{disp}}^{(6),\text{MBD}} &= - \int_0^{\infty} \frac{d\omega}{2\pi} \text{Tr} \left\{ \frac{1}{2} (\mathbf{A}(i\omega)\mathbf{T})^2 \right\} \\
&= - \int_0^{\infty} \frac{d\omega}{2\pi} \frac{1}{2} \sum_K^N \sum_P^N \frac{\alpha^K(i\omega)\alpha^P(i\omega)}{R_{KP}^{10}} f_{\text{damp}}^2 \\
&\quad \times \sum_{\beta}^3 \sum_{\gamma}^3 \left(3R_{KP}^{\beta} R_{KP}^{\gamma} - \delta_{\beta\gamma} R_{KP}^2 \right)^2 \tag{A2.16} \\
&= - \frac{1}{2} \sum_K^N \sum_P^N \frac{C_6^{KP}}{R_{KP}^6} f_{\text{damp}}^2 \\
&\stackrel{!}{=} - \frac{1}{2} \sum_K^N \sum_P^N \frac{C_6^{KP}}{R_{KP}^6} f_{\text{BJD}}^{(6)} = E_{\text{disp}}^{(6)}.
\end{aligned}$$

Hence, the square root of the BJ-damping function is used to damp the MBD interaction tensor. Nevertheless, it should be noted that for higher interaction orders (higher exponentiation of f_{damp}), the respective MBD energy contributions become damped more strongly also in the mid-range distance regime. However, this peculiarity is considered to be small, since the higher-order ($n > 2$) MBD energies represent a smaller fraction of the total dispersion energy (usually one to two magnitudes less than two-body contributions). The final D4-MBD dispersion energy expression consists of two parts. The first compose the two-body dipole-dipole and dipole-quadrupole interaction (denoted as $E_{\text{disp}}^{(6,8)}$). The second part includes all dipole-dipole interactions up to infinite order, $E_{\text{disp}}^{(n),\text{MBD}}$ ($n = 6, 9, 12, 15, \dots, \infty$). To avoid double counting of the two-body dipole-dipole energy, it is removed explicitly from the MBD energy according to

$$E_{\text{disp}}^{\text{D4-MBD}} = E_{\text{disp}}^{(6,8)} + \left(E_{\text{disp}}^{(n),\text{MBD}} - E_{\text{disp}}^{(6),\text{MBD}} \right). \tag{A2.17}$$

Exploiting that $E_{\text{disp}}^{(6)} = E_{\text{disp}}^{(6),\text{MBD}}$ and re-arranging to $E_{\text{disp}}^{\text{D4-MBD}} = E_{\text{disp}}^{(n),\text{MBD}} + E_{\text{disp}}^{(8)}$ is not possible in the general case, as for double hybrid density functionals (abbreviated as DHDF) $s_6 \neq 1$, whereas this scaling cannot be applied to an individual term in the infinite-order MBD energy. Hence, the dispersion energy in DFT-D4-MBD is always calculated as shown in equation A2.17. Similar to Figure 16 of Ref. 17, the contributions to the dispersion energy considered in D4 are put into context with other correction schemes in Figure A2.3.

A2.4. Tight-Binding Two-Body Dispersion Potential (GFN2-xTB)

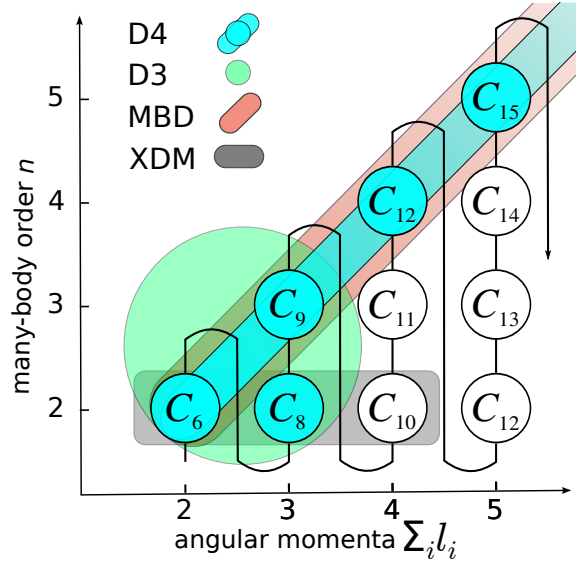


Figure A2.3.: Asymptotic dispersion coefficients from different many-body orders and increasing number of terms in the multipole expansion. The contributions covered by the D3 (including ATM term), D4-MBD, MBD, and XDM methods are highlighted. This Figure is generated in analogy to Figure 16 in Ref. 17.

A2.4. Tight-Binding Two-Body Dispersion Potential (GFN2-xTB)

We developed the GFN2-xTB dispersion potential in terms of density fluctuations (see Ref. 454)

$$\frac{\partial}{\partial c_{vi}} \left[E_{\text{disp}}^{(6,8)} - \sum_j n_j \varepsilon_j \left(\sum_{A,B} \sum_{\kappa \in A} \sum_{\lambda \in B} c_{\kappa j} c_{\lambda j} S_{\kappa \lambda} - 1 \right) \right] = 0$$

A2. Supporting Information to Chapter 2

Take the derivative of $E_{\text{disp}}^{(6,8)}$ with respect to the AO coefficient

$$\begin{aligned}
\frac{\partial E_{\text{disp}}^{(6,8)}}{\partial c_{\nu i}} &= \frac{\partial}{\partial c_{\nu i}} \frac{1}{2} \sum_A \sum_{A,\text{ref}=1}^{N^{A,\text{ref}}} \sum_B \sum_{B,\text{ref}=1}^{N^{B,\text{ref}}} \underbrace{\zeta(z^A, z^{A,\text{ref}})}_{\zeta_A^{A,\text{ref}}} \underbrace{\zeta(z^B, z^{B,\text{ref}})}_{\zeta_B^{B,\text{ref}}} W_A^{A,\text{ref}} W_B^{B,\text{ref}} \\
&\quad \sum_{n=6,8} s_n \frac{C_{AB}^{(n)}}{R_{AB}^{(n)}} f_{\text{BJD}}^{(n)}(R_{AB}) \\
&= \frac{1}{2} \sum_A \sum_{A,\text{ref}=1}^{N^{A,\text{ref}}} \sum_B \sum_{B,\text{ref}=1}^{N^{B,\text{ref}}} \frac{\partial \zeta_A^{A,\text{ref}}}{\partial c_{\nu i}} \zeta_B^{B,\text{ref}} W_A^{A,\text{ref}} W_B^{B,\text{ref}} \sum_{n=6,8} s_n \frac{C_{AB}^{(n)}}{R_{AB}^{(n)}} f_{\text{BJD}}^{(n)}(R_{AB}) \\
&\quad + \frac{1}{2} \sum_A \sum_{A,\text{ref}=1}^{N^{A,\text{ref}}} \sum_B \sum_{B,\text{ref}=1}^{N^{B,\text{ref}}} \frac{\partial \zeta_B^{B,\text{ref}}}{\partial c_{\nu i}} \zeta_A^{A,\text{ref}} W_A^{A,\text{ref}} W_B^{B,\text{ref}} \sum_{n=6,8} s_n \frac{C_{AB}^{(n)}}{R_{AB}^{(n)}} f_{\text{BJD}}^{(n)}(R_{AB}) \\
&= \frac{1}{2} \sum_A \sum_{A,\text{ref}=1}^{N^{A,\text{ref}}} \sum_B \sum_{B,\text{ref}=1}^{N^{B,\text{ref}}} \sum_D \frac{\partial \zeta_A^{A,\text{ref}}}{\partial q_D} \frac{\partial q_D}{\partial c_{\nu i}} \zeta_B^{B,\text{ref}} W_A^{A,\text{ref}} W_B^{B,\text{ref}} \sum_{n=6,8} s_n \frac{C_{AB}^{(n)}}{R_{AB}^{(n)}} f_{\text{BJD}}^{(n)}(R_{AB}) \\
&\quad + \frac{1}{2} \sum_A \sum_{A,\text{ref}=1}^{N^{A,\text{ref}}} \sum_B \sum_{B,\text{ref}=1}^{N^{B,\text{ref}}} \sum_D \frac{\partial \zeta_B^{B,\text{ref}}}{\partial q_D} \frac{\partial q_D}{\partial c_{\nu i}} \zeta_A^{A,\text{ref}} W_A^{A,\text{ref}} W_B^{B,\text{ref}} \sum_{n=6,8} s_n \frac{C_{AB}^{(n)}}{R_{AB}^{(n)}} f_{\text{BJD}}^{(n)}(R_{AB}) \\
&= \frac{1}{2} \sum_A \sum_{A,\text{ref}=1}^{N^{A,\text{ref}}} \sum_B \sum_{B,\text{ref}=1}^{N^{B,\text{ref}}} \frac{\partial \zeta_A^{A,\text{ref}}}{\partial q_A} \frac{\partial q_A}{\partial c_{\nu i}} \zeta_B^{B,\text{ref}} W_A^{A,\text{ref}} W_B^{B,\text{ref}} \sum_{n=6,8} s_n \frac{C_{AB}^{(n)}}{R_{AB}^{(n)}} f_{\text{BJD}}^{(n)}(R_{AB}) \\
&\quad + \frac{1}{2} \sum_A \sum_{A,\text{ref}=1}^{N^{A,\text{ref}}} \sum_B \sum_{B,\text{ref}=1}^{N^{B,\text{ref}}} \frac{\partial \zeta_B^{B,\text{ref}}}{\partial q_B} \frac{\partial q_B}{\partial c_{\nu i}} \zeta_A^{A,\text{ref}} W_A^{A,\text{ref}} W_B^{B,\text{ref}} \sum_{n=6,8} s_n \frac{C_{AB}^{(n)}}{R_{AB}^{(n)}} f_{\text{BJD}}^{(n)}(R_{AB}) \\
&= \frac{1}{2} \sum_A \sum_{A,\text{ref}=1}^{N^{A,\text{ref}}} \sum_B \sum_{B,\text{ref}=1}^{N^{B,\text{ref}}} \frac{\partial \zeta_A^{A,\text{ref}}}{\partial q_A} \left(\delta_{AD} \sum_C \sum_{\kappa \in C} n_i c_{\kappa i} S_{\nu \kappa} + \sum_{\mu \in A} n_i c_{\mu i} S_{\nu \mu} \right) \\
&\quad \times \zeta_B^{B,\text{ref}} W_A^{A,\text{ref}} W_B^{B,\text{ref}} \sum_{n=6,8} s_n \frac{C_{AB}^{(n)}}{R_{AB}^{(n)}} f_{\text{BJD}}^{(n)}(R_{AB}) \\
&\quad + \frac{1}{2} \sum_A \sum_{A,\text{ref}=1}^{N^{A,\text{ref}}} \sum_B \sum_{B,\text{ref}=1}^{N^{B,\text{ref}}} \frac{\partial \zeta_B^{B,\text{ref}}}{\partial q_B} \left(\delta_{BD} \sum_C \sum_{\kappa \in C} n_i c_{\kappa i} S_{\nu \kappa} + \sum_{\mu \in A} n_i c_{\mu i} S_{\nu \mu} \right) \\
&\quad \times \zeta_A^{A,\text{ref}} W_A^{A,\text{ref}} W_B^{B,\text{ref}} \sum_{n=6,8} s_n \frac{C_{AB}^{(n)}}{R_{AB}^{(n)}} f_{\text{BJD}}^{(n)}(R_{AB}) \\
&= \frac{1}{2} \sum_{D,\text{ref}=1}^{N^{D,\text{ref}}} \frac{\partial \zeta_D^{D,\text{ref}}}{\partial q_D} \sum_B \sum_{B,\text{ref}=1}^{N^{B,\text{ref}}} \zeta_B^{B,\text{ref}} W_D^{D,\text{ref}} W_B^{B,\text{ref}} \sum_{n=6,8} s_n \frac{C_{DB}^{(n)}}{R_{DB}^{(n)}} f_{\text{BJD}}^{(n)}(R_{AB}) \sum_C \sum_{\kappa \in C} n_i c_{\kappa i} S_{\nu \kappa} \\
&\quad + \frac{1}{2} \sum_{D,\text{ref}=1}^{N^{D,\text{ref}}} \frac{\partial \zeta_D^d}{\partial q_D} \sum_A \sum_{A,\text{ref}=1}^{N^{A,\text{ref}}} \zeta_A^{A,\text{ref}} W_A^{A,\text{ref}} W_D^{D,\text{ref}} \sum_{n=6,8} s_n \frac{C_{AD}^{(n)}}{R_{AD}^{(n)}} f_{\text{BJD}}^{(n)}(R_{AB}) \sum_C \sum_{\kappa \in C} n_i c_{\kappa i} S_{\nu \kappa} \\
\frac{\partial E_{\text{disp}}^{(6,8)}}{\partial c_{\nu i}} &= \underbrace{\sum_{A,\text{ref}=1}^{N^{A,\text{ref}}} \frac{\partial \zeta_A^{A,\text{ref}}}{\partial q_A} \sum_B \sum_{B,\text{ref}=1}^{N^{B,\text{ref}}} \zeta_B^{B,\text{ref}} W_A^{A,\text{ref}} W_B^{B,\text{ref}} \sum_{n=6,8} s_n \frac{C_{AB}^{(n)}}{R_{AB}^{(n)}} f_{\text{BJD}}^{(n)}(R_{AB})}_{d_A} \sum_C \sum_{\kappa \in C} n_i c_{\kappa i} S_{\nu \kappa}
\end{aligned}$$

Which leads to the two-body DFT-D4 potential used within the GFN2-xTB method

$$F_{\kappa\lambda}^{\text{D4}} = \frac{1}{2} S_{\kappa\lambda} (d_A + d_B), \forall \kappa \in A, \lambda \in B$$

A2.5. Double Hybrid Density Functionals

In the following we give the construction scheme to build the double hybrid density functionals (DHDF) as

$$E_{\text{DHDF}} = (1 - \alpha_x^{\text{Fock}})E_x^{\text{DFT}} + \alpha_x^{\text{Fock}} + \alpha_c^{\text{DFT}}E_c^{\text{DFT}} + \alpha_c^{\text{PT2, OS}}E_{c,\text{OS}}^{\text{PT2}} + \alpha_c^{\text{PT2, SS}}E_{c,\text{SS}}^{\text{PT2}}$$

Table A2.3.: Double hybrid functional definitions as given in the associated literature.

Name	Exchange	Correlation	α_x^{Fock}	α_c^{DFT}	$\alpha_c^{\text{PT2, OS}}$	$\alpha_c^{\text{PT2, SS}}$	Ref.
B2PLYP	B88	LYP	0.5300	0.7300	0.2700	0.2700	455
mPW2PLYP	mPW	LYP	0.5500	0.7500	0.2500	0.2500	456
PWPB95	PW	B95	0.5000	0.7310	0.2690	0.0000	457
DSD-BLYP	B88	LYP	0.6900	0.5400	0.4600	0.3700	285
DSD-PBE	PBE	PBE	0.6800	0.4900	0.5500	0.1300	291
DSD-PBEB95	PBE	B95	0.6600	0.5500	0.4600	0.0900	291
DSD-PBEP86	PBE	P86	0.7000	0.4300	0.5300	0.2500	291
DSD-SVWN	Slater	VWN5	0.7200	0.3300	0.5900	0.1200	291
DOD-BLYP	B88	LYP	0.6500	0.5800	0.5300	0.0000	291
DOD-PBE	PBE	PBE	0.6400	0.5400	0.4200	0.0000	291
DOD-PBEB95	PBE	B95	0.6400	0.5700	0.4600	0.0000	291
DOD-PBEP86	PBE	P86	0.6500	0.4700	0.5400	0.0000	291
DOD-SVWN	Slater	VWN5	0.6900	0.3400	0.5800	0.0000	291
PBE0-2	PBE	PBE	0.7937	0.5000	0.5000	0.5000	458
PBE0-DH	PBE	PBE	0.5000	0.8750	0.1250	0.1250	459

A2.6. BJ-Damping Parameters

Within this section we neglect explicit notation for EEQ charges and denote GFN2-xTB Mulliken-type charges as “TB”. Different parametrizations are created for the application of either ATM or MBD for higher-order dipole-dipole interactions within the DFT-D4 treatment.

Table A2.4.: BJ-damping parameter (DFT-D4-ATM, **default model** also abbreviated as DFT-D4) for various DFAs as derived by fitting to reference data (S66x8²⁰³, S22x5²⁰⁴, NCIBLIND10⁸).

DFA	s_6	s_8	α_1	α_2
B1LYP	1.0000	1.83127296	0.38566678	4.46165003
B1P	1.0000	3.39627782	0.48378848	5.03931438
B3LYP	1.0000	1.93437518	0.40534340	4.46480849

Continued on next page

A2. Supporting Information to Chapter 2

Table A2.4 – Continued from previous page

DFA	s_6	s_8	α_1	α_2
B3P	1.0000	3.16491035	0.47074324	4.98026996
B3PW	1.0000	2.71641216	0.44494036	4.52574006
B97	1.0000	0.89828166	0.30815953	4.44343255
BHLYP	1.0000	1.51193799	0.28352672	5.30677349
BLYP	1.0000	2.29195845	0.43649221	4.07264155
BPBE	1.0000	3.63472763	0.47149679	4.34913593
BP	1.0000	3.09980446	0.41177321	4.91760174
BPW	1.0000	2.94562042	0.45965220	4.16080174
CAMB3LYP	1.0000	1.64013269	0.42783452	5.00658911
HF	1.0000	1.60819947	0.44823943	3.34739336
LB94	1.0000	2.50951042	0.37548645	3.39814397
LCBLYP	1.0000	1.54912035	0.64133251	7.02976707
M062X	1.0000	-0.11498052	0.86398340	7.32464659
M06	1.0000	0.46179592	0.58829427	5.97912883
M06L	1.0000	-0.00187113	0.70990419	6.04454604
MPW1LYP	1.0000	1.32525501	0.30073471	5.17778698
MPW1PW	1.0000	1.62245065	0.41739065	4.60898422
MPWLYP	1.0000	1.35859418	0.28679077	4.91552802
MPWPW	1.0000	1.72053269	0.32744516	4.82196851
O3LYP	1.0000	1.72541878	0.10800765	6.06229794
OLYP	1.0000	2.67570477	0.57149958	2.61804572
OPBE	1.0000	2.90041924	0.62909263	2.36955885
PBE0	1.0000	1.18452505	0.41932554	4.89618246
PBE	1.0000	0.94243311	0.40721568	4.66368352
PW1PW	1.0000	1.17508911	0.47051491	4.88711396
PW6B95	1.0000	-0.23516829	0.07665268	5.86715185
PW86PBE	1.0000	1.43609069	0.42682422	4.67753537
PW91	1.0000	0.85759927	0.39107740	4.99334711
PWP1	1.0000	0.62830540	0.55631871	5.33628863
PWP	1.0000	0.56431039	0.47594244	5.65254449
REVPBE0	1.0000	1.50141170	0.35855796	4.16067532
REVPBE38	1.0000	1.71457164	0.38736794	4.42261301
REVPBE	1.0000	1.70953750	0.52348507	3.08765999
REVPSS	1.0000	1.49570230	0.43220513	4.66456596
RPBE	1.0000	1.28835906	0.45266603	3.17321040
RPW86PBE	1.0000	1.22474218	0.39927128	4.70290460

Continued on next page

Table A2.4 – Continued from previous page

DFA	s_6	s_8	α_1	α_2
SCAN	1.0000	0.45317923	0.61487801	5.89122426
TPSS0	1.0000	1.53512360	0.39794992	4.74628072
TPSS	1.0000	2.22450811	0.44885211	4.64982937
TPSSH	1.0000	2.14405267	0.45324685	4.65909865
WB97	1.0000	1.09057850	0.74881884	7.31791871
WB97X	1.0000	0.33918375	0.57422550	6.43538496
X3LYP	1.0000	1.49832379	0.21295905	5.48908321
XLYP	1.0000	1.52445161	0.09180633	5.36566590
B2PLYP	0.6400	1.03991146	0.42917078	4.64590570
DODBLYP	0.4700	1.21297512	0.40152993	4.29043657
DODPBEB95	0.5400	0.02025159	0.39558022	4.10515132
DODPBE	0.4800	0.81504008	0.38947068	4.40817249
DODPBEP86	0.5600	0.71727708	0.41545419	4.54527783
DODSVWN	0.4200	0.82512933	0.46905029	4.92016057
DSDBLYP	0.5400	0.60520504	0.46267788	4.76592888
DSDPBEB95	0.5400	-0.04387628	0.44578581	4.26570539
DSDPBE	0.4500	0.68957174	0.42311803	4.56085039
DSDPBEP86	0.4700	0.38400895	0.53392682	5.11487807
DSDSVWN	0.4100	0.50548201	0.49342933	4.92304517
MPW2PLYP	0.7500	0.54093706	0.48555673	4.89799320
PBE0-2	0.5000	0.08487184	0.67263608	5.70637126
PBE0-DH	0.8750	0.63911617	0.47372984	4.84410206
PWPB95	0.8200	-0.34312910	0.38199320	4.03853149

Table A2.5.: BJ-damping parameter (DFT-D4-MBD) for various DFAs as derived by fitting to reference data ($S66x8^{203}$, $S22x5^{204}$, $NCIBLIND10^8$).

DFA	s_6	s_8	α_1	α_2
B1LYP	1.0000	1.82880361	0.38501163	4.45594754
B1P	1.0000	3.41489436	0.48259611	5.03433256
B3LYP	1.0000	1.93794471	0.40421683	4.45688214
B3P	1.0000	3.17922279	0.46994391	4.97628954
B3PW	1.0000	2.72554948	0.44382046	4.52143550
B97	1.0000	0.89819432	0.30783131	4.44291091
BHLYP	1.0000	1.51023186	0.28234967	5.28949264
BLYP	1.0000	2.08803266	0.41735956	4.04064805
BPBE	1.0000	3.54765467	0.49393534	4.19603329

Continued on next page

A2. Supporting Information to Chapter 2

Table A2.5 – Continued from previous page

DFA	s_6	s_8	α_1	α_2
BP	1.0000	3.11653507	0.41001465	4.90963955
BPW	1.0000	2.84702187	0.44956163	4.15043391
CAMB3LYP	1.0000	1.65135340	0.42686732	4.99408201
HF	1.0000	1.46466084	0.44789141	3.26970754
LB94	1.0000	2.18919793	0.34183980	3.37328349
LCBLYP	1.0000	1.67842102	0.64789374	7.02690136
M062X	1.0000	-0.04651739	0.86440644	7.33574136
M06	1.0000	0.53733769	0.58813271	5.97262795
M06L	1.0000	0.02532615	0.70915517	6.03265137
MPW1LYP	1.0000	1.33831837	0.29969213	5.17075867
MPW1PW	1.0000	1.63282499	0.41546443	4.59996898
MPWLYP	1.0000	1.36529771	0.28692936	4.90977514
MPWPW	1.0000	1.73006353	0.32572466	4.81445524
O3LYP	1.0000	1.73860949	0.10639457	6.05007081
OLYP	1.0000	2.46450335	0.55516617	2.59873072
OPBE	1.0000	2.69357400	0.61287320	2.35731816
PBE0	1.0000	1.19731044	0.41771977	4.88392353
PBE	1.0000	0.94691612	0.40691345	4.64175930
PW1PW	1.0000	1.18241329	0.46953406	4.88287074
PW6B95	1.0000	-0.15512537	0.08230524	5.93915172
PW86PBE	1.0000	1.46613603	0.42646395	4.67105725
PW91	1.0000	1.20681513	0.46332094	4.85704367
PWP1	1.0000	0.65768072	0.55537751	5.32895289
PWP	1.0000	0.59488896	0.47689543	5.64399980
REVPBE0	1.0000	1.49951783	0.35844324	4.16158145
REVPBE38	1.0000	1.79788536	0.38772841	4.45985024
REVPBE	1.0000	1.52954699	0.49385683	3.10984716
REVPSS	1.0000	1.50953024	0.43005107	4.65617962
RPBE	1.0000	1.14398738	0.44115512	3.14109823
RPW86PBE	1.0000	1.23872511	0.39820283	4.69425839
SCAN	1.0000	0.47101979	0.61572766	5.89955634
TPSS0	1.0000	1.44964396	0.38938772	4.70319441
TPSS	1.0000	1.92120722	0.42887152	4.56481847
TPSSH	1.0000	2.16224973	0.45193499	4.65294862
WB97	1.0000	1.24878344	0.76459986	7.30498442
WB97X	1.0000	0.35331967	0.57760797	6.42117791

Continued on next page

Table A2.5 – Continued from previous page

DFA	s_6	s_8	α_1	α_2
X3LYP	1.0000	1.50510876	0.21172184	5.47818274
XLYP	1.0000	1.50974073	0.09056128	5.36235665
B2PLYP	0.6400	1.01216754	0.41643920	4.63180980
DODBLYP	0.4700	1.08835002	0.37569917	4.23989863
DODPBEB95	0.5400	0.04414267	0.39115971	4.17572877
DODPBE	0.4800	0.81215720	0.38244055	4.37813788
DODPBEP86	0.5600	0.72032712	0.40969100	4.51490751
DODSVWN	0.4200	0.88325732	0.45773819	4.95764154
DSDBLYP	0.5400	0.62682576	0.45454010	4.72957926
SDPBEB95	0.5400	-0.02861403	0.43084778	4.29816817
SDPBE	0.4500	0.69830579	0.41691935	4.53518393
SDPBEP86	0.4700	0.41120180	0.52679302	5.08057386
SDSVWN	0.4100	0.73601001	0.50101270	5.06418673
MPW2PLYP	0.7500	0.55667324	0.48097971	4.87944949
PBE0-2	0.0500	0.26780051	0.67986298	5.76199448
PBE0-DH	0.8750	0.98152896	0.46760392	5.06547798
PWPB95	0.8200	-0.35440136	0.36144369	4.10631855

Table A2.6.: BJ-damping parameter (DFT-D4(TB)-MBD) for various DFAs as derived by fitting to reference data ($S66x8^{203}$, $S22x5^{204}$, $NCIBLIND10^8$).

DFA	s_6	s_8	α_1	α_2
HF	1.0000	1.45828683	0.44712742	3.26487734
BLYP	1.0000	2.08117058	0.41711642	4.03955128
BPBE	1.0000	3.64259175	0.47063878	4.34712279
BP	1.0000	3.11112473	0.40995387	4.91005330
BPW	1.0000	2.52744727	0.40402782	4.22084057
LB94	1.0000	2.09141891	0.30128051	3.45788060
MPWLYP	1.0000	1.36460200	0.28610246	4.91028062
MPWPW	1.0000	1.73130752	0.32547973	4.81372663
OLYP	1.0000	2.30187644	0.54154721	2.53287278
OPBE	1.0000	2.47862243	0.59805792	2.26671322
PBE	1.0000	0.95159605	0.40436318	4.65010856
RPBE	1.0000	1.05401423	0.42599648	3.10146307
REVPBE	1.0000	1.52850098	0.49314034	3.10441225
PW86PBE	1.0000	1.46497296	0.42635774	4.67070001
RPW86PBE	1.0000	1.23782981	0.39785399	4.69412260

Continued on next page

A2. Supporting Information to Chapter 2

Table A2.6 – Continued from previous page

DFA	s_6	s_8	a_1	a_2
PW91	1.0000	0.89648532	0.39592418	4.96320977
PWP	1.0000	0.63806944	0.47390787	5.66515208
XLYP	1.0000	1.50994082	0.09051215	5.36205296
B97	1.0000	0.89799738	0.30819088	4.44324265
TPSS	1.0000	1.88901638	0.42775015	4.55379980
REVTPSS	1.0000	1.50883062	0.43017530	4.65783611
SCAN	1.0000	0.46990209	0.61436450	5.89911495
B1LYP	1.0000	1.83074938	0.38493543	4.45592640
B3LYP	1.0000	1.93642773	0.40445381	4.45704639
BHLYP	1.0000	1.51896770	0.28192218	5.29427469
B1P	1.0000	3.41675121	0.48253511	5.03389354
B3P	1.0000	3.18279035	0.46992325	4.97650253
B3PW	1.0000	2.72363274	0.44377256	4.52215574
O3LYP	1.0000	1.73874942	0.10638982	6.04981736
REVPBE0	1.0000	1.49890714	0.35819541	4.15947955
REVPBE38	1.0000	1.57382508	0.37838702	4.35632432
PBE0	1.0000	1.19661978	0.41734308	4.88432030
PWP1	1.0000	0.64888926	0.55564809	5.32212639
PW1PW	1.0000	1.18364244	0.46953724	4.88272276
MPW1PW	1.0000	1.62788471	0.41557675	4.59973489
MPW1LYP	1.0000	1.33170909	0.29830906	5.17345035
PW6B95	1.0000	-0.16443919	0.07904989	5.94439646
TPSSH	1.0000	2.16468907	0.45254189	4.65553922
TPSS0	1.0000	1.25285163	0.38223499	4.61593529
X3LYP	1.0000	1.50562853	0.21152728	5.47901628
M06L	1.0000	0.01347697	0.70834664	6.03315516
M06	1.0000	0.50785008	0.58953157	5.97317057
M062X	1.0000	0.04672618	0.87098156	7.32988630
WB97	1.0000	1.12736363	0.75396590	7.31052961
WB97X	1.0000	0.35040501	0.56974796	6.44327794
CAMB3LYP	1.0000	1.65213437	0.42676206	4.99450582
LCBLYP	1.0000	1.67459038	0.64772566	7.02691022
LH07TSVWN	1.0000	1.64716468	0.36027550	3.94884094
LH07SSVWN	1.0000	2.54773475	0.37196719	3.89864094
LH12CTSSIRPW92	1.0000	1.90023851	0.33513581	3.53724635
LH12CTSSIFPW92	1.0000	2.04371641	0.33238788	3.47234711

Continued on next page

Table A2.6 – Continued from previous page

DFA	s_6	s_8	α_1	α_2
LH14TCALPBE	1.0000	0.96217113	0.40809799	4.53911955
B2PLYP	0.7800	0.97090085	0.41849225	4.59286243
MPW2PLYP	0.7500	0.55506801	0.48148834	4.88179316
PWPB95	0.8200	-0.02640853	0.43744768	4.53884724
DSDBLYP	0.5400	0.62642144	0.45589598	4.73062294
SDPB	0.4500	0.69229105	0.41584408	4.52896960
SDPBEB95	0.5400	-0.02535683	0.43117570	4.31724907
SDPBEP86	0.4700	0.40437239	0.52692625	5.08678249
SDSVWN	0.4100	0.73668521	0.50541252	5.06078930
DODBLYP	0.4700	1.04384962	0.37001761	4.22041649
DODPB	0.4800	0.80824428	0.38386476	4.37573221
DODPBEB95	0.5600	0.02781676	0.38100406	4.18729280
DODPBEP86	0.4600	0.71163846	0.40907164	4.51396886
DODSVWN	0.4200	0.82959503	0.45957776	4.89671368
PBE0-2	0.5000	0.12481539	0.66150525	5.70164463
PBE0-DH	0.8750	0.65674732	0.47131118	4.82816982

Table A2.7.: BJ-damping parameter (DFT-D4(TB)-ATM) for various DFAs as derived by fitting to reference data ($S_{66 \times 8}$ ²⁰³, $S_{22 \times 5}$ ²⁰⁴, NCIBLIND10⁸).

DFA	s_6	s_8	α_1	α_2
HF	1.0000	1.55736644	0.44217952	3.32410441
BLYP	1.0000	2.19020080	0.42913071	4.05110479
BPBE	1.0000	3.62974920	0.47179311	4.34832782
BP	1.0000	3.08647246	0.41162112	4.91954319
BPW	1.0000	2.85109094	0.45463214	4.14345106
LB94	1.0000	2.39809364	0.36347155	3.34195390
MPWLYP	1.0000	1.36395783	0.28602441	4.91054588
MPWPW	1.0000	1.73185625	0.32534435	4.81318452
OLYP	1.0000	2.30087126	0.54144859	2.53332300
OPBE	1.0000	2.70962530	0.61800352	2.27621123
PBE	1.0000	0.93625094	0.40790049	4.65135944
RPBE	1.0000	1.05164427	0.42592627	3.10037133
REVPBE	1.0000	1.61138201	0.51215200	3.04718355
PW86PBE	1.0000	1.19254614	0.39745489	4.66150128
RPW86PBE	1.0000	1.22289266	0.39946065	4.70231415
PW91	1.0000	0.78221005	0.39097390	4.94408451

Continued on next page

A2. Supporting Information to Chapter 2

Table A2.7 – Continued from previous page

DFA	s_6	s_8	a_1	a_2
PWP	1.0000	0.61218826	0.47778963	5.64605664
XLYP	1.0000	1.50968143	0.09056306	5.36223975
B97	1.0000	0.89818005	0.30891258	4.44379503
TPSS	1.0000	2.22336684	0.44903931	4.65080532
REVPSS	1.0000	1.49374036	0.43199183	4.66405759
SCAN	1.0000	0.45775648	0.61669342	5.90523468
B1LYP	1.0000	1.82819641	0.38561062	4.46105123
B3LYP	1.0000	1.93077774	0.40520781	4.46255249
BHLYP	1.0000	1.50655502	0.28355060	5.30354638
B1P	1.0000	3.39400623	0.48389119	5.03982146
B3P	1.0000	3.16190735	0.47103271	4.98137363
B3PW	1.0000	2.71273965	0.44631895	4.52517962
O3LYP	1.0000	1.72321198	0.10802598	6.06126661
REVPBE0	1.0000	1.50046346	0.35837424	4.15979987
REVPBE38	1.0000	1.61994900	0.38456295	4.37487340
PBE0	1.0000	1.18497326	0.41918588	4.89170085
PWP1	1.0000	0.61368682	0.55682803	5.33266814
PW1PW	1.0000	1.16002822	0.47078518	4.89243094
MPW1PW	1.0000	1.61991331	0.41709790	4.60728322
MPW1LYP	1.0000	1.32539433	0.30123436	5.17574956
PW6B95	1.0000	-0.24364276	0.06861369	5.89370310
TPSSH	1.0000	1.81699305	0.43708555	4.57679351
TPSS0	1.0000	1.46938802	0.39751411	4.71014742
X3LYP	1.0000	1.49493575	0.21310866	5.48746009
M06L	1.0000	0.02539965	0.71110772	6.05063504
M06	1.0000	0.50295755	0.58875642	5.96557487
M062X	1.0000	-0.12770286	0.86289908	7.30761622
WB97	1.0000	1.26204557	0.75437695	7.31527780
WB97X	1.0000	0.34783580	0.57488291	6.41921802
CAMB3LYP	1.0000	1.63966917	0.42427808	5.03109815
LCBLYP	1.0000	1.67838379	0.64705435	7.02883375
LH07TSVWN	1.0000	3.40858218	0.53218598	3.55068620
LH07SSVWN	1.0000	2.01742030	0.49983199	3.53449278
LH12CTSSIRPW92	1.0000	2.46688356	0.56783603	2.83126177
LH12CTSSIFPW92	1.0000	2.70376807	0.58623258	2.72103381
LH14TCALPBE	1.0000	1.23827287	0.43537537	4.63938635

Continued on next page

Table A2.7 – Continued from previous page

DFA	s_6	s_8	a_1	a_2
B2PLYP	0.7800	1.00468553	0.42737183	4.62624158
MPW2PLYP	0.7500	0.54318070	0.48472756	4.89674342
PWPB95	0.8200	-0.35342155	0.37278086	4.03580081
DSDBLYP	0.5400	0.60151254	0.46091302	4.75348449
DSDPBE	0.4500	0.69865539	0.42508371	4.56518930
DSDPBEB95	0.5400	-0.05097431	0.42967019	4.32398958
DSDPBEP86	0.4700	0.38271706	0.53397308	5.11687101
DSDSVWN	0.4100	0.50904643	0.49413232	4.92092377
DODBLYP	0.4700	1.17101452	0.39833737	4.25809811
DODPBE	0.4800	0.80761267	0.38873738	4.40171191
DODPBEB95	0.5600	0.00959016	0.38866713	4.09462693
DODPBEP86	0.4600	0.71327951	0.41631367	4.53851973
DODSVWN	0.4200	0.62186246	0.45590032	4.74298602
PBE0-2	0.5000	0.10740034	0.66706819	5.73936118
PBE0-DH	0.8750	0.74864713	0.47598257	4.90910090

A2.7. Timings of Energy and Gradient Calls

We compare timings for energy and gradient calls between DFT-D4 and DFT-D3(BJ)-ATM for the Tetrakis(isonitrile)rhodium(I) dimer with 106 atoms (doubly positively charged) and a diamond chunk with 430 atoms (286 carbon atoms and 144 hydrogen atoms) derived at four Intel(R) Core(TM) i7-6700 CPU (3.40 GHz).

Property	CPU time(DFT-D4) / s	CPU time(DFT-D3(BJ)-ATM) / s
Tetrakis(isonitrile)rhodium(I) dimer (106 atoms, charge +2)		
single-point	0.01	0.03
gradient	0.01	0.03
Diamond chunk (430 atoms, charge 0)		
single-point	0.34	0.41
gradient	0.51	1.02

A2.8. Extended Statistical Measures

Statistical evaluation: S30L

A2. Supporting Information to Chapter 2

Table A2.8.: Extended statistical evaluation of the S30L²⁵⁹ benchmark set for various different DFAs. For each functional we directly compare DFT–D3 (BJ)-ATM (abbreviated as D3) corrected values with DFT–D4-ATM (abbreviated as D4) corrected values given in kcal mol⁻¹. For further details please check Ref. 257,263. We follow the numbering of the systems regarding Ref. 259

#	DLPNO-	PW6B95		SCAN		revPBE	
	CCSD(T)/CBS*	D4	D3	D4	D3	D4	D3
1	-31.0	-28.2	-30.1	-30.2	-29.7	-29.6	-28.0
2	-20.7	-19.0	-20.4	-19.8	-19.4	-19.6	-18.2
3	-23.3	-19.1	-19.2	-22.5	-21.5	-20.8	-18.0
4	-18.6	-20.9	-20.3	-21.4	-21.0	-20.7	-18.6
5	-27.9	-31.6	-32.9	-33.2	-32.2	-32.7	-28.7
6	-25.2	-21.2	-22.8	-25.6	-25.2	-24.8	-22.2
7	-31.0	-32.1	-33.4	-33.2	-33.2	-34.8	-29.9
8	-35.6	-36.9	-38.7	-38.1	-38.0	-40.2	-34.5
9	-33.7	-31.6	-32.7	-33.6	-29.4	-35.1	-27.0
10	-35.0	-30.5	-32.0	-34.7	-30.2	-36.2	-27.8
11	-35.8	-32.8	-36.7	-40.1	-34.2	-42.5	-32.5
12	-36.9	-33.6	-37.5	-40.1	-34.1	-42.5	-32.4
13	-27.3	-24.2	-25.7	-27.1	-25.5	-24.0	-22.9
14	-28.6	-24.2	-26.7	-28.3	-26.6	-25.6	-23.9
15	-17.5	-17.3	-18.1	-21.8	-21.9	-21.2	-21.1
16	-21.6	-21.4	-23.9	-24.2	-24.2	-25.3	-24.7
17	-34.3	-32.6	-31.7	-36.0	-35.9	-33.4	-32.3
18	-22.8	-20.8	-20.4	-24.4	-24.0	-22.5	-21.3
19	-15.3	-14.4	-14.7	-17.0	-16.1	-15.4	-15.3
20	-18.5	-17.2	-17.9	-20.1	-19.1	-18.0	-18.2
21	-28.0	-22.8	-24.9	-27.3	-25.1	-23.9	-23.5
22	-35.3	-35.2	-33.9	-38.6	-38.8	-39.5	-38.7
23	-62.1	-63.0	-61.8	-66.5	-66.9	-68.7	-68.1
24	-136.3	-130.3	-133.1	-138.0	-134.7	-126.9	-126.5
25	-28.7	-27.4	-31.2	-30.2	-28.9	-29.8	-27.1
26	-28.6	-26.4	-30.3	-27.9	-26.5	-29.8	-27.1
27	-83.4	-80.6	-82.0	-84.3	-83.5	-80.6	-80.7
28	-80.0	-77.4	-78.7	-80.7	-80.1	-77.2	-77.4
29	-52.8	-56.0	-54.2	-58.1	-58.2	-55.8	-54.2
30	-49.6	-51.1	-49.9	-53.6	-53.4	-51.5	-49.7
	MD	1.5	0.3	-1.7	-0.4	-0.8	1.8
	MAD	2.5	1.8	2.0	2.3	2.9	3.1
	RMSD	2.9	2.2	2.6	2.7	3.6	3.8
	SD	13.3	11.7	10.5	14.8	19.5	18.4
	Var	6.1	4.7	3.8	7.6	13.1	11.7
	Max	6.0	4.1	0.9	4.8	9.4	9.8
	Min	-3.7	-5.0	-5.3	-5.4	-6.7	-6.0
	AMax	6.0	5.0	5.3	5.4	9.4	9.8

Statistical evaluation: L7

Table A2.9.: Extended statistical evaluation of the S30L²⁵⁹ benchmark set for various different DFAs. For each functional we directly compare DFT–D3 (BJ)-ATM (abbreviated as D3) corrected values with DFT–D4-MBD (abbreviated as D4) corrected values given in kcal mol⁻¹. For further details please check Ref. 257,263. We follow the numeration of the systems regarding Ref. 259

#	DLPNO-	PW6B95		SCAN		revPBE	
	CCSD(T)/CBS*	D4	D3	D4	D3	D4	D3
1	-31.0	-29.8	-30.1	-30.1	-29.7	-30.2	-28.0
2	-20.7	-20.2	-20.4	-19.7	-19.4	-20.0	-18.2
3	-23.3	-20.8	-19.2	-22.6	-21.5	-21.8	-18.0
4	-18.6	-21.5	-20.3	-21.5	-21.0	-21.1	-18.6
5	-27.9	-33.4	-32.9	-33.2	-32.2	-33.4	-28.7
6	-25.2	-22.9	-22.8	-25.6	-25.2	-25.5	-22.2
7	-31.0	-33.2	-33.4	-33.3	-33.2	-35.2	-29.9
8	-35.6	-38.2	-38.7	-38.1	-38.0	-40.5	-34.5
9	-33.7	-35.2	-32.7	-34.1	-29.4	-37.3	-27.0
10	-35.0	-34.6	-32.0	-35.3	-30.2	-38.6	-27.8
11	-35.8	-38.7	-36.7	-40.9	-34.2	-46.0	-32.5
12	-36.9	-39.4	-37.5	-40.9	-34.1	-45.9	-32.4
13	-27.3	-26.4	-25.7	-27.0	-25.5	-25.3	-22.9
14	-28.6	-26.8	-26.7	-28.2	-26.6	-27.0	-23.9
15	-17.5	-17.9	-18.1	-21.9	-21.9	-21.6	-21.1
16	-21.6	-22.4	-23.9	-24.3	-24.2	-25.9	-24.7
17	-34.3	-33.3	-31.7	-36.0	-35.9	-33.9	-32.3
18	-22.8	-21.6	-20.4	-24.4	-24.0	-23.1	-21.3
19	-15.3	-15.6	-14.7	-17.1	-16.1	-16.3	-15.3
20	-18.5	-19.0	-17.9	-20.2	-19.1	-19.3	-18.2
21	-28.0	-25.9	-24.9	-27.3	-25.1	-25.9	-23.5
22	-35.3	-35.5	-33.9	-38.7	-38.8	-39.8	-38.7
23	-62.1	-63.0	-61.8	-66.6	-66.9	-68.8	-68.1
24	-136.3	-135.9	-133.1	-138.5	-134.7	-130.8	-126.5
25	-28.7	-30.4	-31.2	-30.2	-28.9	-31.0	-27.1
26	-28.6	-29.5	-30.3	-27.8	-26.5	-31.0	-27.1
27	-83.4	-82.8	-82.0	-84.3	-83.5	-81.9	-80.7
28	-80.0	-79.1	-78.7	-80.6	-80.1	-78.2	-77.4
29	-52.8	-55.9	-54.2	-58.1	-58.2	-55.8	-54.2
30	-49.6	-51.3	-49.9	-53.6	-53.4	-51.6	-49.7
	MD	-0.5	0.3	-1.8	-0.4	-1.9	1.8
	MAD	1.5	1.8	2.1	2.3	3.1	3.1
	RMSD	1.9	2.2	2.7	2.7	3.9	3.8
	SD	10.2	11.7	10.8	14.8	18.8	18.4
	Var	3.6	4.7	4.0	7.6	12.2	11.7
	Max	2.5	4.1	1.0	4.8	5.5	9.8
	Min	-5.5	-5.0	-5.3	-5.4	-10.2	-6.0
	AMax	5.5	5.0	5.3	5.4	10.2	9.8

Table A2.10.: Extended statistical evaluations of different DFAs with respect to DLPNO-CCSD(T)/CBS* data. For each functional we directly compare DFT–D3 (BJ)-ATM (abbreviated as D3) corrected values with DFT–D4-ATM (abbreviated as D4) corrected values given in kcal mol⁻¹. We follow the numeration of the systems regarding Ref. 258.

#	DLPNO-	PW6B95		PBE0		TPSS	
	CCSD(T)/CBS*	D4	D3	D4	D3	D4	D3
CBH	-11.6	-8.2	-9.0	-10.8	-11.7	-10.8	-11.6
C2C2PD	-21.3	-18.8	-20.4	-20.1	-18.3	-23.9	-20.1
C3A	-17.0	-14.7	-14.9	-16.0	-14.4	-18.4	-15.3
C3GC	-29.1	-26.2	-26.6	-27.0	-24.2	-31.1	-25.9
GCGC	-12.8	-13.5	-12.4	-14.1	-12.1	-15.8	-12.5
GGG	-1.9	-1.8	-1.4	-2.1	-1.3	-3.0	-1.6
PHE	-23.0	-23.7	-23.7	-25.4	-25.3	-24.2	-23.9
	MD	1.4	1.2	0.2	1.3	-1.5	0.8
	MAD	1.8	1.4	1.3	2.0	1.7	1.1
	RMSD	2.2	1.7	1.5	2.6	1.9	1.5
	SD	4.3	3.1	3.9	5.8	3.1	3.3
	Var	3.1	1.6	2.5	5.7	1.6	1.8
	Max	3.4	2.6	2.1	4.9	0.8	3.2

A2. Supporting Information to Chapter 2

Table A2.11.: Extended statistical evaluations of different DFAs with respect to DLPNO-CCSD(T)/CBS* data. For each functional we directly compare DFT-D3(BJ)-ATM (abbreviated as D3) corrected values with DFT-D4-MBD (abbreviated as D4) corrected values given in kcal mol⁻¹. We follow the numeration of the systems regarding Ref. 258.

#	DLPNO- CCSD(T)/CBS*	PW6B95		PBE0		TPSS	
		D4	D3	D4	D3	D4	D3
CBH	-11.6	-8.6	-9.0	-11.0	-11.7	-10.8	-11.6
C2C2PD	-21.3	-20.5	-20.4	-20.3	-18.3	-23.6	-20.1
C3A	-17.0	-15.6	-14.9	-16.1	-14.4	-18.1	-15.3
C3GC	-29.1	-27.8	-26.6	-27.2	-24.2	-30.7	-25.9
GCGC	-12.8	-13.9	-12.4	-14.1	-12.1	-15.6	-12.5
GGG	-1.9	-2.0	-1.4	-2.1	-1.3	-2.8	-1.6
PHE	-23.0	-24.0	-23.7	-25.6	-25.3	-24.3	-23.9
MD		0.6	1.2	0.1	1.3	-1.3	0.8
MAD		1.2	1.4	1.2	2.0	1.5	1.1
RMSD		1.5	1.7	1.4	2.6	1.7	1.5
SD		3.6	3.1	3.7	5.8	2.8	3.3
Var		2.1	1.6	2.3	5.7	1.3	1.8
Max		3.0	2.6	1.9	4.9	0.8	3.2
Min		-1.1	-0.7	-2.6	-2.3	-2.8	-0.9
AMax		3.0	2.6	2.6	4.9	2.8	3.2

Table A2.12.: Extended statistical evaluations of different DFAs with respect to DLPNO-CCSD(T)/CBS* data. For each functional we directly compare DFT-D3(BJ)-ATM (abbreviated as D3) corrected values with DFT-D4(TB)-ATM (abbreviated as D4) corrected values given in kcal mol⁻¹. We follow the numeration of the systems regarding Ref. 258.

#	DLPNO- CCSD(T)/CBS*	PW6B95		PBE0		TPSS	
		D4	D3	D4	D3	D4	D3
CBH	-11.6	-9.4	-9.0	-12.0	-11.7	-12.0	-11.6
C2C2PD	-21.3	-20.3	-20.4	-20.0	-18.3	-22.9	-20.1
C3A	-17.0	-15.4	-14.9	-15.9	-14.4	-17.7	-15.3
C3GC	-29.1	-27.6	-26.6	-26.9	-24.2	-30.2	-25.9
GCGC	-12.8	-13.7	-12.4	-13.9	-12.1	-15.3	-12.5
GGG	-1.9	-1.9	-1.4	-2.1	-1.3	-2.8	-1.6
PHE	-23.0	-24.2	-23.7	-25.8	-25.3	-24.6	-23.9
	MD	0.6	1.2	0.0	1.3	-1.3	0.8
	MAD	1.2	1.4	1.3	2.0	1.3	1.1
	RMSD	1.4	1.7	1.6	2.6	1.4	1.5
	SD	3.2	3.1	4.1	5.8	1.8	3.3
	Var	1.8	1.6	2.9	5.7	0.5	1.8
	Max	2.2	2.6	2.2	4.9	-0.4	3.2
	Min	-1.2	-0.7	-2.8	-2.3	-2.5	-0.9
	AMax	2.2	2.6	2.8	4.9	2.5	3.2

Statistical evaluation: MOR41 We follow the numberation of the systems regarding Ref. [268](#).

A2. Supporting Information to Chapter 2

Table A2.13.: Extended statistical evaluations of : DOD-PBE and DSD-PBE in kcal mol⁻¹. We abbreviate D3(BJ)-ATM by D3.

#	Ref.	DOD-PBE			DSD-PBE		
		D4-ATM	D4-MBD	D3	D4-ATM	D4-MBD	D3
1	-43.1	-46.2	-46.3	-47.4	-48.4	-48.4	-49.7
2	-46.6	-51.6	-51.8	-52.7	-54.2	-54.2	-55.4
3	-27.6	-35.8	-36.0	-36.6	-39.4	-39.4	-40.3
4	-62.5	-60.3	-60.5	-61.0	-58.5	-58.5	-59.4
5	3.7	2.9	2.7	2.3	3.7	3.7	3.0
6	-23.1	-21.7	-21.7	-20.4	-22.9	-22.9	-21.9
7	-16.2	-14.3	-14.2	-12.5	-14.8	-14.8	-13.3
8	-17.2	-13.5	-13.7	-13.4	-13.2	-13.2	-13.3
9	-18.8	-14.5	-14.6	-12.4	-14.2	-14.2	-13.2
10	-22.6	-21.9	-22.1	-23.2	-23.3	-23.3	-24.6
11	27.0	24.7	24.7	22.6	23.0	23.0	21.4
12	-29.8	-33.4	-33.5	-32.8	-35.5	-35.5	-35.2
13	-43.2	-45.8	-46.0	-47.1	-47.7	-47.7	-49.2
14	-52.0	-53.7	-54.0	-55.6	-55.1	-55.1	-56.7
15	-4.1	7.5	7.3	8.1	11.8	11.8	12.1
16	-39.8	-40.3	-40.8	-42.7	-40.3	-40.3	-41.7
17	-16.1	-13.9	-14.0	-11.2	-14.0	-14.0	-11.8
18	-34.2	-34.0	-34.4	-37.0	-33.7	-33.7	-36.2
19	-40.1	-39.9	-40.3	-43.0	-39.4	-39.4	-41.9
20	-30.2	-29.5	-29.8	-31.8	-28.8	-28.8	-30.9
21	-15.1	-17.2	-17.7	-18.6	-15.8	-15.8	-17.3
22	-35.9	-39.0	-39.4	-41.6	-40.3	-40.3	-42.6
23	-55.0	-55.1	-55.6	-58.9	-54.8	-54.8	-57.9
24	-41.6	-40.2	-41.1	-45.2	-39.9	-39.9	-42.7
25	-45.9	-45.2	-46.3	-50.5	-45.4	-45.4	-48.1
26	-36.4	-34.9	-35.2	-37.1	-33.3	-33.3	-34.7
27	-21.8	-21.1	-21.2	-22.7	-19.8	-19.8	-21.0
28	-36.3	-35.9	-36.1	-37.9	-34.6	-34.6	-36.0
29	-28.3	-28.7	-28.9	-30.3	-27.9	-27.9	-29.2
30	-14.9	-16.0	-16.2	-17.2	-14.9	-14.9	-15.8
31	-29.9	-29.4	-29.8	-31.2	-28.6	-28.6	-30.1
32	-1.9	-2.0	-2.0	-2.0	-2.3	-2.3	-2.1
33	-10.7	-6.7	-6.7	-5.8	-4.2	-4.2	-2.8
34	-25.6	-22.9	-23.0	-23.8	-21.0	-21.0	-21.3
35	-30.9	-28.3	-28.4	-29.9	-26.6	-26.6	-27.4
36	-39.8	-40.2	-40.4	-42.2	-40.0	-40.0	-41.1
37	-14.0	-16.9	-17.4	-17.4	-16.0	-16.0	-16.6
38	-64.4	-68.1	-68.6	-76.3	-67.4	-67.4	-74.0
39	-63.9	-63.3	-63.9	-65.8	-63.7	-63.7	-66.3
40	-65.8	-65.2	-65.4	-68.2	-64.9	-64.9	-67.7
41	-3.2	-2.4	-2.3	-1.4	-2.1	-2.1	-0.7
MD		0.1	-0.2	-1.3	0.2	0.2	-40.9
MAD		2.1	2.1	3.5	2.9	2.9	3.7
RMSD		3.1	3.1	4.4	4.3	4.3	5.0
SD		19.7	19.9	26.7	27.5	27.5	31.8
Var		9.7	9.9	17.8	18.9	18.9	25.3
Max		11.5	11.4	12.1	15.8	15.8	16.2
Min		-8.2	-8.4	-12.0	-11.8	-11.8	-12.7
AMax		11.5	11.4	12.1	15.8	15.8	16.2

Table A2.14.: Extended statistical evaluations of : B3LYP and PBE0 in kcal mol⁻¹. We abbreviate D3(BJ)-ATM by D3.

#	Ref.	B3LYP			PBE0		
		D4-ATM	D4-MBD	D3	D4-ATM	D4-MBD	D3
1	-43.1	-40.5	-40.6	-41.0	-44.6	-44.6	-44.7
2	-46.6	-41.9	-42.0	-42.3	-47.4	-47.4	-47.4
3	-27.6	-22.8	-22.9	-23.0	-26.4	-26.4	-26.4
4	-62.5	-66.2	-66.4	-66.5	-71.3	-71.3	-71.4
5	3.7	-0.1	-0.1	0.1	-2.6	-2.6	-2.4
6	-23.1	-17.4	-17.4	-15.9	-21.0	-21.0	-20.3
7	-16.2	-12.1	-12.0	-11.3	-15.7	-15.7	-15.3
8	-17.2	-12.8	-12.9	-11.8	-16.0	-16.0	-15.3
9	-18.8	-14.3	-14.3	-11.9	-16.1	-16.1	-15.0
10	-22.6	-16.4	-16.6	-16.4	-19.4	-19.4	-19.1
11	27.0	30.0	30.1	28.2	30.9	30.9	30.2
12	-29.8	-24.6	-24.6	-22.8	-29.9	-29.9	-28.9
13	-43.2	-38.0	-38.1	-37.9	-43.9	-43.9	-43.6
14	-52.0	-43.8	-44.0	-43.6	-50.9	-50.9	-50.5
15	-4.1	-5.0	-5.1	-4.2	-4.8	-4.8	-4.4
16	-39.8	-39.3	-39.8	-39.7	-40.4	-40.4	-40.0
17	-16.1	-14.5	-14.6	-9.9	-13.7	-13.7	-11.2
18	-34.2	-31.8	-32.0	-31.7	-33.3	-33.3	-32.8
19	-40.1	-37.2	-37.4	-37.1	-38.7	-38.7	-38.0
20	-30.2	-29.2	-29.4	-28.6	-28.6	-28.6	-27.8
21	-15.1	-18.5	-18.8	-16.5	-18.7	-18.7	-17.1
22	-35.9	-32.3	-32.6	-30.6	-33.5	-33.5	-32.1
23	-55.0	-51.2	-51.4	-51.8	-52.6	-52.6	-52.3
24	-41.6	-40.8	-41.7	-42.9	-41.3	-41.3	-41.7
25	-45.9	-45.4	-46.4	-47.0	-45.6	-45.6	-45.6
26	-36.4	-42.4	-42.6	-43.6	-38.5	-38.5	-39.0
27	-21.8	-26.8	-27.0	-27.5	-25.1	-25.1	-25.5
28	-36.3	-41.7	-41.9	-42.5	-39.2	-39.2	-39.5
29	-28.3	-32.8	-33.0	-33.0	-30.0	-30.0	-30.0
30	-14.9	-21.8	-22.1	-21.6	-16.3	-16.3	-16.1
31	-29.9	-32.8	-33.2	-33.4	-29.4	-29.4	-29.7
32	-1.9	0.1	0.1	0.9	0.2	0.2	0.7
33	-10.7	-18.9	-19.0	-17.9	-9.4	-9.4	-8.8
34	-25.6	-30.3	-30.5	-30.5	-25.1	-25.1	-25.0
35	-30.9	-34.6	-34.7	-35.1	-29.8	-29.8	-29.9
36	-39.8	-39.4	-39.5	-40.9	-34.9	-34.9	-35.3
37	-14.0	-33.0	-33.4	-33.7	-23.3	-23.3	-23.4
38	-64.4	-72.2	-72.6	-78.5	-69.1	-69.1	-71.8
39	-63.9	-58.2	-58.5	-56.7	-60.7	-60.7	-59.5
40	-65.8	-66.4	-66.5	-67.2	-69.0	-69.0	-69.2
41	-3.2	-6.3	-6.3	-6.7	-3.0	-3.0	-3.4
MD		-0.1	-0.3	-0.2	-0.3	-0.3	-0.0
MAD		4.2	4.2	4.8	2.3	2.3	2.6
RMSD		5.3	5.3	6.0	3.1	3.1	3.4
SD		33.7	33.9	38.3	19.7	19.7	21.8
Var		28.3	28.8	36.6	9.7	9.7	11.9
Max		8.2	7.9	8.4	5.0	5.0	4.9
Min		-19.0	-19.4	-19.6	-9.2	-9.2	-9.4
AMax		19.0	19.4	19.6	9.2	9.2	9.4

A2. Supporting Information to Chapter 2

Table A2.15.: Extended statistical evaluations of : PW6B95 and CAM-B3LYP in kcal mol⁻¹. We abbreviate D3(BJ)-ATM by D3.

#	Ref.	PW6B95			CAM-B3LYP		
		D4-ATM	D4-MBD	D3	D4-ATM	D4-MBD	D3
1	-43.1	-41.8	-41.8	-41.4	-40.1	-40.1	-40.1
2	-46.6	-42.9	-43.0	-42.5	-42.7	-42.7	-42.7
3	-27.6	-22.6	-22.6	-22.2	-23.2	-23.2	-23.1
4	-62.5	-63.0	-63.0	-62.4	-64.4	-64.4	-64.2
5	3.7	1.0	1.1	1.6	2.7	2.7	3.0
6	-23.1	-19.8	-19.7	-18.8	-19.5	-19.5	-18.6
7	-16.2	-16.5	-16.0	-15.0	-14.1	-14.1	-13.4
8	-17.2	-12.2	-12.4	-11.3	-15.8	-15.8	-14.8
9	-18.8	-12.5	-12.3	-10.0	-17.8	-17.8	-16.5
10	-22.6	-15.5	-15.6	-14.7	-15.8	-15.8	-15.3
11	27.0	32.8	33.0	32.3	33.6	33.6	33.1
12	-29.8	-28.4	-28.2	-26.7	-24.3	-24.3	-23.0
13	-43.2	-40.9	-40.7	-39.8	-38.4	-38.4	-37.9
14	-52.0	-47.9	-48.1	-47.4	-44.1	-44.1	-43.5
15	-4.1	-3.9	-4.0	-3.1	-9.6	-9.6	-9.1
16	-39.8	-40.0	-40.5	-39.7	-39.0	-39.0	-38.2
17	-16.1	-15.2	-15.2	-12.5	-16.2	-16.2	-13.1
18	-34.2	-29.4	-29.3	-30.9	-30.2	-30.2	-29.8
19	-40.1	-34.5	-34.5	-36.2	-36.4	-36.4	-35.9
20	-30.2	-27.1	-26.9	-26.7	-28.2	-28.2	-27.3
21	-15.1	-16.0	-16.1	-16.0	-14.4	-14.4	-12.8
22	-35.9	-26.1	-26.6	-29.3	-27.4	-27.4	-26.5
23	-55.0	-46.8	-46.7	-50.3	-49.0	-49.0	-49.2
24	-41.6	-39.7	-41.2	-42.0	-40.7	-40.7	-41.0
25	-45.9	-43.0	-44.7	-45.1	-45.0	-45.0	-44.7
26	-36.4	-33.5	-34.2	-35.6	-42.1	-42.1	-42.9
27	-21.8	-21.4	-22.1	-23.7	-27.4	-27.4	-28.2
28	-36.3	-34.3	-34.9	-36.6	-41.8	-41.8	-42.6
29	-28.3	-26.1	-26.7	-27.4	-32.1	-32.1	-32.4
30	-14.9	-9.9	-10.6	-11.6	-17.4	-17.4	-17.7
31	-29.9	-25.4	-26.4	-27.2	-33.3	-33.3	-34.1
32	-1.9	-1.2	-1.1	-1.5	0.5	0.5	0.8
33	-10.7	-10.5	-10.7	-10.7	-18.5	-18.5	-18.1
34	-25.6	-24.1	-24.4	-25.4	-28.6	-28.6	-28.8
35	-30.9	-28.7	-29.0	-31.0	-32.7	-32.7	-33.3
36	-39.8	-33.5	-33.5	-37.2	-36.5	-36.5	-37.7
37	-14.0	-19.6	-20.2	-19.3	-26.7	-26.7	-26.9
38	-64.4	-59.6	-60.5	-64.0	-67.0	-67.0	-70.0
39	-63.9	-61.0	-61.2	-60.5	-60.8	-60.8	-59.8
40	-65.8	-66.2	-66.2	-66.9	-65.9	-65.9	-66.2
41	-3.2	-1.0	-1.4	-2.2	-5.9	-5.9	-6.6
MD		2.7	2.4	2.1	0.5	0.5	0.7
MAD		3.2	3.0	2.7	3.7	3.7	4.3
RMSD		4.0	3.8	3.5	4.6	4.6	5.0
SD		18.9	19.1	18.0	28.9	28.9	31.4
Var		8.9	9.1	8.1	21.0	21.0	24.7
Max		9.8	9.2	8.7	8.5	8.5	9.3
Min		-5.6	-6.2	-5.3	-12.7	-12.7	-12.8
AMax		9.8	9.2	8.7	12.7	12.7	12.8

A2.8. Extended Statistical Measures

Table A2.16.: Extended statistical evaluations of : revPBE and M06L in kcal mol⁻¹. We abbreviate D3(BJ)-ATM by D3.

#	Ref.	revPBE			M06L		
		D4-ATM	D4-MBD	D3	D4-ATM	D4-MBD	D3
1	-43.1	-44.5	-44.6	-44.1	-41.0	-41.0	-40.7
2	-46.6	-47.6	-47.6	-47.0	-45.1	-45.1	-44.9
3	-27.6	-29.0	-29.1	-28.4	-27.1	-27.1	-26.9
4	-62.5	-73.6	-73.8	-72.4	-64.9	-64.9	-64.7
5	3.7	-6.8	-6.7	-5.4	-2.7	-2.7	-2.5
6	-23.1	-17.9	-17.9	-15.5	-18.1	-18.1	-18.1
7	-16.2	-12.9	-12.9	-11.3	-16.8	-16.8	-16.8
8	-17.2	-14.2	-14.3	-12.3	-7.7	-7.7	-7.5
9	-18.8	-14.0	-13.8	-9.7	-7.2	-7.2	-8.2
10	-22.6	-24.6	-24.7	-23.3	-13.2	-13.2	-12.7
11	27.0	24.2	24.5	22.7	30.7	30.7	31.3
12	-29.8	-30.6	-30.4	-26.8	-24.7	-24.7	-24.3
13	-43.2	-44.8	-44.7	-42.9	-39.8	-39.8	-39.4
14	-52.0	-51.2	-51.3	-49.5	-50.0	-50.0	-49.2
15	-4.1	1.9	1.7	4.0	5.4	5.4	5.5
16	-39.8	-41.7	-42.0	-40.4	-42.3	-42.3	-40.6
17	-16.1	-14.8	-14.9	-7.8	-18.2	-18.2	-17.7
18	-34.2	-34.8	-34.5	-32.9	-24.7	-24.7	-23.9
19	-40.1	-39.0	-38.5	-37.2	-28.8	-28.8	-27.7
20	-30.2	-31.2	-30.9	-28.7	-24.6	-24.6	-23.6
21	-15.1	-23.9	-23.7	-18.9	-13.7	-13.7	-12.7
22	-35.9	-37.5	-37.1	-35.2	-21.8	-21.8	-20.7
23	-55.0	-52.2	-51.6	-51.5	-40.8	-40.8	-39.8
24	-41.6	-39.1	-40.0	-41.1	-39.0	-39.0	-36.8
25	-45.9	-43.5	-44.7	-45.4	-44.0	-44.0	-41.1
26	-36.4	-35.5	-35.6	-37.6	-33.7	-33.7	-33.0
27	-21.8	-21.5	-21.7	-24.1	-22.2	-22.2	-22.1
28	-36.3	-36.0	-36.2	-38.1	-33.9	-33.9	-33.5
29	-28.3	-28.9	-29.1	-29.7	-25.7	-25.7	-25.4
30	-14.9	-23.2	-23.2	-23.6	-12.4	-12.4	-12.2
31	-29.9	-28.0	-28.4	-29.3	-23.8	-23.8	-23.9
32	-1.9	-0.5	-0.3	0.0	1.4	1.4	1.4
33	-10.7	-10.5	-10.6	-10.0	-12.1	-12.1	-11.8
34	-25.6	-25.1	-25.1	-25.9	-22.1	-22.1	-21.7
35	-30.9	-29.1	-29.0	-30.3	-23.6	-23.6	-23.2
36	-39.8	-33.6	-33.2	-36.0	-29.8	-29.8	-29.6
37	-14.0	-29.7	-30.4	-28.1	-26.4	-26.4	-26.1
38	-64.4	-73.0	-73.0	-78.5	-59.1	-59.1	-57.4
39	-63.9	-56.7	-56.8	-52.8	-56.1	-56.1	-55.6
40	-65.8	-66.7	-66.5	-66.4	-65.0	-65.0	-64.7
41	-3.2	-1.3	-1.4	-4.3	-4.7	-4.7	-4.9
MD		-0.6	-0.6	0.1	3.6	3.6	4.2
MAD		3.3	3.3	3.8	5.1	5.1	5.4
RMSD		4.8	4.9	5.4	6.4	6.4	6.8
SD		30.7	31.0	34.8	34.1	34.1	34.5
Var		23.6	24.1	30.3	29.1	29.1	29.7
Max		7.2	7.2	11.1	14.2	14.2	15.2
Min		-15.7	-16.3	-14.2	-12.4	-12.4	-12.1
AMax		15.7	16.3	14.2	14.2	14.2	15.2

A2. Supporting Information to Chapter 2

Table A2.17.: Extended statistical evaluations of : PBE and RPBE in kcal mol⁻¹. We abbreviate D3(BJ)-ATM by D3.

#	Ref.	PBE			RPBE		
		D4-ATM	D4-MBD	D3	D4-ATM	D4-MBD	D3
1	-43.1	-46.7	-46.8	-46.6	-44.4	-44.4	-49.0
2	-46.6	-50.0	-50.0	-49.9	-47.3	-47.3	-51.6
3	-27.6	-31.5	-31.5	-31.3	-28.8	-28.8	-31.8
4	-62.5	-75.1	-75.2	-75.0	-74.0	-74.0	-76.4
5	3.7	-7.4	-7.4	-7.0	-7.2	-7.2	-8.6
6	-23.1	-20.4	-20.4	-19.6	-17.7	-17.7	-11.6
7	-16.2	-14.9	-14.8	-14.7	-12.1	-12.1	-4.3
8	-17.2	-14.4	-14.5	-13.7	-14.1	-14.1	-13.6
9	-18.8	-16.0	-15.9	-15.0	-15.3	-15.3	-10.5
10	-22.6	-24.5	-24.6	-23.9	-24.6	-24.6	-28.1
11	27.0	25.0	25.0	24.6	24.4	24.4	18.2
12	-29.8	-30.8	-30.7	-29.4	-30.8	-30.8	-26.0
13	-43.2	-45.2	-45.2	-44.7	-44.9	-44.9	-48.9
14	-52.0	-52.3	-52.5	-51.4	-51.2	-51.2	-55.5
15	-4.1	1.2	1.1	1.7	1.2	1.2	3.8
16	-39.8	-39.5	-39.9	-38.5	-40.5	-40.5	-42.2
17	-16.1	-14.4	-14.5	-11.7	-14.6	-14.6	-2.1
18	-34.2	-32.5	-32.6	-31.0	-36.0	-36.0	-44.7
19	-40.1	-36.3	-36.4	-34.6	-39.9	-39.9	-48.6
20	-30.2	-28.1	-28.1	-26.5	-32.2	-32.2	-38.0
21	-15.1	-20.4	-20.6	-18.0	-25.2	-25.2	-28.0
22	-35.9	-35.2	-35.4	-32.5	-38.5	-38.5	-48.8
23	-55.0	-50.2	-50.3	-48.5	-53.8	-53.8	-65.6
24	-41.6	-36.8	-37.6	-36.3	-38.1	-38.1	-47.5
25	-45.9	-41.4	-42.3	-40.4	-41.6	-41.6	-50.6
26	-36.4	-34.9	-35.1	-34.9	-35.6	-35.6	-41.8
27	-21.8	-21.9	-22.1	-22.0	-21.8	-21.8	-30.1
28	-36.3	-35.5	-35.7	-35.4	-36.3	-36.3	-44.2
29	-28.3	-27.7	-27.8	-27.4	-29.0	-29.0	-35.5
30	-14.9	-19.9	-20.1	-19.2	-23.6	-23.6	-28.7
31	-29.9	-26.6	-26.9	-26.6	-28.9	-28.9	-36.5
32	-1.9	0.9	0.9	1.5	-0.5	-0.5	-0.4
33	-10.7	-9.5	-9.6	-8.8	-10.1	-10.1	-5.2
34	-25.6	-23.8	-23.9	-23.3	-25.0	-25.0	-27.0
35	-30.9	-28.1	-28.2	-27.6	-29.2	-29.2	-34.1
36	-39.8	-32.8	-32.9	-32.8	-34.3	-34.3	-41.5
37	-14.0	-29.8	-30.0	-29.8	-30.3	-30.3	-31.1
38	-64.4	-68.5	-68.8	-70.0	-73.9	-73.9	-99.4
39	-63.9	-57.0	-57.2	-55.1	-58.6	-58.6	-68.8
40	-65.8	-68.4	-68.5	-68.1	-67.4	-67.4	-79.4
41	-3.2	-2.8	-2.9	-3.6	-1.1	-1.1	2.6
MD		-0.1	-0.3	0.5	-0.9	-0.9	-4.7
MAD		3.5	3.4	3.9	3.4	3.4	8.3
RMSD		4.8	4.7	5.1	5.0	5.0	10.1
SD		30.5	30.4	32.4	31.4	31.4	57.5
Var		23.3	23.0	26.3	24.6	24.6	82.6
Max		7.0	6.9	8.8	5.5	5.5	14.0
Min		-15.7	-16.0	-15.8	-16.2	-16.2	-35.0
AMax		15.7	16.0	15.8	16.2	16.2	35.0

Statistical evaluation: SCONF

Table A2.18.: Reference values are calculated on a DLPNO-CCSD(T)/TightPNO/CBS(aug-cc-pVTZ/aug-cc-pVQZ) level of theory. We follow the nomenclature of the GMTKN55⁵⁷ database. We abbreviate D3(BJ)-ATM by D3 and D4-ATM by D4.

#	Ref.	DSDBLYP		B3LYP		PW6B95		PBE	
		D4	D3	D4	D3	D4	D3	D4	D3
ANGOL15									
C1-C2	0.9	0.9	0.9	0.8	0.8	0.9	0.9	0.8	0.8
C1-C3	2.3	2.2	2.2	2.5	2.6	2.5	2.5	3.2	3.2
C1-C4	3.1	3.1	3.1	3.2	3.3	3.3	3.3	3.9	3.9
C1-C5	4.6	4.5	4.5	4.5	4.4	4.7	4.7	5.1	5.1
C1-C6	4.9	4.8	4.8	4.7	4.7	5.1	5.1	5.4	5.4
C1-C7	4.2	4.2	4.2	4.6	4.5	4.3	4.2	5.3	5.3
C1-C8	4.4	4.3	4.3	4.7	4.5	4.4	4.3	5.3	5.2
C1-C9	6.2	6.2	6.1	6.2	6.0	6.4	6.3	6.8	6.6
C1-C10	6.2	6.1	6.1	6.3	6.1	6.5	6.4	7.1	6.9
C1-C11	5.7	5.6	5.6	5.9	5.7	5.8	5.7	6.5	6.4
C1-C12	5.6	5.6	5.6	6.0	5.8	5.8	5.7	6.7	6.6
C1-C13	5.9	5.8	5.8	6.0	5.7	6.7	6.5	6.8	6.7
C1-C14	6.3	6.3	6.3	6.4	6.2	6.5	6.4	6.8	6.7
C1-C15	6.2	6.3	6.2	6.5	6.0	6.2	6.0	6.8	6.5
GLC4									
G1-G2	0.2	0.2	0.2	0.1	0.1	0.2	0.2	0.2	0.2
G1-G3	6.2	6.2	6.3	5.3	5.6	4.8	5.0	4.6	4.8
G1-G4	5.5	5.1	5.2	3.5	3.8	4.8	5.0	2.6	2.8
MD	>0.1	>0.1	-0.1	-0.1	0.0	-0.0	0.3	0.3	
MAD	0.1	0.1	0.3	0.3	0.3	0.2	0.9	0.8	
RMSD	0.1	0.1	0.6	0.5	0.4	0.4	1.1	1.0	
SD	0.5	0.4	2.4	1.9	1.8	1.6	4.3	3.9	
Var	0.0	0.0	0.3	0.2	0.2	0.2	1.1	0.9	
Max	0.1	0.1	0.4	0.3	0.7	0.6	1.2	1.1	
Min	-0.4	-0.4	-2.1	-1.7	-1.3	-1.2	-3.0	-2.7	
AMax	0.4	0.4	2.1	1.7	1.3	1.2	3.0	2.7	

Statistical evaluation: PCONF21

A2. Supporting Information to Chapter 2

Table A2.19.: The reference energies were generated on the DLPNO-CCSD(T)/TightPNO/CBS(aug-cc-pVTZ/aug-cc-pVQZ) level of theory while the original geometries were kept. We follow the nomenclature of the GMTKN55⁵⁷ database. We abbreviate D3(BJ)-ATM by D3 and D4-ATM by D4.

#	Ref.	DSDBLYP		B3LYP		PW6B95		PBE		
		D4	D3	D4	D3	D4	D3	D4	D3	
Tripeptides										
99-444	0.0	0.2	0.1	-0.3	-0.7	0.9	0.7	-2.2	-2.5	
99-357	1.0	1.0	0.8	0.9	0.1	0.9	0.6	-1.0	-1.5	
99-366	0.7	1.1	1.0	1.2	1.1	1.7	1.7	0.6	0.5	
99-215	0.8	1.1	0.9	0.6	0.2	1.6	1.4	-1.2	-1.4	
99-300	0.8	1.3	1.2	1.5	1.2	1.6	1.5	0.8	0.6	
99-114	1.9	1.8	1.6	1.7	1.1	1.6	1.3	0.1	-0.3	
99-412	2.2	2.2	2.1	2.0	1.9	2.1	2.1	1.4	1.4	
99-691	1.6	1.9	1.8	1.9	1.8	2.3	2.3	1.1	1.1	
99-470	1.9	2.0	1.9	2.3	1.7	2.6	2.3	1.4	1.0	
99-224	2.1	1.8	1.7	1.2	1.0	2.9	2.8	-0.2	-0.4	
GLY										
GLY_ab-GLY_aR	1.1	1.1	1.2	0.9	1.3	1.2	1.4	1.3	1.6	
GLY_ab-GLY_pII	1.2	1.5	1.5	1.8	1.9	2.2	2.3	2.3	2.4	
GLY_ab-GLY_aL	2.4	2.5	2.7	2.4	3.0	2.2	2.5	2.8	3.2	
GLY_ab-GLY_b	2.1	1.8	1.9	1.8	1.8	2.1	2.1	1.3	1.3	
SER										
SER_ab-SER_aR	1.5	1.6	1.6	1.6	1.9	1.6	1.7	2.0	2.2	
SER_ab-SER_pII	2.8	3.1	3.2	3.2	3.5	3.6	3.7	3.9	4.0	
SER_ab-SER_aL	2.3	2.7	2.8	2.6	3.2	1.8	2.1	3.4	3.7	
SER_ab-SER_b	2.7	2.5	2.6	2.5	2.5	2.9	2.9	2.3	2.3	
MD	0.1	0.1	0.0	0.0	0.0	0.4	0.3	-0.5	-0.5	
MAD	0.2	0.2	0.3	0.3	0.5	0.5	0.5	1.0	1.2	
RMSD	0.3	0.3	0.4	0.6	0.6	0.6	0.6	1.2	1.4	
SD	1.0	1.2	1.7	2.6	2.0	2.0	2.0	4.8	5.7	
Var	0.1	0.1	0.2	0.4	0.2	0.2	0.2	1.4	1.9	
Max	0.5	0.6	0.7	0.9	1.0	1.0	1.0	1.1	1.5	
Min	-0.3	-0.4	-0.9	-1.1	-0.5	-0.6	-0.6	-2.3	-2.5	
AMax	0.5	0.6	0.9	1.1	1.0	1.0	1.0	2.3	2.5	

Statistical evaluation: ICONF

Table A2.20.: Reference energies are obtained with the W1-F12 protocol on TPSS-D3(BJ)/def2-TZVP optimised geometries without spin-orbit and DBOC. We follow the nomenclature of the GMTKN55⁵⁷ database. We abbreviate D3(BJ)-ATM by D3 and D4-ATM by D4.

#	Ref.	DSDBLYP		B3LYP		PW6B95		PBE	
		D4	D3	D4	D3	D4	D3	D4	D3
N ₃ H ₅ _1-N ₃ H ₅ _2	0.9	1.0	1.0	1.0	1.0	1.0	1.0	1.2	1.2
N ₃ H ₅ _1-N ₃ H ₅ _3	5.3	5.3	5.4	5.2	5.3	5.2	5.2	5.6	5.6
N ₄ H ₆ _1-N ₄ H ₆ _2	0.1	0.5	0.5	0.6	0.6	0.8	0.9	0.4	0.4
N ₄ H ₆ _1-N ₄ H ₆ _3	2.3	2.7	2.7	3.0	3.1	3.2	3.2	3.0	3.0
N ₃ P ₃ H ₁₂ _1-N ₃ P ₃ H ₁₂ _2	12.2	12.5	12.5	12.2	12.3	12.2	12.2	11.9	11.9
Si ₅ H ₁₂ _1-Si ₅ H ₁₂ _2	0.1	-0.1	-0.0	0.1	0.2	-0.1	0.0	0.1	0.2
Si ₅ H ₁₂ _1-Si ₅ H ₁₂ _3	1.0	1.0	1.0	1.0	0.9	0.9	0.9	0.9	0.9
Si ₅ H ₁₂ _1-Si ₅ H ₁₂ _4	3.5	3.7	3.7	3.3	3.3	3.5	3.4	3.1	3.1
Si ₆ H ₁₂ _1-Si ₆ H ₁₂ _2	1.7	1.8	1.8	1.7	1.5	1.4	1.4	1.6	1.4
P ₇ H ₇ _1-P ₇ H ₇ _2	1.4	1.6	1.6	1.6	1.6	1.5	1.6	1.2	1.2
S ₄ O ₄ _1-S ₄ O ₄ _2	4.4	4.5	4.5	4.2	4.3	3.8	3.9	5.0	5.0
S ₈ _1-S ₈ _2	9.2	9.1	9.1	9.4	9.1	9.1	9.2	10.3	10.0
H ₂ S ₂ O ₇ _1-H ₂ S ₂ O ₇ _2	0.6	0.5	0.5	0.6	0.6	0.6	0.6	0.5	0.4
H ₂ S ₂ O ₇ _1-H ₂ S ₂ O ₇ _3	3.5	3.2	3.2	3.1	3.2	3.6	3.6	3.1	3.2
H ₄ P ₂ O ₇ _1-H ₄ P ₂ O ₇ _2	1.3	1.4	1.4	1.2	1.2	1.2	1.2	1.2	1.2
H ₄ P ₂ O ₇ _1-H ₄ P ₂ O ₇ _3	3.7	3.4	3.4	3.0	3.0	3.6	3.6	3.8	3.8
H ₄ P ₂ O ₇ _1-H ₄ P ₂ O ₇ _4	4.3	3.7	3.7	3.2	3.4	4.5	4.4	4.2	4.3
MD	0.0	0.0	-0.1	-0.1	0.0	0.0	0.1	0.1	0.1
MAD	0.2	0.2	0.3	0.3	0.2	0.2	0.3	0.3	0.3
RMSD	0.3	0.3	0.4	0.4	0.3	0.3	0.4	0.4	0.4
SD	1.1	1.1	1.7	1.6	1.4	1.4	1.6	1.5	1.5
Var	0.1	0.1	0.2	0.2	0.1	0.1	0.2	0.1	0.1
Max	0.4	0.4	0.7	0.8	0.8	0.9	1.1	0.8	0.8
Min	-0.7	-0.6	-1.1	-1.0	-0.6	-0.5	-0.4	-0.4	-0.4
AMax	0.7	0.6	1.1	1.0	0.8	0.9	1.1	0.8	0.8

Statistical evaluation: UPU23

A2. Supporting Information to Chapter 2

Table A2.21.: Reference values are obtained at the DLPNO-CCSD(T)/CBS*//TPSS-D3(BJ)/def2-TZVP(COSMO) level of theory. We follow the nomenclature of the GMTKN55⁵⁷ database. We abbreviate D3(BJ)-ATM by D3 and D4-ATM by D4.

#	Ref.	DSDBLYP		B3LYP		PW6B95		PBE	
		D4	D3	D4	D3	D4	D3	D4	D3
2p-1a	4.9	5.4	5.5	5.6	6.0	6.0	6.1	5.5	5.7
2p-1b	3.0	3.7	3.8	3.6	4.1	4.2	4.3	4.0	4.2
2p-1c	8.9	9.4	9.6	9.7	10.1	10.4	10.6	9.6	9.8
2p-1g	2.2	2.6	2.6	2.7	2.7	3.2	3.2	2.9	2.9
2p-1p	2.0	2.7	2.8	2.4	2.7	3.0	3.0	2.5	2.6
2p-2a	3.1	3.0	3.0	3.5	3.5	2.9	2.9	3.1	3.1
2p-5z	0.6	0.2	0.4	-0.3	0.1	0.9	0.9	0.8	1.0
2p-6p	3.3	3.2	3.2	3.1	3.2	3.0	3.1	2.9	2.9
2p-7a	7.3	8.4	8.4	8.8	8.8	8.4	8.4	8.9	8.9
2p-aa	4.0	4.4	4.4	4.8	4.9	4.2	4.2	5.0	5.2
2p-1e	11.1	11.8	11.8	11.8	12.0	12.2	12.3	11.7	11.9
2p-0a	4.8	5.9	6.0	6.0	6.2	5.7	5.8	5.6	5.7
2p-1f	14.4	14.1	14.1	14.3	14.4	14.1	14.2	13.8	13.9
2p-9a	5.2	5.5	5.5	5.8	5.7	5.5	5.4	5.7	5.7
2p-4b	5.5	5.6	5.6	5.5	5.6	5.7	5.7	5.3	5.4
2p-3a	6.8	7.2	7.2	7.3	7.3	7.6	7.6	6.7	6.7
2p-7p	3.9	3.7	3.7	3.6	3.6	3.5	3.5	3.5	3.5
2p-8d	6.4	6.4	6.5	6.7	6.8	6.4	6.5	6.5	6.6
2p-3d	5.4	5.5	5.5	5.7	5.8	5.7	5.8	5.6	5.7
2p-0b	6.7	6.5	6.5	6.1	6.2	6.3	6.3	5.9	6.0
2p-1m	5.6	6.8	6.8	6.7	6.7	6.7	6.7	5.9	5.9
2p-2h	10.4	10.9	10.9	11.5	11.4	10.7	10.8	10.4	10.4
2p-3b	6.1	6.5	6.5	6.4	6.4	6.6	6.6	6.2	6.2
MD	0.3	0.4	0.4	0.6	0.6	0.5	0.5	0.3	0.4
MAD	0.4	0.5	0.6	0.7	0.7	0.6	0.7	0.5	0.6
RMSD	0.6	0.6	0.7	0.8	0.8	0.8	0.8	0.6	0.7
SD	2.1	2.2	2.7	2.8	2.8	2.9	2.8	2.8	2.9
Var	0.2	0.2	0.3	0.3	0.4	0.4	0.3	0.4	0.4
Max	1.2	1.2	1.5	1.6	1.5	1.7	1.6	1.6	1.7
Min	-0.3	-0.3	-0.9	-0.5	-0.4	-0.4	-0.8	-0.8	-0.8
AMax	1.2	1.2	1.5	1.6	1.5	1.7	1.6	1.6	1.7

Statistical evaluation: ROT34

Table A2.22.: Statistical data for the results of the ROT34 test set for three DFAs using the def2-QZVP basis set. Anharmonic corrections have been performed at the HF/DZ level of theory as described in the literature²²⁰. All values are given in MHz. We abbreviate D3(BJ)-ATM by D3 and D4-ATM by D4.

#	rot. const	Ref.	PBE0		PBE		TPSS	
			D3	D4	D3	D4	D3	D4
1	A	4293.9	4299.8	4298.1	4240.8	4238.8	4235.9	4235.8
	B	1395.9	1400.7	1400.7	1383.9	1382.9	1384.5	1384.1
	C	1130.2	1133.1	1132.9	1119.3	1118.3	1119.5	1119.1
2	A	3322.5	3309.3	3307.7	3247.0	3247.8	3239.0	3240.4
	B	719.8	718.8	719.0	707.2	707.5	709.5	709.4
	C	698.0	697.0	697.2	686.0	686.0	687.7	687.6
3	A	3071.1	3071.9	3071.3	3023.0	3022.8	3021.0	3022.3
	B	1285.0	1289.9	1290.4	1271.9	1270.9	1271.1	1270.2
	C	1248.7	1249.0	1249.3	1232.4	1231.7	1231.0	1230.7
4	A	2755.9	2765.6	2765.8	2731.3	2731.7	2729.3	2730.3
	B	2675.6	2689.5	2689.3	2652.4	2652.1	2653.3	2653.1
	C	2653.3	2666.5	2666.8	2631.5	2631.8	2633.1	2634.1
5	A	2336.9	2339.1	2339.9	2307.0	2306.5	2306.0	2307.1
	A	1464.2	1471.0	1471.1	1440.0	1439.7	1439.1	1439.9
6	B	768.2	767.6	768.3	756.4	757.1	762.1	763.0
	C	580.6	580.9	581.4	572.3	572.7	576.1	576.8
	A	1165.7	1170.2	1170.4	1152.1	1153.5	1154.6	1155.9
7	B	661.2	660.6	661.3	653.3	653.8	654.0	654.6
	C	454.0	454.6	454.9	448.9	449.4	449.6	450.2
	A	1166.3	1167.7	1168.3	1147.9	1148.4	1153.1	1155.3
8	B	767.6	766.4	767.0	752.7	753.0	754.3	755.0
	C	513.0	512.5	512.9	504.3	504.5	505.6	506.4
	A	862.5	865.9	866.0	852.4	852.4	853.2	853.8
9	B	754.2	752.8	752.8	741.8	741.7	742.6	742.9
	C	513.7	513.6	513.7	505.7	505.6	506.5	506.8
	A	3086.2	3101.0	3100.5	3060.2	3059.9	3061.3	3061.6
10	B	723.7	725.3	725.2	716.2	715.9	715.8	716.0
	C	685.0	686.7	686.6	678.0	677.8	677.7	677.9
	A	1432.1	1436.0	1435.5	1416.5	1416.5	1418.6	1418.9
11	B	820.5	822.8	822.9	810.9	811.4	812.1	813.3
	C	679.4	683.0	682.9	674.1	675.0	675.4	676.1
	A	1523.2	1523.3	1521.2	1496.3	1495.8	1497.2	1497.4
12	B	1070.5	1075.0	1076.0	1059.8	1060.6	1060.9	1061.9
	C	719.9	721.1	721.5	709.3	709.7	711.0	711.9
	MD		2.6	2.7	-18.1	-18.1	-17.6	-17.0
MAD		3.8	3.9	18.1	18.1	17.6	17.0	
RMSD		5.7	5.8	23.3	23.4	24.1	23.7	
SD		29.4	30.0	85.5	86.5	96.5	95.9	
Var		26.1	27.3	221.8	226.5	282.2	278.9	
Max		14.8	14.3	-5.1	-4.4	-4.0	-3.3	
Min		-13.2	-14.8	-75.5	-74.7	-83.5	-82.1	
AMax		14.8	14.8	75.5	74.7	83.5	82.1	

A2. Supporting Information to Chapter 2

Table A2.23.: Statistical data for the results of the ROT34 test set for three DFAs using the def2-QZVP basis set. Anharmonic corrections have been performed at the HF/DZ level of theory as described in the literature²²⁰. All values are given in MHz. We abbreviate D3(BJ)-ATM by D3 and D4(TB)-ATM by D4.

#	rot. const	Ref.	PBE0		PBE		TPSS		
			D3	D4	D3	D4	D3	D4	
1	A	4293.9	4299.8	4300.5	4240.8	4239.3	4235.9	4239.0	
	B	1395.9	1400.7	1400.3	1383.9	1383.6	1384.5	1384.9	
	C	1130.2	1133.1	1132.8	1119.3	1118.8	1119.5	1119.9	
2	A	3322.5	3309.3	3308.4	3247.0	3247.9	3239.0	3243.4	
	B	719.8	718.8	718.9	707.2	708.0	709.5	710.5	
	C	698.0	697.0	697.1	686.0	686.3	687.7	688.3	
3	A	3071.1	3071.9	3072.6	3023.0	3023.1	3021.0	3024.1	
	B	1285.0	1289.9	1290.0	1271.9	1271.9	1271.1	1272.3	
	C	1248.7	1249.0	1248.8	1232.4	1232.0	1231.0	1231.8	
4	A	2755.9	2765.6	2766.1	2731.3	2732.3	2729.3	2732.0	
	B	2675.6	2689.5	2689.8	2652.4	2652.8	2653.3	2654.7	
	C	2653.3	2666.5	2667.2	2631.5	2632.2	2633.1	2635.1	
5	A	2336.9	2339.1	2339.1	2307.0	2307.1	2306.0	2308.6	
6	A	1464.2	1471.0	1471.4	1440.0	1440.2	1439.1	1440.7	
	B	768.2	767.6	768.5	756.4	757.3	762.1	764.5	
	C	580.6	580.9	581.5	572.3	572.8	576.1	577.9	
7	A	1165.7	1170.2	1170.1	1152.1	1153.4	1154.6	1156.2	
	B	661.2	660.6	661.0	653.3	653.8	654.0	654.7	
	C	454.0	454.6	454.8	448.9	449.4	449.6	450.2	
8	A	1166.3	1167.7	1168.3	1147.9	1149.6	1153.1	1158.8	
	B	767.6	766.4	766.9	752.7	753.3	754.3	755.8	
	C	513.0	512.5	512.8	504.3	504.8	505.6	507.2	
9	A	862.5	865.9	866.0	852.4	852.6	853.2	854.7	
	B	754.2	752.8	752.8	741.8	741.9	742.6	743.6	
	C	513.7	513.6	513.7	505.7	505.8	506.5	507.3	
10	A	3086.2	3101.0	3100.8	3060.2	3060.5	3061.3	3063.5	
	B	723.7	725.3	725.3	716.2	716.1	715.8	716.6	
	C	685.0	686.7	686.6	678.0	677.9	677.7	678.5	
11	A	1432.1	1436.0	1435.6	1416.5	1416.4	1418.6	1421.2	
	B	820.5	822.8	822.6	810.9	810.9	812.1	813.2	
	C	679.4	683.0	682.7	674.1	674.1	675.4	676.3	
12	A	1523.2	1523.3	1520.1	1496.3	1495.5	1497.2	1499.0	
	B	1070.5	1075.0	1076.4	1059.8	1060.6	1060.9	1062.5	
	C	719.9	721.1	721.5	709.3	710.1	711.0	712.7	
			MD	2.6	2.7	-18.1	-17.8	-17.6	-15.8
			MAD	3.8	4.0	18.1	17.8	17.6	15.8
			RMSD	5.7	5.9	23.3	23.1	24.1	22.4
			SD	29.4	30.6	85.5	86.0	96.5	92.7
			Var	26.1	28.3	221.8	224.3	282.2	260.3
			Max	14.8	14.6	-5.1	-4.6	-4.0	-2.7
			Min	-13.2	-14.1	-75.5	-74.6	-83.5	-79.1
			AMax	14.8	14.6	75.5	74.6	83.5	79.1

Statistical evaluation: LMGB35

Table A2.24.: The LMGB35 benchmark set contains of systems from the first and second row of the periodic system. All bond lengths are given in pm. Reference distances are taken from Ref. 460. We abbreviate D3(BJ)-ATM by D3 and D4-ATM by D4.

system(bond)	Ref.	PBE0		PBE		TPSS	
		D3	D4	D3	D4	D3	D4
H ₂ (H-H)	74.1	74.5	74.4	75.0	75.0	74.3	74.2
HF(H-F)	91.7	91.8	91.7	93.0	93.0	92.9	92.9
H ₂ O(H-O)	95.7	95.7	95.7	96.9	96.9	96.7	96.7
HOF(O-H)	96.6	96.6	96.6	97.9	97.9	97.7	97.7
OH(O-H)	97.0	97.0	97.0	98.3	98.3	98.2	98.1
NH ₃ (N-H)	101.2	101.1	101.1	102.1	102.1	101.9	101.8
OH ⁺ (O-H)	102.9	103.2	103.2	104.7	104.7	104.0	103.9
NH(N-H)	103.6	103.7	103.7	105.0	104.9	104.4	104.4
C ₂ H ₂ (C-H)	106.2	106.4	106.4	107.0	107.0	106.5	106.5
NO ⁺ (N-O)	106.3	105.3	105.3	106.9	106.9	106.6	106.6
HCN(H-C)	106.5	106.8	106.8	107.5	107.5	107.0	107.0
NH ⁺ (N-H)	107.0	107.6	107.6	109.1	109.1	108.3	108.3
C ₂ H ₄ (C-H)	108.1	108.3	108.3	109.1	109.1	108.6	108.6
CH ₄ (C-H)	108.6	108.8	108.8	109.5	109.5	109.1	109.1
N ₂ (N-N)	109.8	108.9	108.9	110.2	110.2	109.9	109.9
CH ₂ O(O-H)	109.9	110.7	110.7	111.7	111.7	111.0	111.0
N ₂ ⁺ (N-N)	111.6	110.1	110.1	111.4	111.4	111.2	111.2
O ₂ ⁺ (O-O)	111.6	109.8	109.8	112.1	112.1	112.0	112.0
CH(C-H)	112.0	112.4	112.4	113.6	113.6	112.9	112.9
CO(C-O)	112.8	112.2	112.2	113.5	113.5	113.3	113.3
HCN(C-N)	115.3	114.5	114.5	115.7	115.7	115.4	115.4
CO ₂ (C-O)	116.0	115.6	115.6	117.0	117.0	116.8	116.8
C ₂ H ₂ (C-C)	120.3	119.6	119.6	120.6	120.6	120.2	120.2
CH ₂ O(C-O)	120.3	119.5	119.5	120.8	120.8	120.7	120.7
BO(B-O)	120.5	119.9	119.9	121.3	121.3	121.2	121.2
O ₂ (O-O)	120.8	119.2	119.2	121.8	121.8	121.9	121.9
BH(B-H)	123.2	124.0	124.0	125.1	125.1	123.6	123.6
BF(B-F)	126.3	125.9	125.9	127.3	127.3	127.3	127.3
CF(C-F)	127.2	126.7	126.7	128.5	128.5	128.9	128.9
NF(N-F)	131.7	130.3	130.3	132.7	132.7	133.3	133.3
F ₂ ⁺ (F-F)	132.2	127.2	127.3	131.6	131.6	131.7	131.7
C ₂ H ₄ (C-C)	133.4	132.2	132.2	133.2	133.2	133.0	133.0
F ₂ (F-F)	141.2	137.5	137.6	141.4	141.4	141.6	141.6
HOF(O-F)	143.5	140.5	140.6	144.5	144.5	145.0	145.0
B ₂ (B-B)	159.0	161.3	161.3	161.8	161.8	161.9	161.9
MD		-0.5	-0.6	1.0	1.0	0.7	0.7
MAD		0.9	0.9	1.0	1.0	0.8	0.8
RMSD		1.4	1.4	1.2	1.2	1.0	1.0
SD		7.8	7.7	4.0	3.9	3.9	3.9
Var		1.8	1.7	0.5	0.5	0.5	0.5
Max		2.3	2.3	2.8	2.8	2.9	2.9
Min		-5.0	-4.9	-0.6	-0.6	-0.5	-0.5
AMax		5.0	4.9	2.8	2.8	2.9	2.9

A2. Supporting Information to Chapter 2

Table A2.25.: The LMGB35 benchmark set contains of systems from the first and second row of the periodic system. All bond lengths are given in pm. Reference distances are taken from Ref. ⁴⁶⁰. We abbreviate D3(BJ)-ATM by D3 and D4(TB)-ATM by D4.

system(bond)	Ref.	PBE0		PBE		TPSS	
		D3	D4	D3	D4	D3	D4
H ₂ (H-H)	74.1	74.5	74.4	75.0	74.2	74.3	74.2
HF(H-F)	91.7	91.8	91.7	93.0	92.9	92.9	92.9
H ₂ O(H-O)	95.7	95.7	95.7	96.9	96.7	96.7	96.7
HOF(O-H)	96.6	96.6	96.6	97.9	97.7	97.7	97.7
OH(O-H)	97.0	97.0	97.0	98.3	98.1	98.2	98.1
NH ₃ (N-H)	101.2	101.1	101.1	102.1	101.9	101.9	101.9
OH ⁺ (O-H)	102.9	103.2	103.2	104.7	103.9	104.0	103.9
NH(N-H)	103.6	103.7	103.7	105.0	104.4	104.4	104.4
C ₂ H ₂ (C-H)	106.2	106.4	106.4	107.0	106.5	106.5	106.5
NO ⁺ (N-O)	106.3	105.3	105.3	106.9	106.6	106.6	106.6
HCN(H-C)	106.5	106.8	106.8	107.5	107.0	107.0	107.0
NH ⁺ (N-H)	107.0	107.6	107.6	109.1	108.3	108.3	108.3
C ₂ H ₄ (C-H)	108.1	108.3	108.3	109.1	108.6	108.6	108.6
CH ₄ (C-H)	108.6	108.8	108.8	109.5	109.1	109.1	109.1
N ₂ (N-N)	109.8	108.9	108.9	110.2	109.9	109.9	109.9
CH ₂ O(O-H)	109.9	110.7	110.7	111.7	111.0	111.0	111.0
N ₂ ⁺ (N-N)	111.6	110.1	110.1	111.4	111.2	111.2	111.2
O ₂ ⁺ (O-O)	111.6	109.8	109.8	112.1	112.0	112.0	112.0
CH(C-H)	112.0	112.4	112.4	113.6	112.9	112.9	112.9
CO(C-O)	112.8	112.2	112.2	113.5	113.3	113.3	113.3
HCN(C-N)	115.3	114.5	114.5	115.7	115.4	115.4	115.4
CO ₂ (C-O)	116.0	115.6	115.6	117.0	116.8	116.8	116.8
C ₂ H ₂ (C-C)	120.3	119.6	119.6	120.6	120.2	120.2	120.2
CH ₂ O(C-O)	120.3	119.5	119.5	120.8	120.7	120.7	120.7
BO(B-O)	120.5	119.9	119.9	121.3	121.2	121.2	121.2
O ₂ (O-O)	120.8	119.2	119.2	121.8	121.9	121.9	121.9
BH(B-H)	123.2	124.0	124.0	125.1	123.6	123.6	123.6
BF(B-F)	126.3	125.9	125.9	127.3	127.3	127.3	127.3
CF(C-F)	127.2	126.7	126.7	128.5	128.9	128.9	128.9
NF(N-F)	131.7	130.3	130.3	132.7	133.3	133.3	133.3
F ₂ ⁺ (F-F)	132.2	127.2	127.3	131.6	131.7	131.7	131.7
C ₂ H ₄ (C-C)	133.4	132.2	132.2	133.2	133.0	133.0	133.0
F ₂ (F-F)	141.2	137.5	137.6	141.4	141.6	141.6	141.6
HOF(O-F)	143.5	140.5	140.6	144.5	145.0	145.0	145.0
B ₂ (B-B)	159.0	161.3	161.3	161.8	161.9	161.9	161.9
MD		-0.5	-0.6	1.0	0.7	0.7	0.7
MAD		0.9	0.9	1.0	0.8	0.8	0.8
RMSD		1.4	1.4	1.2	1.0	1.0	1.0
SD		7.8	7.7	4.0	3.9	3.9	3.9
Var		1.8	1.7	0.5	0.5	0.5	0.5
Max		2.3	2.3	2.8	2.9	2.9	2.9
Min		-5.0	-4.9	-0.6	-0.5	-0.5	-0.5
AMax		5.0	4.9	2.8	2.9	2.9	2.9

Statistical evaluation: HMGB11

Table A2.26.: Experimental reference bond distances for 11 molecules from Ref. 243 containing third-row or higher main group elements. All distances are given in pm. We abbreviate D3(BJ)-ATM by D3 and D4-ATM by D4.

system(bond)	Ref.	PBE0		PBE		TPSS	
		D3	D4	D3	D4	D3	D4
Cl ₂ (Cl-Cl)	198.8	197.9	197.9	200.4	200.5	200.8	200.8
S ₂ H ₂ (S-S)	205.5	204.4	204.4	206.3	206.3	206.4	206.4
P ₂ (CH ₃) ₄ (P-P)	221.2	219.2	219.2	221.3	221.4	220.9	221.0
Br ₂ (Br-Br)	228.1	227.8	227.8	230.8	230.8	230.5	230.5
Se ₂ H ₂ (Se-Se)	234.6	232.4	232.4	235.0	235.0	234.4	234.4
Ge ₂ H ₆ (Ge-Ge)	241.0	242.1	242.1	243.3	243.3	242.5	242.5
As ₂ (CH ₃) ₄ (As-As)	242.9	243.8	243.8	247.3	247.2	246.1	246.1
Te ₂ (CH ₃) ₂ (Te-Te)	268.6	267.3	267.3	269.7	269.6	268.5	269.1
Sn ₂ (CH ₃) ₆ (Sn-Sn)	277.6	277.7	278.0	279.6	280.1	278.4	278.9
Sb ₂ (CH ₃) ₄ (Sb-Sb)	281.8	282.5	282.6	286.2	286.1	284.9	285.0
Pb ₂ (CH ₃) ₆ (Pb-Pb)	288.0	287.1	287.2	292.0	291.9	289.8	290.3
MD	-0.5	-0.5	2.2	2.2	1.4	1.5	
MAD	1.0	1.1	2.2	2.2	1.5	1.6	
RMSD	1.2	1.2	2.6	2.6	1.8	1.9	
SD	3.6	3.6	4.9	4.8	4.0	3.8	
Var	1.3	1.3	2.4	2.3	1.6	1.5	
Max	1.1	1.1	4.4	4.3	3.2	3.2	
Min	-2.2	-2.2	0.1	0.2	-0.3	-0.2	
AMax	2.2	2.2	4.4	4.3	3.2	3.2	

Table A2.27.: Experimental reference bond distances for 11 molecules from Ref. 243 containing third-row or higher main group elements. All distances are given in pm. We abbreviate D3(BJ)-ATM by D3 and D4(TB)-ATM by D4.

system(bond)	Ref.	PBE0		PBE		TPSS	
		D3	D4	D3	D4	D3	D4
Cl ₂ (Cl-Cl)	198.8	197.9	197.9	200.4	200.5	200.8	200.8
S ₂ H ₂ (S-S)	205.5	204.4	204.4	206.3	206.4	206.4	206.4
P ₂ (CH ₃) ₄ (P-P)	221.2	219.2	219.2	221.3	221.7	220.9	221.3
Br ₂ (Br-Br)	228.1	227.8	227.8	230.8	230.8	230.5	230.6
Se ₂ H ₂ (Se-Se)	234.6	232.4	232.4	235.0	235.0	234.4	234.5
Ge ₂ H ₆ (Ge-Ge)	241.0	242.1	242.1	243.3	243.3	242.5	242.6
As ₂ (CH ₃) ₄ (As-As)	242.9	243.8	243.8	247.3	247.4	246.1	246.3
Te ₂ (CH ₃) ₂ (Te-Te)	268.6	267.3	267.3	269.7	269.8	268.5	269.2
Sn ₂ (CH ₃) ₆ (Sn-Sn)	277.6	277.7	278.0	279.6	280.7	278.4	279.3
Sb ₂ (CH ₃) ₄ (Sb-Sb)	281.8	282.5	282.6	286.2	286.8	284.9	285.5
Pb ₂ (CH ₃) ₆ (Pb-Pb)	288.0	287.1	287.2	292.0	292.7	289.8	291.0
MD	-0.5	-0.5	2.2	2.4	1.4	1.8	
MAD	1.0	1.1	2.2	2.4	1.5	1.8	
RMSD	1.2	1.2	2.6	2.9	1.8	2.1	
SD	3.6	3.6	4.9	5.3	4.0	4.1	
Var	1.3	1.3	2.4	2.9	1.6	1.7	
Max	1.1	1.1	4.4	5.0	3.2	3.7	
Min	-2.2	-2.2	0.1	0.4	-0.3	-0.1	
AMax	2.2	2.2	4.4	5.0	3.2	3.7	

Statistical evaluation: TMC32

A2. Supporting Information to Chapter 2

Table A2.28.: Diverse set of 32 metal complexes from the first transition row, for which precise gas- phase geometries are known from electron diffraction or microwave spectroscopy. Compilation by Bühl *et al.*²⁹⁴. We abbreviate D3(BJ)-ATM by D3 and D4-ATM by D4.

system(bond)	Ref.	PBE0		PBE		TPSS	
		D3	D4	D3	D4	D3	D4
Sc(acac) ₃ (Sc-O)	207.6	209.0	208.8	210.4	210.3	210.0	209.8
TiCl ₄ (Ti-Cl)	216.9	216.4	216.4	218.3	218.2	218.3	218.3
Ti(CH ₃)Cl ₃ (Ti-C)	204.7	202.3	202.3	204.5	204.7	205.3	205.3
Ti(CH ₃)Cl ₃ (Ti-Cl)	218.5	218.0	217.9	219.3	219.2	219.5	219.4
Ti(CH ₃) ₂ Cl ₂ (Ti-C)	205.8	203.5	203.6	205.5	205.5	206.3	206.3
Ti(CH ₃) ₂ Cl ₂ (Ti-Cl)	219.6	219.6	219.6	220.5	220.4	220.7	220.6
Ti(BD ₄) ₃ (Ti-B)	217.5	214.3	214.3	214.7	214.6	214.9	214.8
Ti(BD ₄) ₃ (Ti-D ^{br})	198.4	193.4	193.5	193.7	193.7	193.2	193.1
VOF ₃ (V=O)	157.0	154.1	154.1	157.5	157.5	157.6	157.5
VOF ₃ (V-F)	172.9	171.6	171.6	173.7	173.7	173.4	173.4
VF ₅ (V-F ^{ax})	173.4	173.5	173.5	176.4	176.4	175.9	175.9
VF ₅ (V-F ^{eq})	170.8	169.9	169.9	172.7	172.6	172.3	172.3
VOCl ₃ (V=O)	157.3	153.9	153.9	157.2	157.2	157.3	157.3
VOCl ₃ (V-Cl)	213.8	213.0	213.0	215.0	214.9	214.9	214.9
V(N(CH ₃) ₂) ₄ (V-N)	187.9	186.1	186.1	188.2	188.1	188.1	187.9
V(Cp)(CO) ₄ (V-C ^{CO})	196.3	192.3	192.3	192.7	192.7	194.4	194.3
CrO ₂ F ₂ (Cr=O)	157.4	153.7	153.6	157.1	157.1	157.0	157.0
CrO ₂ F ₂ (Cr-F)	171.9	170.2	170.2	172.4	172.3	172.0	172.0
CrO ₂ Cl ₂ (Cr=O)	157.7	153.8	153.8	157.2	157.2	157.2	157.1
CrO ₂ Cl ₂ (Cr-Cl)	212.2	210.6	210.6	212.4	212.4	212.4	212.3
CrO ₂ (NO ₃) ₂ (Cr=O)	158.4	153.8	153.8	157.4	157.4	157.4	157.4
CrO ₂ (NO ₃) ₂ (Cr-O)	195.4	191.0	191.0	193.2	193.2	193.0	192.9
Cr(C ₆ H ₆) ₂ (Cr-C)	215.0	213.0	212.9	213.8	213.7	213.6	213.5
Cr(C ₆ H ₆)(CO) ₃ (Cr-C ^{Ar})	220.8	219.1	219.2	221.0	221.1	220.2	220.2
Cr(C ₆ H ₆)(CO) ₃ (Cr-C ^{CO})	186.3	183.8	183.8	183.9	183.9	185.2	185.0
Cr(NO) ₄ (Cr-N)	175.0	171.5	171.5	174.1	174.1	174.1	174.0
MnO ₃ F(Mn-O)	158.6	154.2	154.2	159.2	157.7	157.6	157.6
MnO ₃ F(Mn-F)	172.4	170.1	170.1	171.0	172.0	171.6	171.6
MnCp(CO) ₃ (Mn-C ^{Cp})	214.7	213.7	213.7	215.2	215.1	214.3	214.2
MnCp(CO) ₃ (Mn-C ^{CO})	180.6	178.3	178.3	178.4	178.3	179.4	179.3
Fe(CO) ₅ (Fe-C ^{mean})	182.9	179.7	179.7	180.2	180.1	181.0	180.9
Fe(CO) ₃ (tmm)(Fe-C ^{CO})	181.0	177.9	177.9	178.0	178.0	178.8	178.8
Fe(CO) ₃ (tmm)(Fe-C ^{ent})	193.8	192.2	192.2	194.6	194.6	194.3	194.3
Fe(CO) ₃ (tmm)(Fe-C ^{H2})	212.3	209.8	209.9	213.1	213.2	212.0	212.2
Fe(CO) ₂ (NO) ₂ (Fe-C ^{mean})	187.2	180.8	180.8	181.5	181.3	182.3	182.2
Fe(CO) ₂ (NO) ₂ (Fe-N)	167.4	164.1	164.1	167.1	167.0	166.9	166.9
FeCp ₂ (Fe-C)	206.4	204.2	204.2	204.0	204.1	203.7	203.5
Fe(C ₂ H ₄)(CO) ₄ (Fe-C ^{et})	211.7	209.7	216.2	213.0	216.7	212.3	216.7
Fe(C ₂ H ₄)(CO) ₄ (Fe-C ^{ax})	181.5	180.0	180.1	179.9	179.9	180.7	180.7
Fe(C ₂ H ₄)(CO) ₄ (Fe-C ^{eq})	180.6	178.1	177.8	178.9	178.7	179.6	179.3
Fe(C ₅ (CH ₃) ₅)(P ₅)(Fe-P)	237.7	235.7	235.7	236.3	236.1	234.9	234.7
CoH(CO) ₄ (Co-C ^{eq})	181.8	178.4	178.4	179.0	179.0	179.5	179.5
Co(CO) ₃ (NO)(Co-N)	165.8	162.9	162.9	166.1	166.1	165.8	165.8
Co(CO) ₃ (NO)(Co-C)	183.0	180.1	180.1	180.5	180.4	181.1	181.0
Ni(CO) ₄ (Ni-C)	182.5	182.1	182.0	182.3	182.2	182.7	182.6
Ni(acac) ₂ (Ni-O)	187.6	185.1	184.3	185.8	185.3	185.4	184.6
Ni(PF ₃) ₄ (Ni-P)	209.9	209.0	208.8	210.6	210.3	210.0	209.5
CuCH ₃ (Cu-C)	188.4	190.1	190.1	189.3	189.4	189.6	189.6
CuCN(Cu-C)	183.2	184.3	184.3	182.0	182.0	182.3	182.3
Cu(acac) ₂ (Cu-O)	191.4	191.9	191.8	194.3	194.2	193.2	193.1
MD		-2.1	-2.0	-0.6	-0.5	-0.6	-0.5
MAD		2.3	2.4	1.5	1.6	1.3	1.4
RMSD		2.7	2.8	1.9	2.1	1.7	1.9
SD		11.6	13.3	13.0	14.0	11.3	12.8
Var		2.7	3.6	3.5	4.0	2.6	3.3
Max		1.7	4.5	3.0	5.0	2.5	5.0
Min		-6.4	-6.4	-5.7	-5.9	-5.2	-5.3
AMax		6.4	6.4	5.7	5.9	5.2	5.3

Table A2.29.: Diverse set of 32 metal complexes from the first transition row, for which precise gas- phase geometries are known from electron diffraction or microwave spectroscopy. Compilation by Bühl *et al.*²⁹⁴. We abbreviate D3(BJ)-ATM by D3 and D4(TB)-ATM by D4.

system(bond)	Ref.	PBE0		PBE		TPSS	
		D3	D4	D3	D4	D3	D4
Sc(acac) ₃ (Sc-O)	207.6	209.0	208.9	210.4	210.3	210.0	209.8
TiCl ₄ (Ti-Cl)	216.9	216.4	216.4	218.3	218.2	218.3	218.3
Ti(CH ₃)Cl ₃ (Ti-Cl)	204.7	202.3	202.3	204.5	204.5	205.3	205.4
Ti(CH ₃) ₂ Cl ₂ (Ti-Cl)	218.5	218.0	217.9	219.3	219.3	219.5	219.5
Ti(CH ₃) ₂ Cl ₂ (Ti-C)	205.8	203.5	203.6	205.5	205.5	206.3	206.4
Ti(CH ₃) ₂ Cl ₂ (Ti-Cl)	219.6	219.6	219.5	220.5	220.5	220.7	220.7
Ti(BD ₄) ₃ (Ti-B)	217.5	214.3	214.3	214.7	214.6	214.9	214.8
Ti(BD ₄) ₃ (Ti-D ^{br})	198.4	193.4	193.4	193.7	193.7	193.2	193.1
VOF ₃ (V=O)	157.0	154.1	154.1	157.5	157.5	157.6	157.5
VOF ₃ (V-F)	172.9	171.6	171.6	173.7	173.7	173.4	173.4
VF ₅ (V-F ^{ax})	173.4	173.5	173.5	176.4	176.4	175.9	175.9
VF ₅ (V-F ^{eq})	170.8	169.9	169.8	172.7	172.6	172.3	172.4
VOCl ₃ (V=O)	157.3	153.9	153.9	157.2	157.2	157.3	157.3
VOCl ₃ (V-Cl)	213.8	213.0	213.0	215.0	214.9	214.9	214.9
V(N(CH ₃) ₂) ₄ (V-N)	187.9	186.1	186.2	188.2	188.1	188.1	188.0
V(Cp)(CO) ₄ (V-C ^{CO})	196.3	192.3	192.3	192.7	192.7	194.4	194.3
CrO ₂ F ₂ (Cr=O)	157.4	153.7	153.7	157.1	157.1	157.0	157.0
CrO ₂ F ₂ (Cr-F)	171.9	170.2	170.2	172.4	172.4	172.0	172.0
CrO ₂ Cl ₂ (Cr=O)	157.7	153.8	153.8	157.2	157.2	157.2	157.2
CrO ₂ Cl ₂ (Cr-Cl)	212.2	210.6	210.6	212.4	212.4	212.4	212.4
CrO ₂ (NO ₃) ₂ (Cr=O)	158.4	153.8	153.8	157.4	157.4	157.4	157.4
CrO ₂ (NO ₃) ₂ (Cr-O)	195.4	191.0	191.0	193.2	193.2	193.0	192.9
Cr(C ₆ H ₆) ₂ (Cr-C)	215.0	213.0	213.0	213.8	213.7	213.6	213.6
Cr(C ₆ H ₆)(CO) ₃ (Cr-C ^{Ar})	220.8	219.1	219.2	221.0	221.1	220.2	220.3
Cr(C ₆ H ₆)(CO) ₃ (Cr-C ^{CO})	186.3	183.8	183.8	183.9	183.9	185.2	185.1
Cr(NO) ₄ (Cr-N)	175.0	171.5	171.5	174.1	174.1	174.1	174.1
MnO ₃ F(Mn=O)	158.6	154.2	154.2	159.2	157.7	157.6	157.6
MnO ₃ F(Mn-F)	172.4	170.1	170.1	171.0	172.0	171.6	171.6
MnCp(CO) ₃ (Mn-C ^{Cp})	214.7	213.7	213.7	215.2	215.1	214.3	214.3
MnCp(CO) ₃ (Mn-C ^{CO})	180.6	178.3	178.3	178.4	178.4	179.4	179.4
Fe(CO) ₅ (Fe-C) ^{mean}	182.9	179.7	179.7	180.2	180.2	181.0	181.0
Fe(CO) ₃ (tmm)(Fe-C ^{CO})	181.0	177.9	177.9	178.0	178.0	178.8	178.8
Fe(CO) ₃ (tmm)(Fe-C ^{ent})	193.8	192.2	192.2	194.6	194.7	194.3	194.4
Fe(CO) ₃ (tmm)(Fe-C ^{H₂})	212.3	209.8	209.8	213.1	213.1	212.0	212.2
Fe(CO) ₂ (NO) ₂ (Fe-C) ^{mean}	187.2	180.8	180.7	181.5	181.4	182.3	182.3
Fe(CO) ₂ (NO) ₂ (Fe-N)	167.4	164.1	164.2	167.1	167.1	166.9	166.9
FeCp ₂ (Fe-C)	206.4	204.2	204.2	204.0	204.1	203.7	203.6
Fe(C ₂ H ₄)(CO) ₄ (Fe-C ^{et})	211.7	209.7	209.9	213.0	213.1	212.3	212.6
Fe(C ₂ H ₄)(CO) ₄ (Fe-C ^{ax})	181.5	180.0	180.0	179.9	179.9	180.7	180.7
Fe(C ₂ H ₄)(CO) ₄ (Fe-C ^{eq})	180.6	178.1	178.1	178.9	178.8	179.6	179.6
Fe(C ₅ (CH ₃) ₅)(P ₅)(Fe-P)	237.7	235.7	244.7	236.3	236.2	234.9	234.8
CoH(CO) ₄ (Co-C ^{eq})	181.8	178.4	178.4	179.0	179.0	179.5	179.5
Co(CO) ₃ (NO)(Co-N)	165.8	162.9	162.9	166.1	166.1	165.8	165.8
Co(CO) ₃ (NO)(Co-C)	183.0	180.1	180.1	180.5	180.5	181.1	181.1
Ni(CO) ₄ (Ni-C)	182.5	182.1	182.0	182.3	182.3	182.7	182.7
Ni(acac) ₂ (Ni-O)	187.6	185.1	184.3	185.8	185.3	185.4	184.6
Ni(PF ₃) ₄ (Ni-P)	209.9	209.0	208.4	210.6	209.8	210.0	209.1
CuCH ₃ (Cu-C)	188.4	190.1	190.1	189.3	189.4	189.6	189.6
CuCN(Cu-C)	183.2	184.3	184.3	182.0	182.0	182.3	182.3
Cu(acac) ₂ (Cu-O)	191.4	191.9	191.8	194.3	194.2	193.2	193.1
MD		-2.1	-2.0	-0.6	-0.6	-0.6	-0.6
MAD		2.3	2.5	1.5	1.5	1.3	1.3
RMSD		2.7	2.9	1.9	1.9	1.7	1.7
SD		11.6	14.7	13.0	12.9	11.3	11.5
Var		2.7	4.4	3.5	3.4	2.6	2.7
Max		1.7	7.0	3.0	3.0	2.5	2.5
Min		-6.4	-6.5	-5.7	-5.8	-5.2	-5.3
AMax		6.4	7.0	5.7	5.8	5.2	5.3

A3. Supporting Information to Chapter 3

Appendix A3 contains:

- Periodic DFT-D4 methodologies for ζ -function, CN definition, EEQ model, dispersion energy
- Quasi-harmonic approximation (QHA) definition
- Technical details of reference polarizabilities
- Computational details for solid state volumes, QHA, timings, refractive indices, and salt polarizabilities

A3.1. Appendix: Extension and Evaluation of the D4 London Dispersion Model for Periodic Systems

A3.1.1. Periodic DFT-D4 Methodologies

Let us begin with a review of the theoretical framework of the D4 approach³⁰⁸ as this will provide the context for the introduction of the new features. The underlying concept of D4 and its predecessors is to model the dispersion energy based on atomic pairwise dispersion coefficients C_6^{jk} , which are obtained from a Casimir–Polder integration of the respective atomic polarizabilities $\alpha^{\text{eff}}(i\omega)$

$$C_6^{jk} = \frac{3}{\pi} \int_0^{\infty} d\omega \alpha_j^{\text{eff}}(i\omega) \alpha_k^{\text{eff}}(i\omega). \quad (\text{A3.1})$$

Note that atomic units are used throughout in this work. To account for the influence of the chemical environment, the atomic polarizabilities used in the D4 model are not fixed at the values of the isolated atoms $\alpha(i\omega)$, but depend (i) on geometric parameters captured by the atomic coordination number (CN_j , as in D3), as well as (ii) on effective atomic charges (z_j , new in D4) obtained *via* an electronegativity-equilibration (EEQ) scheme. The idea behind the introduction of this charge scaling is to allow for a more “natural” behavior of the effective

A3.1. Extension and Evaluation of the D4 London Dispersion Model for Periodic Systems

polarizabilities, *i.e.*, to render atoms with negative partial charge more polarizable and *vice versa*.

In practice, the geometry and charge dependence of the polarizabilities is implemented using an interpolation based on a set of molecular reference systems. To do this efficiently and avoid an interpolation in two dimensions, the atomic polarizabilities of all reference systems are, in a first step, rescaled to match the effective charge of the atom under consideration of z_j *via*

$$\bar{\alpha}_i^{\text{ref}}(i\omega) = \alpha_i^{\text{ref}}(i\omega)\zeta(z_j, z_i^{\text{ref}}), \quad (\text{A3.2})$$

where ζ describes an empirical relation between the polarizability of an atom and its effective charge. Its analytical form

$$\zeta(z_i, z_i^{\text{ref}}) = \exp\left(\beta \left\{1 - \exp\left[\gamma_i \left(1 - \frac{z_i^{\text{ref}}}{z_i}\right)\right]\right\}\right), \quad (\text{A3.3})$$

with β as a global parameter set to 3 and γ_i as the chemical hardness taken from Ref. 461 is discussed in more detail in Ref. 308. The calculation of the necessary effective charges z done with an EEQ model is described in section. A3.1.2

In a second step, the effective polarizability of the atom j is obtained *via* interpolation from the charge-scaled reference polarizabilities using a Gaussian weighting based on the coordination number (CN)

$$\alpha_j^{\text{eff}}(i\omega) = \sum_{i, \text{ref}=1}^{N^{i, \text{ref}}} \bar{\alpha}_i^{\text{ref}}(i\omega) W_j^{i, \text{ref}}(\text{CN}_i^{i, \text{ref}}, \text{CN}_j). \quad (\text{A3.4})$$

However, to use this CN-based approach in periodic systems, a different formula for the CN is used compared to the molecular implementation to avoid CN-divergences. The expression for the CN in periodic systems reads

$$\begin{aligned} \text{CN}_i = & \sum_{\mathbf{T}} \sum_j' \frac{\delta_{ij}^{\text{EN}}}{2} \left(1 + \text{erf}\left(-k_0 \left(\frac{(\mathbf{R}_{ij} + \mathbf{T}) - \mathbf{R}_{ij}^{\text{cov}}}{\mathbf{R}_{ij}^{\text{cov}}}\right)\right)\right) \\ \delta_{ij}^{\text{EN}} = & \left(k_1 \exp(|\text{EN}_i - \text{EN}_j| + k_2)^2\right) / k_3, \end{aligned} \quad (\text{A3.5})$$

where, $\mathbf{T} = t_1 \mathbf{a}_1 + t_2 \mathbf{a}_2 + t_3 \mathbf{a}_3$ denotes the translation vector with \mathbf{a}_1 , \mathbf{a}_2 , and \mathbf{a}_3 being the lattice vectors (t_1 , t_2 , and $t_3 \in \mathbb{Z}$). The primed sum over j indicates that the case $i = j$ is omitted for $\mathbf{T} = \mathbf{0}$. One of the central changes is the use of Pauling electronegativities (EN),²⁴² as well as the inter-nuclear distance R_{ij} of the pair ij , and the covalent atomic radii²⁴³ ($R_{ij}^{\text{cov}} = R_i^{\text{cov}} + R_j^{\text{cov}}$). Note that the CN has become EN-dependent to differentiate between covalent and ionic bonding

A3. Supporting Information to Chapter 3

(e.g., differentiate F₂ from HF). The parameters in equation A3.5 ($k_0 = 7.5$, $k_1 = 4.1$, $k_2 = 19.09$, and $k_3 = 254.56$) were taken from Ref. 308.

This charge and geometry dependent calculation of atomic polarizabilities from molecular reference systems, which may be described as an atom-in-molecule approach to polarizabilities, presumes the additivity of atomic polarizabilities,²⁴¹ which is reflected in the following equation

$$\alpha_i^{\text{ref}}(i\omega) = \frac{1}{m} \left[\alpha^{\text{I}_m\text{X}_n}(i\omega) - \frac{n}{l} \alpha^{\text{X}_l}(i\omega) \zeta(z_X, z_X^{\text{ref}}) \right]. \quad (\text{A3.6})$$

Here, $\alpha^{\text{I}_m\text{X}_n}(i\omega)$ is the molecular polarizability of one I-reference, $\alpha^{\text{X}_l}(i\omega)$ refers to the homonuclear compound (e.g., $\alpha^{\text{H}_2}(i\omega)$ as dihydrogen) and m , n , and l are the particular stoichiometric coefficients. All I atoms inside the reference molecules and the X atoms in the homonuclear compounds are electronically equal and thus symmetry equivalent. By exploiting this symmetry equivalence, the approximation of additive polarizabilities is justified. Furthermore, the charge scaling of all X atoms in the respective reference system is directly incorporated.

This more general scheme has no disadvantage compared to the hydrogenated reference systems used in the D3 model. With it, any diatomic molecular polarizabilities, e.g., dihalide molecular polarizabilities (chlorine or fluorine) and oxygen molecular polarizabilities can be used in the subtraction scheme of equation A3.6 as briefly discussed in Ref. 170. This generalization of the approach opens up the possibility to provide specialized C₆ dispersion coefficients, which will be exploited here to properly describe interactions in ionic solids.

A3.1.2. Periodic Electronegativity Equilibration Model

For the generation of atomic partial charges q under periodic boundary conditions, a classical geometry dependent EEQ charge model is developed in the present work. For this purpose, a cyclic cluster model (CCM) is implemented which applies periodic boundary conditions to a cluster that uses a non-primitive unit cell of a solid, a surface, or an infinite chain by directly employing cyclic Born-van-Kármán boundary conditions. The environment of each atom is replaced by a notional cyclic arrangement of cluster atoms, where the interaction zone of each atom within the cyclic cluster is described by a Wigner-Seitz cell, constructed by the translation vectors of the unit cell and centered at the atom. The cluster is constructed as a supercell of the primitive unit cell, so that a repetition of this unit cell of N_1 , N_2 , and N_3 cells along the lattice vectors \mathbf{a}_1 , \mathbf{a}_2 , and \mathbf{a}_3 leads to a total cell number of $N = N_1 \cdot N_2 \cdot N_3$. In the CCM, the WSCs are stoichiometrically and symmetrically constructed to ensure local electroneutrality. This is guaranteed by the fact that each WSC central atom i is surrounded by Ξ_i neighbours j with an inverted partial charge. When setting up the cluster, the

A3.1. Extension and Evaluation of the D4 London Dispersion Model for Periodic Systems

number of all neighbours of each WSC central atom is determined and weighting factors $w_{ij} = 1/\Xi_i$ for the respective neighbours are assigned, accordingly. Since the CCM is a finite-size method, the clusters used can also carry a net charge without running into convergence problems occurring within the employed Ewald sums. In contrast to a supercell model, no summation over special \mathbf{k} -points has to be carried out. Instead, a discrete number of \mathbf{k} -points is contained implicitly by placing them equally distributed in space.

$$\{\mathbf{k}\} = \prod_j^3 \frac{g_j}{N_j} \mathbf{b}_j \text{ with } g_j = 0, \dots, N_j^{-1} \quad (\text{A3.7})$$

Here, we introduce the reciprocal lattice vectors \mathbf{b} . The periodic charge density $\rho(\mathbf{r})$ of the system is supposed to be a superposition of spherically symmetric Gaussian functions centered at the atoms position, each normalized to the corresponding nuclear charge q_i given by the following expression

$$\rho_i(\mathbf{r}) = \sum_{\mathbf{T}} \frac{q_i}{\alpha_i^3 \pi^{3/2}} \exp\left(-\frac{|\mathbf{r} - \mathbf{R}_i + \mathbf{T}|^2}{\alpha_i^2}\right). \quad (\text{A3.8})$$

Here, the atomic van der Waals radii α_i are introduced. By choosing such atomic charge densities the total isotropic electrostatic (IES) energy is amenable by the following expression given in matrix notation

$$E_{\text{IES}} = \mathbf{q}^T \left(\frac{1}{2} \mathbf{A} \cdot \mathbf{q} - \mathbf{X} \right). \quad (\text{A3.9})$$

The interaction matrix \mathbf{A} contains all periodic Coulomb interactions, which are developed in Ewald sums by splitting the Coulomb operator into short-range and long-range contributions (Ewald splitting parameter $\xi = \sqrt{\pi}/V^{1/3}$). Here, the previously determined weighting factors w_{ij} (as obtained from the CCM) are applied for all off-diagonal elements

$$\begin{aligned} A_{ij}^{\text{rec}} &= \frac{4\pi}{V} \sum_{\mathbf{k} \neq 0} \cos(\mathbf{k} \cdot (\mathbf{R}_{ij} + \mathbf{T})) \exp\left\{-\frac{k^2}{4\xi^2}\right\} \frac{w_{ij}}{k^2} \\ A_{ii}^{\text{rec}} &= \frac{4\pi}{V} \sum_{\mathbf{k} \neq 0} \exp\left\{-\frac{k^2}{4\xi^2}\right\} \frac{1}{k^2} \\ A_{ij}^{\text{dir}} &= \sum_{\mathbf{T}} \left(\frac{\text{erf}(\gamma_{ij} |\mathbf{R}_{ij} + \mathbf{T}|)}{|\mathbf{R}_{ij} + \mathbf{T}|} - \frac{\text{erf}(\xi |\mathbf{R}_{ij} + \mathbf{T}|)}{|\mathbf{R}_{ij} + \mathbf{T}|} \right) w_{ij} \\ A_{ii}^{\text{dir}} &= \sum_{\mathbf{T} \neq 0} \frac{\text{erf}(\gamma_{ii} |\mathbf{T}|)}{|\mathbf{T}|} - \frac{\text{erf}(\xi |\mathbf{T}|)}{|\mathbf{T}|} \\ A_{ii}^{\text{self/back}} &= J_{ii} + \frac{2\gamma_{ii}}{\sqrt{\pi}} - \frac{\pi}{\xi^2 V}. \end{aligned} \quad (\text{A3.10})$$

A3. Supporting Information to Chapter 3

Furthermore, we define γ_{ij} to be equal to $(\alpha_i^2 + \alpha_j^2)^{-1/2}$. The Lagrangian is constructed under the constraint that the sum of the atomic charges conserves the total charge of the cluster, *i.e.*,

$$L = E_{IES} + \lambda \left(\sum_k q_k - q_{\text{cluster}} \right) \quad (\text{A3.11})$$

with $\frac{\partial L}{\partial \mathbf{q}} = \mathbf{0} \wedge \frac{\partial L}{\partial \lambda} = \sum_i q_i - q_{\text{cluster}} = 0,$

which leads to a set of $(N + 1)$ linear equations. The right-hand side (RHS) of this set of equations is given by $X_i = -\chi_i$, where χ_i consists of the fitted atomic electronegativity EN_i which is shifted according to the following expression

$$\chi_i = EN_i - \Omega_i. \quad (\text{A3.12})$$

The molecular EEQ model uses for this shift the square root of a modified error function CN as described in Ref. 308. Since high coordination numbers can be reached very quickly in a periodic system, artificial polarity reversals can occur. An instructive example is displayed in figure A3.1, where the polarity between cations and anions within the sodium chloride crystal is reversed (*i.e.*, sodium formally becomes anionic and chlorine cationic). This is an artifact of the definition of

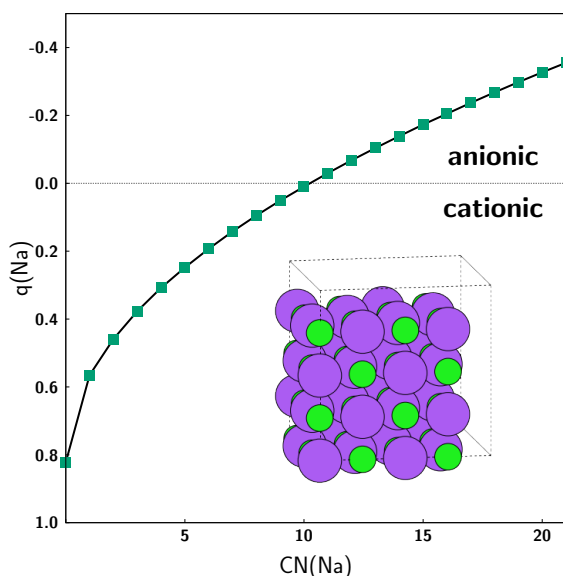


Figure A3.1.: Functional dependence on the sodium partial charge $q(\text{Na})$ with increasing $\text{CN}(\text{Na})$ using the molecular EEQ model within the sodium chloride crystal.

the CN, which depends on the covalent radius R^{cov} of the respective atom. As a result, the atom with the larger covalent radius also gets a higher CN (here $R_{\text{Na}}^{\text{cov}} = 3.5 \text{ Bohr}$ and $R_{\text{Cl}}^{\text{cov}} = 2.5 \text{ Bohr}$) and thus a higher EN shift resulting in

A3.1. Extension and Evaluation of the D4 London Dispersion Model for Periodic Systems

nonphysical polarity changes. In order to avoid such artifacts, the procedure is modified for periodic boundary conditions. Here, Ω_i is used which includes the global parameter $\gamma = 8$ and is given as

$$\Omega_i = \kappa_i \left(\log \left(\frac{1 + \exp(\gamma)}{1 + \exp(\gamma - CN_i)} \right) \right)^{1/2}. \quad (\text{A3.13})$$

This classical charge model requires overall five empirical parameters (J_{ii} , α_i , EN_i , κ_i , and R_i^{cov}) per element and achieves for molecules across the entire periodic table of elements an average deviation of about $0.04 e^-$ ($0.03 e^-$ for organic molecules) with respect to PBE0 based Hirshfeld charges.³⁰⁸

By using the definition of the Lagrangian given in equation A3.11 the analytical charge gradients is derived as

$$\frac{\partial \mathbf{q}}{\partial \mathbf{R}_j} = \tilde{\mathbf{A}}^{-1} \left[-\frac{\partial (\mathbf{A} \cdot \mathbf{q})}{\partial \mathbf{R}_j} + \frac{\partial \mathbf{X}}{\partial \mathbf{R}_j} \right] \quad (\text{A3.14})$$

where the inverse of the indefinite $(N+1)$ matrix has been obtained by a Bunch–Kaufman factorization²⁴⁹ and inversion.

A3.1.3. Dispersion Energy

The periodic DFT-D4 energy expression is constructed as follows

$$E_{\text{disp}}^{\text{D4}} = E_{\text{disp}}^{(6,8)} + E_{\text{disp}}^{(9),\text{ATM}}. \quad (\text{A3.15})$$

The left part of equation A3.15 corresponds to the pairwise dispersion energy which is given by

$$E_{\text{disp}}^{(6,8)} = -\frac{1}{2} \sum_i \sum_{\mathbf{T}} \sum_j' \sum_{n=6,8} s_n \frac{C_{ij}^{(n)}}{R_{ij\mathbf{T}}^{(n)}} f_{\text{damp}}^{(n)}(R_{ij\mathbf{T}}). \quad (\text{A3.16})$$

Here, the primed sum over j indicates that the case $i = j$ is omitted for $\mathbf{T} = \mathbf{0}$. In equation A3.16, s_n scales the individual multi-polar contributions— s_6 and s_8 for the dipole–dipole and dipole–quadrupole term—and $f_{\text{damp}}^{(n)}$ denotes the rational Becke–Johnson (BJ) damping function (denoted as BJ-damping (BJD) in the following) which is used to couple this approach to standard DFAs.

$$f_{\text{BJD}}^{(n)}(R_{ij\mathbf{T}}) = \frac{R_{ij\mathbf{T}}^{(n)}}{R_{ij\mathbf{T}}^{(n)} + \left(\alpha_1 R_0^{ij} + \alpha_2 \right)^{(n)}} \quad (\text{A3.17})$$

A3. Supporting Information to Chapter 3

Equation A3.17 incorporates the DFA-specific parameters α_1 and α_2 and the cutoff-radii defined as

$$R_0^{ij} = \sqrt{\frac{C_8^{ij}}{C_6^{ij}}}, \quad (\text{A3.18})$$

where the recursive relation between dipole–dipole and dipole–quadrupole dispersion coefficients is used. Furthermore, we define the following expression for the rational damping term

$$R_{0,BJ}^{ij} = (\alpha_1 R_0^{ij} + \alpha_2). \quad (\text{A3.19})$$

The simplest way to include three-body effects uses the well-known Axilrod–Teller–Muto^{167,168} (ATM) term (*cf.*, right side of equation A3.15) which is defined as the sum over ijk energy contributions each defined by

$$E^{ijk} = \frac{C_9^{ijk} (3 \cos \theta_i \cos \theta_j \cos \theta_k + 1)}{(R_{ij} R_{jk} R_{ki})^3}. \quad (\text{A3.20})$$

Here, θ_i , θ_j , and θ_k are the internal angles of the triangle formed by R_{ij} , R_{jk} , and R_{ki} while C_9^{ijk} is the triple-dipole constant given by

$$C_9^{ijk} \approx \sqrt{C_6^{ij} C_6^{jk} C_6^{ki}}. \quad (\text{A3.21})$$

The C_9^{ijk} coefficients are derived from C_6 coefficients which are obtained from charge-neutral atomic polarizabilities (i.e., neutral atoms with $z_i = Z_i$). The finally used three-body dispersion energy expression is as follows

$$E_{\text{disp}}^{(9),\text{ATM}} = -k \sum_i \sum_{\mathbf{T}} \sum_j \sum_{\mathbf{T}'}' \sum_k'' f_{\text{damp}}^{(9)}(\bar{R}_{ij\mathbf{T}k\mathbf{T}'}) E^{ij\mathbf{T}k\mathbf{T}'}, \quad (\text{A3.22})$$

where the sum is over all atom triples ijk applied with a zero-damping scheme proposed by Chai and Head-Gordon¹²²

$$f_{\text{damp}}^{(9)}(\bar{R}_{ij\mathbf{T}k\mathbf{T}'}) = \frac{1}{1 + 6 (\bar{R}_{ij\mathbf{T}k\mathbf{T}'})^{-16}}. \quad (\text{A3.23})$$

To avoid multiple counting of three-body interactions the factor k is set to $\frac{1}{3}$ if atoms i , j , k are within the reference cell and to $\frac{1}{2}$ in all other cases. As previously, the primed sum over j indicates that the case $i = j$ is omitted for $\mathbf{T} = \mathbf{0}$, the double primed sum over k indicates that the case $j = k$ is omitted for $\mathbf{T} = \mathbf{T}'$ and $i = k$ is omitted for $\mathbf{T} = \mathbf{0}$. Equation A3.23 includes the averaged inter-atomic

distance

$$\bar{R}_{ijTk_T'} = \left(R_{ijT} R_{jTk_T'} R_{k_T'i} / R_{0,BJ}^{ij} R_{0,BJ}^{jk} R_{0,BJ}^{ki} \right)^{1/3}, \quad (\text{A3.24})$$

which incorporates $R_{0,BJ}^{ij/jk/ki}$ (cf. equation A3.19). Since dispersion interactions are much faster decaying (leading order term $\propto R^{-6}$) than, e.g., Coulomb interactions we employ for this energy contribution a real-space cutoff within the periodic implementation. Furthermore, analytical gradients are available for the dispersion energy expression in equation A3.15.

A3.1.4. Theory of the Quasi-Harmonic Approximation

In order to account for thermodynamic properties to crystals, the knowledge of phonon modes is required over the complete first Brillouin zone (FBZ) of the system. The easiest way to account for ZPVE contributions includes harmonic lattice dynamics where each \mathbf{k} -point in the FBZ is associated with $3M$ harmonic oscillators (*i.e.* phonons) which are labeled by a phonon band index n ($n = 1, \dots, 3N$) and whose energy levels are given by the usual harmonic expression as

$$\varepsilon_m^{n,\mathbf{k}} = \left(m + \frac{1}{2} \right) \omega_{\mathbf{k}n}, \quad (\text{A3.25})$$

where m is an integer, $\omega_{\mathbf{k}n} = 2\pi\nu_{\mathbf{k}n}$, and N is the number of atoms per primitive cell. The overall vibrational canonical partition function of a crystal at a given temperature T is given as

$$Q_{\text{vib}}(T) = \prod_{\mathbf{k}} \prod_{n=1}^{3N} \sum_{m=0}^{\infty} \exp\left(-\frac{\varepsilon_m^{n,\mathbf{k}}}{k_B T}\right), \quad (\text{A3.26})$$

where k_B is Boltzmann's constant. From this expression it is straightforward to obtain harmonic expressions to the internal energy given as

$$\mathcal{E}(T) = k_B T^2 \left(\frac{\partial \log(Q_{\text{vib}})}{\partial T} \right) = \sum_{\mathbf{k}n} \hbar \omega_{\mathbf{k}n} \left(\frac{1}{2} + \frac{1}{\exp\left(\frac{\hbar \omega_{\mathbf{k}n}}{k_B T}\right) - 1} \right). \quad (\text{A3.27})$$

However, the harmonic approximation has its limitations like zero thermal expansion, temperature independence of elastic constants and bulk modulus, equality of constant-pressure and constant-volume specific heats, as well as infinite thermal conductivity and phonon lifetimes.⁴⁶² To overcome such drawbacks, the simplest way includes quasi-harmonic quantities in the sense of the quasi-harmonic approximation (QHA).^{463–466} According to the QHA the Helmholtz free energy of a crystal is written retaining the same harmonic expression but introducing an

A3. Supporting Information to Chapter 3

explicit dependence of vibrational phonon frequencies on volume as given by

$$F^{\text{QHA}}(T, V) = U_0(V) + F_{\text{vib}}^{\text{QHA}}(T, V), \quad (\text{A3.28})$$

where $U_0(V)$ is the zero-temperature internal energy of the crystal without any vibrational contribution (similar to volume constrained geometry optimizations) and the vibrational part is given by

$$F_{\text{vib}}^{\text{QHA}}(T, V) = \sum_{\mathbf{kn}} \frac{\hbar\omega_{\mathbf{kn}}(V)}{2} + k_{\text{B}}T \left[\ln \left(1 - \exp \left(-\frac{\hbar\omega_{\mathbf{kn}}(V)}{k_{\text{B}}T} \right) \right) \right], \quad (\text{A3.29})$$

where the first part refers to the zero-point energy of the system. The equilibrium volume at a given temperature T is obtained by minimizing $F^{\text{QHA}}(T, V)$ with respect to volume V while keeping T constant.

A3.1.5. Technical Details

All molecular dynamic dipole polarizabilities $\alpha(i\omega)$ were calculated using time-dependent density functional theory (TD-DFT).^{164,165} A variant of the PBE0 hybrid functional was used, with a Fock-exchange admixture of 37.5% (dubbed PBE38). This method has already proved its accuracy and robustness in previous works.^{46,210,308} The atomic orbital (AO) basis sets used in the TD-DFT calculations are of def2-QZVP^{251,254} quality closely representing the complete basis set (CBS) limit for this property. The following def2-ECPs are used: ECP-28⁴⁶⁷⁻⁴⁶⁹ covering 28 core electrons (for Rb, Sr, Y-Cd, In-Sb, Te-Xe, Ce-Lu), ECP-46 covering 46 core electrons (for Cs, Ba, La), and ECP-60 covering 60 core electrons (for Hf-Hg, Tl-Bi, Po-Rn) as defined in Ref. 251. Crystal structures have been extracted from MATERIALS PROJECT⁴⁷⁰ (for alkali metals Li, Na, K, Rb, and Cs; for alkaline earth metals Be, Mg, Ca, Sr, and Ba; for d -block elements Sc and Y) and used within the PEECM to obtain dynamic polarizabilities. Since some elements have experimental crystal structures that exhibit high dipole moments, the PEECM calculation could not be successfully converge (e.g, for Ti, Zr, Hf, V, Nb, and Ta). For these elements closed-shell monomers without dipole moments were extracted from the crystal structure and dynamic polarizabilities were calculated using the presented level of theory. Furthermore, periodic coordination numbers were assigned to those six extracted clusters to be used as approximated “periodic” reference system. The ECPs used to create the shells within part (II) of the particular clusters have been extracted from the TURBOMOLE^{206,471} basis set library (nomenclature reads as follows element/ecp-electrons in core-name; for alkali metals we used: Li/ecp-2-sdf, Na/ecp-10-sdf, K/ecp-18-sdf, Rb/ecp-36-sdf, and Cs/ecp-54-sdf; for earth alkali metals we used: Be/ecp-2-sdf, Mg/ecp-10-sdf⁴⁷²,

A3.1. Extension and Evaluation of the D4 London Dispersion Model for Periodic Systems

Ca/ecp-18-sdf, Sr/ecp-36-sdf, and Ba/ecp-54-sdf; for *d*-block elements we used: Sc/ecp-10-mdf⁴⁷³, Y/ecp-28-mwb⁴⁷⁴; for halogen we applied Cl/ecp-10-sdf and F/ecp-2-sdf and for oxygen we applied O/ecp-2-sdf).

A3.1.6. Computational Details

X23: Solid State Volumina For the determination of the 23 molecular crystal structure volumes we applied the VASP 6.0.8 software package. All PBE PAW calculations used an 800eV plane-wave cutoff (convergence criteria: energy difference $\propto 10^{-6}$). The DFT conjugated gradient method has been used within the optimization where all atomic positions and the cell has been relaxed. For all calculations standard pseudopotentials have been used.

ICE10: QHA Calculations Quasi-harmonic approximation calculations have been performed for eight different ice polymorphs. For this purpose the QHA implementation within the CRYSTAL17 code has been applied in combination with HSE-3c. Here, four different volumina have been used (steps of 2.5%) for which overall ten different temperatures have been applied (ranging from 10 K to 100 K applying 10 K steps). V_0 has been extracted from Helmholtz free energy calculations at a pressure of 0 GPa.

Timings for the Cyclohexanedione Crystal A self-consistent field (SCF) calculation has been performed for the cyclohexanedione crystal using the PBE/800eV setup in VASP 6.0.8 (convergence criteria: energy difference $\propto 10^{-6}$). The converged wave function has been applied to determine the pure timing arising from each dispersion correction. For SCAN-rVV10 and vdW-DF2 we applied an PAW cutoff of 800eV. For all calculations standard pseudopotentials have been used.

Refractive Indices Salt polarizabilities have been calculated for an organic polymer database. For D3 and D4 we use polarizabilities from the DFTD3 and DFTD4 standalone programs. For other dispersion corrections we have calculated polarizabilities using VASP 6.0.8 with a PBE/500eV setup using standard pseudopotentials.

Salt Polarizabilities Salt polarizabilities have been calculated for several alkali halides. For D3 and D4 we use polarizabilities from the DFTD3 and DFTD4 standalone programs. For other dispersion corrections we have calculated polarizabilities using VASP 6.0.8 with a PBE/500eV setup using standard pseudopotentials. All values are given in table A3.1 together with statistical measures covering the mean absolute deviation (MAD), the mean deviation (MD), the root mean squared deviation (RMSD), and the absolute maximum deviation (AMAX) all given in %.

A3. Supporting Information to Chapter 3

Table A3.1.: Static polarizabilities as obtained by experimental measurements (polarizabilities are extracted from Ref. 315), and theoretical values for D4, D3, TS, TS/Hi, MBD, MBD/Hi, and MBD/FI. All polarizabilities and statistical measures are given in Bohr³. Statistical values are given in %. All crystal structures have the Fm $\bar{3}$ m space group.

#	Compound	Salt polarizabilities							
		α_{exp}	α_{D4}	α_{D3}	α_{TS}	α_{MBD}	$\alpha_{\text{TS/Hi}}$	$\alpha_{\text{MBD/Hi}}$	$\alpha_{\text{MBD/FI}}$
1	LiF	6.1	9.0	40.8	144.4	crash	89.0	8.4	14.4
2	LiCl	19.6	20.7	52.6	163.9	crash	112.4	27.3	31.5
3	LiBr	27.9	27.1	59.2	171.4	crash	124.2	41.2	48.7
4	LiI	42.0	39.4	71.0	189.4	130.5	149.6	73.0	75.9
5	NaF	7.8	10.8	27.8	139.7	crash	77.4	17.8	16.0
6	NaCl	22.0	22.5	39.6	158.3	crash	93.1	34.3	30.7
7	NaBr	29.6	29.1	46.1	166.2	137.5	102.1	41.2	42.7
8	NaI	42.3	41.6	58.0	184.5	153.8	122.4	61.5	60.9
9	KF	13.6	16.4	53.4	244.6	crash	144.6	57.1	27.2
10	KCl	28.2	28.1	65.3	261.8	230.6	161.7	67.9	34.7
11	KBr	35.7	34.7	71.8	270.7	242.7	172.5	73.7	46.9
12	KI	49.9	47.3	83.6	291.0	260.2	195.6	93.9	65.2
13	RbF	17.4	19.7	62.1	269.3	crash	165.9	83.5	35.9
14	RbCl	31.8	31.5	73.9	282.7	257.6	180.1	89.1	38.1
15	RbBr	40.0	37.8	80.5	290.8	268.3	190.2	96.0	50.4
16	RbI	54.6	50.5	92.3	310.9	285.4	212.8	116.0	68.7
	MD	5.7	156.2	873.7	222.6	511.2	120.6	59.2	
	MAD	10.1	156.2	873.7	310.1	511.2	120.6	59.2	
	RMSD	16.7	203.4	1037.1	383.6	602.4	154.6	69.0	
	AMAX	47.1	568.7	2267.2	717.6	1359.2	379.6	135.9	

A4. Supporting Information to Chapter 4

Appendix A4 contains:

- TPM crystal structure (HSE-3c)
- TPM gas phase dimer structure (HSE-3c)
- TPM dimer dissociation energies (B3LYP-D3(BJ)-ATM/def2-TZVPP)
- TPM gas phase dimer structure (B3LYP-D3(BJ)-ATM/def2-TZVPP)
- Triphenylmethane dimer dissociation energies (B3LYP-D3(BJ)-ATM/def2-TZVPP)
- Triphenylmethane gas phase dimer structure (B3LYP-D3(BJ)-ATM/def2-TZVPP)

A4.1. Appendix: London Dispersion Enables the Shortest Intermolecular Hydrocarbon H···H Contact

A4.2. Computations

Molecular computations were performed at the HSE-3c³⁴³ (crystal structure as well as dimer calculations, CRYSTAL14⁷¹), at the B3LYP-D3(BJ)-ATM/def2-TZVPP^{46,117,166,475,476} (energy decomposition analysis, TURBOMOLE 7.0.2^{205,206,208,209}) and at the B3LYP-D3(BJ)-ATM/def2-TZVPP//PBEh-3c (dissociation free energy//thermo statistic contributions, TURBOMOLE 7.0.2) level of theory. Coordinates are given in Angström [Å], energies in Hartree [E_h]. The HSE-3c solid state computations of $\mathbf{1}_2$ were performed within the P2₁3 space group. All gas phase computations of $\mathbf{1}_2$ were performed without restrictions and converged to point group S₆.

A4.2.1. Crystal Structure

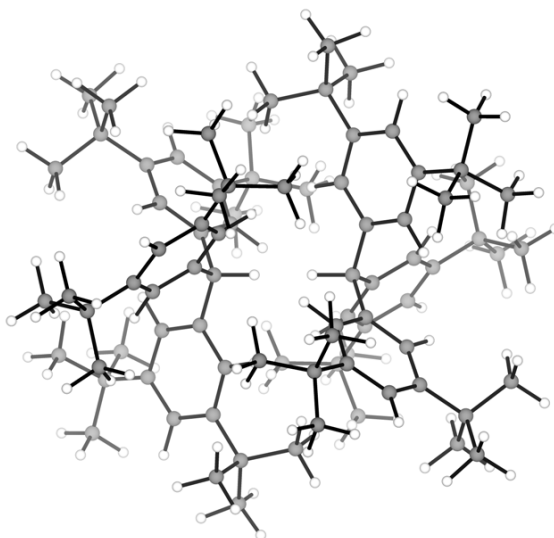


Figure A4.1.: Structure of **1**₂ obtained by solid state HSE-3c computations.

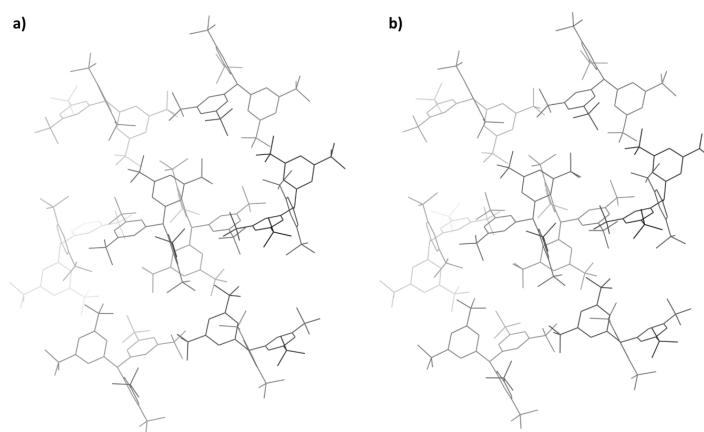


Figure A4.2.: Comparison of the wireframe representation of the unit cell of **1** obtained by a) neutron diffraction and b) solid state HSE-3c computations.

Table A4.1.: The Coordinates of the crystal structure of tri(3,5-di-tert-butylphenyl)methane optimized with the HSE-3c composite scheme in space group $P2_13$.

Element	x	y	z	Element	x	y	z
856							
H	13.360	3.458	8.991	H	11.273	7.096	15.794
H	20.600	6.367	13.321	H	13.796	8.454	16.959
H	16.269	-0.873	16.231	H	12.631	5.931	18.317
H	13.280	3.611	13.261	H	13.287	3.365	16.018

Continued on next page

Table A4.1 – Continued from previous page

Element	x	y	z	Element	x	y	z
H	16.329	6.447	13.474	H	13.572	6.440	13.229
H	16.116	3.398	16.311	H	16.362	6.155	16.303
H	16.986	3.861	11.204	H	14.374	5.353	15.216
H	18.387	2.741	13.724	H	9.020	3.498	16.226
H	15.866	1.340	12.605	H	13.364	10.707	13.361
H	15.948	3.463	6.537	H	16.229	6.363	20.571
H	23.053	3.779	13.326	H	6.589	6.110	16.177
H	16.264	-3.326	13.642	H	13.414	13.138	15.974
H	15.272	4.455	14.318	H	13.617	6.313	23.001
H	9.900	3.520	9.824	H	7.308	4.701	15.416
H	19.766	9.827	13.384	H	14.175	12.419	14.565
H	16.207	-0.039	19.690	H	15.026	5.552	22.282
H	14.745	2.524	7.409	H	7.448	4.935	17.161
H	22.181	4.982	12.387	H	12.429	12.279	14.799
H	17.203	-2.454	14.846	H	14.792	7.298	22.143
H	14.574	4.274	7.268	H	9.921	0.023	15.662
H	22.323	5.153	14.138	H	13.928	9.806	9.886
H	15.453	-2.596	15.016	H	19.704	5.799	19.670
H	17.758	2.482	7.851	H	7.917	7.926	17.118
H	21.739	1.969	12.346	H	12.473	11.810	17.789
H	17.245	-2.012	11.833	H	11.801	7.254	21.674
H	17.457	5.032	7.676	H	12.264	-0.041	15.859
H	21.915	2.270	14.896	H	13.732	7.463	9.823
H	14.695	-2.188	12.133	H	19.768	5.995	17.326
H	16.145	5.815	8.564	H	7.757	7.587	14.585
H	21.027	3.582	15.678	H	15.006	11.970	17.451
H	13.912	-1.300	13.446	H	12.140	4.721	21.833
H	17.805	2.591	9.605	H	8.594	6.225	13.827
H	19.986	1.922	12.454	H	15.763	11.133	16.089
H	17.136	-0.259	11.786	H	13.502	3.964	20.997
H	9.897	4.339	12.071	H	9.514	7.590	14.446
H	17.520	9.830	14.202	H	15.144	10.213	17.453
H	15.388	2.207	19.694	H	12.137	4.583	20.077
H	17.522	5.149	9.433	H	10.080	1.855	18.231
H	20.158	2.205	15.012	H	11.360	9.647	11.719
H	14.578	-0.431	12.069	H	17.872	8.367	19.511
H	16.634	1.532	8.824	H	12.534	1.269	14.711
H	20.767	3.093	11.396	H	14.879	7.193	11.133
H	18.195	-1.040	12.956	H	18.458	4.848	17.057
H	11.226	4.563	9.338	H	9.669	7.972	16.991
H	20.253	8.501	14.427	H	12.600	10.058	17.836
H	15.164	-0.526	18.364	H	11.755	7.127	19.922
H	10.173	1.853	11.682	H	8.901	6.829	18.088
H	17.909	9.554	11.716	H	11.502	10.826	16.692
H	17.874	1.818	19.418	H	12.898	8.225	20.690
H	11.307	2.823	9.048	H	13.267	1.319	16.307
H	20.543	8.420	12.686	H	13.283	6.460	11.183
H	16.904	-0.816	18.283	H	18.408	6.444	16.323
H	11.647	1.813	12.648	H	8.947	1.433	15.991
H	16.943	8.080	11.676	H	13.600	10.780	11.297
H	17.914	2.784	17.944	H	18.294	6.127	20.644
H	11.231	5.450	11.773	H	11.834	1.842	18.353
H	17.818	8.496	15.313	H	11.237	7.893	11.706
H	14.277	1.909	18.360	H	17.885	8.490	17.756

Continued on next page

A4. Supporting Information to Chapter 4

Table A4.1 – Continued from previous page

Element	x	y	z	Element	x	y	z
H	11.299	4.317	13.121	H	10.965	0.349	17.989
H	16.470	8.428	14.181	H	11.602	8.762	10.212
H	15.410	3.257	18.291	H	19.378	8.125	18.625
H	11.667	1.219	10.989	H	9.910	1.363	14.516
H	18.602	8.060	11.083	H	15.075	9.817	11.226
H	18.508	1.125	17.924	H	18.364	4.652	19.681
C	15.263	3.640	9.940	C	11.224	6.019	15.896
C	19.650	4.464	13.504	C	13.694	8.503	15.883
C	16.087	0.077	14.328	C	13.708	6.033	18.367
C	13.819	3.632	12.320	C	13.746	5.981	15.844
C	17.270	5.908	13.495	C	11.102	1.723	16.304
C	16.095	2.457	15.772	C	13.287	8.625	11.586
C	15.901	3.826	13.690	C	18.004	6.440	18.489
C	15.292	3.467	7.409	C	9.970	4.003	16.131
C	22.182	4.435	13.331	C	13.460	9.757	13.866
C	16.260	-2.455	14.299	C	15.724	6.267	19.620
C	17.137	2.498	8.749	C	9.902	1.110	15.577
C	20.842	2.590	12.362	C	14.013	9.825	10.974
C	17.229	-1.115	12.454	C	18.617	5.714	19.689
C	15.203	3.749	12.354	C	12.352	3.911	16.010
C	17.237	4.524	13.612	C	13.580	7.375	13.775
C	15.978	2.490	14.388	C	15.816	6.147	17.239
C	13.875	3.537	9.936	C	8.733	6.253	15.996
C	19.654	5.852	13.401	C	13.594	10.994	16.117
C	16.190	0.073	15.716	C	13.474	6.133	20.857
C	13.129	3.536	11.119	C	7.455	5.446	16.198
C	18.472	6.598	13.399	C	13.393	12.272	15.310
C	16.191	1.255	16.462	C	14.281	6.334	22.136
C	10.984	4.433	12.083	C	11.144	3.238	16.122
C	17.507	8.743	14.296	C	13.469	8.583	13.102
C	15.294	2.220	18.606	C	16.489	6.258	18.446
C	16.117	3.644	8.678	C	12.400	5.299	15.903
C	20.912	3.610	13.508	C	13.688	7.327	15.163
C	16.083	-1.185	13.474	C	14.428	6.039	17.190
C	11.608	3.394	11.141	C	10.987	1.426	17.805
C	18.449	8.119	13.258	C	11.786	8.740	11.289
C	16.333	1.278	17.982	C	18.301	7.941	18.603
C	15.909	3.758	11.167	C	8.648	6.956	14.636
C	18.424	3.818	13.621	C	14.954	11.079	16.819
C	15.969	1.303	13.681	C	12.771	4.773	20.943
C	16.854	4.986	8.586	C	9.987	5.387	16.017
C	21.005	2.873	14.849	C	13.574	9.740	15.251
C	14.741	-1.278	12.736	C	14.340	6.153	19.603
C	11.256	1.988	11.645	C	8.815	7.305	17.111
C	17.946	8.471	11.852	C	12.480	10.912	17.168
C	17.739	1.781	18.334	C	12.422	7.247	20.776
C	10.987	3.586	9.760	C	12.364	1.042	15.765
C	19.831	8.740	13.449	C	13.825	7.363	10.906
C	16.141	-0.104	18.604	C	18.685	5.902	17.227
H	16.231	16.269	-0.873	H	18.317	12.631	5.931
H	8.991	13.360	3.458	H	15.794	11.273	7.096
H	13.321	20.600	6.367	H	16.959	13.796	8.454
H	16.311	16.116	3.398	H	16.303	16.362	6.155
H	13.261	13.280	3.611	H	16.018	13.287	3.365

Continued on next page

Table A4.1 – Continued from previous page

Element	x	y	z	Element	x	y	z
H	13.474	16.329	6.447	H	13.229	13.572	6.440
H	12.605	15.866	1.340	H	15.216	14.374	5.353
H	11.204	16.986	3.861	H	20.571	16.229	6.363
H	13.724	18.387	2.741	H	16.226	9.020	3.498
H	13.642	16.264	-3.326	H	13.361	13.364	10.707
H	6.537	15.948	3.463	H	23.001	13.617	6.313
H	13.326	23.053	3.779	H	16.177	6.589	6.110
H	14.318	15.272	4.455	H	15.974	13.414	13.138
H	19.690	16.207	-0.039	H	22.282	15.026	5.552
H	9.824	9.900	3.520	H	15.416	7.308	4.701
H	13.384	19.766	9.827	H	14.565	14.175	12.419
H	14.846	17.203	-2.454	H	22.143	14.792	7.298
H	7.409	14.745	2.524	H	17.161	7.448	4.935
H	12.387	22.181	4.982	H	14.799	12.429	12.279
H	15.016	15.453	-2.596	H	19.670	19.704	5.799
H	7.268	14.574	4.274	H	15.662	9.921	0.023
H	14.138	22.323	5.153	H	9.886	13.928	9.806
H	11.833	17.245	-2.012	H	21.674	11.801	7.254
H	7.851	17.758	2.482	H	17.118	7.917	7.926
H	12.346	21.739	1.969	H	17.789	12.473	11.810
H	12.133	14.695	-2.188	H	17.326	19.768	5.995
H	7.676	17.457	5.032	H	15.859	12.264	-0.041
H	14.896	21.915	2.270	H	9.823	13.732	7.463
H	13.446	13.912	-1.300	H	21.833	12.140	4.721
H	8.564	16.145	5.815	H	14.585	7.757	7.587
H	15.678	21.027	3.582	H	17.451	15.006	11.970
H	11.786	17.136	-0.259	H	20.997	13.502	3.964
H	9.605	17.805	2.591	H	13.827	8.594	6.225
H	12.454	19.986	1.922	H	16.089	15.763	11.133
H	19.694	15.388	2.207	H	20.077	12.137	4.583
H	12.071	9.897	4.339	H	14.446	9.514	7.590
H	14.202	17.520	9.830	H	17.453	15.144	10.213
H	12.069	14.578	-0.431	H	19.511	17.872	8.367
H	9.433	17.522	5.149	H	18.231	10.080	1.855
H	15.012	20.158	2.205	H	11.719	11.360	9.647
H	12.956	18.195	-1.040	H	17.057	18.458	4.848
H	8.824	16.634	1.532	H	14.711	12.534	1.269
H	11.396	20.767	3.093	H	11.133	14.879	7.193
H	18.364	15.164	-0.526	H	19.922	11.755	7.127
H	9.338	11.226	4.563	H	16.991	9.669	7.972
H	14.427	20.253	8.501	H	17.836	12.600	10.058
H	19.418	17.874	1.818	H	20.690	12.898	8.225
H	11.682	10.173	1.853	H	18.088	8.901	6.829
H	11.716	17.909	9.554	H	16.692	11.502	10.826
H	18.283	16.904	-0.816	H	16.323	18.408	6.444
H	9.048	11.307	2.823	H	16.307	13.267	1.319
H	12.686	20.543	8.420	H	11.183	13.283	6.460
H	17.944	17.914	2.784	H	20.644	18.294	6.127
H	12.648	11.647	1.813	H	15.991	8.947	1.433
H	11.676	16.943	8.080	H	11.297	13.600	10.780
H	18.360	14.277	1.909	H	17.756	17.885	8.490
H	11.773	11.231	5.450	H	18.353	11.834	1.842
H	15.313	17.818	8.496	H	11.706	11.237	7.893
H	18.291	15.410	3.257	H	18.625	19.378	8.125

Continued on next page

A4. Supporting Information to Chapter 4

Table A4.1 – Continued from previous page

Element	x	y	z	Element	x	y	z
H	13.121	11.299	4.317	H	17.989	10.965	0.349
H	14.181	16.470	8.428	H	10.212	11.602	8.762
H	17.924	18.508	1.125	H	19.681	18.364	4.652
H	10.989	11.667	1.219	H	14.516	9.910	1.363
H	11.083	18.602	8.060	H	11.226	15.075	9.817
C	14.328	16.087	0.077	C	18.367	13.708	6.033
C	9.940	15.263	3.640	C	15.896	11.224	6.019
C	13.504	19.650	4.464	C	15.883	13.694	8.503
C	15.772	16.095	2.457	C	15.844	13.746	5.981
C	12.320	13.819	3.632	C	18.489	18.004	6.440
C	13.495	17.270	5.908	C	16.304	11.102	1.723
C	13.690	15.901	3.826	C	11.586	13.287	8.625
C	14.299	16.260	-2.455	C	19.620	15.724	6.267
C	7.409	15.292	3.467	C	16.131	9.970	4.003
C	13.331	22.182	4.435	C	13.866	13.460	9.757
C	12.454	17.229	-1.115	C	19.689	18.617	5.714
C	8.749	17.137	2.498	C	15.577	9.902	1.110
C	12.362	20.842	2.590	C	10.974	14.013	9.825
C	14.388	15.978	2.490	C	17.239	15.816	6.147
C	12.354	15.203	3.749	C	16.010	12.352	3.911
C	13.612	17.237	4.524	C	13.775	13.580	7.375
C	15.716	16.190	0.073	C	20.857	13.474	6.133
C	9.936	13.875	3.537	C	15.996	8.733	6.253
C	13.401	19.654	5.852	C	16.117	13.594	10.994
C	16.462	16.191	1.255	C	22.136	14.281	6.334
C	11.119	13.129	3.536	C	16.198	7.455	5.446
C	13.399	18.472	6.598	C	15.310	13.393	12.272
C	18.606	15.294	2.220	C	18.446	16.489	6.258
C	12.083	10.984	4.433	C	16.122	11.144	3.238
C	14.296	17.507	8.743	C	13.102	13.469	8.583
C	13.474	16.083	-1.185	C	17.190	14.428	6.039
C	8.678	16.117	3.644	C	15.903	12.400	5.299
C	13.508	20.912	3.610	C	15.163	13.688	7.327
C	17.982	16.333	1.278	C	18.603	18.301	7.941
C	11.141	11.608	3.394	C	17.805	10.987	1.426
C	13.258	18.449	8.119	C	11.289	11.786	8.740
C	13.681	15.969	1.303	C	20.943	12.771	4.773
C	11.167	15.909	3.758	C	14.636	8.648	6.956
C	13.621	18.424	3.818	C	16.819	14.954	11.079
C	12.736	14.741	-1.278	C	19.603	14.340	6.153
C	8.586	16.854	4.986	C	16.017	9.987	5.387
C	14.849	21.005	2.873	C	15.251	13.574	9.740
C	18.334	17.739	1.781	C	20.776	12.422	7.247
C	11.645	11.256	1.988	C	17.111	8.815	7.305
C	11.852	17.946	8.471	C	17.168	12.480	10.912
C	18.604	16.141	-0.104	C	17.227	18.685	5.902
C	9.760	10.987	3.586	C	15.765	12.364	1.042
C	13.449	19.831	8.740	C	10.906	13.825	7.363
H	3.496	6.406	10.736	H	1.410	2.768	3.933
H	6.406	10.736	3.496	H	2.768	3.933	1.410
H	10.736	3.496	6.406	H	3.933	1.410	2.768
H	3.416	6.253	6.466	H	3.424	6.498	3.709
H	6.253	6.466	3.416	H	6.498	3.709	3.424
H	6.466	3.416	6.253	H	3.709	3.424	6.498

Continued on next page

Table A4.1 – Continued from previous page

Element	x	y	z	Element	x	y	z
H	7.122	6.003	8.523	H	4.511	4.511	4.511
H	6.003	8.523	7.122	H	-0.844	6.366	3.501
H	8.523	7.122	6.003	H	6.366	3.501	-0.844
H	6.085	6.401	13.190	H	3.501	-0.844	6.366
H	6.401	13.190	6.085	H	-3.274	3.753	3.550
H	13.190	6.085	6.401	H	3.753	3.550	-3.274
H	5.409	5.409	5.409	H	3.550	-3.274	3.753
H	0.037	6.343	9.903	H	-2.555	5.162	4.311
H	6.343	9.903	0.037	H	5.162	4.311	-2.555
H	9.903	0.037	6.343	H	4.311	-2.555	5.162
H	4.881	7.340	12.318	H	-2.416	4.928	2.566
H	7.340	12.318	4.881	H	4.928	2.566	-2.416
H	12.318	4.881	7.340	H	2.566	-2.416	4.928
H	4.711	5.589	12.459	H	0.057	9.841	4.065
H	5.589	12.459	4.711	H	9.841	4.065	0.057
H	12.459	4.711	5.589	H	4.065	0.057	9.841
H	7.894	7.381	11.876	H	-1.947	1.938	2.609
H	7.381	11.876	7.894	H	1.938	2.609	-1.947
H	11.876	7.894	7.381	H	2.609	-1.947	1.938
H	7.594	4.831	12.051	H	2.401	9.904	3.868
H	4.831	12.051	7.594	H	9.904	3.868	2.401
H	12.051	7.594	4.831	H	3.868	2.401	9.904
H	6.281	4.049	11.163	H	-2.106	2.276	5.142
H	4.049	11.163	6.281	H	2.276	5.142	-2.106
H	11.163	6.281	4.049	H	5.142	-2.106	2.276
H	7.941	7.273	10.122	H	-1.270	3.638	5.900
H	7.273	10.122	7.941	H	3.638	5.900	-1.270
H	10.122	7.941	7.273	H	5.900	-1.270	3.638
H	0.033	5.525	7.656	H	-0.350	2.274	5.281
H	5.525	7.656	0.033	H	2.274	5.281	-0.350
H	7.656	0.033	5.525	H	5.281	-0.350	2.274
H	7.658	4.715	10.294	H	0.216	8.008	1.496
H	4.715	10.294	7.658	H	8.008	1.496	0.216
H	10.294	7.658	4.715	H	1.496	0.216	8.008
H	6.771	8.331	10.903	H	2.670	8.594	5.016
H	8.331	10.903	6.771	H	8.594	5.016	2.670
H	10.903	6.771	8.331	H	5.016	2.670	8.594
H	1.363	5.300	10.389	H	-0.195	1.891	2.736
H	5.300	10.389	1.363	H	1.891	2.736	-0.195
H	10.389	1.363	5.300	H	2.736	-0.195	1.891
H	0.309	8.011	8.045	H	-0.963	3.035	1.639
H	8.011	8.045	0.309	H	3.035	1.639	-0.963
H	8.045	0.309	8.011	H	1.639	-0.963	3.035
H	1.444	7.041	10.679	H	3.404	8.544	3.420
H	7.041	10.679	1.444	H	8.544	3.420	3.404
H	10.679	1.444	7.041	H	3.420	3.404	8.544
H	1.783	8.051	7.079	H	-0.917	8.430	3.736
H	8.051	7.079	1.783	H	8.430	3.736	-0.917
H	7.079	1.783	8.051	H	3.736	-0.917	8.430
H	1.367	4.414	7.954	H	1.971	8.021	1.374
H	4.414	7.954	1.367	H	8.021	1.374	1.971
H	7.954	1.367	4.414	H	1.374	1.971	8.021
H	1.436	5.546	6.606	H	1.102	9.515	1.738
H	5.546	6.606	1.436	H	9.515	1.738	1.102

Continued on next page

A4. Supporting Information to Chapter 4

Table A4.1 – Continued from previous page

Element	x	y	z	Element	x	y	z
H	6.606	1.436	5.546	H	1.738	1.102	9.515
H	1.803	8.644	8.738	H	0.046	8.501	5.211
H	8.644	8.738	1.803	H	8.501	5.211	0.046
H	8.738	1.803	8.644	H	5.211	0.046	8.501
C	5.399	6.223	9.787	C	1.360	3.844	3.831
C	6.223	9.787	5.399	C	3.844	3.831	1.360
C	9.787	5.399	6.223	C	3.831	1.360	3.844
C	3.955	6.232	7.407	C	3.883	3.883	3.883
C	6.232	7.407	3.955	C	1.238	8.141	3.423
C	7.407	3.955	6.232	C	8.141	3.423	1.238
C	6.037	6.037	6.037	C	3.423	1.238	8.141
C	5.428	6.396	12.318	C	0.107	5.861	3.596
C	6.396	12.318	5.428	C	5.861	3.596	0.107
C	12.318	5.428	6.396	C	3.596	0.107	5.861
C	7.273	7.365	10.978	C	0.038	8.753	4.150
C	7.365	10.978	7.273	C	8.753	4.150	0.038
C	10.978	7.273	7.365	C	4.150	0.038	8.753
C	5.339	6.115	7.373	C	2.488	5.952	3.717
C	6.115	7.373	5.339	C	5.952	3.717	2.488
C	7.373	5.339	6.115	C	3.717	2.488	5.952
C	4.011	6.326	9.791	C	-1.130	3.610	3.731
C	6.326	9.791	4.011	C	3.610	3.731	-1.130
C	9.791	4.011	6.326	C	3.731	-1.130	3.610
C	3.265	6.328	8.608	C	-2.409	4.417	3.529
C	6.328	8.608	3.265	C	4.417	3.529	-2.409
C	8.608	3.265	6.328	C	3.529	-2.409	4.417
C	1.121	5.431	7.644	C	1.281	6.625	3.605
C	5.431	7.644	1.121	C	6.625	3.605	1.281
C	7.644	1.121	5.431	C	3.605	1.281	6.625
C	6.253	6.219	11.049	C	2.537	4.564	3.824
C	6.219	11.049	6.253	C	4.564	3.824	2.537
C	11.049	6.253	6.219	C	3.824	2.537	4.564
C	1.745	6.469	8.586	C	1.124	8.438	1.922
C	6.469	8.586	1.745	C	8.438	1.922	1.124
C	8.586	1.745	6.469	C	1.922	1.124	8.438
C	6.046	6.106	8.560	C	-1.216	2.908	5.091
C	6.106	8.560	6.046	C	2.908	5.091	-1.216
C	8.560	6.046	6.106	C	5.091	-1.216	2.908
C	6.991	4.878	11.141	C	0.124	4.476	3.710
C	4.878	11.141	6.991	C	4.476	3.710	0.124
C	11.141	6.991	4.878	C	3.710	0.124	4.476
C	1.393	7.875	8.082	C	-1.049	2.559	2.616
C	7.875	8.082	1.393	C	2.559	2.616	-1.049
C	8.082	1.393	7.875	C	2.616	-1.049	2.559
C	1.123	6.278	9.967	C	2.500	8.821	3.962
C	6.278	9.967	1.123	C	8.821	3.962	2.500
C	9.967	1.123	6.278	C	3.962	2.500	8.821
H	6.367	13.321	20.600	H	8.454	16.959	13.796
H	3.458	8.991	13.360	H	7.096	15.794	11.273
H	-0.873	16.231	16.269	H	5.931	18.317	12.631
H	6.447	13.474	16.329	H	6.440	13.229	13.572
H	3.611	13.261	13.280	H	3.365	16.018	13.287
H	3.398	16.311	16.116	H	6.155	16.303	16.362
H	2.741	13.724	18.387	H	5.353	15.216	14.374

Continued on next page

Table A4.1 – Continued from previous page

Element	x	y	z	Element	x	y	z
H	3.861	11.204	16.986	H	10.707	13.361	13.364
H	1.340	12.605	15.866	H	3.498	16.226	9.020
H	3.779	13.326	23.053	H	6.363	20.571	16.229
H	3.463	6.537	15.948	H	13.138	15.974	13.414
H	-3.326	13.642	16.264	H	6.110	16.177	6.589
H	4.455	14.318	15.272	H	6.313	23.001	13.617
H	9.827	13.384	19.766	H	12.419	14.565	14.175
H	3.520	9.824	9.900	H	4.701	15.416	7.308
H	-0.039	19.690	16.207	H	5.552	22.282	15.026
H	4.982	12.387	22.181	H	12.279	14.799	12.429
H	2.524	7.409	14.745	H	4.935	17.161	7.448
H	-2.454	14.846	17.203	H	7.298	22.143	14.792
H	5.153	14.138	22.323	H	9.806	9.886	13.928
H	4.274	7.268	14.574	H	0.023	15.662	9.921
H	-2.596	15.016	15.453	H	5.799	19.670	19.704
H	1.969	12.346	21.739	H	11.810	17.789	12.473
H	2.482	7.851	17.758	H	7.926	17.118	7.917
H	-2.012	11.833	17.245	H	7.254	21.674	11.801
H	2.270	14.896	21.915	H	7.463	9.823	13.732
H	5.032	7.676	17.457	H	-0.041	15.859	12.264
H	-2.188	12.133	14.695	H	5.995	17.326	19.768
H	3.582	15.678	21.027	H	11.970	17.451	15.006
H	5.815	8.564	16.145	H	7.587	14.585	7.757
H	-1.300	13.446	13.912	H	4.721	21.833	12.140
H	1.922	12.454	19.986	H	11.133	16.089	15.763
H	2.591	9.605	17.805	H	6.225	13.827	8.594
H	-0.259	11.786	17.136	H	3.964	20.997	13.502
H	9.830	14.202	17.520	H	10.213	17.453	15.144
H	4.339	12.071	9.897	H	7.590	14.446	9.514
H	2.207	19.694	15.388	H	4.583	20.077	12.137
H	2.205	15.012	20.158	H	9.647	11.719	11.360
H	5.149	9.433	17.522	H	1.855	18.231	10.080
H	-0.431	12.069	14.578	H	8.367	19.511	17.872
H	3.093	11.396	20.767	H	7.193	11.133	14.879
H	1.532	8.824	16.634	H	1.269	14.711	12.534
H	-1.040	12.956	18.195	H	4.848	17.057	18.458
H	8.501	14.427	20.253	H	10.058	17.836	12.600
H	4.563	9.338	11.226	H	7.972	16.991	9.669
H	-0.526	18.364	15.164	H	7.127	19.922	11.755
H	9.554	11.716	17.909	H	10.826	16.692	11.502
H	1.853	11.682	10.173	H	6.829	18.088	8.901
H	1.818	19.418	17.874	H	8.225	20.690	12.898
H	8.420	12.686	20.543	H	6.460	11.183	13.283
H	2.823	9.048	11.307	H	1.319	16.307	13.267
H	-0.816	18.283	16.904	H	6.444	16.323	18.408
H	8.080	11.676	16.943	H	10.780	11.297	13.600
H	1.813	12.648	11.647	H	1.433	15.991	8.947
H	2.784	17.944	17.914	H	6.127	20.644	18.294
H	8.496	15.313	17.818	H	7.893	11.706	11.237
H	5.450	11.773	11.231	H	1.842	18.353	11.834
H	1.909	18.360	14.277	H	8.490	17.756	17.885
H	8.428	14.181	16.470	H	8.762	10.212	11.602
H	4.317	13.121	11.299	H	0.349	17.989	10.965
H	3.257	18.291	15.410	H	8.125	18.625	19.378

Continued on next page

A4. Supporting Information to Chapter 4

Table A4.1 – Continued from previous page

Element	x	y	z	Element	x	y	z
H	8.060	11.083	18.602	H	9.817	11.226	15.075
H	1.219	10.989	11.667	H	1.363	14.516	9.910
H	1.125	17.924	18.508	H	4.652	19.681	18.364
C	4.464	13.504	19.650	C	8.503	15.883	13.694
C	3.640	9.940	15.263	C	6.019	15.896	11.224
C	0.077	14.328	16.087	C	6.033	18.367	13.708
C	5.908	13.495	17.270	C	5.981	15.844	13.746
C	3.632	12.320	13.819	C	8.625	11.586	13.287
C	2.457	15.772	16.095	C	1.723	16.304	11.102
C	3.826	13.690	15.901	C	6.440	18.489	18.004
C	4.435	13.331	22.182	C	9.757	13.866	13.460
C	3.467	7.409	15.292	C	4.003	16.131	9.970
C	-2.455	14.299	16.260	C	6.267	19.620	15.724
C	2.590	12.362	20.842	C	9.825	10.974	14.013
C	2.498	8.749	17.137	C	1.110	15.577	9.902
C	-1.115	12.454	17.229	C	5.714	19.689	18.617
C	4.524	13.612	17.237	C	7.375	13.775	13.580
C	3.749	12.354	15.203	C	3.911	16.010	12.352
C	2.490	14.388	15.978	C	6.147	17.239	15.816
C	5.852	13.401	19.654	C	10.994	16.117	13.594
C	3.537	9.936	13.875	C	6.253	15.996	8.733
C	0.073	15.716	16.190	C	6.133	20.857	13.474
C	6.598	13.399	18.472	C	12.272	15.310	13.393
C	3.536	11.119	13.129	C	5.446	16.198	7.455
C	1.255	16.462	16.191	C	6.334	22.136	14.281
C	8.743	14.296	17.507	C	8.583	13.102	13.469
C	4.433	12.083	10.984	C	3.238	16.122	11.144
C	2.220	18.606	15.294	C	6.258	18.446	16.489
C	3.610	13.508	20.912	C	7.327	15.163	13.688
C	3.644	8.678	16.117	C	5.299	15.903	12.400
C	-1.185	13.474	16.083	C	6.039	17.190	14.428
C	8.119	13.258	18.449	C	8.740	11.289	11.786
C	3.394	11.141	11.608	C	1.426	17.805	10.987
C	1.278	17.982	16.333	C	7.941	18.603	18.301
C	3.818	13.621	18.424	C	11.079	16.819	14.954
C	3.758	11.167	15.909	C	6.956	14.636	8.648
C	1.303	13.681	15.969	C	4.773	20.943	12.771
C	2.873	14.849	21.005	C	9.740	15.251	13.574
C	4.986	8.586	16.854	C	5.387	16.017	9.987
C	-1.278	12.736	14.741	C	6.153	19.603	14.340
C	8.471	11.852	17.946	C	10.912	17.168	12.480
C	1.988	11.645	11.256	C	7.305	17.111	8.815
C	1.781	18.334	17.739	C	7.247	20.776	12.422
C	8.740	13.449	19.831	C	7.363	10.906	13.825
C	3.586	9.760	10.987	C	1.042	15.765	12.364
C	-0.104	18.604	16.141	C	5.902	17.227	18.685

A4.2.2. Gas Phase Structures

Table A4.2.: The Coordinates of the crystal structure of tri(3,5-di-tert-butylphenyl)methane optimized with the HSE-3c composite scheme in space group $P2_13$.

Element	x	y	z	Element	x	y	z
214							
H	10.331	10.333	10.331	H	9.389	9.385	9.389
H	11.364	11.366	8.376	H	8.357	8.353	11.344
H	8.377	11.366	11.365	H	11.343	8.354	8.354
H	11.364	8.378	11.362	H	8.353	11.341	8.360
H	15.621	11.042	8.317	H	4.099	8.672	11.403
H	8.319	15.623	11.041	H	11.402	4.096	8.671
H	11.040	8.316	15.619	H	8.672	11.405	4.102
H	13.482	10.654	11.990	H	6.238	9.063	7.731
H	11.991	13.483	10.654	H	7.730	6.235	9.065
H	10.654	11.990	13.483	H	9.066	7.730	6.237
H	14.723	11.409	4.913	H	4.995	8.304	14.807
H	4.912	14.722	11.382	H	14.807	4.994	8.316
H	11.393	4.910	14.716	H	8.307	14.808	5.003
H	15.098	10.188	6.125	H	4.610	9.519	13.593
H	6.128	15.083	10.161	H	13.591	4.619	9.534
H	10.169	6.123	15.081	H	9.527	13.596	4.624
H	15.613	11.863	6.353	H	4.112	7.839	13.365
H	6.348	15.621	11.830	H	13.367	4.105	7.858
H	11.839	6.348	15.614	H	7.850	13.368	4.113
H	12.388	10.903	4.897	H	7.327	8.836	14.823
H	4.898	12.383	10.912	H	14.822	7.328	8.824
H	10.916	4.897	12.377	H	8.819	14.822	7.338
H	12.564	9.635	6.108	H	7.137	10.098	13.608
H	6.112	12.537	9.644	H	13.606	7.154	10.088
H	9.645	6.108	12.537	H	10.086	13.611	7.157
H	11.380	10.916	6.328	H	8.335	8.830	13.392
H	6.327	11.374	10.945	H	13.392	8.338	8.805
H	10.941	6.328	11.370	H	8.808	13.390	8.344
H	12.199	13.293	6.925	H	7.541	6.441	12.804
H	6.926	12.229	13.307	H	12.799	7.519	6.428
H	13.306	6.929	12.218	H	6.429	12.795	7.531
H	13.113	13.285	5.417	H	6.626	6.446	14.311
H	5.416	13.140	13.285	H	14.308	6.606	6.440
H	13.289	5.420	13.129	H	6.436	14.304	6.618
H	13.921	13.651	6.943	H	5.823	6.065	12.786
H	6.942	13.956	13.641	H	12.782	5.797	6.069
H	13.644	6.946	13.944	H	6.066	12.778	5.810
H	16.844	9.053	12.292	H	2.874	10.661	7.430
H	12.294	16.845	9.054	H	7.431	2.871	10.663
H	9.057	12.293	16.845	H	10.664	7.434	2.873
H	15.802	8.428	11.010	H	3.913	11.287	8.713
H	11.012	15.805	8.428	H	8.716	3.908	11.287
H	8.428	11.014	15.802	H	11.290	8.715	3.914
H	15.094	9.190	12.428	H	4.623	10.527	7.295
H	12.429	15.096	9.190	H	7.297	4.621	10.532
H	9.194	12.431	15.096	H	10.530	7.297	4.623
H	16.232	12.689	11.571	H	3.493	7.025	8.146

Continued on next page

A4. Supporting Information to Chapter 4

Table A4.2 – Continued from previous page

Element	x	y	z	Element	x	y	z
H	11.574	16.233	12.690	H	8.140	3.493	7.026
H	12.691	11.565	16.233	H	7.028	8.149	3.491
H	17.089	11.565	12.628	H	2.632	8.148	7.092
H	12.631	17.090	11.566	H	7.087	2.631	8.151
H	11.569	12.624	17.091	H	8.152	7.095	2.630
H	15.343	11.741	12.758	H	4.379	7.977	6.960
H	12.760	15.343	11.741	H	6.957	4.378	7.982
H	11.746	12.754	15.344	H	7.980	6.962	4.376
H	17.188	9.801	9.358	H	2.529	9.909	10.362
H	9.361	17.191	9.803	H	10.361	2.524	9.905
H	9.799	9.357	17.187	H	9.912	10.366	2.531
H	18.132	10.412	10.710	H	1.587	9.297	9.010
H	10.712	18.134	10.414	H	9.008	1.584	9.293
H	10.412	10.707	18.132	H	9.301	9.015	1.587
H	17.376	11.542	9.598	H	2.345	8.167	10.122
H	9.600	17.378	11.544	H	10.118	2.344	8.164
H	11.540	9.593	17.375	H	8.171	10.126	2.346
C	10.962	10.963	10.962	C	8.758	8.756	8.758
C	12.300	11.002	10.256	C	7.420	8.716	9.464
C	10.257	12.301	11.001	C	9.463	7.418	8.717
C	11.001	10.257	12.299	C	8.718	9.463	7.421
C	12.312	11.213	8.881	C	7.409	8.505	10.840
C	8.881	12.314	11.212	C	10.839	7.406	8.505
C	11.211	8.881	12.310	C	8.506	10.838	7.411
C	13.498	11.242	8.161	C	6.222	8.475	11.560
C	8.162	13.500	11.240	C	11.558	6.219	8.476
C	11.239	8.161	13.496	C	8.476	11.559	6.225
C	14.689	11.039	8.861	C	5.031	8.676	10.859
C	8.863	14.691	11.039	C	10.858	5.028	8.675
C	11.038	8.860	14.688	C	8.677	10.860	5.033
C	14.713	10.828	10.235	C	5.007	8.887	9.486
C	10.236	14.715	10.828	C	9.484	5.004	8.887
C	10.828	10.234	14.712	C	8.889	9.487	5.008
C	13.499	10.821	10.921	C	6.221	8.896	8.800
C	10.922	13.501	10.821	C	8.799	6.218	8.897
C	10.820	10.921	13.499	C	8.899	8.800	6.221
C	13.469	11.537	6.664	C	6.253	8.185	13.057
C	6.665	13.473	11.533	C	13.056	6.249	8.184
C	11.536	6.664	13.467	C	8.182	13.056	6.257
C	14.804	11.230	5.986	C	4.914	8.480	13.733
C	5.985	14.803	11.206	C	13.733	4.913	8.492
C	11.214	5.983	14.798	C	8.485	13.735	4.921
C	12.386	10.702	5.970	C	7.326	9.034	13.749
C	5.972	12.378	10.714	C	13.748	7.331	9.021
C	10.715	5.970	12.374	C	9.019	13.749	7.337
C	13.157	13.027	6.477	C	6.580	6.699	13.250
C	6.477	13.182	13.028	C	13.247	6.561	6.694
C	13.030	6.480	13.172	C	6.692	13.243	6.573
C	16.004	10.596	11.013	C	3.716	9.118	8.707
C	11.015	16.005	10.597	C	8.706	3.713	9.118
C	10.597	11.012	16.004	C	9.121	8.710	3.716
C	15.928	9.240	11.727	C	3.790	10.475	7.995
C	11.729	15.930	9.241	C	7.996	3.786	10.476
C	9.243	11.729	15.929	C	10.478	7.997	3.790

Continued on next page

Table A4.2 – Continued from previous page

Element	x	y	z	Element	x	y	z
C	16.173	11.712	12.052	C	3.549	8.003	7.667
C	12.055	16.174	11.713	C	7.663	3.548	8.005
C	11.715	12.048	16.174	C	8.006	7.669	3.547
C	17.238	10.590	10.111	C	2.482	9.121	9.609
C	10.114	17.239	10.591	C	9.606	2.479	9.118
C	10.589	10.109	17.237	C	9.124	9.613	2.483

A4.2.3. Determination of the Dissociation Energies

Dissociation energies of the dimers to two monomers were obtained by the following equation:

$$E_d = 2 \cdot E(\text{Monomer}) - E(\text{Dimer}) \quad (\text{A4.1})$$

Tri(3,5-di-tert-butylphenyl)methane dimer

Table A4.3.: Energies for tri(3,5-di-tert-butylphenyl)methane and the corresponding dimer at the B3LYP-D3(BJ)-ATM/def2-TZVPP level. Thermostatistical corrections at the PBEh-3c level.

Energy	Unit	Monomer	Dimer
EE	Hartree	-1676.8746179	-3353.7934933
U	Hartree	-1675.9300409	-3351.9033033
H	Hartree	-1675.8798279	-3351.8020233
S	cal mol ⁻¹	259.003	454.653
G ^{298K}	Hartree	-1676.0028889	-3352.0180433
C-H...H-C	Å	n/a	1.601

Table A4.4.: Coordinates of the structure of tri(3,5-di-tert-butylphenyl)methane optimized at B3LYP-D3(BJ)-ATM/def2-TZVPP.

Element	x	y	z	Element	x	y	z
107							
C	-0.803	4.014	2.919	H	-3.360	1.405	4.886
C	-0.035	3.808	1.777	H	-3.994	4.350	5.406
C	0.182	2.490	1.368	H	-4.026	3.622	3.794
C	-0.346	1.416	2.069	H	-3.077	5.079	4.087
C	-1.118	1.660	3.203	H	-1.886	4.212	6.829
C	-1.355	2.956	3.648	H	-0.941	4.939	5.529
C	1.395	-0.412	2.061	H	-0.448	3.390	6.208
C	2.067	-1.391	1.345	H	5.305	-3.724	2.515
C	3.321	-1.860	1.746	H	6.068	-2.479	1.518
C	3.880	-1.311	2.896	H	5.840	-4.106	0.882
C	3.232	-0.319	3.641	H	3.276	-2.212	-0.997

Continued on next page

A4. Supporting Information to Chapter 4

Table A4.4 – Continued from previous page

Element	x	y	z	Element	x	y	z
C	1.989	0.122	3.203	H	4.716	-3.223	-1.115
C	-1.889	-2.632	3.667	H	4.845	-1.558	-0.531
C	-0.888	-1.778	3.219	H	2.977	-4.585	1.925
C	-1.058	-1.006	2.071	H	3.611	-5.003	0.328
C	-2.243	-1.108	1.358	H	2.156	-4.014	0.474
C	-3.273	-1.958	1.770	H	3.566	1.689	6.466
C	-3.073	-2.706	2.926	H	2.079	0.936	5.895
C	-0.005	-0.001	1.626	H	2.877	2.171	4.917
C	0.582	4.959	0.975	H	5.749	1.254	5.426
C	-2.186	3.250	4.900	H	5.135	1.668	3.820
C	4.017	-2.951	0.927	H	5.929	0.117	4.090
C	3.898	0.237	4.903	H	4.583	-0.530	6.821
C	-1.735	-3.475	4.936	H	4.747	-1.691	5.502
C	-4.568	-2.025	0.954	H	3.156	-1.361	6.185
C	0.229	6.333	1.556	H	-0.309	-3.894	6.502
C	0.068	4.904	-0.476	H	-0.224	-2.235	5.915
C	2.115	4.813	0.980	H	0.450	-3.550	4.949
C	-2.716	1.971	5.560	H	-1.772	-5.582	5.478
C	-3.392	4.130	4.522	H	-1.110	-5.269	3.868
C	-1.311	3.995	5.926	H	-2.850	-5.185	4.140
C	5.387	-3.331	1.501	H	-2.739	-3.671	6.858
C	4.223	-2.454	-0.517	H	-3.830	-3.249	5.537
C	3.134	-4.213	0.912	H	-2.752	-2.026	6.207
C	3.049	1.321	5.579	H	-5.877	-2.741	2.552
C	5.261	0.854	4.535	H	-5.181	-4.033	1.565
C	4.110	-0.907	5.912	H	-6.478	-3.030	0.923
C	-0.372	-3.271	5.609	H	-3.562	-1.769	-0.975
C	-1.878	-4.968	4.582	H	-5.157	-2.514	-1.082
C	-2.833	-3.081	5.943	H	-3.777	-3.451	-0.493
C	-5.579	-3.018	1.540	H	-5.464	-0.300	1.939
C	-4.244	-2.464	-0.486	H	-6.146	-0.656	0.346
C	-5.222	-0.631	0.928	H	-4.564	0.114	0.482
H	0.597	6.447	2.576	H	-0.010	0.000	0.533
H	-0.848	6.506	1.559	H	-0.984	5.023	3.255
H	0.688	7.115	0.949	H	0.789	2.288	0.494
H	0.331	3.965	-0.961	H	-1.530	0.818	3.734
H	0.501	5.717	-1.062	H	1.591	-1.805	0.465
H	-1.018	5.003	-0.505	H	4.846	-1.657	3.228
H	2.503	4.852	1.999	H	1.460	0.888	3.745
H	2.575	5.622	0.408	H	0.041	-1.697	3.759
H	2.431	3.868	0.539	H	-2.367	-0.497	0.473
H	-3.303	2.231	6.442	H	-3.854	-3.368	3.265
H	-1.904	1.317	5.883				

Table A4.5.: Coordinates of the structure of tri(3,5-di-tert-butylphenyl)methane dimer optimized at B3LYP-D3(BJ)-ATM/def2-TZVPP.

Element	x	y	z	Element	x	y	z
214							
C	-0.804	4.083	2.896	H	2.450	-3.060	-0.668
C	0.001	3.799	1.794	H	4.035	-3.656	-1.112
C	0.253	2.457	1.508	H	3.761	-1.921	-0.943

Continued on next page

Table A4.5 – Continued from previous page

Element	x	y	z	Element	x	y	z
C	-0.296	1.436	2.276	H	3.804	-4.484	2.542
C	-1.102	1.756	3.363	H	3.937	-5.179	0.920
C	-1.365	3.082	3.694	H	2.412	-4.467	1.459
C	1.394	-0.463	2.277	H	3.921	1.647	6.484
C	2.004	-1.448	1.509	H	2.409	0.847	6.061
C	3.292	-1.902	1.796	H	3.060	2.117	5.021
C	3.940	-1.347	2.899	H	5.997	1.303	5.188
C	3.354	-0.361	3.696	H	5.178	1.703	3.672
C	2.074	0.075	3.365	H	6.056	0.183	3.826
C	-1.988	-2.725	3.694	H	5.066	-0.515	6.703
C	-0.970	-1.835	3.363	H	5.128	-1.671	5.373
C	-1.095	-0.976	2.276	H	3.613	-1.406	6.233
C	-2.254	-1.010	1.508	H	-0.533	-4.226	6.478
C	-3.291	-1.898	1.795	H	-0.463	-2.517	6.056
C	-3.136	-2.737	2.897	H	0.304	-3.719	5.013
C	0.001	-0.001	1.887	H	-1.877	-5.846	5.186
C	0.805	-4.083	-2.896	H	-1.123	-5.341	3.668
C	1.365	-3.082	-3.694	H	-2.878	-5.334	3.826
C	1.103	-1.755	-3.363	H	-2.976	-4.126	6.703
C	0.296	-1.436	-2.276	H	-4.009	-3.598	5.374
C	-0.252	-2.457	-1.508	H	-3.016	-2.422	6.232
C	0.000	-3.799	-1.794	H	-5.647	-3.506	2.001
C	1.095	0.977	-2.276	H	-4.609	-4.076	0.690
C	2.254	1.011	-1.508	H	-6.136	-3.265	0.332
C	3.291	1.898	-1.795	H	-3.865	-0.598	-0.675
C	3.135	2.738	-2.896	H	-5.180	-1.667	-1.114
C	1.988	2.725	-3.694	H	-3.546	-2.306	-0.942
C	0.969	1.835	-3.362	H	-5.779	-1.031	2.537
C	-3.354	0.361	-3.696	H	-6.446	-0.802	0.914
C	-2.074	-0.075	-3.364	H	-5.061	0.156	1.449
C	-1.394	0.463	-2.277	H	1.116	-5.271	-5.373
C	-2.005	1.448	-1.508	H	2.089	-4.639	-6.701
C	-3.292	1.901	-1.796	H	0.591	-3.824	-6.232
C	-3.940	1.347	-2.899	H	3.185	-5.153	-3.824
C	-0.001	0.001	-1.887	H	4.065	-3.634	-3.668
C	0.626	4.911	0.945	H	4.127	-4.541	-5.185
C	-2.259	3.469	4.876	H	3.369	-1.590	-5.014
C	3.943	-3.000	0.948	H	1.944	-1.657	-6.057
C	4.136	0.219	4.879	H	3.392	-2.569	-6.478
C	-1.878	-3.693	4.876	H	-1.137	-5.320	1.118
C	-4.569	-1.909	0.947	H	-1.409	-3.647	0.677
C	2.260	-3.469	-4.876	H	0.231	-4.221	0.942
C	-0.626	-4.912	-0.945	H	-0.229	-6.946	-0.329
C	4.569	1.910	-0.947	H	1.234	-6.025	-0.689
C	1.878	3.692	-4.876	H	0.221	-6.642	-1.998
C	-4.136	-0.219	-4.879	H	-2.520	-5.989	-0.908
C	-3.944	3.000	-0.948	H	-1.992	-5.525	-2.532
C	-0.203	6.204	1.002	H	-2.662	-4.311	-1.444
C	0.739	4.491	-0.530	H	5.181	1.666	1.114
C	2.038	5.200	1.490	H	3.867	0.596	0.673
C	-2.767	2.244	5.646	H	3.545	2.303	0.943
C	-3.481	4.249	4.355	H	6.134	3.267	-0.331
C	-1.464	4.356	5.852	H	4.606	4.077	-0.687
C	5.477	-2.921	0.997	H	5.644	3.509	-1.999

Continued on next page

A4. Supporting Information to Chapter 4

Table A4.5 – Continued from previous page

Element	x	y	z	Element	x	y	z
C	3.515	-2.898	-0.525	H	6.447	0.805	-0.915
C	3.497	-4.367	1.502	H	5.780	1.035	-2.538
C	3.327	1.269	5.651	H	5.063	-0.154	-1.451
C	5.420	0.891	4.358	H	4.009	3.597	-5.375
C	4.509	-0.914	5.853	H	2.976	4.126	-6.703
C	-0.562	-3.522	5.645	H	3.015	2.421	-6.232
C	-1.946	-5.141	4.356	H	2.878	5.334	-3.827
C	-3.042	-3.444	5.853	H	1.123	5.341	-3.669
C	-5.276	-3.272	1.003	H	1.877	5.846	-5.187
C	-4.264	-1.599	-0.528	H	-0.304	3.718	-5.013
C	-5.522	-0.830	1.496	H	0.463	2.516	-6.056
C	1.464	-4.356	-5.852	H	0.532	4.226	-6.478
C	3.482	-4.249	-4.355	H	-5.128	1.671	-5.373
C	2.767	-2.244	-5.646	H	-5.066	0.514	-6.703
C	-0.740	-4.491	0.530	H	-3.612	1.406	-6.233
C	0.204	-6.204	-1.001	H	-6.056	-0.183	-3.826
C	-2.037	-5.202	-1.491	H	-5.178	-1.704	-3.672
C	4.264	1.597	0.527	H	-5.996	-1.304	-5.188
C	5.274	3.274	-1.001	H	-3.060	-2.118	-5.021
C	5.523	0.833	-1.498	H	-2.408	-0.848	-6.061
C	3.042	3.444	-5.853	H	-3.921	-1.647	-6.484
C	1.945	5.141	-4.356	H	-4.035	3.657	1.111
C	0.562	3.522	-5.645	H	-2.449	3.063	0.666
C	-4.509	0.913	-5.853	H	-3.758	1.923	0.944
C	-5.420	-0.891	-4.358	H	-5.904	3.666	-0.325
C	-3.327	-1.269	-5.651	H	-5.831	1.937	-0.678
C	-3.514	2.899	0.525	H	-5.872	3.117	-1.992
C	-5.477	2.919	-0.996	H	-3.939	5.179	-0.922
C	-3.499	4.367	-1.504	H	-3.808	4.483	-2.544
H	-0.218	6.642	2.000	H	-2.414	4.468	-1.462
H	-1.233	6.026	0.691	H	0.002	-0.001	0.801
H	0.230	6.946	0.330	H	-0.002	0.001	-0.800
H	1.407	3.647	-0.678	H	-1.019	5.113	3.136
H	1.135	5.320	-1.118	H	0.877	2.189	0.667
H	-0.234	4.222	-0.942	H	-1.536	0.951	3.935
H	1.994	5.523	2.531	H	1.461	-1.854	0.667
H	2.521	5.987	0.906	H	4.939	-1.676	3.139
H	2.663	4.308	1.441	H	1.593	0.853	3.937
H	-3.392	2.570	6.479	H	-0.056	-1.810	3.934
H	-1.944	1.658	6.057	H	-2.334	-0.336	0.668
H	-3.368	1.590	5.014	H	-3.921	-3.437	3.137
H	-4.127	4.541	5.185	H	1.019	-5.112	-3.136
H	-4.064	3.634	3.668	H	1.536	-0.951	-3.935
H	-3.185	5.153	3.824	H	-0.876	-2.190	-0.667
H	-2.089	4.640	6.701	H	2.334	0.336	-0.667
H	-1.116	5.271	5.373	H	3.921	3.437	-3.137
H	-0.591	3.824	6.232	H	0.056	1.810	-3.934
H	5.870	-3.120	1.994	H	-1.593	-0.853	-3.936
H	5.832	-1.939	0.680	H	-1.461	1.854	-0.667
H	5.904	-3.668	0.326	H	-4.939	1.676	-3.139

Triphenylmethane dimer

Table A4.6.: Energies for the triphenylmethane and the corresponding dimer at the B3LYP-D3(BJ)-ATM/def2-TZVPP level. Thermostatistical corrections at the PBEh-3c level.

Energy	Unit	Monomer	Dimer
EE	Hartree	-733.5369732	-1467.087047
U	Hartree	-733.2520992	-1466.516800
H	Hartree	-733.2359432	-1466.485733
S	cal mol ⁻¹	120.837	184.166
G ^{298K}	Hartree	-733.2933572	-1466.573236
C-H...H-C	Å	n/a	1.717

Table A4.7.: Coordinates of the structure of triphenylmethane optimized at B3LYP-D3(BJ)-ATM/def2-TZVPP.

Element	x	y	z	Element	x	y	z
35							
C	-0.706	4.072	3.144	C	0.080	0.014	1.876
C	0.086	3.814	2.029	H	0.092	0.036	0.783
C	0.316	2.505	1.629	H	-0.888	5.091	3.458
C	-0.238	1.432	2.328	H	0.941	2.308	0.766
C	-1.033	1.701	3.439	H	-1.482	0.884	3.986
C	-1.264	3.012	3.846	H	1.638	-1.830	0.687
C	1.468	-0.437	2.309	H	4.964	-1.746	3.383
C	2.120	-1.423	1.568	H	1.614	0.843	4.022
C	3.370	-1.893	1.948	H	0.033	-1.815	3.950
C	3.990	-1.383	3.084	H	-2.295	-0.368	0.671
C	3.349	-0.401	3.829	H	-3.886	-3.391	3.253
C	2.099	0.070	3.442	H	3.861	-2.656	1.358
C	-1.912	-2.686	3.724	H	3.824	0.005	4.713
C	-0.879	-1.824	3.370	H	-4.122	-1.904	1.283
C	-1.004	-0.980	2.270	H	-1.797	-3.335	4.582
C	-2.184	-1.023	1.527	H	-1.884	3.202	4.712
C	-3.216	-1.884	1.874	H	0.522	4.632	1.472
C	-3.084	-2.719	2.979				

Table A4.8.: Coordinates of the structure of triphenylmethane dimer optimized at B3LYP-D3(BJ)-ATM/cc-pVDZ.

Element	x	y	z	Element	x	y	z
70							
C	-0.734	4.091	3.109	C	-3.360	1.917	-1.970
C	0.006	3.815	1.964	C	-4.013	1.390	-3.080
C	0.257	2.499	1.598	C	-0.090	-0.012	-1.938
C	-0.228	1.439	2.366	H	0.118	0.041	0.850
C	-0.973	1.724	3.507	H	-0.113	-0.029	-0.850
C	-1.221	3.042	3.879	H	-0.932	5.115	3.396

Continued on next page

A4. Supporting Information to Chapter 4

Table A4.8 – Continued from previous page

Element	x	y	z	Element	x	y	z
C	1.477	-0.446	2.361	H	0.838	2.291	0.708
C	2.106	-1.440	1.611	H	-1.369	0.913	4.102
C	3.363	-1.911	1.964	H	1.604	-1.853	0.744
C	4.011	-1.394	3.082	H	4.992	-1.757	3.360
C	3.393	-0.404	3.834	H	1.667	0.851	4.057
C	2.135	0.070	3.474	H	0.006	-1.861	3.966
C	-1.937	-2.724	3.681	H	-2.274	-0.307	0.698
C	-0.897	-1.851	3.373	H	-3.899	-3.417	3.149
C	-1.005	-0.972	2.299	H	0.931	-5.119	-3.364
C	-2.173	-0.988	1.534	H	1.372	-0.923	-4.096
C	-3.209	-1.861	1.835	H	-0.838	-2.278	-0.695
C	-3.094	-2.734	2.913	H	2.274	0.331	-0.698
C	0.092	0.017	1.938	H	3.897	3.414	-3.184
C	0.733	-4.093	-3.084	H	-0.005	1.843	-3.987
C	1.222	-3.049	-3.860	H	-1.673	-0.864	-4.043
C	0.975	-1.730	-3.496	H	-1.596	1.869	-0.755
C	0.229	-1.437	-2.357	H	-4.994	1.751	-3.358
C	-0.257	-2.492	-1.583	H	1.804	-3.260	-4.748
C	-0.006	-3.810	-1.940	H	-0.386	-4.614	-1.324
C	1.006	0.975	-2.308	H	3.837	-2.678	1.367
C	2.173	1.002	-1.542	H	3.891	0.008	4.702
C	3.207	1.873	-1.852	H	-3.899	-0.027	-4.688
C	3.093	2.732	-2.941	H	-3.832	2.690	-1.378
C	1.936	2.712	-3.710	H	1.836	3.379	-4.556
C	0.898	1.841	-3.393	H	4.101	1.884	-1.242
C	-3.398	0.392	-3.826	H	-4.103	-1.863	1.225
C	-2.138	-0.078	-3.466	H	-1.837	-3.401	4.519
C	-1.476	0.447	-2.360	H	-1.802	3.246	4.769
C	-2.102	1.449	-1.616	H	0.385	4.623	1.353

A4.3. Interaction Energies

A4.3.1. Energy Decomposition Analysis

Table A4.9.: Energies of the energy decomposition analysis of the (3,5-di-tert-butylphenyl)methane dimer in C_3 on the B3LYP-D3(BJ)-ATM/def2-TZVPP level of theory.

	[Hartree]	[kcal mol ⁻¹]
E_{elst}	-0.02894088	-18.16048
$E_{\text{nuc-nuc}}$	7235.12086	4540060
$E_{1\text{-electron}}$	-14470.7822	-9080459
$E_{2\text{-electron}}$	7235.63237	4540381
$E_{\text{exch-rep}}$	0.11836262	74.27289
E_{exch}	-0.02976382	-18.67688
$E_{\text{exch-rep}}$	0.14812644	92.94978
$E_{\text{orbital Relax.}}$	-0.02068952	-12.98273
$E_{\text{corr.}}$	-0.08309221	-52.14061
E_{tot}	-0.0584361	-36.66883

A4. Supporting Information to Chapter 4

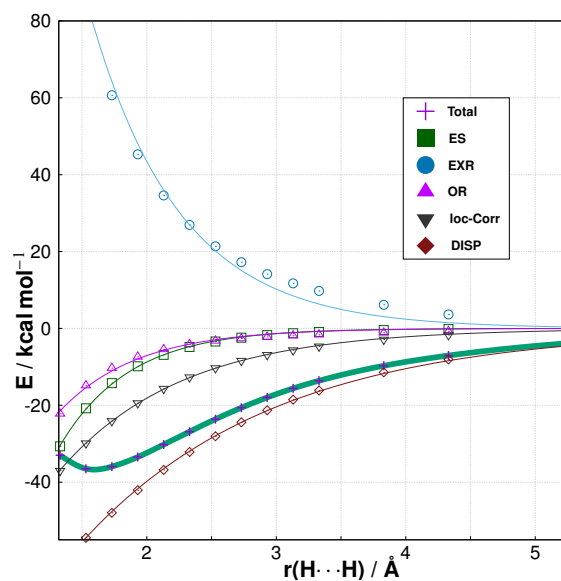


Figure A4.3.: Representation of the energy decomposition analysis at the B3LYP-D3(BJ)-ATM/def2-TZVPP level of theory with respect to the H \cdots H distance within the (3,5-di-tert-butylphenyl)methane dimer. The total interaction energy (bold, green curve) shows a minimum around 1.59 Å. Dispersion interactions (termed “DISP”) are dominant within the complex mirroring long-range correlation effects. The local correlation energy (termed “loc-Corr”) represents the short-range correlation part, already described by the B3LYP hybrid functional.

A5. Supporting Information to Chapter 5

Appendix A5 contains:

- Computational details for DFT calculations, DFT-D corrections, DLPNO-CCSD(T), and geometry optimization
- Benchmark data for MOR41, WCCR10, and HEAVY28
- LED for $[[\text{Rh}(\text{CNPh})_4]_2]^+$ dication
- Timings
- Structure of indenyl complexes

A5.1. Appendix: Understanding and Quantifying London Dispersion Effects in Organometallic Complexes

A5.1.1. Computational Details

Density Functional Theory Calculations

All ground state DFT calculations were performed with TURBOMOLE 7.0.2,^{143,205} TURBOMOLE 7.33⁵⁹ or ORCA 4.0.1^{144,145} program packages. Standard exchange-correlation energy integration grids (TURBOMOLE: *m4*, ORCA: *grid4*, *finalgrid5*) and usual convergence criteria for the self-consistent field convergence (10^{-7} Hartree) were used. The resolution of the identity (RI) approximation^{207,209} was applied in all calculations for the electronic Coulomb energy contribution. Ahlrichs' type quadruple- ζ basis sets with (def2-QZVPP) and without (def2-QZVP)²⁵⁴ additional polarization functions were used and for timings also def2-SVP was employed.

DFT-D Corrections

Our standalone dftd3 and dftd4 was used for all D3(BJ)-ATM⁴⁶ and D4^{210,308} (All partial charges used in D4 calculations were obtained self-consistently by GFN2-xTB²⁴⁴ if not noted otherwise) single point calculations, respectively. For

A5. Supporting Information to Chapter 5

geometry optimization the TURBOMOLE 7.3 implementation of D4 was used. All calculations employing the D3 and D4 correction scheme apply Becke-Johnson (BJ) damping¹⁶⁶ and include Axilrod-Teller-Muto (ATM) type three-body dispersion^{167,168} to the total dispersion energy. Molecular dispersion coefficients were calculated with the D4 method standalone.

DLPNO-CCSD(T)

For generation of reference energies DLPNO-CCSD(T)²⁶¹ was used in its sparse maps implementation²² as available in ORCA 4.0.1^{144,145} with def2-TZVPP and def2-QZVPP²⁵⁴ basis sets and corresponding auxiliary basis sets. The auxiliary basis sets def2-TZVPP/C and def2-QZVPP/C⁴⁷⁷ were applied for the correlation part. For complete basis set (CBS) extrapolation the scheme proposed by Neese and Valeev²⁷¹ was employed. *VeryTightPNO*²⁷⁰ settings for def2-TZVPP and *TightPNO* settings⁴⁷⁸ for def2-QZVPP and ORCA *TightSCF* convergence criteria for the HF energy were used. The LED⁴⁴⁷ scheme was carried out with ORCA 4.0.1 as well.

Geometries

The Tetrakis(isonitrile)rhodium(I) dimer structure has been obtained with the dispersion corrected composite method PBEh-3c²⁷² and the monomers have been cut out of this dimer structure without further optimization. For the transition state structure of the oxidative addition of methane to Pd(PCy₃)₂ and the structure of the heavy carbene analogue Pb{C₆H₂-2,4,6-iPr₃)₂ structures were optimized at the PBE0-D4/def2-TZVP level of theory. The structures of the sumanene and the bimetallic indenyl complexes were optimized on the PBE0-D4/def2-QZVP level of theory. Minimum structures were verified as minima on the potential energy hyper surface by the absence of imaginary frequencies in harmonic frequency calculations.

A5.1.2. Benchmark Data

Table A5.1.: MOR41 reaction energies given in kcal mol⁻¹. DFT calculations employ the def2-QZVPP basis set. Given are PBE0 (termed as "Pure") and dispersion corrected PBE0 values. We abbreviate D3(BJ)-ATM as D3 and D4(q^{TB})-ATM as D4. Reference: DLPNO-CCSD(T)/*TightPNO*/CBS(def2-TZVPP/def2-QZVPP)

#	Ref.	Pure	D3	D4	NL
1	-43.1	-42.1	-44.7	-44.7	-45.8
2	-46.6	-45.2	-47.4	-46.9	-48.8
3	-27.6	-24.7	-26.4	-26.4	-27.6
4	-62.5	-69.0	-71.4	-71.7	-72.4

Continued on next page

A5.1. Understanding and Quantifying London Dispersion Effects in Organometallic Complexes

Table A5.1 – Continued from previous page

#	Ref.	Pure	D3	D4	NL
5	3.7	-0.1	-2.4	-2.3	-3.3
6	-23.1	-19.8	-20.3	-21.0	-21.9
7	-16.2	-15.3	-15.3	-15.4	-17.4
8	-17.2	-12.7	-15.3	-17.0	-15.6
9	-18.8	-21.0	-15.0	-16.8	-16.2
10	-22.6	-13.3	-19.1	-19.5	-20.6
11	27.0	37.1	30.2	29.0	29.6
12	-29.8	-25.6	-28.9	-30.2	-31.4
13	-43.2	-39.3	-43.6	-43.8	-45.4
14	-52.0	-42.4	-50.5	-52.8	-53.8
15	-4.1	-3.7	-4.4	-5.1	-5.4
16	-39.8	-24.0	-40.0	-41.1	-41.3
17	-16.1	-8.2	-11.2	-14.5	-15.5
18	-34.2	-23.3	-32.8	-33.1	-33.0
19	-40.1	-26.8	-38.0	-38.4	-38.3
20	-30.2	-18.1	-27.8	-28.3	-28.4
21	-15.1	-8.2	-17.1	-17.5	-18.1
22	-35.9	-22.5	-32.1	-33.4	-32.4
23	-55.0	-41.2	-52.3	-52.4	-52.2
24	-41.6	-20.7	-41.7	-41.5	-41.6
25	-45.9	-21.2	-45.6	-45.6	-45.8
26	-36.4	-31.4	-39.0	-38.9	-34.6
27	-21.8	-24.4	-25.5	-25.5	-21.4
28	-36.3	-36.0	-39.6	-39.6	-35.4
29	-28.3	-27.5	-30.0	-29.9	-26.6
30	-14.9	-13.1	-16.1	-16.4	-12.3
31	-29.9	-28.4	-29.7	-29.8	-25.9
32	-1.9	0.4	0.7	0.4	0.1
33	-10.7	-6.6	-8.8	-10.0	-7.7
34	-25.6	-20.9	-25.0	-25.8	-23.1
35	-30.9	-25.4	-29.9	-30.3	-27.9
36	-39.8	-32.0	-35.3	-34.7	-34.0
37	-14.0	-20.2	-23.5	-23.3	-21.2
38	-64.4	-51.5	-71.8	-69.7	-65.0
39	-63.9	-54.9	-59.6	-61.2	-61.5
40	-65.8	-64.5	-69.2	-68.4	-69.9
41	-3.2	-6.0	-3.4	-3.4	-1.4
MD	5.5	< -0.1	-0.5	0.2	
MAD	6.6	2.6	2.2	2.4	
RMSD	8.7	3.4	3.0	3.1	
SD	6.9	3.5	3.0	3.2	
Var	47.0	11.9	9.2	10.0	
Max	24.7	4.9	5.1	5.8	
Min	-6.5	-9.4	-9.3	-9.9	
AMax	24.7	9.4	9.3	9.9	

A5. Supporting Information to Chapter 5

Table A5.2.: WCCR10 ligand binding energies given in kcal mol⁻¹. DFT calculations employ the def2-QZVPP basis set. Given are PBE0 (termed as “Pure”) and dispersion corrected PBE0 values. We abbreviate D3(BJ)-ATM as D3 and D4(q^{TB})-ATM as D4. Reference: DLPNO-CCSD(T)/NormalPNO/CBS(cc-pVTZ-PP/cc-pVQZ-PP)

#	Ref.	Pure	D3	D4
1	25.60	21.46	24.30	24.18
2	63.36	37.14	61.59	63.54
3	63.00	37.60	61.80	63.77
4	52.70	30.98	52.90	52.64
5	45.08	33.86	46.36	46.08
6	67.38	62.27	66.57	66.75
7	59.75	56.32	60.74	60.67
8	50.12	46.20	50.60	50.80
9	36.38	33.14	38.54	38.40
10	23.78	17.63	22.96	23.56
MD	-11.1	-0.1	0.3	
MAD	11.1	1.1	0.8	
RMSD	14.3	1.2	1.0	
SD	9.6	1.3	1.0	
Var	91.9	1.7	0.9	
Max	-3.2	2.2	2.0	
Min	-26.2	-1.8	-1.4	
AMax	26.2	2.2	2.0	

Table A5.3.: HEAVY28 interaction energies given in kcal mol⁻¹. DFT calculations employ the def2-QZVP basis set. Given are PBE0 (termed as “Pure”) and dispersion corrected PBE0 values. We abbreviate D3(BJ)-ATM as D3 and D4(q^{TB})-ATM as D4. Reference: CCSD(T)/CBS(aug-cc-pwCVTZ-PP/aug-cc-pwCVQZ-PP)

#	Ref.	Pure	D3	D4
1	1.16	0.12	1.42	1.46
2	2.49	2.02	2.83	2.89
3	1.36	0.42	1.52	1.51
4	0.77	0.18	0.88	0.86
5	0.98	0.27	1.11	1.07
6	1.30	0.48	1.56	1.47
7	0.60	0.38	0.88	0.90
8	1.25	-0.04	1.38	1.30
9	0.55	0.02	0.80	0.73
10	0.36	0.12	0.42	0.44
11	0.75	-0.01	0.77	0.79
12	0.93	0.03	0.94	0.92
13	1.18	0.00	1.20	1.14
14	0.65	0.04	0.85	0.82
15	1.28	0.13	1.60	1.60
16	1.57	1.55	2.13	2.03
17	1.06	0.73	1.51	1.39
18	2.02	2.03	2.85	2.66
19	1.89	1.84	2.74	2.55
20	1.49	1.28	2.30	2.12
21	2.84	2.46	3.50	3.51
22	0.52	-0.15	0.76	0.72

Continued on next page

A5.1. Understanding and Quantifying London Dispersion Effects in Organometallic Complexes

Table A5.3 – Continued from previous page

#	Ref.	Pure	D3	D4
23	0.68	0.36	0.81	0.87
24	0.48	-0.09	0.60	0.62
25	1.23	0.52	1.41	1.36
26	1.22	0.42	1.38	1.35
27	0.80	0.23	1.11	1.06
28	3.35	3.10	4.07	4.07
MD	-0.58	0.31	0.27	
MAD	0.58	0.31	0.27	
RMSD	0.68	0.40	0.34	
SD	0.36	0.26	0.22	
Var	0.13	0.07	0.05	
Max	0.01	0.85	0.72	
Min	-1.29	0.01	-0.04	
AMax	1.29	0.85	0.72	

A5.1.3. LED

Table A5.4.: Energy contributions as coming from the LED analysis given in kcal mol⁻¹.

ΔE_{int}	$\Delta E_{\text{el-prep}}$	ΔE_{elint}	$\Delta E_{\text{exch}}^{(X,Y)}$	ΔE_{disp}	$\Delta E_{\text{C-(T)}}^{\text{red},(X,Y)}$	$\left \frac{E_{\text{disp}}}{\Delta E_{\text{int}}} \right $
13.1	164.5	-71.4	-30.1	-47.9	-2.1	3.7
Absolute dispersion energy deviations: $\Delta E_{\text{disp}} - \Delta E_{\text{disp}}^{\text{HF/DFT-D}}$						
			HF-D3	-1.7		
			B3LYP-D3	-6.0		
			PBE0-D3	-19.6		
			HF-D4	4.6		
			B3LYP-D4	-1.9		
			PBE0-D4	-16.6		

In order to obtain a more accurate dispersion energy the triples contributions is further decomposed into charge transfer and dispersion interaction by an estimation scheme, where the ratio of the dispersion part of the strong pairs $E_{\text{C-SP}}^{\text{disp}(X,Y)}$ is divided by the total interaction energy of the strong pairs $E_{\text{C-SP}}^{(X,Y)}$ to obtain the ratio r_{sp} . For the total dispersion contribution the triples contribution are scaled by r_{sp} . The remaining triples contribution is termed $E_{\text{C-(T)}}^{\text{red},(X,Y)}$.

$$r_{\text{sp}} = \frac{E_{\text{C-SP}}^{\text{disp}(X,Y)}}{E_{\text{C-SP}}^{(X,Y)}} \quad (\text{A5.1})$$

$$E_{\text{disp}} = E_{\text{C-SP}}^{\text{disp}(X,Y)} + E_{\text{C-WP}}^{(X,Y)} + r_{\text{sp}} E_{\text{C-(T)}}^{(X,Y)} \quad (\text{A5.2})$$

A5.1.4. Timings

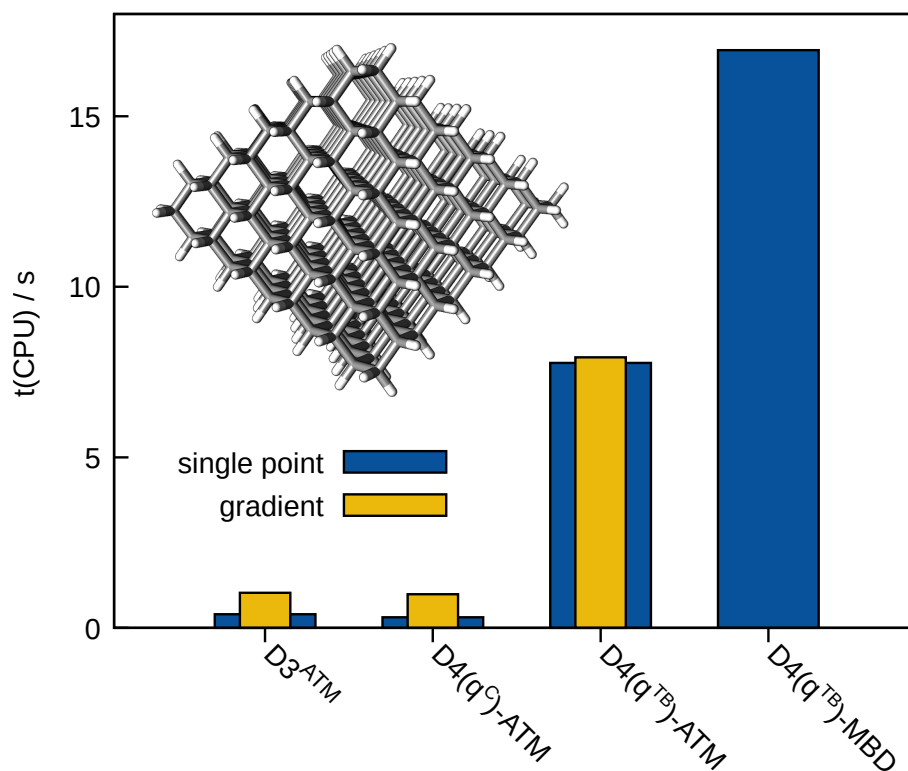


Figure A5.1.: CPU timings of selected DFT-D combinations for a diamondoid with 430 atoms. q^{TB} indicates the use of charges obtained from the GFN2-xTB Tight-Binding method,²⁴⁴ q^{c} the use of classical charges.

A5.1.5. Indenyl Complexes

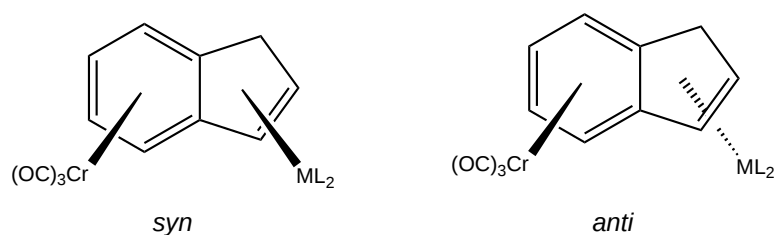


Figure A5.2.: Structures of the *syn*- and *anti*-facial bimetallic indenyl species (1: $\text{ML}_2=\text{Rh}(\text{norbornadiene})$, 2: $\text{ML}_2=[\text{Rh}(\text{CO})_2]$, 3: $\text{ML}_2=[\text{Rh}(\text{cyclooctadiene})]$, 4: $\text{ML}_2=[\text{Ir}(\text{CO})_2]$).

Acknowledgements

This dissertation would not have been possible without the great support of different people. I want to thank my supervisor Prof. Dr Stefan Grimme, for many points. First, I thank Stefan for the opportunity to work on exciting scientific problems, where I had the freedom to realize my ideas. Second, I am thankful for his scientific and financial support, which allowed me to attend many scientific conferences to present my research.

I am grateful to Prof. Dr Thomas Bredow for being my second referee, but also for all scientific and non-scientific interactions I had with him.

I thank Jana Pisarek, Dr Jan Gerit Brandenburg, Sebastian Ehlert, Philipp Pracht, Sebastian Spicher, and Joachim Laun for proof-reading parts of this dissertation.

Additionally, I am grateful to my current and former colleagues Dr Jan Gerit Brandenburg, Dr Christoph Bannwarth, Sebastian Ehlert, Fabian Bohle, Jakob Seibert, Philipp Pracht, Mirko Bauer, Dr Andreas Hansen, Sebastian Dohm, Rebecca Sure, Christoph Bauer, Sebastian Spicher, Hagen Neugebauer, Markus Bursch, Dr Jan Mewes, Dr Christoph Reimann, Jeroen Koopman, Sarah Schmitz, and Karola Schmitz for the great teamwork during joint projects and for general support.

Next, I wish to thank all of my collaborators outside the Grimme group that I had the pleasure to work with. In the context, I would like to express my gratitude to Dr Sören Rösel and Prof. Dr Peter Schreiner for the fruitful collaboration.

Throughout my studies, I had the pleasure to work in a welcoming and scientifically productive atmosphere. I want to thank all past and current members of the Grimme and Bredow group for contributing to it in their own way. Furthermore, I enjoyed sharing an office with Fabian Bohle and Dr Christoph Reimann.

Special thanks go to my girlfriend, Jana Pisarek, for her ongoing support and patience. I also want to take this opportunity to thank my family: my sister Kinka my sister in law Natalie, my brothers Nicko and Max, and in particular my parents for their continuous support. As part of my family, I also want to thank Maximilian Metzler and Markus Winnen in particular. Without my family and my friends, my studies would not have been possible in this way.

Abbreviations

ACFD *Adiabatic Connection Fluctuation Dissipation*

AE *All-Electron*

AIM *Atom-in-Molecule*

AMAX *Absolute Maximum deviation*

AOs *Atomic Orbitals*

ATM *Axilrod–Teller–Muto*

B88 *Becke Exchange*

BOA *Born–Oppenheimer Approximation*

BSIE *Basis Set Incompleteness Error*

BSSE *Basis Set Superposition Error*

CI *Configuration Interaction*

CNs *Fractional Coordination Numbers*

C *Correlation*

DFAs *Density Functional Approximations*

DFT *Density Functional Theory*

ES *Electrostatics*

EXR *Pauli Exchange Repulsion*

FBZ *First Brillouin Zone*

GGA *Generalized Gradient Approximation*

GTOs *Gaussian Type Orbitals*

HF *Hartree–Fock*

HK *Hohenberg and Kohn*

IND *Induction*

INT *total interaction energy*

KS *Kohn–Sham*

LCAO-MO *Linear Combinations of Atomic Orbitals*

LD *London Dispersion*

LED *Local Energy Decomposition*

LRD *Local-Response Dispersion*

LR *Long-Range*

LSDA *Local Spin Density Approximation*

LYP *Lee–Yang–Parr*

MAD *Mean Absolute Deviation*

MBD@scsTS *Many-Body Dispersion*

MD *Mean Deviation*

mGGA *meta-GGA*

MP2 *Møller–Plesset Perturbation Theory of Second-Order*

NAOs *Numerically Tabulated Atom-Centered Orbitals*

NHCs *N-heterocyclic Carbenes*

NCIs *Noncovalent Interactions*

OS *Opposite-Spin*

PAW *Projector Augmented-Wave*

PBCs *Periodic Boundary Conditions*

PBE *Perdew–Burke–Erzerhof*

PHS *Pseudo Hilbert Space*

PT *Rayleigh–Schrödinger Perturbation Theory*

QM *Quantum Mechanical*

RMSD *Root Mean Squared Deviation*

RPA *Random Phase Approximation*

RSH *Range-Separated Hybrids*

SAPT *Symmetry-Adapted Perturbation Theory*

SCAN *Strongly Constrained and Appropriately Normed*

SIE *Self-Interaction Error*

SR *Short-Range*

SS *Same-Spin*

STOs *Slater Type Orbitals*

TD-DFT *Time-Dependent Density Functional Theory*

TPM *tris(3,5-di-tert-butylphenyl)methane*

TPSS *Tao-Perdew-Staroverov-Scuseria*

TS *Tkatchenko-Scheffler*

vdw-DF *van der Waals Density Functionals*

WFT *Wave Function Theory*

XC *Exchange-Correlation*

XDM *Exchange Dipole Moment*

X *Exchange*

